LOAN DOCUMENT

PHOTOGRAPH THIS SHEET

AD-A252 283

DTIC ACCESSION NUMBER

LEVEL

(1)

INVENTORY

12th Moving Base Gravity/Gradiometer Conference

DOCUMENT IDENTIFICATION

14-15 Feb 84

DISTRIBUTION STATEMENT A

Approved for public release;
Distribution Unlimited

DISTRIBUTION STATEMENT

HANDLE WITH CARE

ACCESSION FOR

NTIS GRA&I ☑

DTIC TRAC ☐

UNANNOUNCED ☐

JUSTIFICATION

BY

DISTRIBUTION/

AVAILABILITY CODES

DISTRIBUTION	AVAILABILITY AND/OR SPECIAL	
A-1		

DISTRIBUTION STAMP

DTIC
ELECTE
JUN 2 4 1992
S C D

DATE ACCESSIONED

DATE RETURNED

92 024

DATE RECEIVED IN DTIC

92-16505

REGISTERED OR CERTIFIED NUMBER

PHOTOGRAPH THIS SHEET AND RETURN TO DTIC-FDAC

DTIC FORM 70A JUN 90

DOCUMENT PROCESSING SHEET

PREVIOUS EDITIONS MAY BE USED UNTIL STOCK IS EXHAUSTED.

LOAN DOCUMENT

Twelfth Moving Base
Gravity/Gradiometer Conference
United States Air Force Academy
Colorado Springs, Colorado

Agenda

Tuesday 14 February

0800 - Buses depart USAFA Officers' Club for Fairchild Hall

0815 - Registration - 3rd floor Fairchild Hall, South End

0900 - Welcome/Introduction - 2Lt Warner

0910 - Opening Remarks - Dr. Martin (DMA)

0920 - "AFGL/DMA GGSS Program Review" - Mr. Borgeson (AFGL)

0935 - "Review of 1983 Moving Base Gravity Gradiometer Activities at Bell Aerospace Textron" - Mr. Metzger (Bell Aerospace Textron)

1010 - "Comparison of at Sea Gradiometer Test Results with an Independent Gravity Gradient Reference" - Mr. Zorn, Mr. Benson (Dynamics Research Inc.)

1040 - Break

1055 - "Current GGSS Performance Expectation and Error Allocation" - Dr. Heller (TASC)

1145 - Buses depart Fairchild Hall for USAFA Officers' Club

1200 - Luncheon - Officers' Club

1300 - Buses depart Officers' Club for Fairchild Hall

1315 - "Efficient Processing of Gradiometer Output Using a Kalman Filter" - Dr. Hutcheson (Bell Aerospace Textron)

1345 - "On-Going Work in Post-Mission Data Processing Algorithm Development" - Dr. Heller (TASC)

1410 - "Three-axis Super Conducting Gravity Gradiometer" - Dr. Paik (University of Maryland)

1500 - Break

1515 - "Overview of Airborne Gravity and Comparison of Gravity and Gradient Anomolies" - Dr. Hammer (University of Wisconsin)

1535 - "WGS 72 Gravity Gradient Reference Ellipsoid and Earth Gravitational Model" - Mr. May (NADC)

1600 - Buses depart Fairchild Hall for USAFA Officers' Club

1615 - Reception - USAFA Officers' Club

Wednesday 15 February

0800 - Buses depart USAFA Officers' Club for Fairchild Hall

0815 - "Relooking at MASCONS for Representing Gravity Survey Data" - Dr. Breakwell (Stanford University)

0840 - "Integral Formulas Relating Gravity Gradients to Vertical Deflection" - Mr. Zorn (Dynamics Research Inc.)

0910 - "Real-time Vertical Deflection Estimation Using Gradient Data" - Dr. Feldman (Sperry Corp) (Mr. B. Epstein, Co-Author, US Navy SSPO)

0940 - Break

1000 - "Gravity Gradiometer Application to Tunnel Detection" - Mr. Jircitano (Bell Aerospace Textron)

1040 - ***Time Permitting*** "A Simplification of the Least Squares Determination of the Gravity Field..." - Dr. Reinhardt (Bendix)

1050 - DoD Executive Session

1200 - Buses leave

DISCLAIMER NOTICE

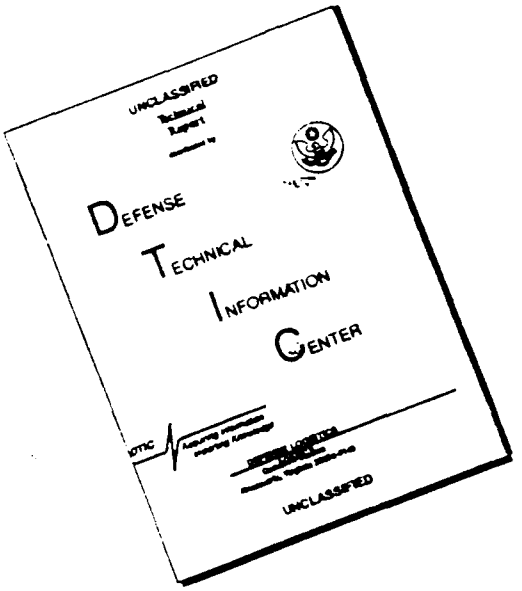

THIS DOCUMENT IS BEST QUALITY AVAILABLE. THE COPY FURNISHED TO DTIC CONTAINED A SIGNIFICANT NUMBER OF PAGES WHICH DO NOT REPRODUCE LEGIBLY.

MISSING PAGES WILL BE INSERTED AT AN LATER DATE
AS ERRATA(S)

MINUTES OF THE TWELFTH ANNUAL
MOVING BASE GRAVITY GRADIOMETER CONFERENCE

United States Air Force Academy
Colorado Springs, Colorado

14-15 February 1984

Tuesday Morning Session

Welcome/Introduction - 2Lt D.L. Warner (AFGL)
As coordinator of the two-day conference, Lt. Warner opened the meeting on behalf of the co-sponsoring agencies, the Air Force Geophysics Laboratory (AFGL) and the Defense Mapping Agency (DMA). She then introduced Dr. C. Martin, Director of the Advanced Technology Division, DMA.

Opening remarks - Dr. C. Martin
Dr. Martin welcomed participants and attendees. He made reference to the agenda noting his enthusiasm over topics of data processing and algorithm development, and the breaking from topics of hardware development. He expressed the urgency of the need to develop the necessary means to analyze the data. Software development has a long lead time, therefore Dr. Martin urged the gravity community to share insights, applicable software, anything that might keep individual software developers from "reinventing the wheel".

AFGL/DMA GGSS Program Review - Mr. R. Borgeson (AFGL)
Mr. Borgeson, program manager of the Gravity Gradiometer Survey System, presented a review of those milestones that have been accomplished, and those soon to be accomplished. He gave a brief description of the two modes of the system: the land based and the airborne modes, including mockup models and viewgraph sketches. He stated the accuracy requirements of the system and showed diagrams and pictures of the actual three-axis gravity gradiometer that Bell Aerospace Textron is under contract to develop and build. Mr. Borgeson stated that AFGL and DMA are in the process of determining which aircraft would best suit the needs of the GGSS program. The present choices are the P3, the Convair 580, and the C130.

Questions:
Dr. S. Hammer (University of Wisconsin) - To what accuracy can we estimate gravity using the gradiometer? Is it a prediction or demonstrated performance?

Mr. Borgeson - .18 arc seconds, .9 milligals and it is a specification and predicted accuracy.

Mr. M. May (NADC) - What navigation system would be used on the P3, and will a gravimeter be used?

Mr. Borgeson - GPS navigation and no gravimeter.

Review of 1983 Moving Base Gravity Gradiometer Activities at Bell Aerospace Textron - Mr. E. Metzger (Bell Aerospace Textron)

Mr. Metzger described the two programs Bell is working on: the Navy Gravity Survey System (GSS) and the AFGL/DMA GGSS Program. He described the performance of the Advanced Development Model (ADM) #1 (Navy) aboard the USNS Vanguard. Having been in operation since February 1982 the instrument failed less often than expected and met the feasibility requirements in all tests. The ADM #2 has been in operation since September 1983. Mr. Metzger outlined the status and future plans of ADM #2 stating that the objective was to provide a test bed for verifying modifications considered for operational systems. Since Mr. Borgeson had already covered the physical or hardware portions of the GGSS, Mr. Metzger focused his attention on a discussion of error analysis and track spacing.

Questions:

Dr. H.J. Paik (University of Maryland) - What is the origin of the red noise?

Mr. Metzger - Drift in the even order calibration coefficients of the accelerometers.

Dr. Paik - Is the noise proportional to 1/f?

Mr. Metzger - It is proportional to between 1/f and $(1/f)^{1.6}$.

Comparison of At-Sea Gradiometer Test Results With An Independent Gravity Gradient Reference - Mr. D. Benson, Jr. and Mr. A. Zorn (Dynamics Research Corporation)

Mr. B. Regenauer, Mr. Benson, and Mr. Zorn are co-authors of this paper and it was presented by the latter two. Mr. Benson discussed the generation of a gravity gradient reference off the north coast of Puerto Rico and subsequent comparison of Gravity Gradiometer gradients with the reference. The gradient reference was derived using position differences between an accurate marine inertial system and an accurate geodetic position reference, Autotape. Similar techniques have been used for vertical deflections over land but, in contrast, require frequent stopping for gyro recalibration. Mr. Zorn presented part two, the feasibility of the at-sea survey technique which was established using covariance error analysis. Subsequently a test plan was developed to acquire data for map development, and the survey was performed with equipment onboard the USNS Vanguard. Returns over the same paths and crossing paths during the survey allow separation of time varying gyro and acclerometer errors from position varying gradients and deflections when the survey data is processed. The analysis and data processing include local geodetic constraints on the gradients to satisfy the conditions of the earth's gravitational potential. Mr. Zorn concluded by mentioning that the survey paths were repeated on a later at-sea test with the Bell Gravity Gradiometer onboard. Gravity gradients from the gradiometer compared remarkably well with the gravity gradient reference along the survey paths.

Questions:

Mr. Borgeson - Is the program under contract?

Mr. Benson - Yes, under contract with Sperry Management Systems, SP24.

Mr. S. Jordan (Geospace) - Can you give an actual accuracy for test results?

Mr. Benson - No, it is classified.

Mr. P. Fell (DMAHTC) - What is the Autotape system?

Mr. Benson - A radar navigation line of sight positioning system.

Mr. W. Gumert (Carson Geoscience) - What speed were you surveying at?

Mr. Zorn - 5 to 8 knots.

Dr. W. Heller (TASC) - Is there an RMS difference between map and measured gradients?

Mr. Benson - They exist but are classified.

A discussion followed between Dr. Heller and Mr. Benson concerning possible RMS differences and how they depend on data processing and use of low frequency information.

Current GGSS Performance Expectation and Error Analysis Allocation - *Dr. W. Heller (TASC)*

Dr. Heller opened with a review of test and survey geometry of the GGSS and the desired goals. He discussed the error sources as well as the GGSS sensitivity to variation in the frequency content of the gravity field. Mentioned as well were the contribution of each class of errors and the sensitivity to survey altitude. In his conclusions Dr. Heller stated that the bottom-line is that the performance of the GGSS is expected to fall well within prescribed specifications.

Questions:
Mr. J. Brozena (NRL) - The downward continuation and truncation errors refer to the center of the survey. What happens as you go away from the center?

Dr. Heller - We have to be concerned with edge effects. Testing will be done at the center of the survey region to minimize edge effects.

Mr. Zorn - Was only one gradient, Tzz, used?

Dr. Heller - Yes.

Mr. Zorn - What if other gradients are used, such as those that are more directly related to the vertical deflection by integration? The error could be overstated because these gradients are not used.

Dr. Heller - We used Breakwell's results that the best gradient to use is Tzz. We incurred a penalty of a factor of 2 by not using other gradients and the errors in Tzz were correspondingly scaled.

Mr. M. Molny (Sperry) - Why not put in a wider grid spacing for the outside areas?

Dr. Heller - That's a good introduction to the next talk!

Dr. Jordan - Is the downward continuation to the physical surface or to a reference surface?

Dr. Heller - This has to be resolved. We don't want to continue the data below the surface. For convenience we chose the physical surface.

Dr. Jordan - I don't believe we can meet the goals of the program using the physical surface as a reference. We can't downward continue in a mountainous area.

Benson, Jordan, and Heller further dicussed the choice of the reference surface.

Dr. H. Baussus von Luetzow (ETL) - We need to consider the shortcomings of least squares collocation at high frequencies (the use of stationary models could introduce errors of 10-20%). No terrain effects have to be considered.

Dr. Heller - We plan to survey over smooth areas to test and demonstrate the gradiometer and should be able to handle mountainous terrain in the future.

Mr. M. Trageser - Why do we need to downward continue at all? Why not estimate gravity at altitude?

Dr. Heller - We want point estimates at the surface.

There was further discussion on this question between Heller, Trageser, and Martin.

Tuesday Afternoon Session

Efficient Processing of Gradiometer Output Using a Kalman Filter - Dr. J. Hutcheson (Bell Aerospace Textron)

Dr. Hutcheson made several points concerning the processing of the data to be collected by the gravity gradiometer system. First, there are just too many data points; they must be compressed. He presented a method to process gradient data using a straight line Kalman filter. Dr. Hutcheson showed comparisons of the STAG model and state space approximations. He compared results of fixed point smoothing and least squares collocation. Results were simulated using a MASCON synthetic gravity field.

Questions:
Unidentified questioner - What wavelengths were modeled with the MASCON model?

Dr. Hutcheson - The North Atlantic Gravity Model was used. The wavelengths are possibly classified.

Dr. C. Jekeli (AFGL) - When using the straight line filter, are correlations from track to track taken into account?

Dr. Hutcheson - Two dimensional correlations are taken into account in a subsequent stage of processing.

Mr. P. Ugincius (NSWC) - What about estimating away from the track?

Dr. Hutcheson - One can always contract the estimation point to the nearest grid point.

On-going Work in Post Mission Data Processing Algorithm Development - Dr. W. Heller (TASC)

Dr. Heller presented some background information on the GGSS program and described what will be required for post mission analysis of the data collected. He discussed various survey and data processing issues as well as prefilter design considerations. On this topic Dr. Heller concludes that a 12 second filter time constant will be needed. On the topic of estimation approaches to the gravity disturbance vector, Dr. Heller proposed two alternatives:

a) a sequential complementary filter.
b) an optimized template algorithm.

Numerical data showing applications of these alternatives were presented. Dr. Heller summarized by stating that on-going development is not a neat "packaged deal" but an active process. He then proceeded to outline the development of the algorithms.

Questions:
Mr. Zorn - How sensitive is the estimation if the aircraft is not able to follow the regular grid?

Dr. Heller - The system noise includes navigation error. If the navigation error becomes too great, we may cease data collection.

Dr. S. Hammer - How did you simulate the test data?

Dr. Heller - With ocean trench data by computing gradients which were reinverted creating an anomaly field.

Mr. Molny - What is the actual mapping area?

Dr. Heller - 320 X 320 kilometers.

Mr. Borgeson - There are two test sites. Central Florida and Cheyenne, Wyoming, are being considered based on weather data and available gravity

data.

Mr. Molny - When condensing data, averaging, etc., do you consider the survey design?

Dr. Heller - We must make sure the data are regular.

Mr. Molny - One could enlarge the size of the square by having larger track intervals in the outside areas to pick up larger wavelength information.

Dr. Heller - We may do this for the test if we are interested only in gravity estimates in the inner zone.

Ugincius, Hutcheson, Fell, Zorn, Benson, and Heller discussed use of the template method.

Three-axis Super Conducting Gravity Gradiometer - Dr. H.J. Paik (University of Maryland)

Dr. Paik opened his presentation with a review of his program to develop a single axis version of a cryogenic gravity gradiometer. Dr. Paik then went on to describe plans to develop a three-axis superconducting gravity gradiometer. He elaborated mathematically on the expected sensitivity of the instrument and explained its physical design with slides and viewgraphs. Dr. Paik described the new pendulum suspension and error compensation. For adequate error compensation Dr. Paik proposed the development of a six-axis superconducting accelerometer and described in detail its configuration, design features, and sensitivity as well as its operation with a gradiometer. He concluded with a proposed time line for the development of both a three-axis GGM and a six-axis accelerometer. His ultimate aspirations include space born testing of the GGM in an earth orbit aboard the space shuttle by the year 1990.

Questions:

Dr. Heller - At what time will an eror of 10^{-1} E/$(Hz)^{1/2}$ be demonstrated?

Dr. Paik - This is difficult to predict. We may have to do temperature control experiments to get rid of squid noise. We had hoped to have had data 2 years ago, but we need to improve the platform. With a little confidence and if the platform is OK, maybe next week. We are trying to get better noise levels in the platform. Maybe next year.

Mr. Hastings (Sperry) - If you were to add proportional feed back, would it improve the accuracy?

Dr. Paik - This would not improve the accuracy. It would increase the dynamic range.

Dr. Jordan - GRM will get 100 km resolution at a cost of 1/3 billion dollars. Would you care to comment on the resolution and cost of the satellite gradiometer?

Dr. Paik - For 10^{-2} E sensitivity we get 100 km resolution. To improve

the resolution by a factor of two we need to improve the gradiometer by a factor of 100.

Overview of Airborne Gravity and Comparison of Gravity and Gradient Anomalies - Dr. S. Hammer (University of Wisconsin)
Dr. Hammer introduced his topic with a very brief history of gravity measurements in a moving vehicle and a description of the Carson Helicopter Gravity Measuring System (HGMS). HGMS has been operational for about four years and observes an average of 5000 km of line data per month with a probable error of the order of 1 mgal and anomaly resolution limit of about 3 km. Survey altitude, as specified, can vary from low terrain clearance up to about 14,000 ft (4300 m) above sea level and over any type of terrain including environmentally restricted areas such as the Wildlife Reserve in Alaska. In his presentation Dr. Hammer compared the magnitudes and rates of attenuation with altitude of gradient and gravity anomalies. He emphasized that the rate of attenuation of all components of the gravity gradient is the same for a given type of anomaly. The gradient attenuates with altitude an order of magnitude faster than the corresponding gravity anomaly. In conclusion Dr. Hammer raised the question: to accomplish the basic objectives of this conference, what is the best way to proceed? (a) Concentrate efforts on the development of theory and instrumentation for gravity gradiometry; or (b) Undertake a world-wide gravity mapping program with the rapid and precise HGMS which is now available.

Questions: (deferred to Mr. W. Gumert of Carson Geoscience)
Mr. Borgeson - Did you have any problems with civil air traffic?

Mr. Gumert - There were no problems, as long as we filed a flight plan and flew low.

Dr. Heller - How far out to sea did you fly?

Mr. Gumert - 160-180 km using line of sight radar.

Mr. Molny - How do you separate vertical acceleration from gravity anomalies?

Dr. Hammer - Using barometric and radar altimeters.

Wednesday Morning Session

(Due to unexpected circumstances, the order of presentation as shown on the agenda was slightly rearranged.)

A Simplification of the Least Squares Determination of the Gravity Field from Low-low Satellite Tracking Data Utilizing An Operator Representation of the Range Observable - Dr. V. Reinhardt (Bendix Field Engineering Corporation)
Dr. Reinhardt introduced his paper by explaining that one of the purposes of NASA/Goddard Space Flight Center's proposed Geopotential Research Mission is to map the gravity field of the Earth to 1-2 mgal in 41,253 1 degree by 1 degree blocks using range rate tracking data between two

polar low orbiting satellites in the same orbit. Because there are 41,253 blocks in the gravity map, it takes, in general, at least 9.4×10^{13} real floating point operations (flop) to solve the least squares fit (LSQF) matrix equation used to determine the gravity potential from the tracking data. Dr. Reinhardt showed that with the circular orbit infinite trajectory length approximation, and an iterative method, one obtains an approximate covariance matrix for the coefficients in less than 1.5×10^{12} flop. In his presentation Dr. Reinhardt also demonstrated the application of this method to airborne gradiometry.

WGS Gravity Gradient Reference Ellipsoid and Earth Gravitational Model - Mr. M. May (NADC)
Mr. May described the gravity gradient ellipsoid in terms of geographic latitude using WGS-72 reference ellipsoid parameters. Additionally, he described a representation of earth's gravity gradients by a Fourier series for wavelengths down to 120 nautical miles.

Questions:
Dr. Hammer - What wavelength ranges were used?

Mr. May - 180 X 180 degree field which corresponds to wavelengths down to 120 nautical miles.

Dr. Heller - Comment: for stochastic modeling, models have been determined for the degree variances of the gravity field.

Dr. Jekeli - What is the advantage of using gradient maps over gravity maps?

Mr. May - It is advantageous to mix data for vertical deflection determination at the instrument (gradient) level.

Re-looking at MASCONS for Representing Gravity Survey Data - Dr. J. Breakwell (Stanford University)
Dr. Breakwell introduced his presentation with the statement that the representation of the higher harmonic part of the Earth's gravity field by a finite grid of MASCONS in two layers, one at the Earth's surface and one at the bottom of the Earth's crust, leads to an error in the gravity components at altitude (in addition to the error from the estimation of density fluctuations in the two layers). His discussion examined these errors for various ratios of grid size to gradiometer altitude.

Integral Formulas Relating Gravity Gradients to Vertical Deflections - Mr. A. Zorn (Dynamics Research Corporation)
Mr. Zorn presented a number of integral formulas relating gravity gradients to vertical deflections. The formulas are derived from standard geodesy theory and are similar to the Stokes and Vening-Meinesz integral formulas. He explained that the deterministic formulas provide a physical explanation of certain properties common to various self-consistent stochastic gravity models. For example, the high degree of correlation between the gravity gradient, Txz, and the vertical deflection Tx, in most gravity models can be physically justified based on a deterministic

integral formula. The integral formulas may lead to insight into the construction of gradiometer filters to estimate vertical deflections which are insensitive to stochastic gravity models. Mr. Zorn discussed implementation considerations involving discretization and truncation of the integral formulas using surface gravity data over the Blake Escarpment. He concluded with several statements including that vertical deflection maps can be constructed from gradiometer survey data using Stokes' formula.

Questions:

Mr. Ugincius - Going from Tzz one can get any other gradient quantity. Why measure these other components?

Mr. Zorn - To get other components we need Tzz over the entire earth's surface. We therefore measure the other components to get more information especially in limited areas.

Mr. Ugincius - Would the tree diagram hold for spherical formulations?

Mr. Zorn - Yes

Dr. D. DeBra (Stanford University) - Are some paths more sensitive?

Mr. Zorn indicated on his diagram certain paths that would be affected by low frequency errors.

Mr. May - The tree diagram can be derived from spherical harmonic expansion. Is there distinction between gravity anomaly and gravity disturbance?

Mr. Zorn - The difference is negligible.

Mr. A. Rufty (NSWC) - If we have gradient information only, we need integration constants to get gravity quantities.

Zorn - We would need low frequency information to obtain the constant of integration.

Real-Time Vertical Deflection Estimation Using Gradient Data -
Dr. W. Feldman (Sperry; Co-author, Mr. B. Epstein)
Dr. Feldman discussed techniques and algorithms for making real-time estimates of vertical deflections from gravity gradient measurements. First he outlined the techniques and algorithms used to condition sensor data for effects of high-frequency noise, pressure sensitivity, self-gradients, bias/trend, and carouselling. He then showed plots of typical gradient data before and after preprocessing to illustrate the effectiveness of the preprocessing. Second, a batch filter formulation for estimating deflections from gradient and SEASAT map data was illustrated. Finally, Dr. Feldman demonstrated filter results by plots of filter estimates of vertical deflection vs. reference values for several ship tracks.

Questions:
Dr. Heller - Why pull out the reference field in the instrument frame

rather than in the NED frame?

Dr. Feldman - It is equivalent.

Dr. Heller - What are the practical considerations?

Dr. Feldman - It was simpler to do in the instrument frame and there was less chance of error.

Gravity Gradiometer Application to Tunnel Detection - Mr. Jircitano (Bell)
Mr. Jircitano described a project being conducted by the Army in the field of tunnel detection by means of measuring differences in gravity gradients. There are two tunnel detection problems: 1) the detection of new tunnels (those which had been dug after a previous survey of the area) 2) the detection of old tunels (those that were present before any previous survey).

Questions:
Dr. Reinhardt - What is the feasibility of tunnel detection if they were masked by high density fill?

Mr. Jircitano - The possibility exists but to compensate one would have to half fill the tunnel with steel which is impractical.

Dr. DeBra - Seasonal groundwater has a significant mass. Is this a problem for new tunnel detection?

Mr. Jircitano - Could be, but water would not collect in a tunnel formation.

Closing Remarks - Lt. D. Warner
Lt. Warner thanked everyone for attending this year's conference, especially those who presented papers. She also offered a special thanks to her AFGL colleagues who helped with audio/visual equipment and note taking. As a date for next year's conference had not yet been established, she assured all that they would be informed of the date as soon as it was reserved.

CONFERENCE ATTENDEES

TWELFTH ANNUAL MOVING BASE GRAVITY GRADIOMETER REVIEW

14, 15 February 1984

AFFLECK, C.	Bell
ANDERLE, R.	NSWC
BAUSSUS von Luetzow, H.	ETL-RI
BENSON, D.	Dynamics Research Corporation
BERNSTEIN, R.	Navy
BLANTON, J.	NSWC
BODIFORD, L.	SSPO, Navy
BORGESON, R.	AFGL
BRADLEY, L.	Geospace
BREAKWELL, J.	Stanford University
BROZENA, J.	NRL
CHATFIELD, A.	Geodynamics
CONFER, M.	CIGTF
DEBRA, D.	Stanford University
DECKER, L.	DMAAC
DELGADO, L.	HQAFSC
DEMATTEO, J.	NADC
DOWNS, H.	CIGTF
ECKHARDT, D.	AFGL
FELDMAN, W.	Sperry Systems Management
FELL, P.	DMAHTC
FLEETWOOD, J.	Mobil
FRANSON, J.	Johns Hopkins University
FUNDAK, T.	AFGL
GOLDSBOROUGH, R.	AFGL
GOUKER, R.	DMAHTC
GRAHAM, J.	DMAAC
GSCHWIND, J.	DMAHTC
GUMERT, W.	Carson Geoscience
HADFIELD, M.	Honeywell
HAMMER, S.	University of Wisconsin
HARRIMAN, D.	Geodynamics
HASTINGS, R.	Sperry Management Systems, U2T20
HEACOCK, J.	ONR
HELLER, W.	TASC
HOWLAND, J.	Johns Hopkins University

HUTCHESON, J.	Bell
JEKELI, C.	AFGL
JIRCITANO, A.	Bell
JORDAN, S.	Geospace
KOWALSKI, M.	SOHIO
KURKOWSKI, J.	DMAHTC
LAZAREWICZ, A.	AFGL
LIST, R.	Sperry Systems Management
LUCAS, S.	Carson Geoscience
LUMAN, R.	Johns Hopkins University
MARTIN, C.	DMA
MAY, M.	NADC
MAYO, W.	DMAHTC
MERTZ, B.	DMAHTC
METZGER, E.	Bell
MOLNY, M.	Sperry Systems Management
NAVAZIO, F.	Carson Geoscience
PAIK, H.J.	University of Maryland
PFEIFER, L.	DMAHTC
PFOHL, L.	Bell
PINSON, E.	DMAHTC
PRICE, C.	TASC
REGANAUER, B.	Dynamics Research Corporation
REINHARDT, V.	Bendix
ROONEY, T.	AFGL
RUFTY,A.	NSWC
RUTSCHEIDT, E.	DMA
RYCHEL, J.	NSWC
SENUS, W.	DMA
SHAW, C.	USAFA
SHULTZ, M.	DMAAC
SIMMS, T.	NSWC
SUMNER, D.	Sperry Systems Management
TANG, W.	TASC
TRAGESER, M.	C.S. Draper
UGINCIUS, P.	NSWC
WARNER, D.	AFGL
WIRTANEN, T.	AFGL
ZERZAN, J.	SOHIO
ZORN, A.	Dynamics Research Corporation

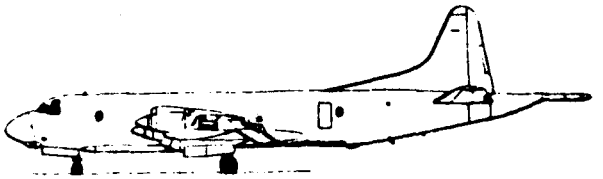

GRAVITY GRADIOMETER SURVEY SYSTEM (GGSS) PROGRAM

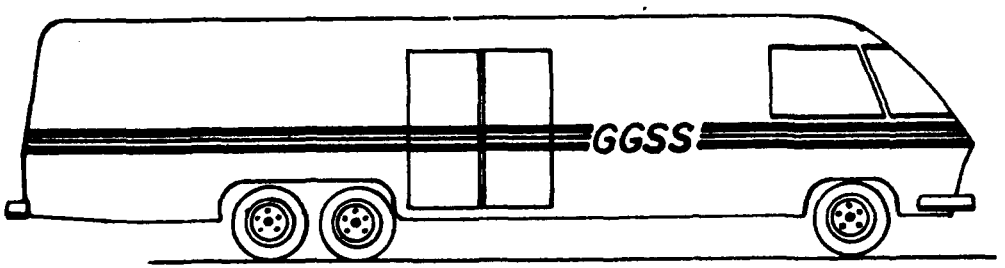

AIRBORNE GRAVITY GRADIOMETRY

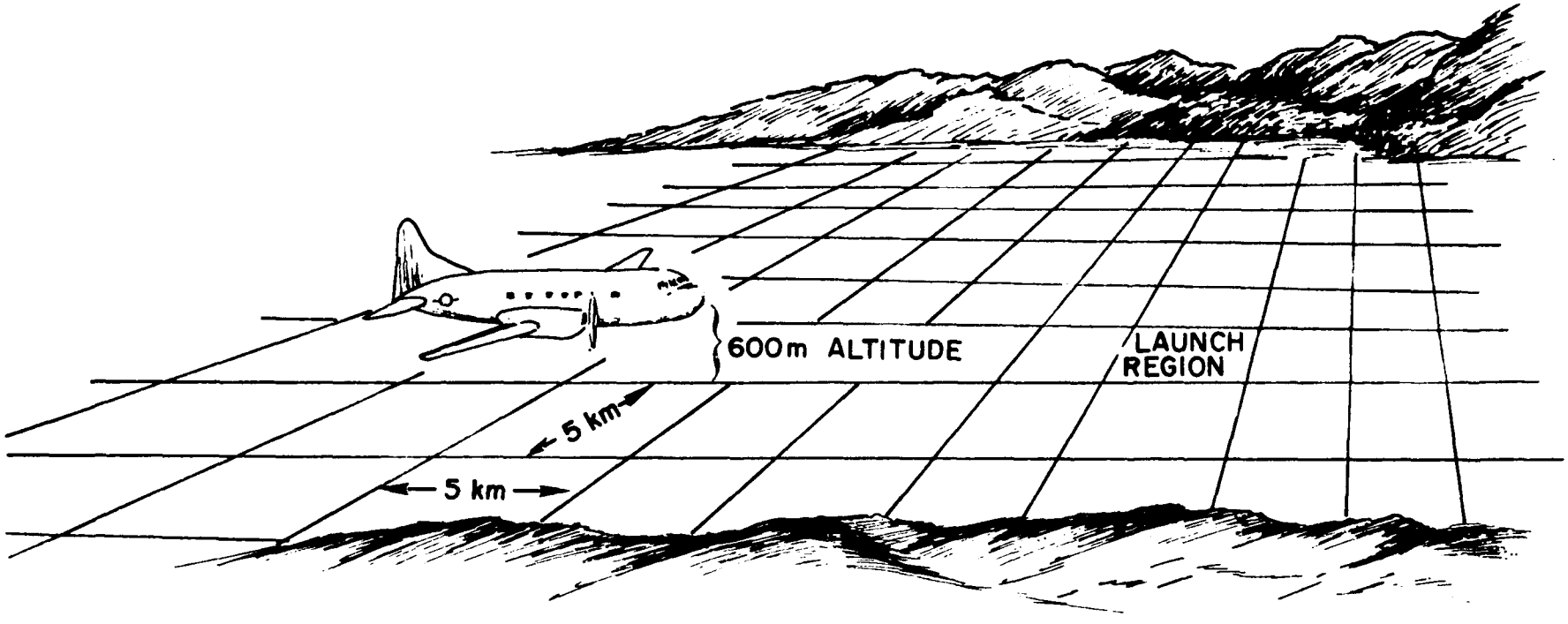

GRID SPACING, ALTITUDE AND SPEED OPTIMIZED FOR GEOGRAPHY, ACCURACY, ETC.

GGSS

ACCURACY REQUIREMENTS

- RMS FOR SPATIAL FREQUENCIES > 0.002 CYCLES/KM
- DEFLECTION OF THE VERTICAL - 0.18 ARC SEC RMS
- GRAVITY DISTURBANCE VECTOR - 0.90 MGAL RMS

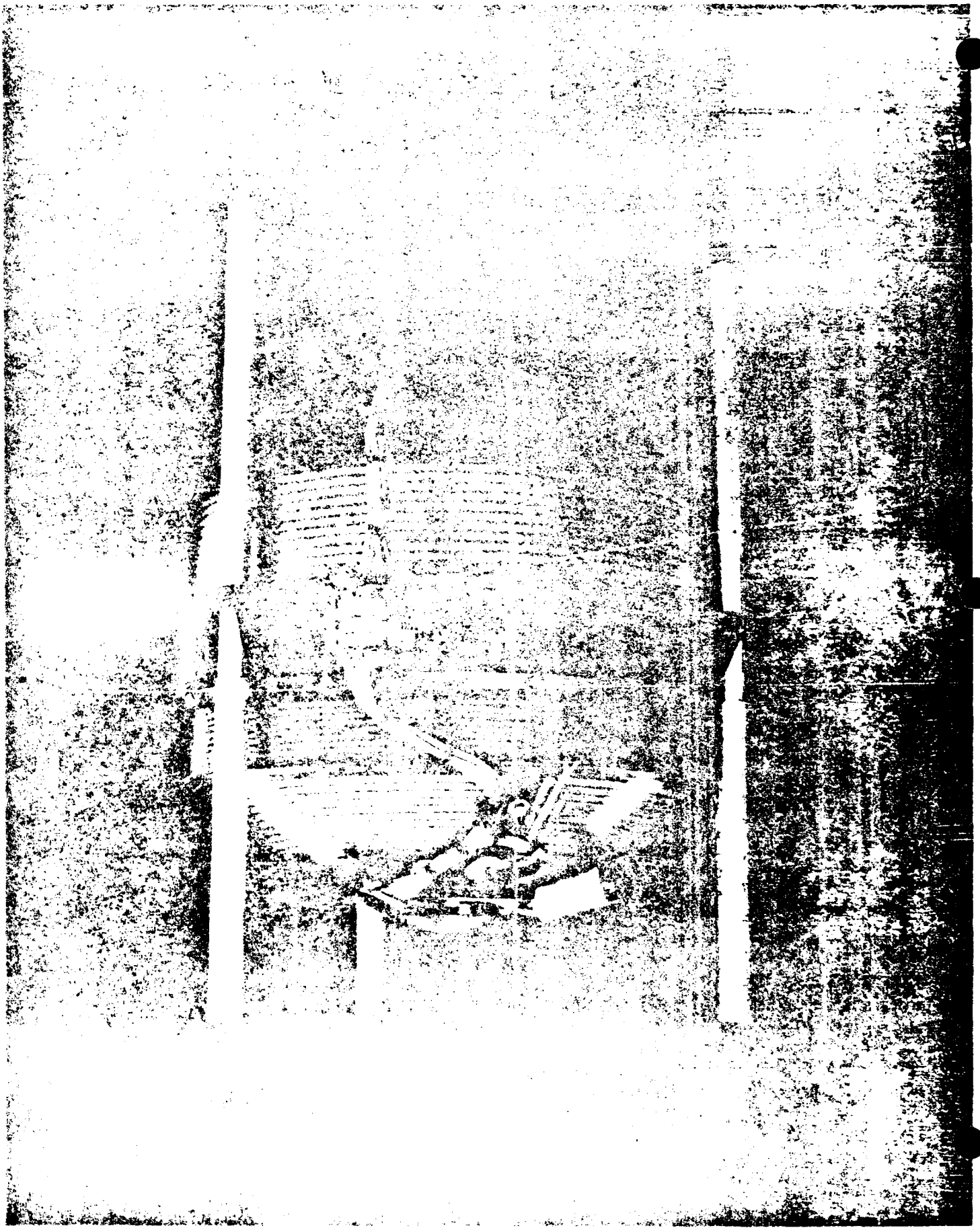

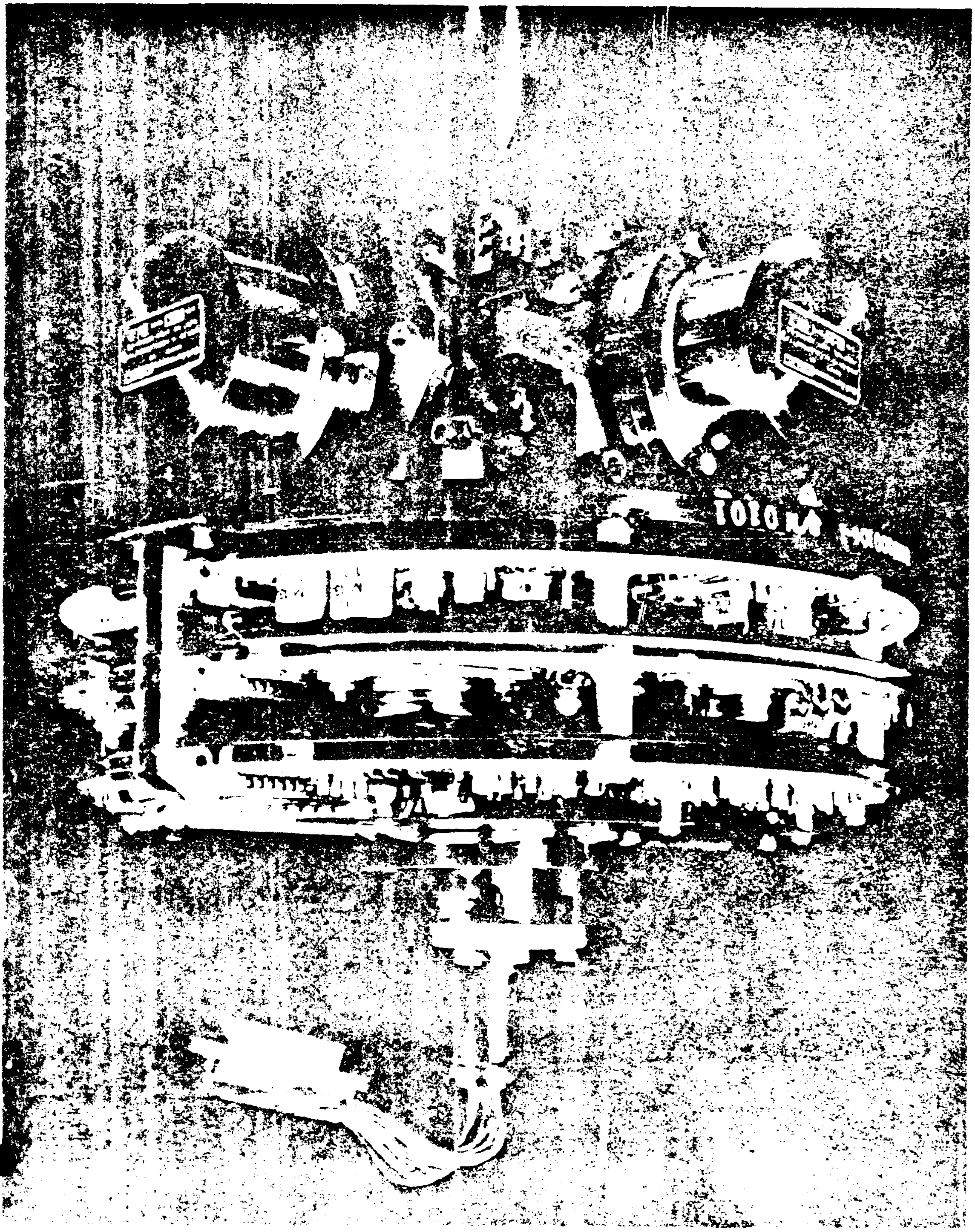

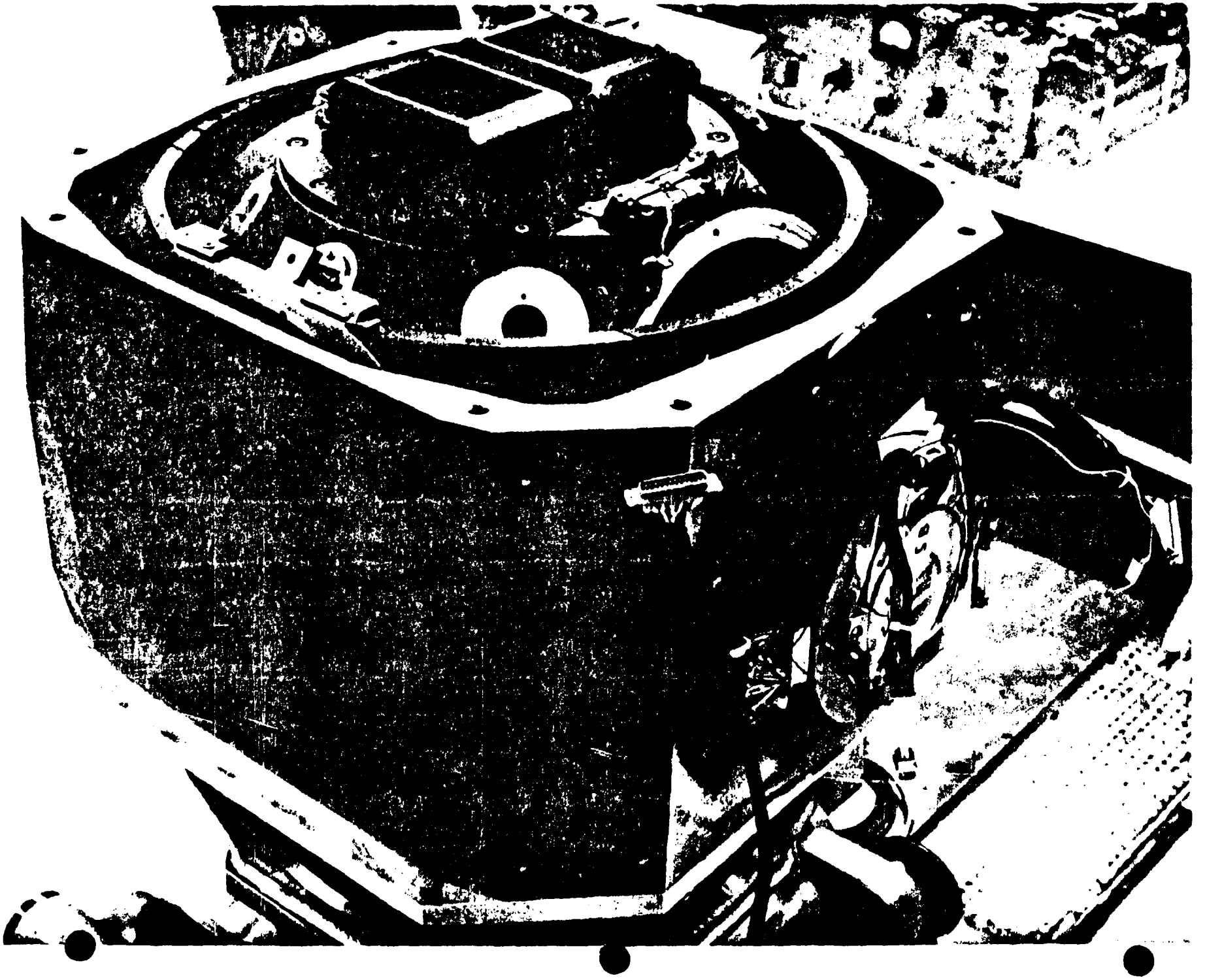

LAND VEHICLE INSTALLATION

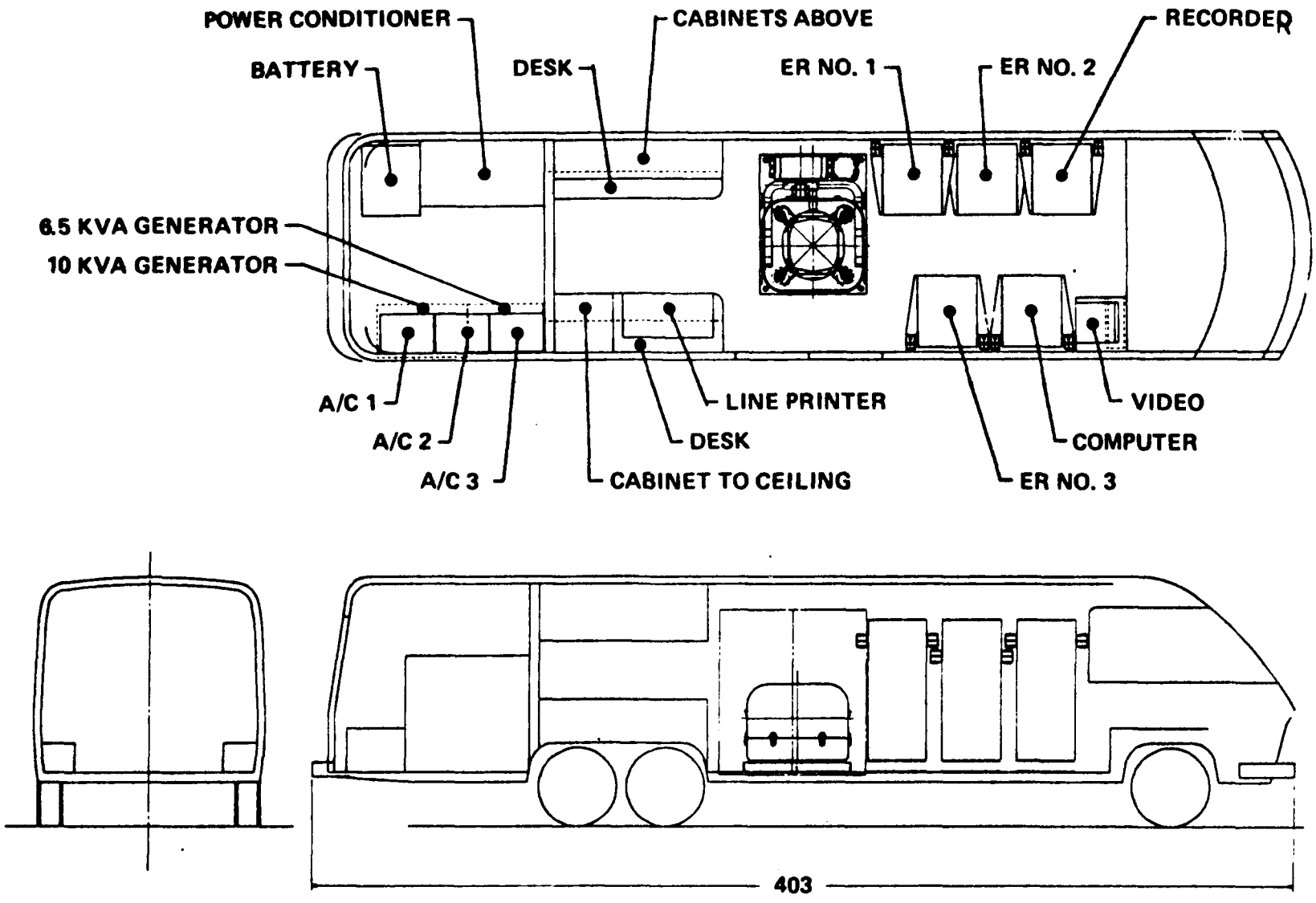

P-3 INSTALLATION

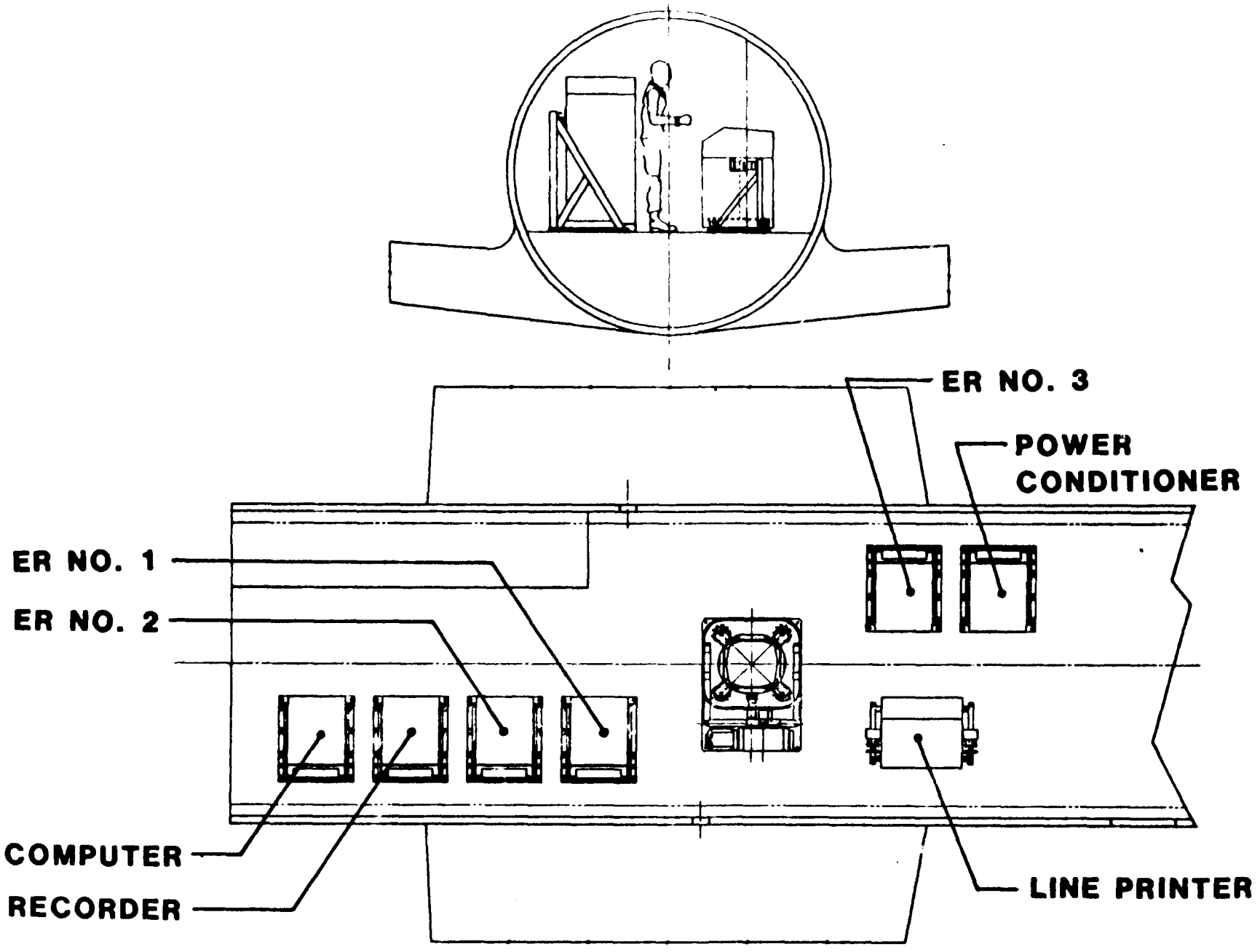

Bell Aerospace TEXTRON

GGSS PROGRAM MILESTONES

⬆ CONTRACT AWARD	FEB 83
⬆ SRR	MAY 83
⬆ PDR	AUG 83
⬆ CDR	NOV 83
⇧ CDR (FINAL)	MAR 84
⇧ SYSTEM INTEGRATION	FEB 85
⇧ LAB TESTS	SEP 85
⇧ LAND SYSTEM TESTS	MAY 86
⇧ AIRBORNE SYSTEM TESTS	SEP 86
⇧ DELIVERY	NOV 86

PROGRAM SCHEDULE

GRAVITY GRADIOMETER SURVEY SYSTEM

LINE	PROGRAM MILESTONES	PRIOR SCHED		FISCAL YEAR 1983												FISCAL YEAR 1984												FY 1985				FY 1986				FY 1987				COMPL DATE	
		MO	YR	O	N	D	J	F	M	A	M	J	J	A	S	O	N	D	J	F	M	A	M	J	J	A	S	1	2	3	4	1	2	3	4	1	2	3	4	QTR	FY
1	CONTRACT AWARD							▲																																	
2																																									
3	SRR									▲																																
4																																									
5	PDR													▲																												
6																																									
7	CDR															▲																										
8																																									
9	CDR (FINAL)																				⇧																				
10																																									
11	SYSTEM INTEGRATION																											⇧													
12																																									
13	LAB TESTS																														⇧										
14																																									
15	LAND VEHICLE TESTS																																⇧								
16																																									
17	AIRBORNE TESTS																																	⇧							
18																																									
19	DELIVERY																																	⇧							

MOVING BASE GRAVITY GRADIOMETER REVIEW

AIR FORCE ACADEMY

REPORT NO. 6501-927024

FEBRUARY 14-15, 1984

Bell Aerospace TEXTRON
Division of Textron Inc.

POST OFFICE BOX ONE • BUFFALO, NEW YORK 14240

KEY MILESTONES FOR 1983

- Conducted GSS Studies Toward Operation System Under Sperry Management for SP 24
- Continued Good Operation of GSS ADM System Aboard USNS Vanguard
- Received GGSS Program Award from AFGL under DMA Funding - April 1983
- Placed GSS ADM No. 2 into Operation at Bell - August 1983
- Implemented GGI Platform Perturbation Calibration Technique - May 1983
- Verified Operation of Two Experimental GGIs on Vanguard - September 1983
- Received GSS OSDP Purchase Order from Sperry for SP24 - October 1983

ADM GSS

GSS ADM PLATFORM AND GGI BEING INSTALLED ON THE USNS VANGUARD

GSS ADM ELECTRONIC CABINETS INSTALLED ON THE USNS VANGUARD

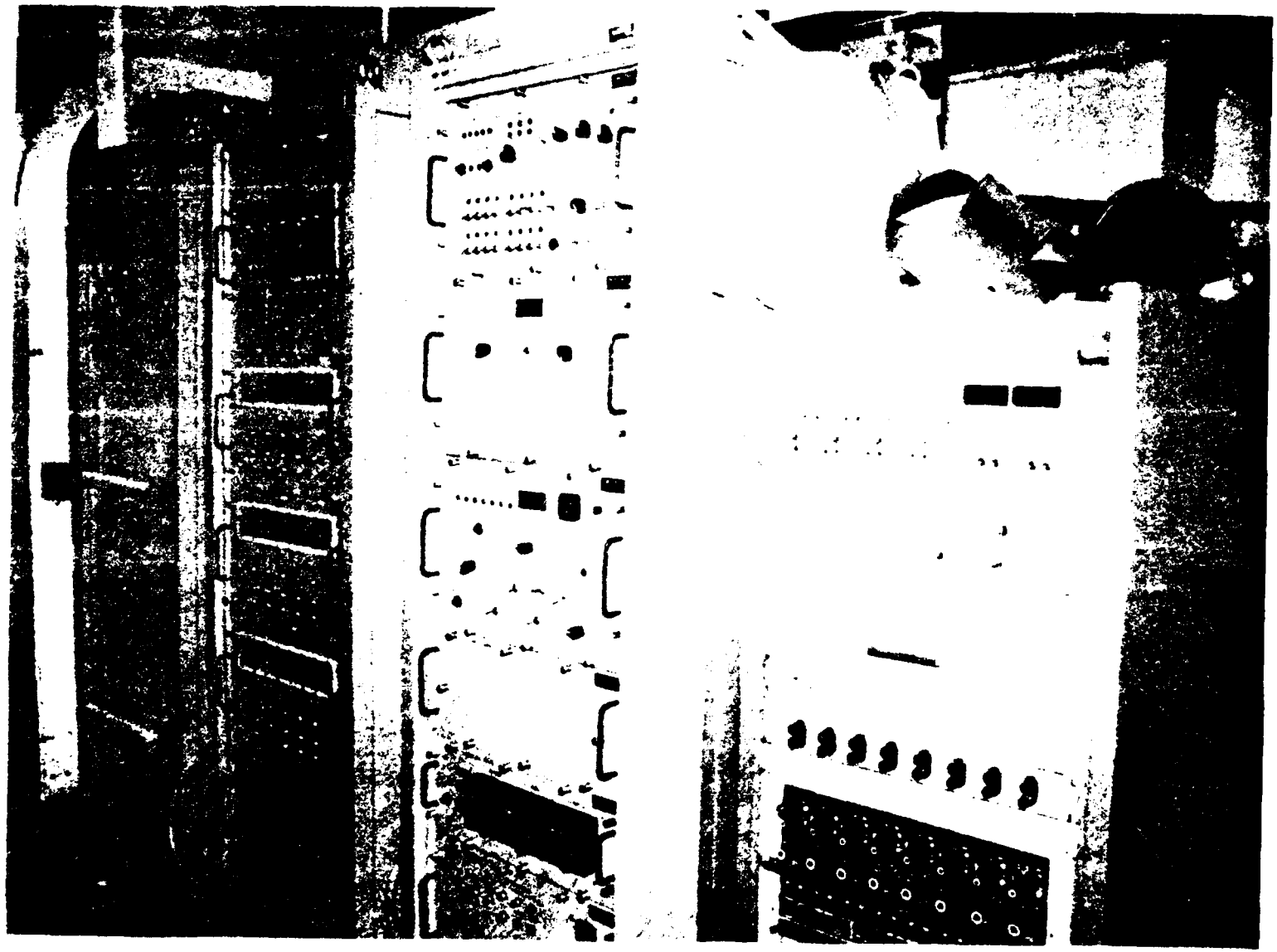

PLATFORM CUTAWAY DRAWING

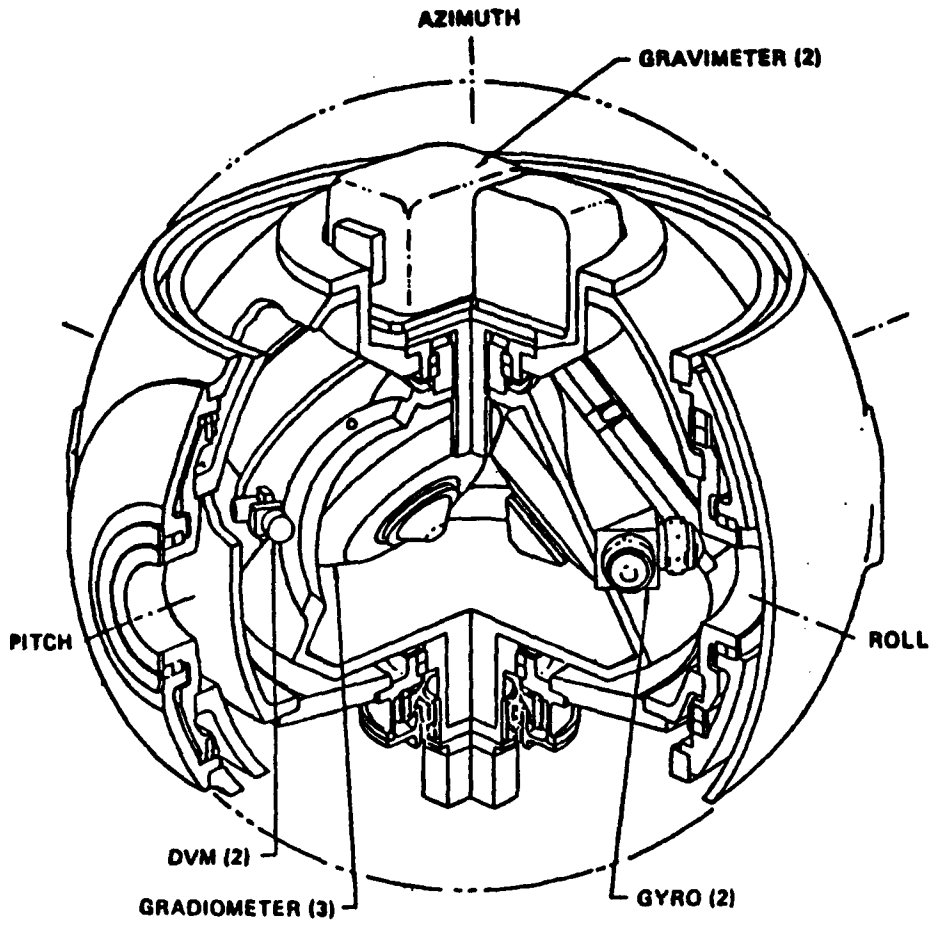

GSS ADM NO. 1 EXPERIENCE ONBOARD USNS VANGUARD

- In Continuous Operation Since February 1982
- 16,500 Hours of Operation
- Completed 34 Cruises (Generally Two Weeks at Sea and 10 Days in Port)
- Fewer Failures then Predicted by Theoretical MTBF Analysis
- No GGI Failures
- Carouseling (500 O/hr) Confirmed as Prime Operating Mode
- Implemented Perturbation Technique for Dockside GGI Calibration
- Two Experimental GGIs Tested at Sea to Evaluate Modifications for Operation System
- Performance Met Feasibility Requirements in all Tests
    - Low Frequency Performance as Expected
    - High Frequency Performance Degraded by Ship Motion

GSS ADM NO. 1 FAILURE HISTORY

	Comment
- (1) Synchro to Digital Converter	Random Failure
- One (1) G 1200 Gyro	Bearing Failure
- One (1) Back Plane Wire Short	Contamination
- Four (4) Blower Fans	Wrong Component for Application
- Power Supply	Taken Out by Fan Failure
- Azimuth Gimbal Stiction	Motor and Bearing Contamination Design Deficiencies

GSS ADM NO. 2

OBJECTIVE: Provide Test Bed for Verifying Modifications Considered for Operational Systems Systems

STATUS: Placed into Operation - September 1983

Transferred GGI Compensation Constants from Hardware to Software

Gravity Sensor Platform Can Operate With G-7 Gyros as Well as G1200

Confirmed that GSP Grounding Method is Far from Optimum.

Grounding Improvements are Being Explored

Confirmed that Considerable Circuit Goupling Occurs in GSP Wire Harnesses. Requirements for Additional Shielded Twisted Pairs are Being Explored.

FUTURE PLANS: Verify Performance of GSS OS Operating Modes

Verify Performance of GSS OS Calibration Modes

Explore Start Up at Sea Procedures

Systems Test with Various GGIs Configurations

Check Out of Critical Maintainability/Testability Features

GGSS

GRAVITY GRADIOMETER SURVEY SYSTEM

GGSS OBJECTIVE

Measure Elements of Gravity Gradient Tensor Onboard Aircraft or Landvehicle and Determine Gravity Disturbance Vector by Postmission Smoothing Analysis Under Following Conditions.

	Aircraft	Landvehicle
Speed (KM/HR)	300	30 to 90
Maximum Wavelength (KM)	500	NA
Maximum Track Length (KM)	NA	200 KM
Altitude Above Terrain (M)	600	0
Track Spacing (KM)	5	NA
Deflection Survey Accuracy (Arc Sec)	0.18	0.18
Vertical Component Accuracy (mgal)	0.9	0.9

GGSS SUMMARY ERROR ANALYSIS

STANDARD TWO DIMENSIONAL SURVEY ANALYSIS CONDITIONS

GGI Red Noise (A)	10^{-5} E^2 x Rad/Sec
GGI White Noise (B)	51 E^2/Rad/Sec
Aircraft Velocity (V_A)	300 Km/Hr
Aircraft Altitude (H_A)	600 M
Track Spacing	5 Km

SUMMARY ERROR ANALYSIS

	DISTURBING PSD	GGSS SPECIFICATION		BELL GOAL	
		SENSITIVITY	PSD CONT. E^2/RAD/SEC	SENSITIVITY	PSD CONT E^2/RAD/SEC
GGI SELF NOISE					
RED	–	–	$\frac{10^{-5}}{\omega^2}$		$\frac{10^{-5}}{\omega^2}$
WHITE	–	–	25		5
LINEAR ACCELERATIONS					
1R	10^{-4} g^2/RAD/SEC	1000 E/g	100	200 E/g	20
2R	3×10^{-5} g^2/RAD/SEC	1000 E/g	30	200 E/g	6
3R	10^{-5} g^2/RAD/SEC	1000 E/g	10	200 E/g	2
LINEAR ACCELERATION (DC)	10^{-4} g^2/RAD/SEC	400 E/g	16	100 E/g	1
SELF GRADUAL RESIDUAL	$\frac{0.035 \text{ (RAD}^2\text{/RAD/SEC}}{1+\left(\frac{\omega_0}{0.0013}\right)^2}$	8 E/RAD	2	8 E/RAD	2
3° ω_0 = 0.0013 RAD/SEC					
NAVIGATION ERROR	$\frac{1.9 \times 10^6 \text{ M}^2\text{/RAD/SEC}}{1+\left(\frac{\omega_0}{0.0013}\right)^2}$	7×10^{-4} E/M	1	7×10^{-4} E/M	1
50 M, 7×10^{-4} E/M, ω_0 = 0.0013 RAD/SEC					
MAGNETIC			NEGLIGIBLE		NEGLIGIBLE
JITTER			184		37
TEMPERATURE			0.87		0.50
Γ_Z MGAL			0.63		0.35
Γ_X AND Γ_Y MGAL					

RESIDUAL GRAVITY DISTURBANCE AS FUNCTION OF GGI WHITE NOISE (B)

V_A = 300 KM/HR

H_A = 600M

TRACK SPACING 5 KM

GGI NOISE

WHITE (B) = 51 E^2/RAD/SEC

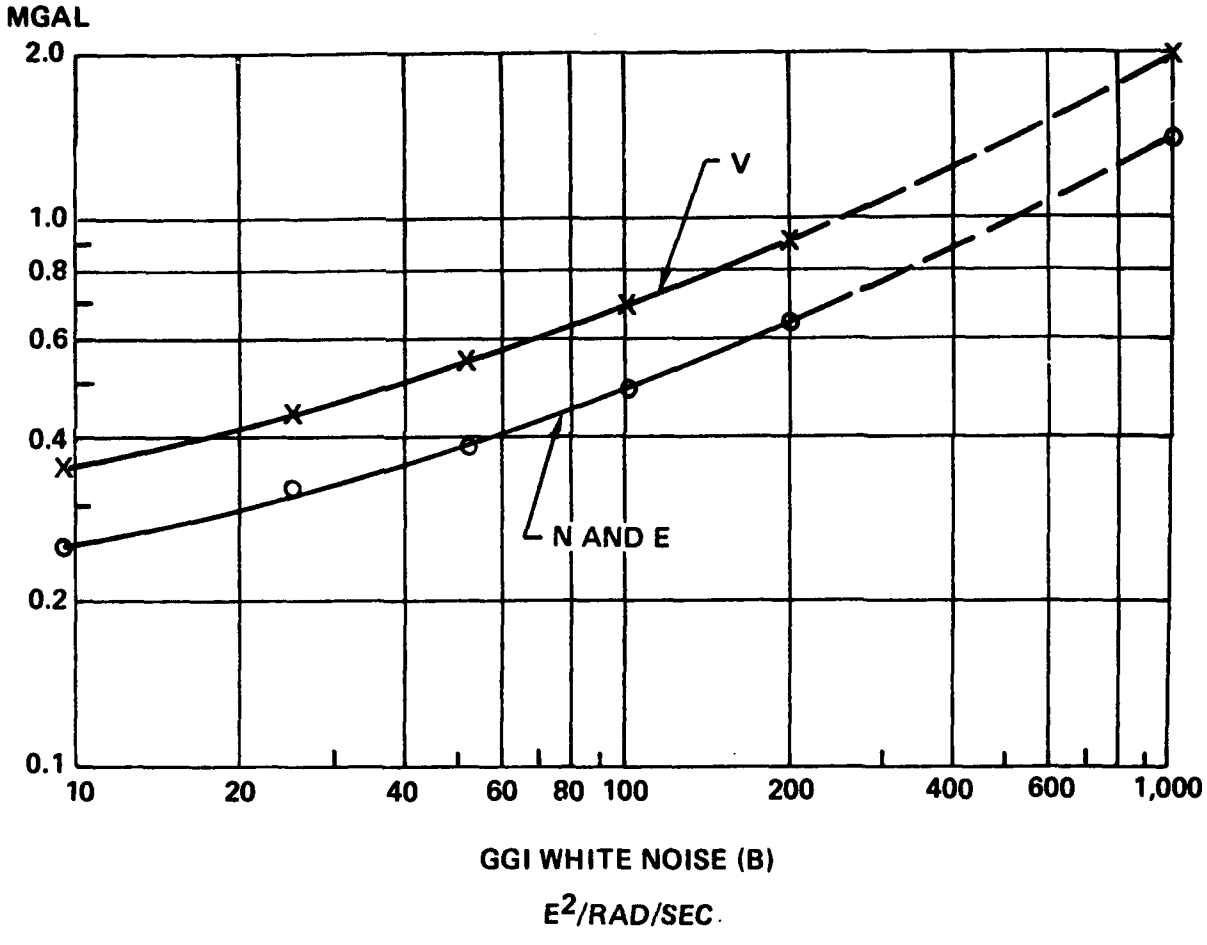

RESIDUAL GRAVITY DISTURBANCE AS FUNCTION OF AIRCRAFT VELOCITY

H_A = 600M

GGI NOISE

RED (A) = 10^{-5} x E^2 RAD/SEC

WHITE (B) = 51 E^2/RAD/SEC

TRACK SPACING = 5 KM

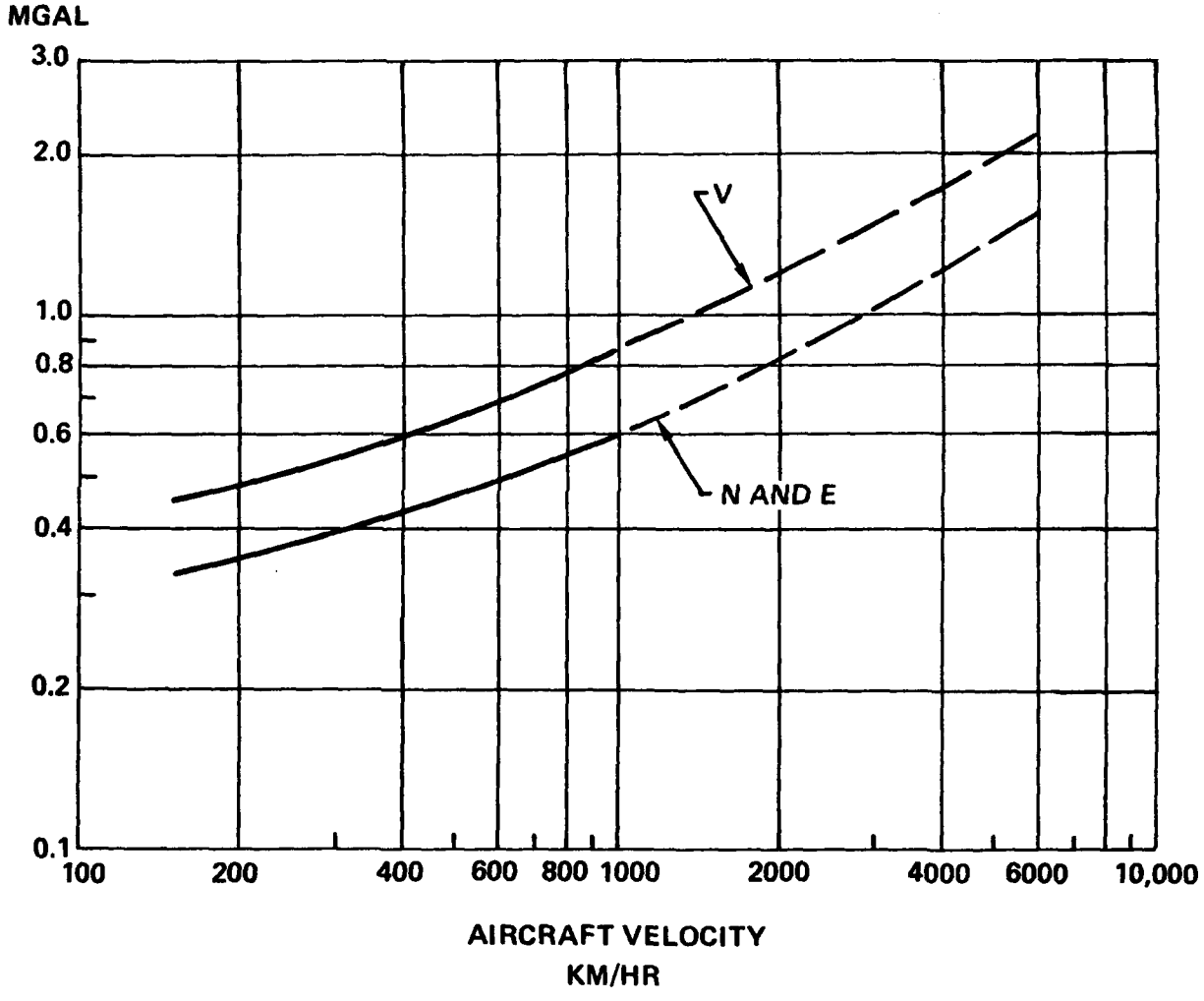

RESIDUAL GRAVITY DISTURBANCE AS FUNCTION OF AIRCRAFT ALTITUDE

V_A = 300 KM/HR

GGI NOISE

WHITE (B) = 51 E^2/RAD/SEC

RED (A) = 10^{-5} E^2/RAD/SEC

TRACK SPACING 5 KM

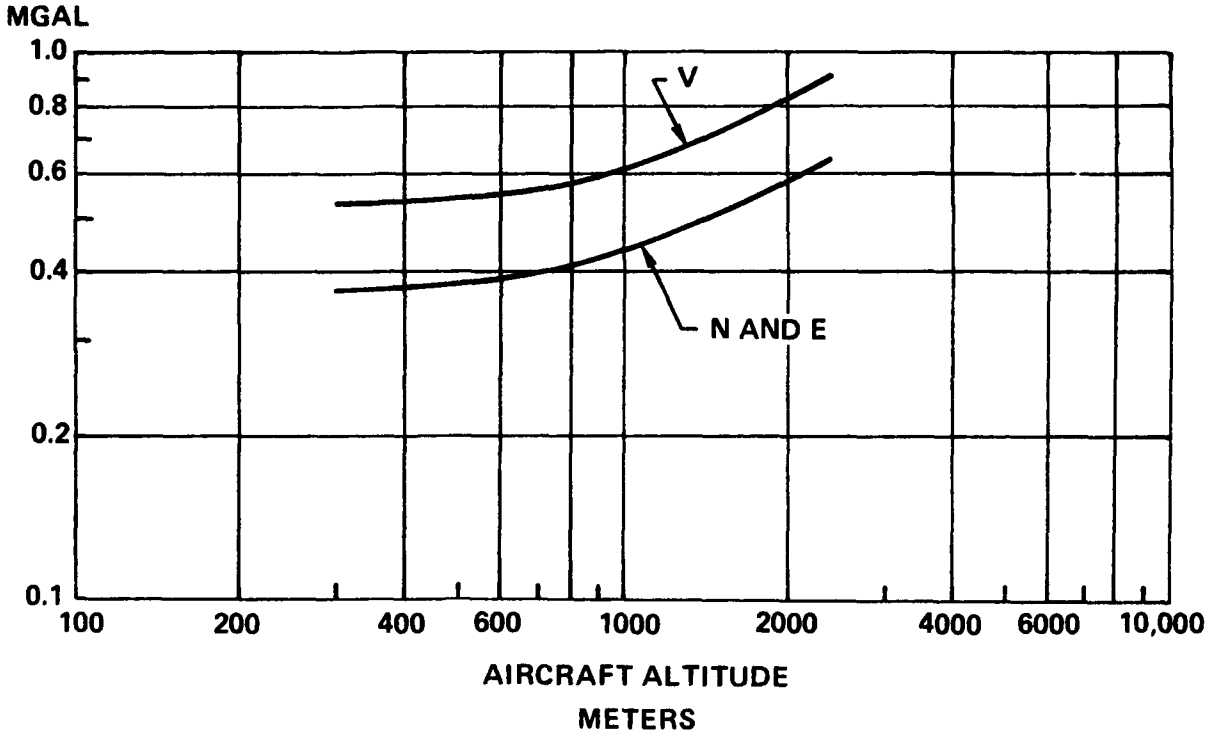

RESIDUAL GRAVITY DISTURBANCE AS FUNCTION OF TRACK SPACING

V_A = 300 KM/HR

H_A = 600M

GGI NOISE

RED (A) = $10^{-5}E^2$ x RAD/SEC

WHITE (B) = 51 E^2/RAD/SEC

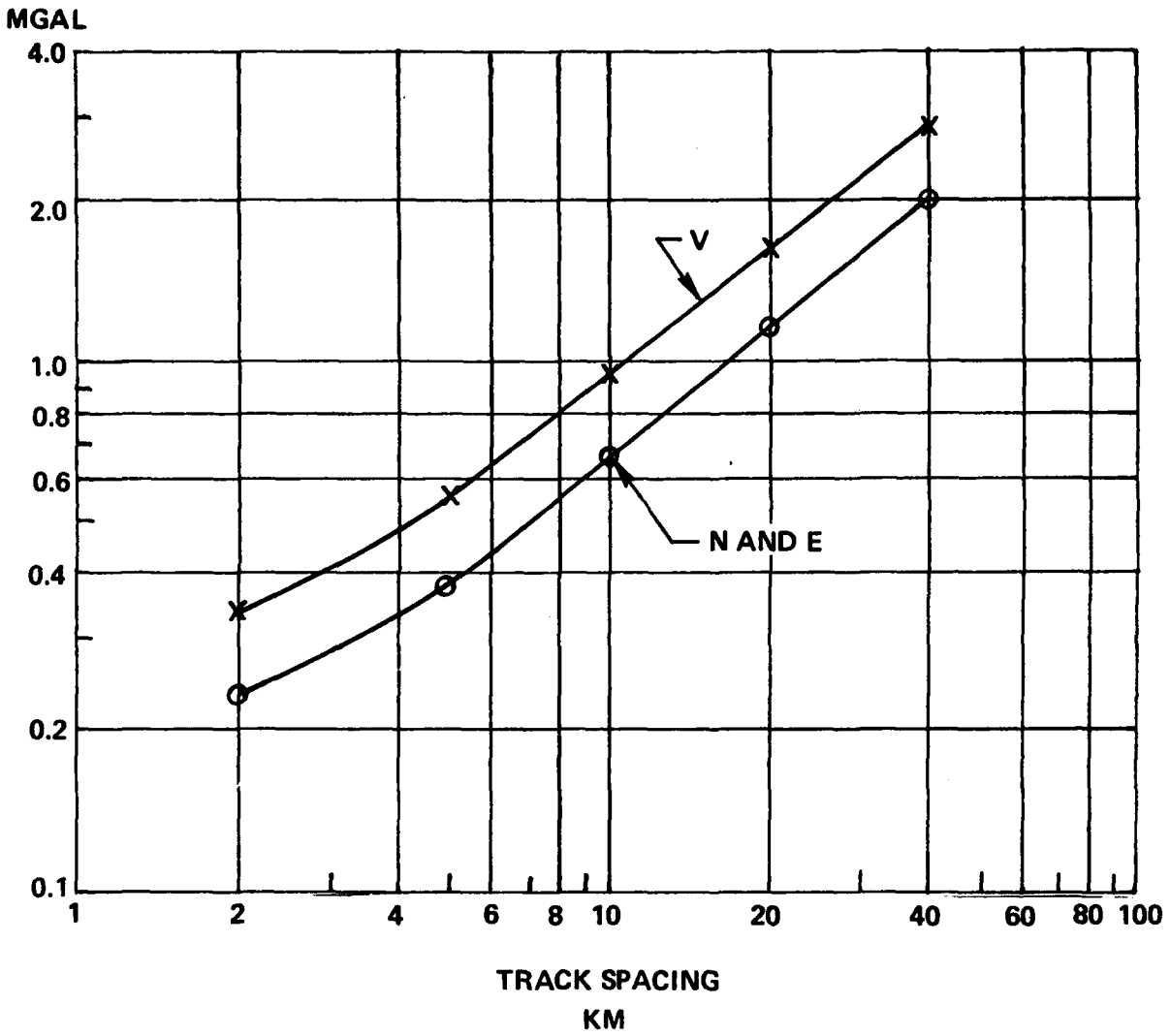

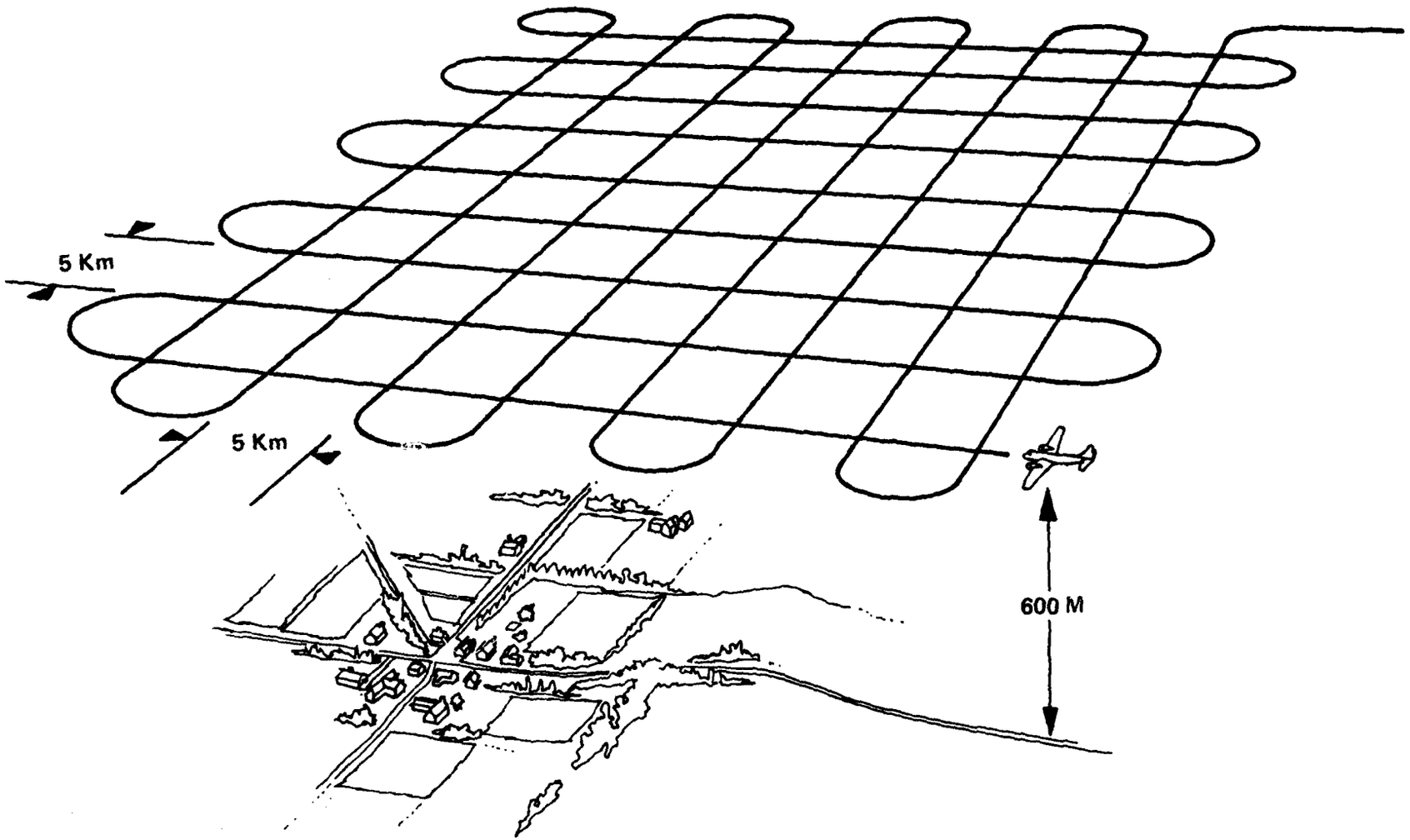
5 Km
5 Km
600 M

GGSS FUNCTIONAL BLOCK DIAGRAM

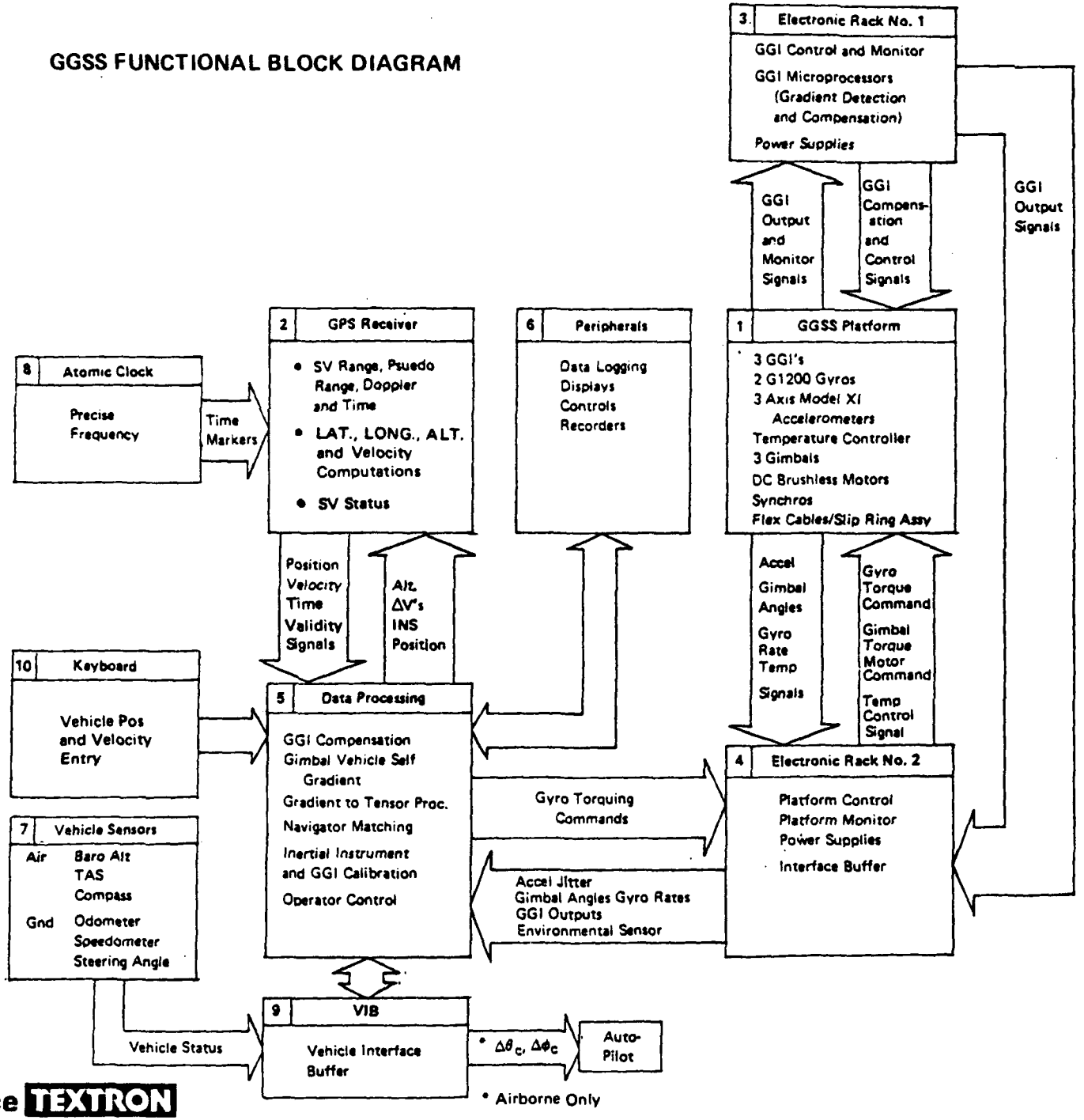

Bell Aerospace TEXTRON

P-3 INSTALLATION

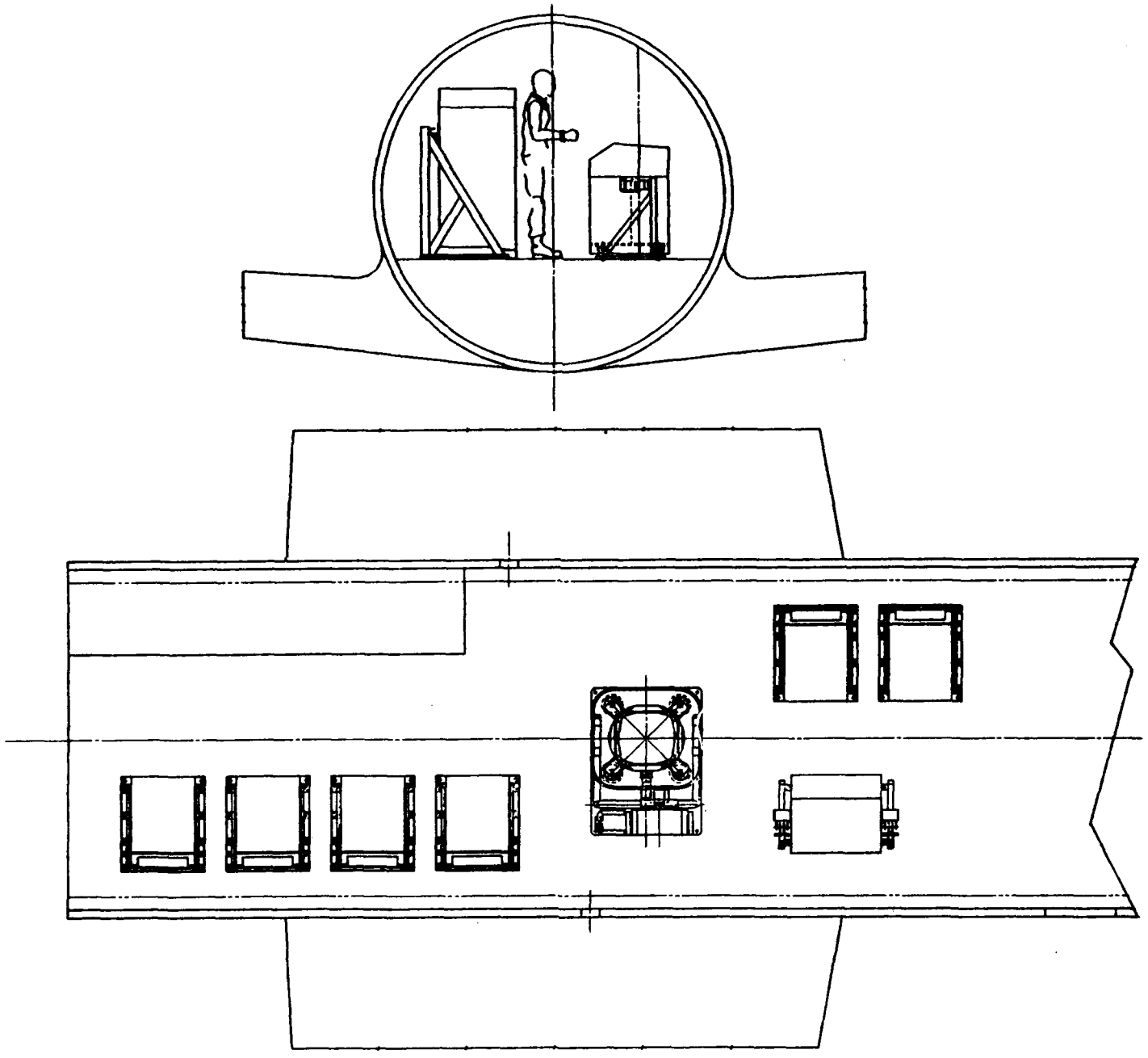

C130 INSTALLATION

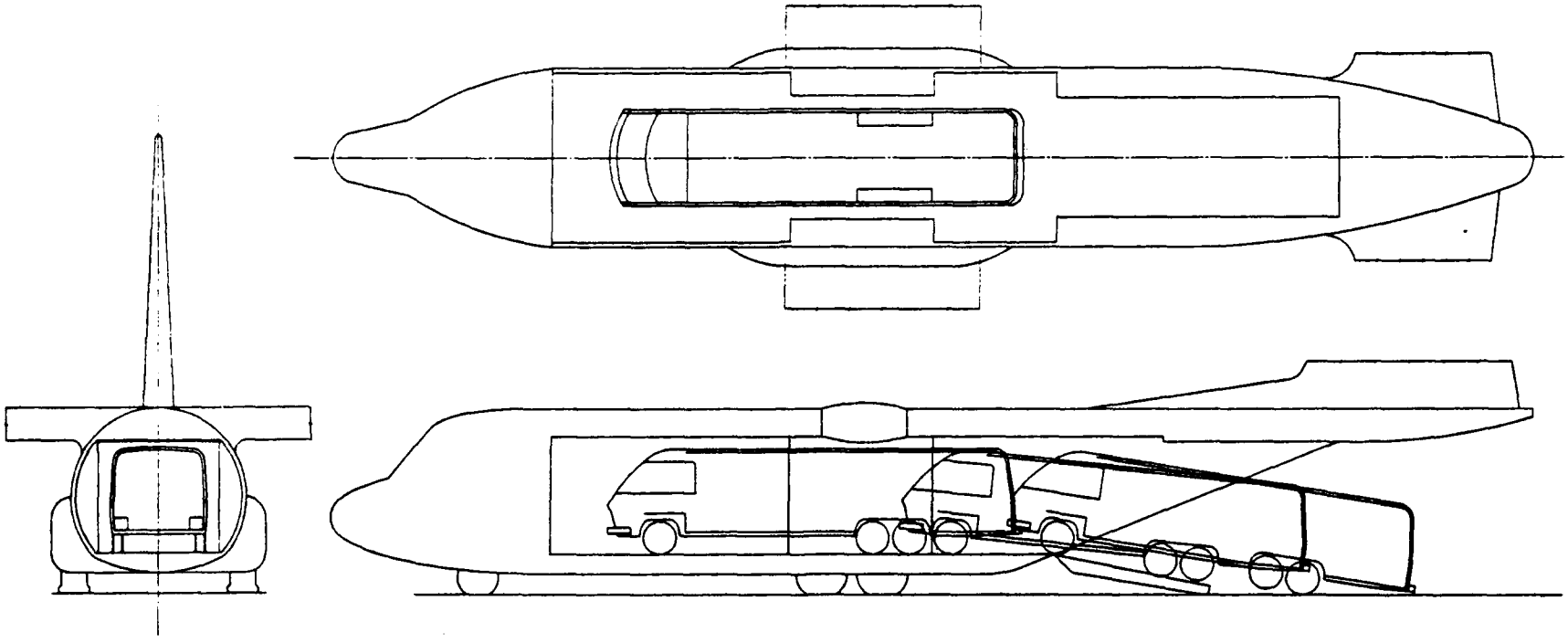

LAND VEHICLE INSTALLATION

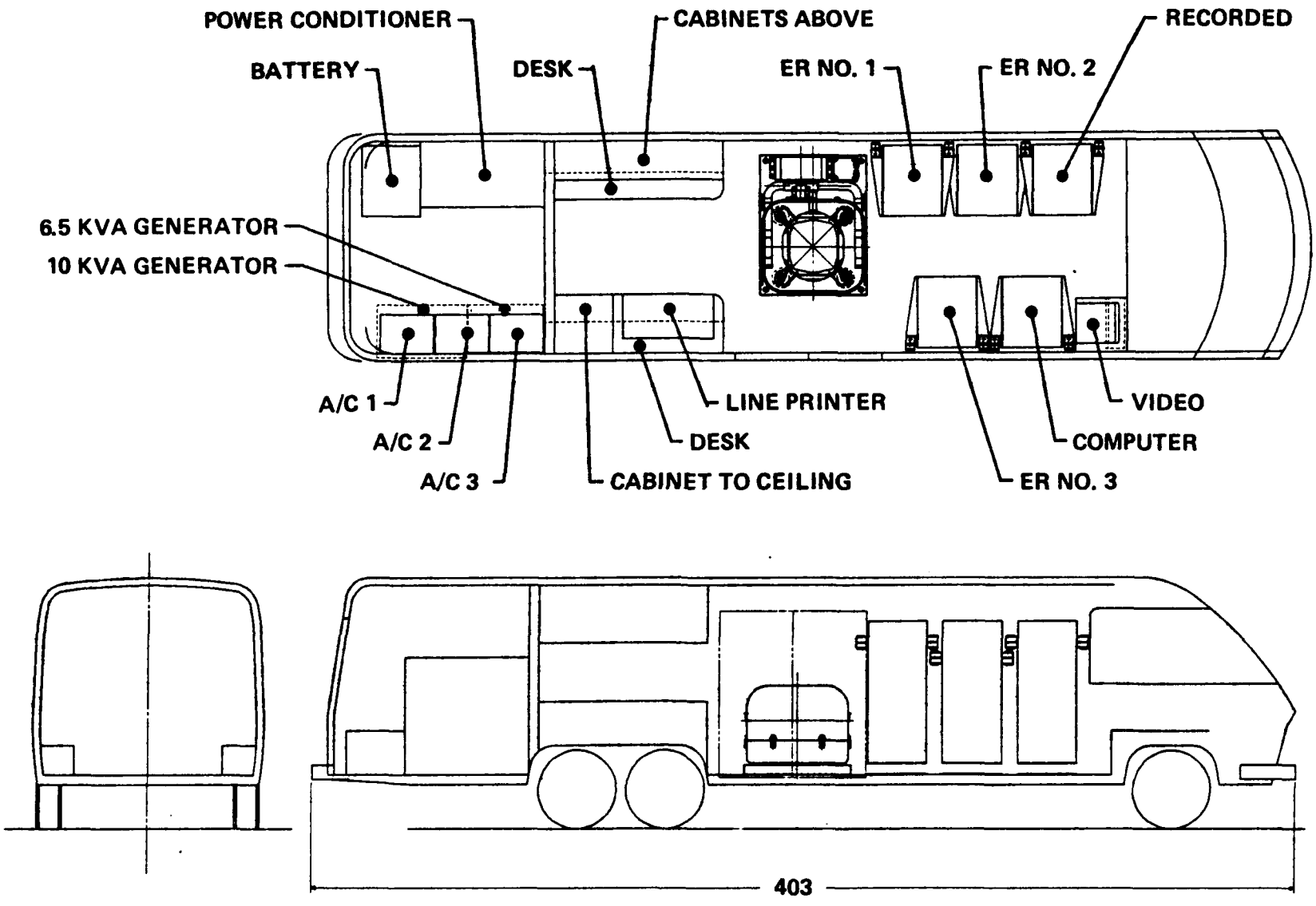

GGSS BASE STATION SUPPORT EQUIPMENT

- REVCON ON-BOARD EQUIPMENT
  - REVCON COMPLETELY SELF CONTAINED
    - ENVIRONMENTAL CONTROL
      - THREE AC UNITS
      - DEDICATED 6.5 KVA ONAN OR KOHLER MOTOR GENERATOR SET
        - 60 Hz, 3ϕ, 120/208 VAC POWER
    - GGSS POWER SUPPLY
      - DEDICATED 10 KVA WENCO OR KOHLER MOTOR GENERATOR SET
        - 60 Hz, 3ϕ, 120/208 VAC POWER
  - CAN ACCEPT 3ϕ, 60-400 Hz, 120/208 VAC GROUND POWER FROM:
    - MOBILE GROUND POWER UNIT (MGPU)
    - PUBLIC UTILITY

AIRCRAFT ON-BOARD CAPABILITY AND GROUND SUPPORT REQUIREMENTS-LOCKHEED C-120

- Environmental Control
  - Capability
    - Revcon Contains Its Own Air Conditioning
    - Revcon AC Units Powered In-Flight Via 6.5 KVA Frequency Changer from Aircraft On-Board Power
    - Aircraft APU Can Supply Trevcon AC Unit Ground Power
  - Ground Support Requirements
    - If APU Desired Off and Revcon On-Board
      - Ten KVA of Ground Power Required Via Aircraft
      - 6.5 KVA of 60 Hz Ground Power Required of Power Supplies Directly to Revcon
    - No Support Required if Revcon Deplaned
- GGSS Power
  - Capability
    - Aircraft APU Can Supply GGSS Ground Power
    - Revcon Motor Generator Can Supply GGSS Ground Power If Revcon If Revcon Deplaned
  - Ground Support Requirements
    - None Strictly Required
    - C-130/Revcon Can Accept Ground Power If So Desired
      - 16.5 KVA of 60 Hz Power Direct to Revcon
      - 20 KVA of 400 Hz Power Via Aircraft Bus

ENCLOSURE DESIGN

- Skid Mounted on Light Weight Aluminum Extrusion
- Self Contained Unit With Air Conditioner and Thermal Control unit
- Enclosure Wall Construction
  - Similar to ADM 1 Inch Thick Fiberglass-Foam Sandwich Construction
- EMI Shielded
  - Fiberglass Enclosure Will Be Coated With Flame Sprayed Aluminum
  - Inside and Out and Sealed Around Split Lines With EMI Gasket
  - Connectors Will be Mounted on Shielded Base

PLATFORM & ENCLOSURE - TOP VIEW

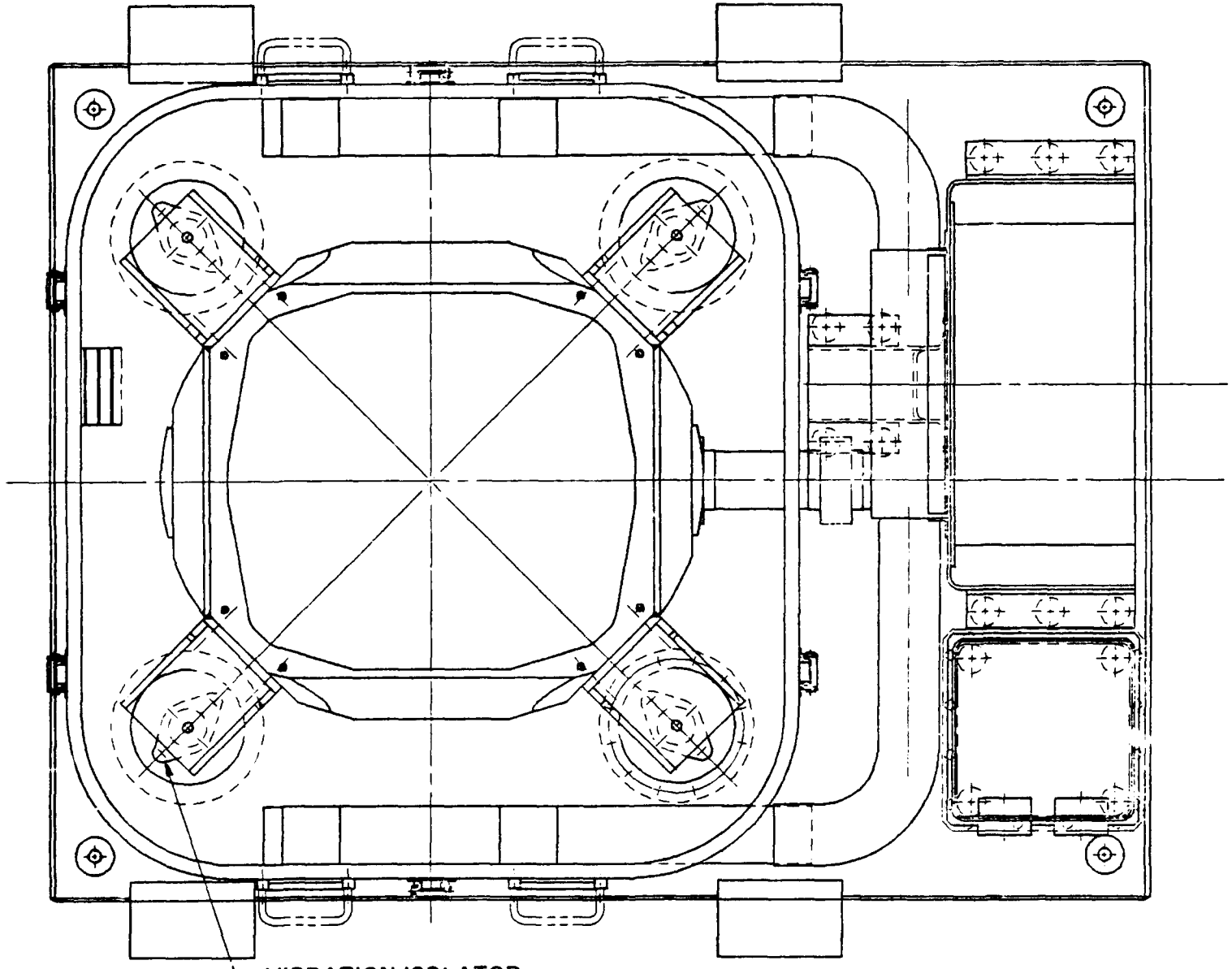

PLATFORM & ENCLOSURE - SIDE VIEW

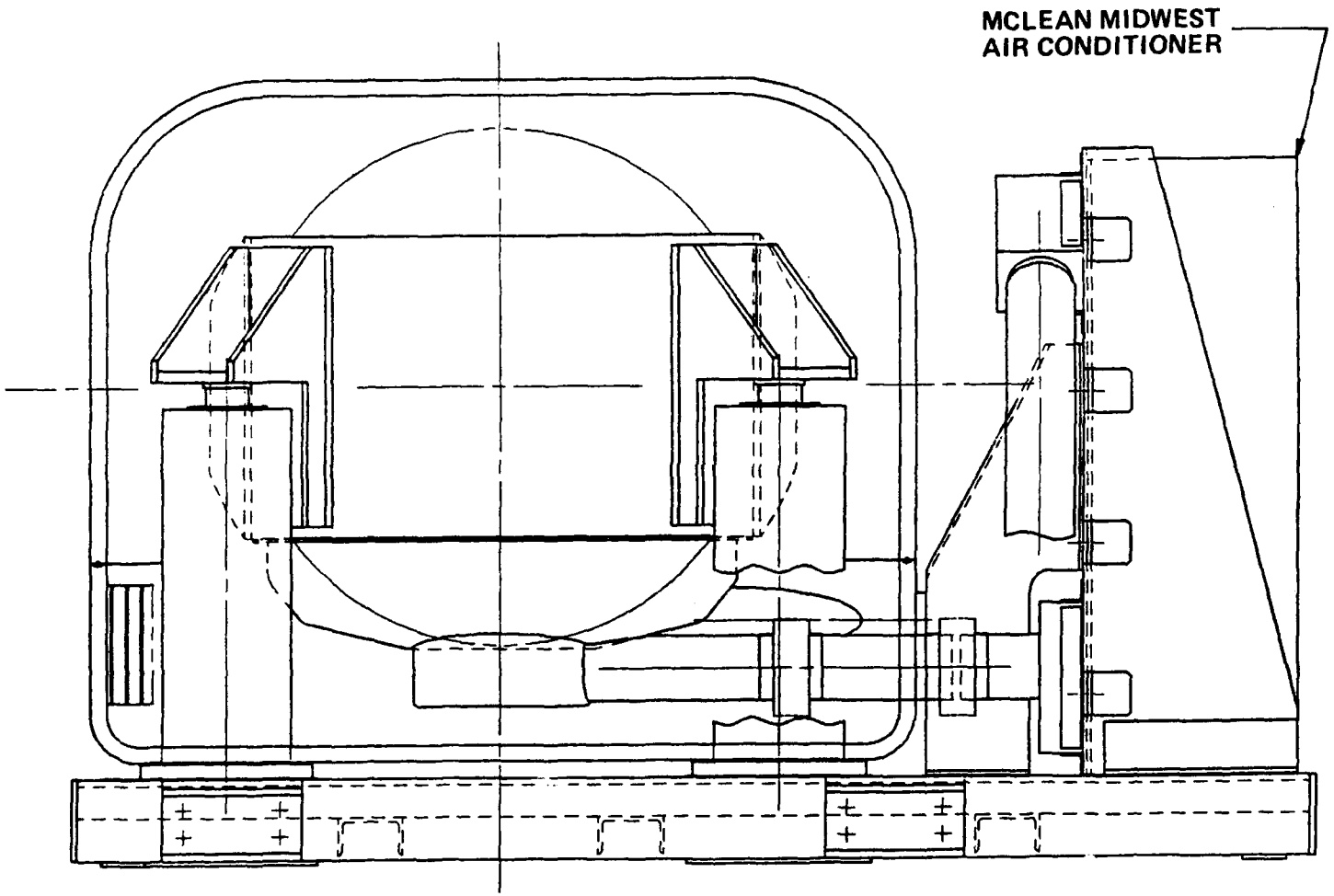

PLATFORM DESIGN

- Minimal Changes From ADM Platform
- Same Gimbal Sequence Pitch Outer, Roll Center, Azimuth Inner
- Same Synchros
- Cable Harness Will Be New - 3 Axis Accelerometer
  GGI Rotor Speed Control
  Better Gimbal Clearances
- Flex Capsules of the Same Type But Revised Lead Count
- Azimuth Slip Ring Assy of the Same Type but Revised Lead Count
- Platform Airflow - Has Been Improved From ADM to FSD
  - Plan to Use FSD Design for Lower Part of Azimuth Gimbal (Torque Motor/Bearing Adapter Assy) for Increased AirFlow Past GGI's
- Terminal Block of ADM Azimuth Gimbal Replaced by 4 Connectors as on FSD
- All Major Components are Drawn and Being Checked

AIRCRAFT ACCELERATION MEASUREMENTS

U.S. NAVY	P3 ORION
U.S. AIR FORCE	C-130 HERCULES
	CONVAIR 240
	CONVAIR 580

FINDINGS:

- ACCELERATION LEVELS AT 1/4 TO 3/4 Hz RANGE BETWEEN $10^{-5} G^2/RAD/SEC$ AND $10^{-3} G^2/RAD/SEC$
- PROVISIONS FOR POST MISSION ACCELERATION CORRECTION WILL BE MADE

RACK MOUNTING

LAND VEHICLE

- Manufacturers Say They Can Provide Walls Sufficiently Stiff to Provide Tie Down Points for Sway Stabilizers.
- Therefore There Will BE No Frames Around Racks as Previously Envisaged.
- For Bases it is Planned to Use Barry VHC Type Isolators.
  - Provides a 12 Hz System
  - Good Attenuation of Vertical Shock
  - Would Survive 9G Shock Without Failure (Any Direction)
  - Q of Approximately 7 With Damping Ratio of Approximately 0.07
- Stabilizers
  - Barry 2K Stabilizers
  - No Vertical Stiffness - All Vibration Isolation Achieved by Base
  - Safe
- Cabinets Have Been Analyzed for Structural Strength. They Are Safe to a Shock Level Greater Than 20 gs.
- Cabinets Will be in EQUIPTO Racks - Two Sizes.

COMPLETED DESIGN FOR GGSS AND GSS

PROVIDES FLEXIBILITY FOR SLIP RING SELECTION AND MODEL VII PENDULOSITY. ELECTRICALLY AND MECHANICALLY INTERCHANGEABLE WITH ADM GGI CONFIGURATION.

GGS UNINTERRUPTABLE POWER SUPPLY (UPS)

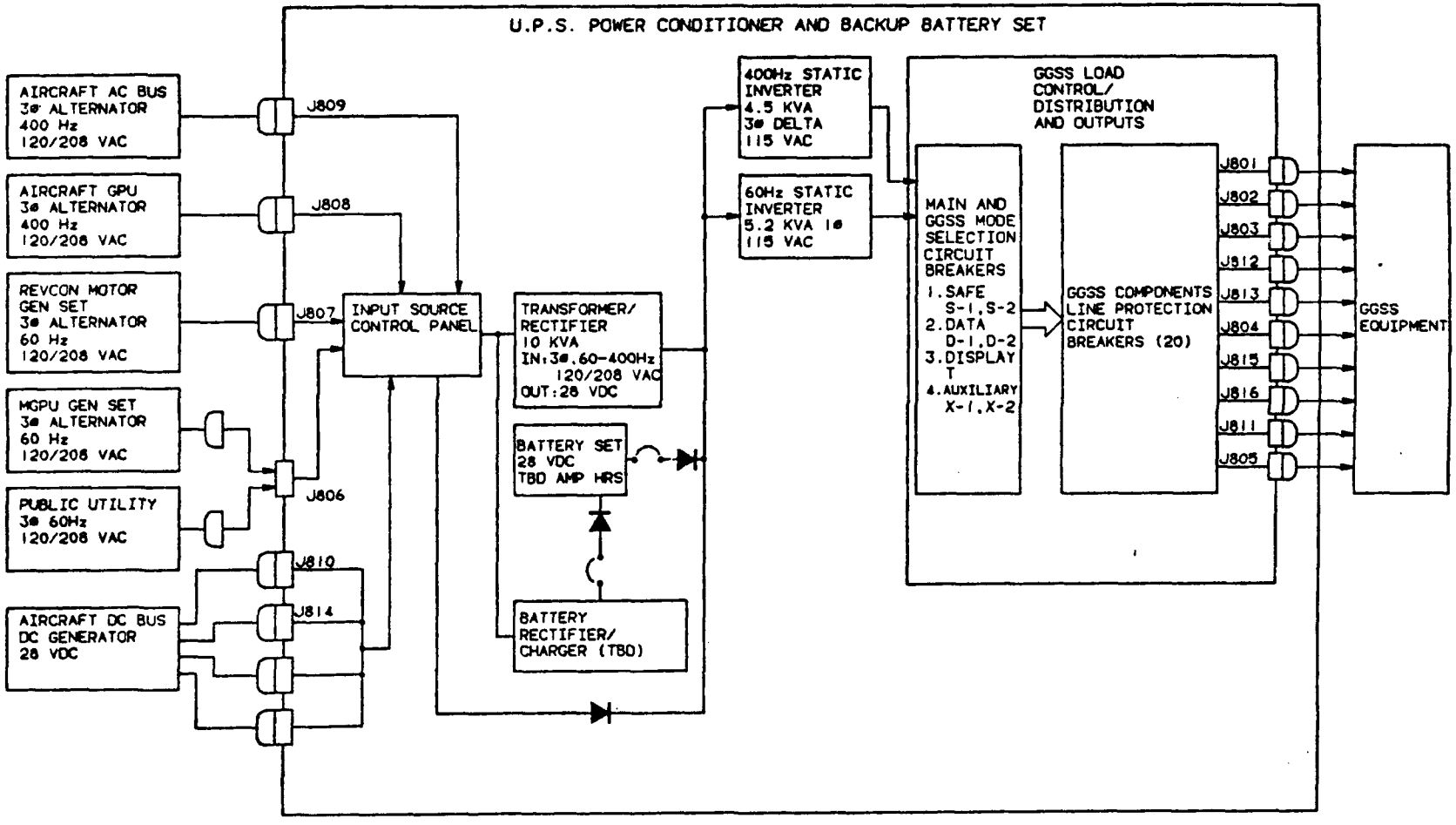

GGI

GRAVITY GRADIENT INSTRUMENT

SCHEMATIC ILLUSTRATION OF ROTATING FIXTURE

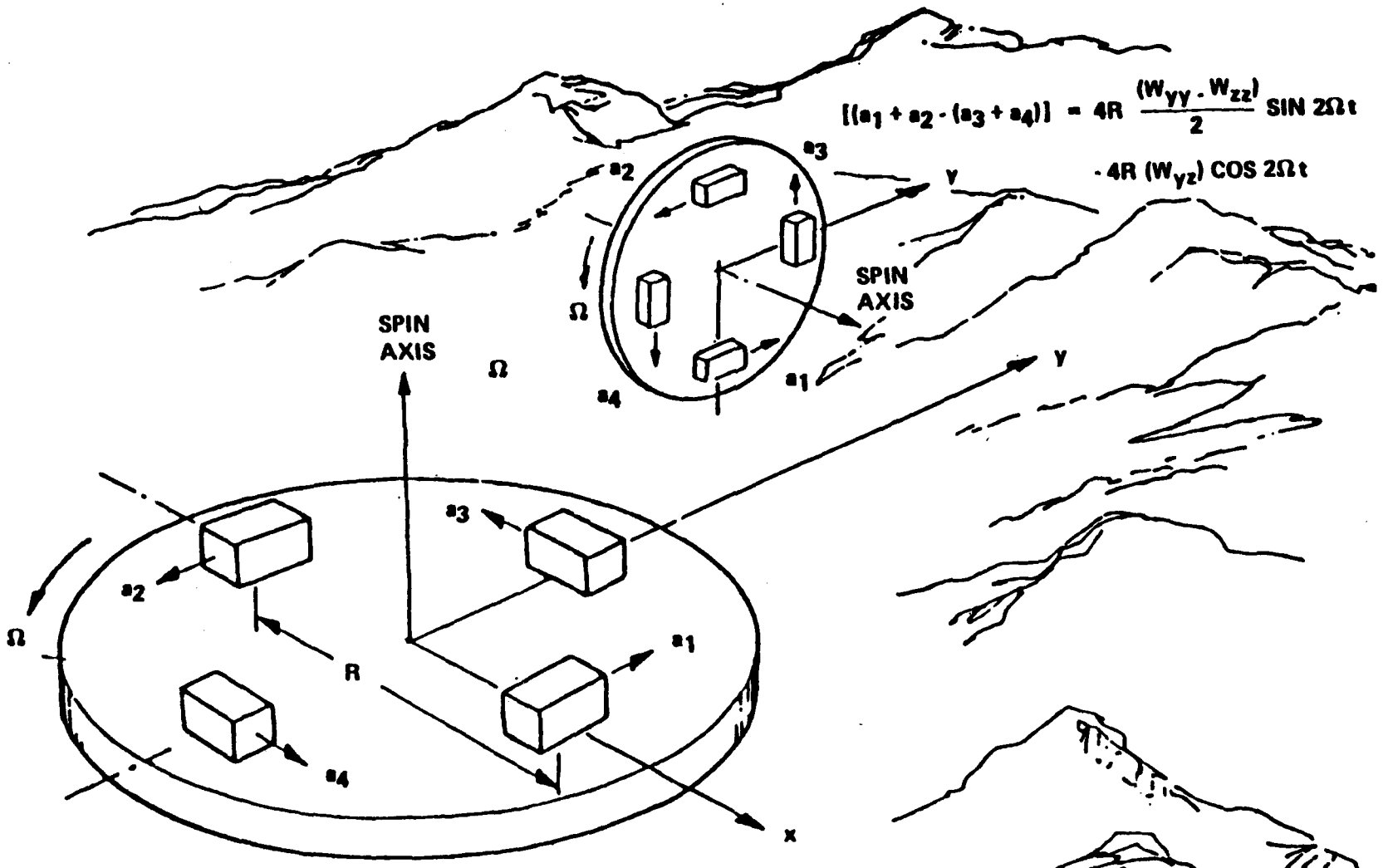

$$[(a_1 + a_2) - (a_3 + a_4)]_V = 2R\,(W_{xx} - W_{yy})\,\text{SIN}\,2\Omega t + 4R\,(W_{xy})\,\text{COS}\,2\Omega t$$

$$[(a_1 + a_2 - (a_3 + a_4)] = 4R\,\frac{(W_{yy} - W_{zz})}{2}\,\text{SIN}\,2\Omega t - 4R\,(W_{yz})\,\text{COS}\,2\Omega t$$

GGI SIGNAL PROCESS BLOCK DIAGRAM

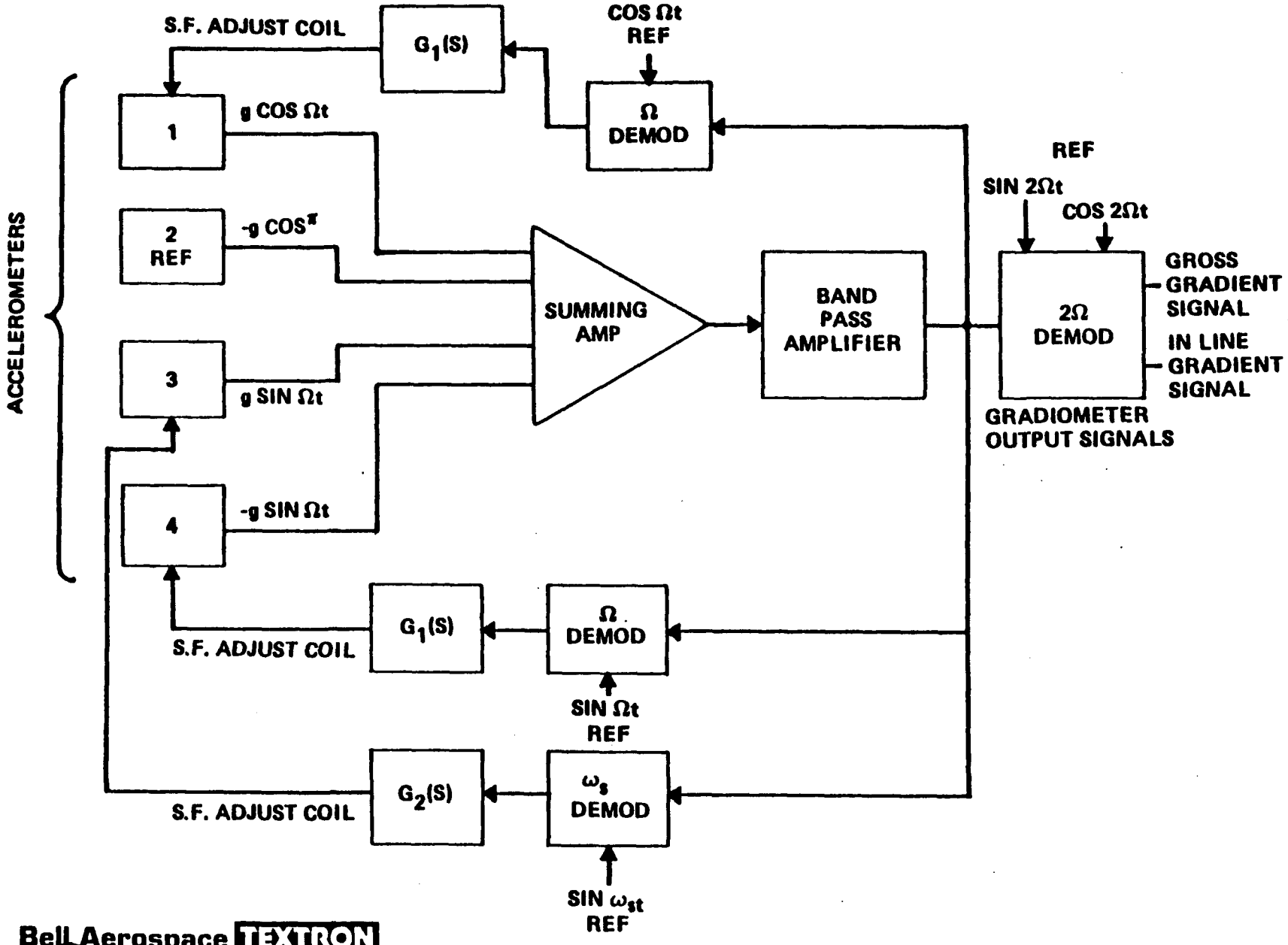

MODEL VIIB ACCELEROMETER

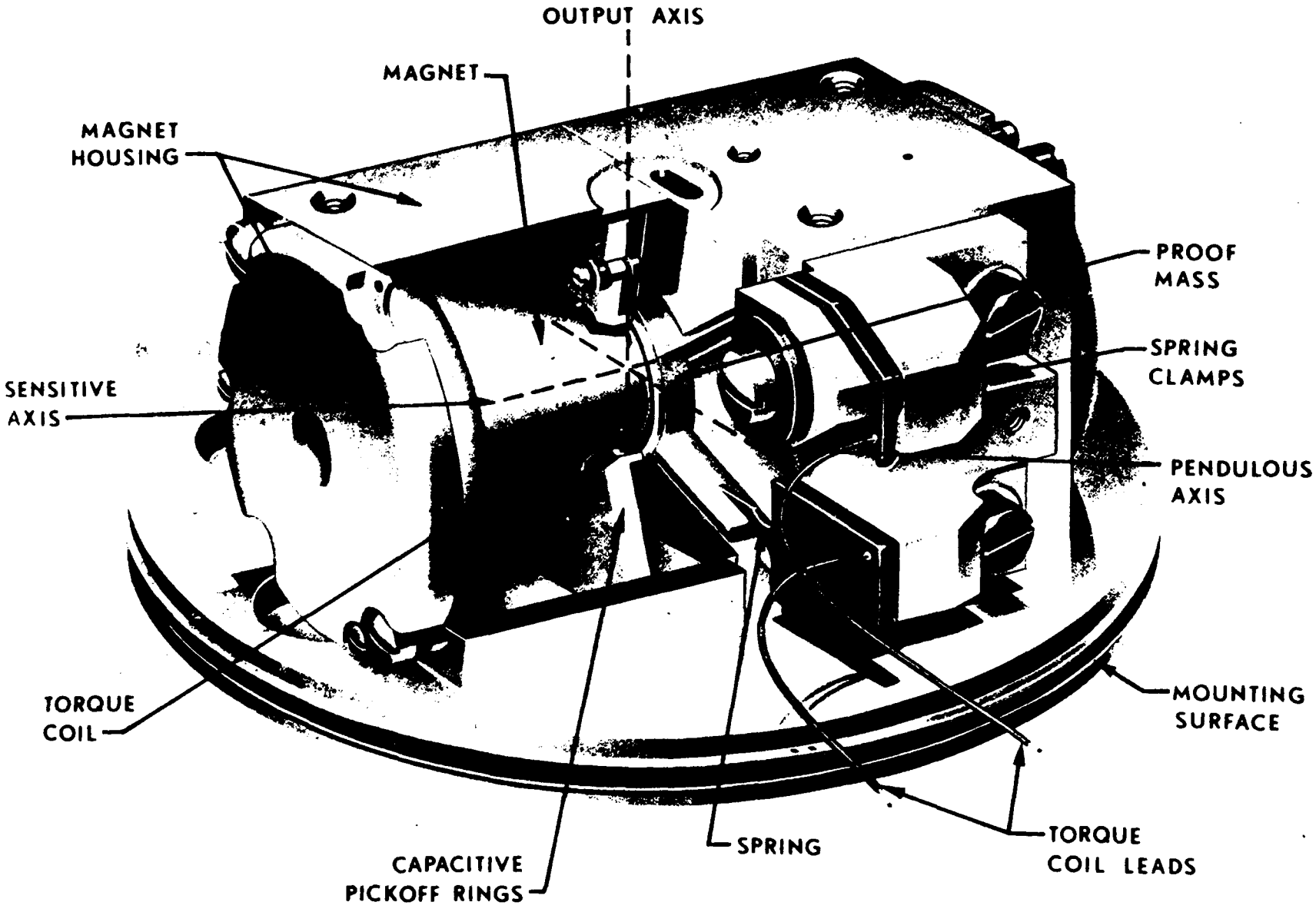

ADM GGI

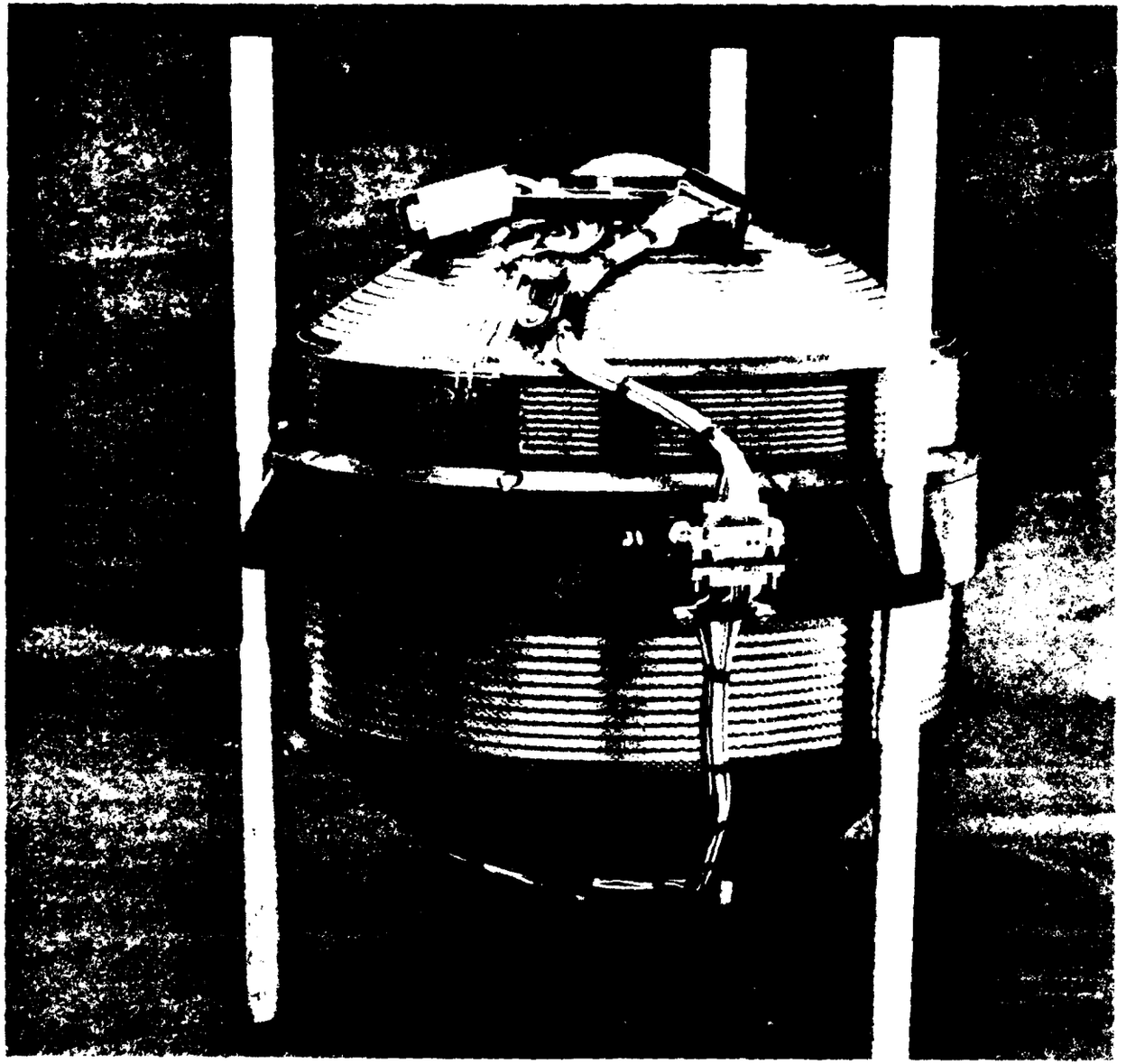

INSTRUMENT BLOCK AND ELECTRONICS

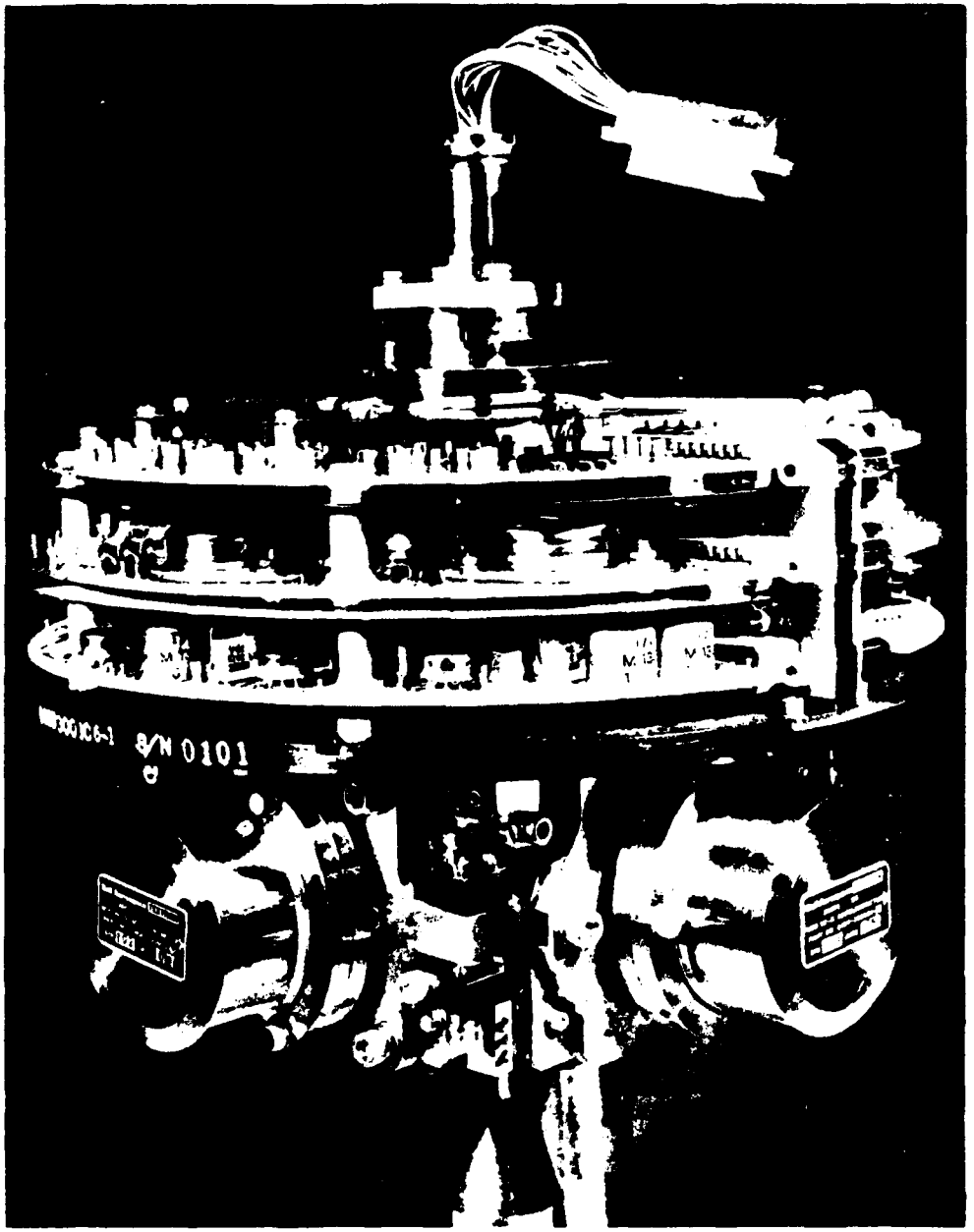

1983 GGI DEVELOPMENTS

Tested on USNS Vanguard	
- ADM GGI With Low Pendulosity Model VIIs (1/3)	Higher Shock Survivability Easier to Handle and Fabricate
- IR&D GGI With Duplex Preload Bearings	Provide More Space for Slip Ring Assembly Reduce Bearing Induced Periodicity
- GGI Platform Perturbation Technique	Dockside Calibration of Fixed Level K_4, K_8 and Differential $K_2 - K_5$ Compensation
Tested In Laboratory	
- GGI with High Pendulosity Model VIIs (2X)	Reduce High Frequency GGI Noise
- Noise Measurements of Various Slip Ring Assemblies	Extent Maintenance Interval - Goal is 20,000 Hrs
Completed Design for GGSS and GSS OS GGIs	Provides Flexibility for Slip Ring Selection and Model VII Pendulosity. Electrically and Mechanically Interchangeable with ADM GGI Configuration.

BOBBIN AND LEG ASSEMBLY – STANDARD PROOF MASS MODEL VII G

1200 DYN cm/g

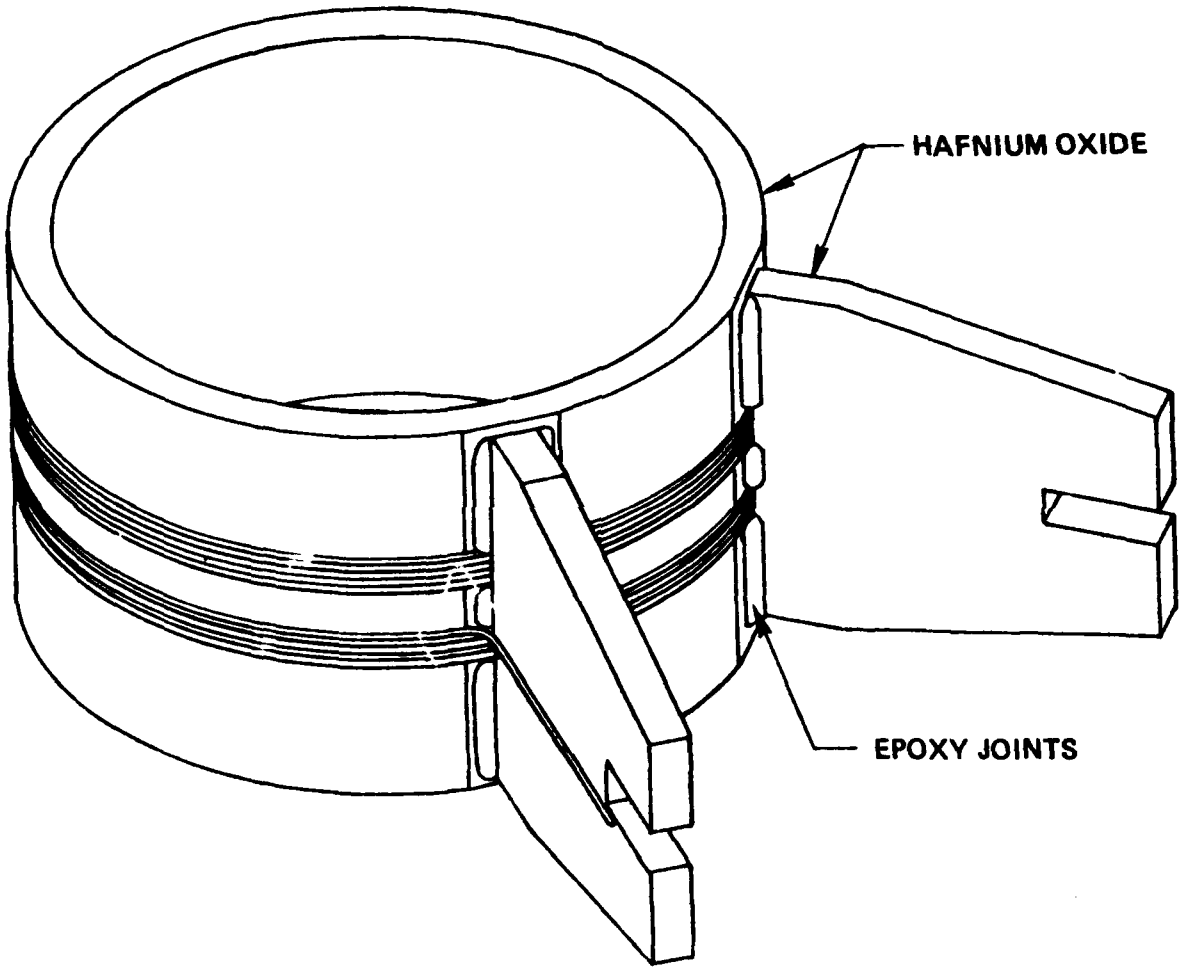

BOBBIN AND LEG ASSEMBLY – LIGHT PROOF MASS MODEL VII G

400 DYN cm/g

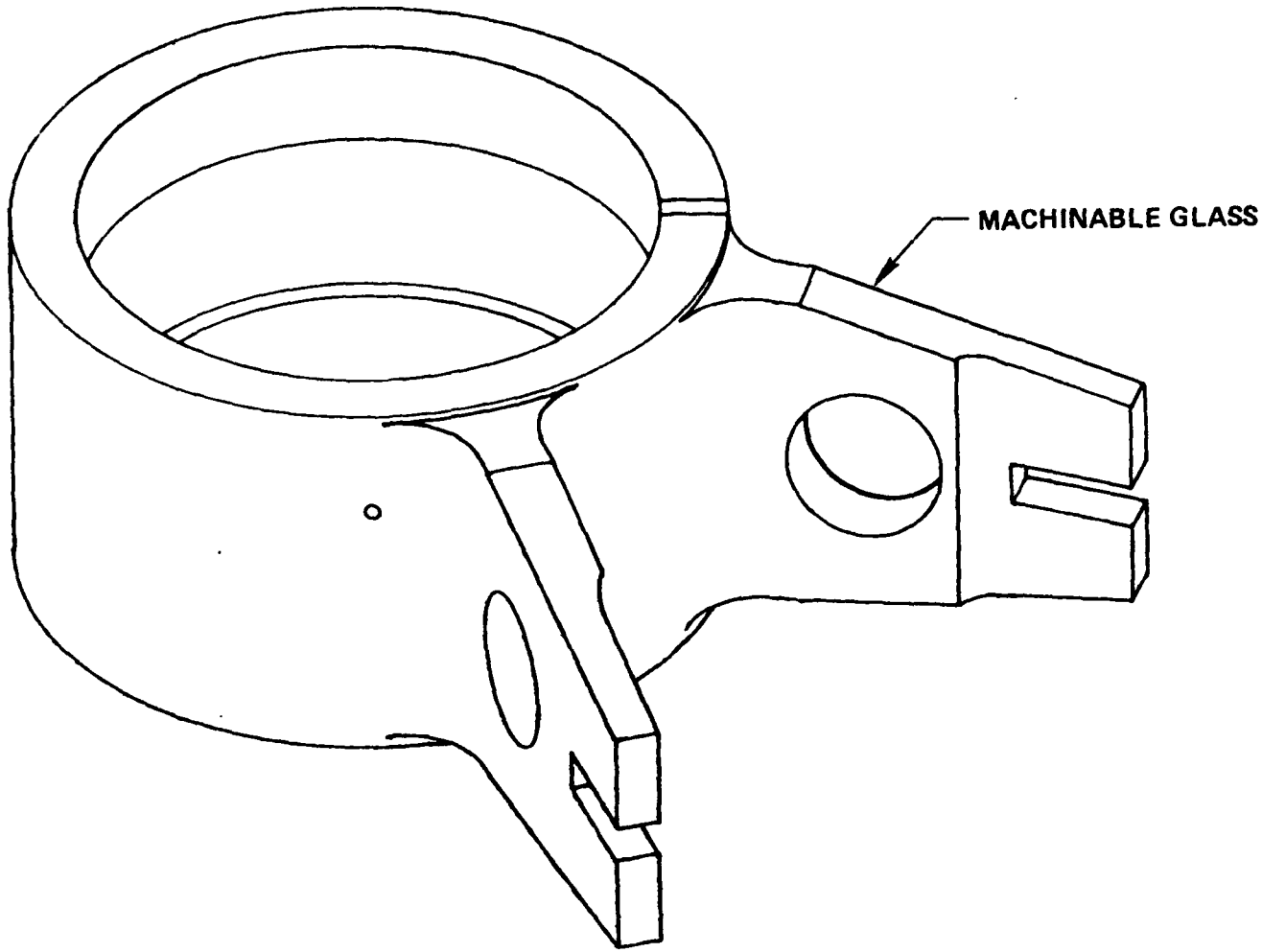

BOBBIN – HEAVY PROOF MASS MODEL VII G

2400 DYN cm/g

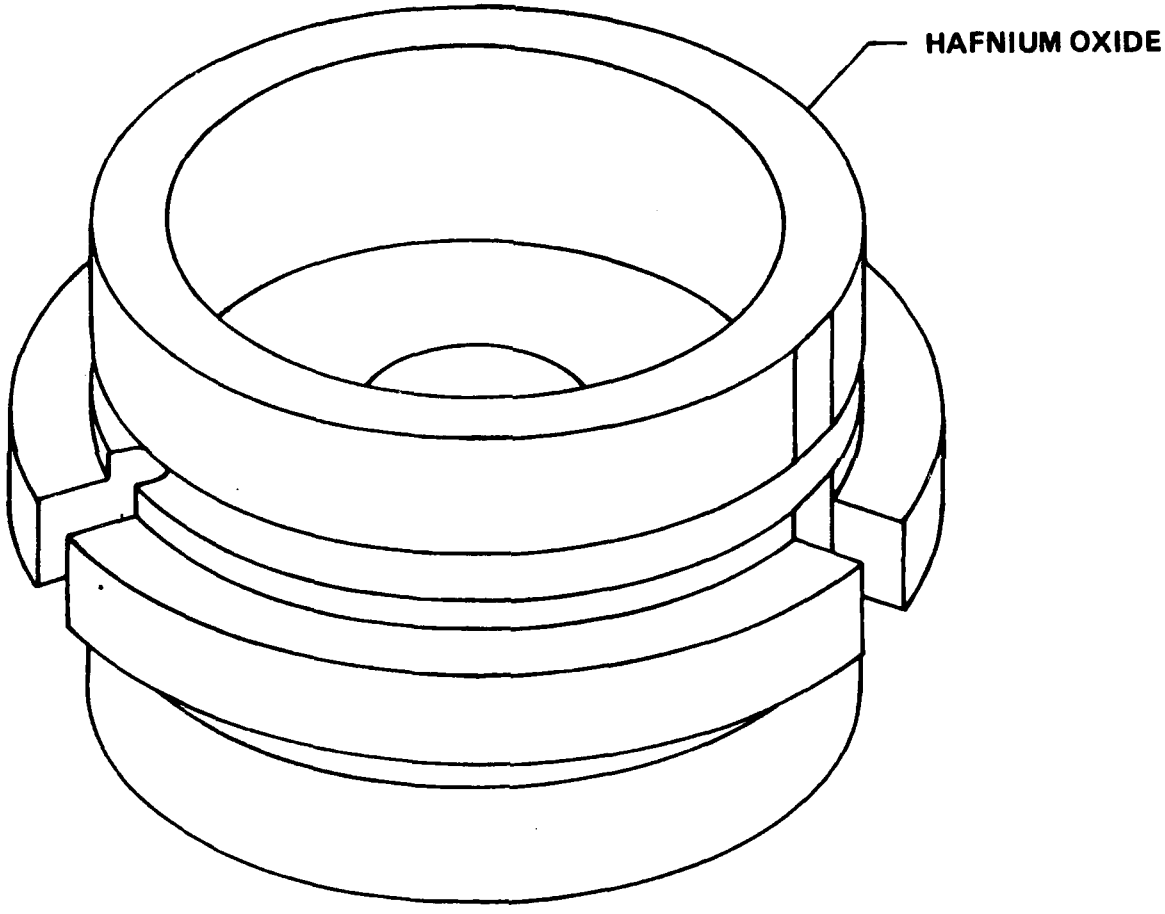

PLATFORM PERTURBATION

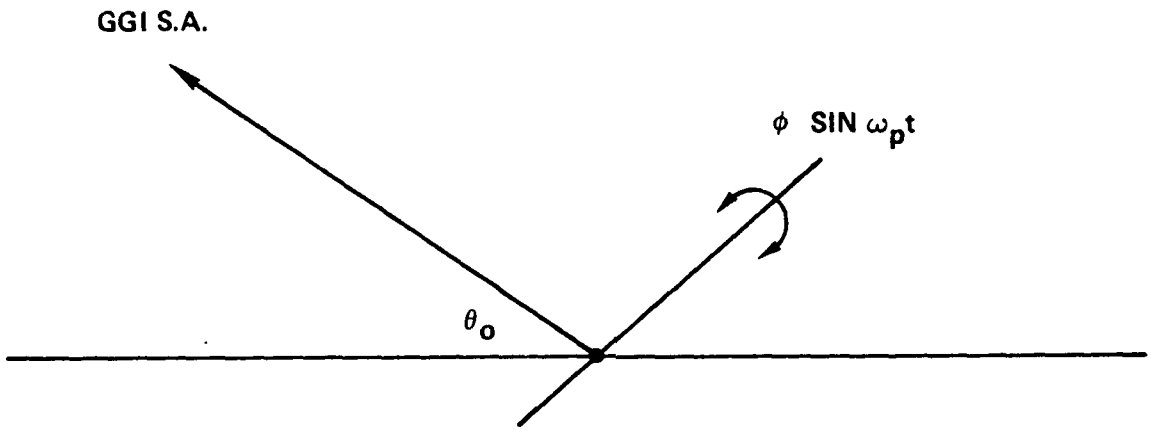

$$\theta = \theta_o + \phi \text{ SIN } \omega_p t$$

GGI PLATFORM PERTURBATION CALIBRATION TECHNIQUE

ACCELEROMETER ERROR MODEL

$$A_M = K_1 A_I + K_2 A_I^2 + K_4 A_I A_P + K_5 A_O^2 + K_6 A_I A_O + K_7 A_P^2 + K_8 A_O A_P + \alpha A_P$$

A_I, A_O, A_P	ARE ACCELERATIONS ALONG ACCELEROMETER INPUT, OUTPUT AND PENDULOUS AXIS
K_1	SCALE FACTOR
K_2, K_4, K_5, K_6, K_7, K_8	ARE ACCELEROMETER EVEN ORDER ERROR COEFFICIENTS
α_O	IS ACCELEROMETER INPUT AXIS MISALIGNMENT INTO GGI SPIN AXIS

GGI OUTPUT ERRORS AS A FUNCTION OF ACCELERATION DISTURBANCES ERROR COEFFICIENTS AND ATTITUDE

ACCELERATION INPUTS	ERROR COEFFICIENTS	FUNCTION OF θ	METHOD OF COMP
g PERPENDICULAR SA	$\Sigma K_2, K_5, K_6$	$\cos^2\theta$	SIMPLE DOCKSIDE
a PERPENDICULAR SA	$\Sigma K_2, K_5, K_6$	$\cos\theta$	ADJUSTMENT
a_Ω PERPENDICULAR SA	ΣK_1	-	SCALE FACTOR BALANCE LOOPS
$a_{2\Omega}$ PARALLEL SA	$\Sigma \alpha_0$	-	AXIAL SHAKE LOOP
	ΣK_7	2 SINE θ	AXIAL SHAKE LOOP
$a_{2\Omega}$ PERPENDICULAR SA	ΣDIFF K_2, K_5	$\cos\theta$	FACTORY CALIBRATION FIXED LEVEL COMP
a_Ω PARALLEL SA	$\Sigma K_4, K_8$	$\cos\theta$	FACTORY CALIBRATION FIXED LEVEL COMP

PLATFORM PERTURBATION WITH AXIAL SHAKE LOOP SETTING

$\left(\Sigma a_0 + \Sigma 2 \text{ SIN } \theta \ K_7 \right)$ TO 0

PLATFORM PERTURBATION WITH GGI SA AT θ_U

COEFFICIENT	DETECTION SIGNAL
$\Sigma K_4 K_8$	$\phi_g \Sigma K_4 K_8 \text{ Cos } \theta_U \text{ SIN } \Omega t \text{ SIN } \omega_p t$
$\Sigma K_8 K_4$	$\phi_g \Sigma K_8 K_4 \text{ Cos } \theta_U \text{ Cos } \Omega t \text{ SIN } \omega_p t$
$\Sigma \text{DIFF } K_2 K_5$	$\frac{\phi}{2}_g \Sigma \text{DIFF } K_2 K_5 \text{ SIN } \omega_p t$

FSD GGI SLIP RING DESIGN APPROACH

- Increase Capsule Diameter to Enhance Slip Ring Vendors Prospects of Achieving a Design With a Significantly Increased Maintenance Interval

- Design In a Connector For the Slip Ring Capsule to Facilitate Slip Ring Replacement as the Maintenance Operation

- Evaluate the Alternative Design Principles/Techniques Currently Available
  - Pandect (UK) - Conventional
  - Poly-Scientific - Fibre Brush
  - Encoder Research - Rolling Element

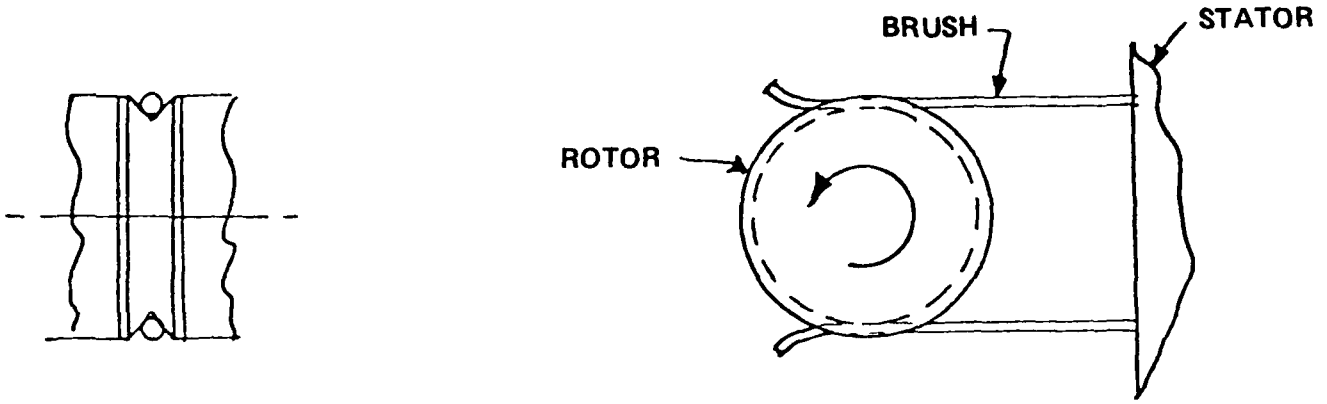

SLIDING CONTACT SLIP RING

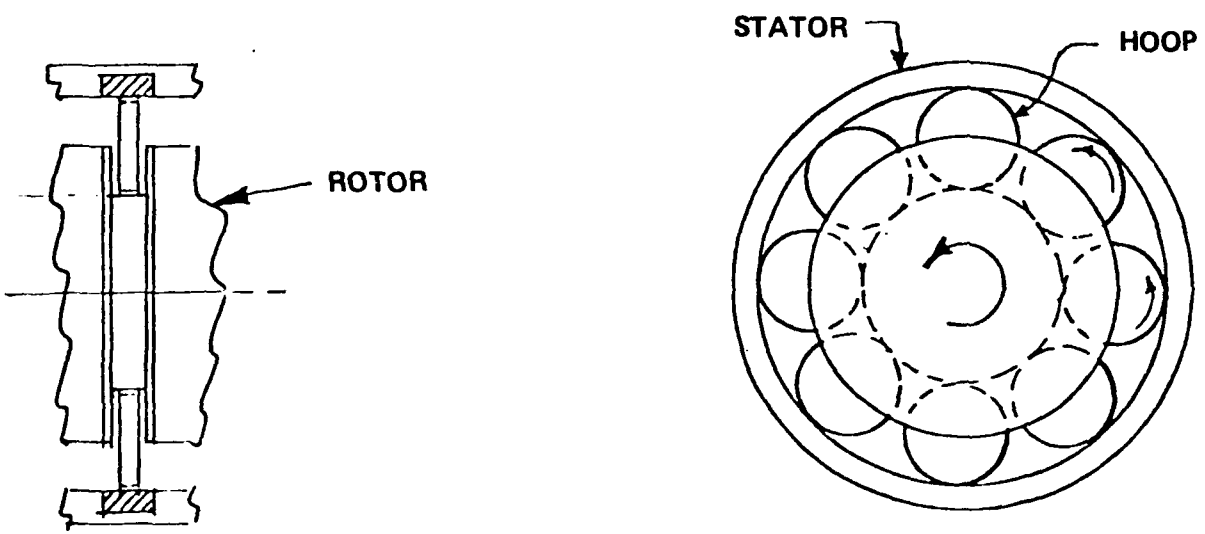

ROLLING ELEMENT SLIP RING

SLIDING CONTACT TYPE SLIP RINGS

ADM TYPE
POLY-SCIENTIFIC

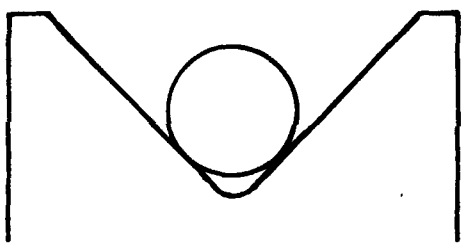

GOLD PLATED RINGS

BRUSH FORCE 1-1/2 ± 1/2 gm

LUBRICATED

PANDECT (U.K.)

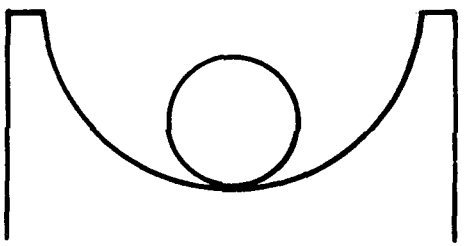

SOLID GOLD RINGS

BRUSH FORCE 1 ± 0.1 gm

UNLUBRICATED

FIBRE BRUSH
POLY-SCIENTIFIC

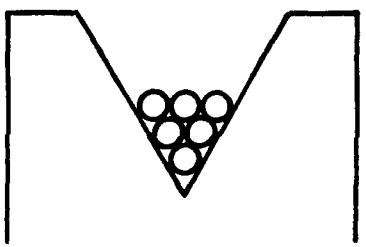

GOLD PLATED RINGS

BRUSH FORCE 2/3 gm

UNLUBRICATED

SLIP RING EVALUATION TESTING

- 8 Test Stations
  - 2 for Pandect
  - For Poly-Scientific Fibre Brush
  - For Rolling Element
  - 2 for ADM Type (Control)

- 2 Evaluation Scenarios for Each Type
  - Continuous Running at 1/4 Hz (GGI Rotor Speed)
  - 1 Week Running at 1/4 Hz Followed by Continuous Running at 3/4 Hz

- Tests Evaluate
  - 2 Series Slip Ring Circuit Resistance
  - Insulation Resistance Adjacent Circuits

PRELIMINARY FSD GGI LAYOUT

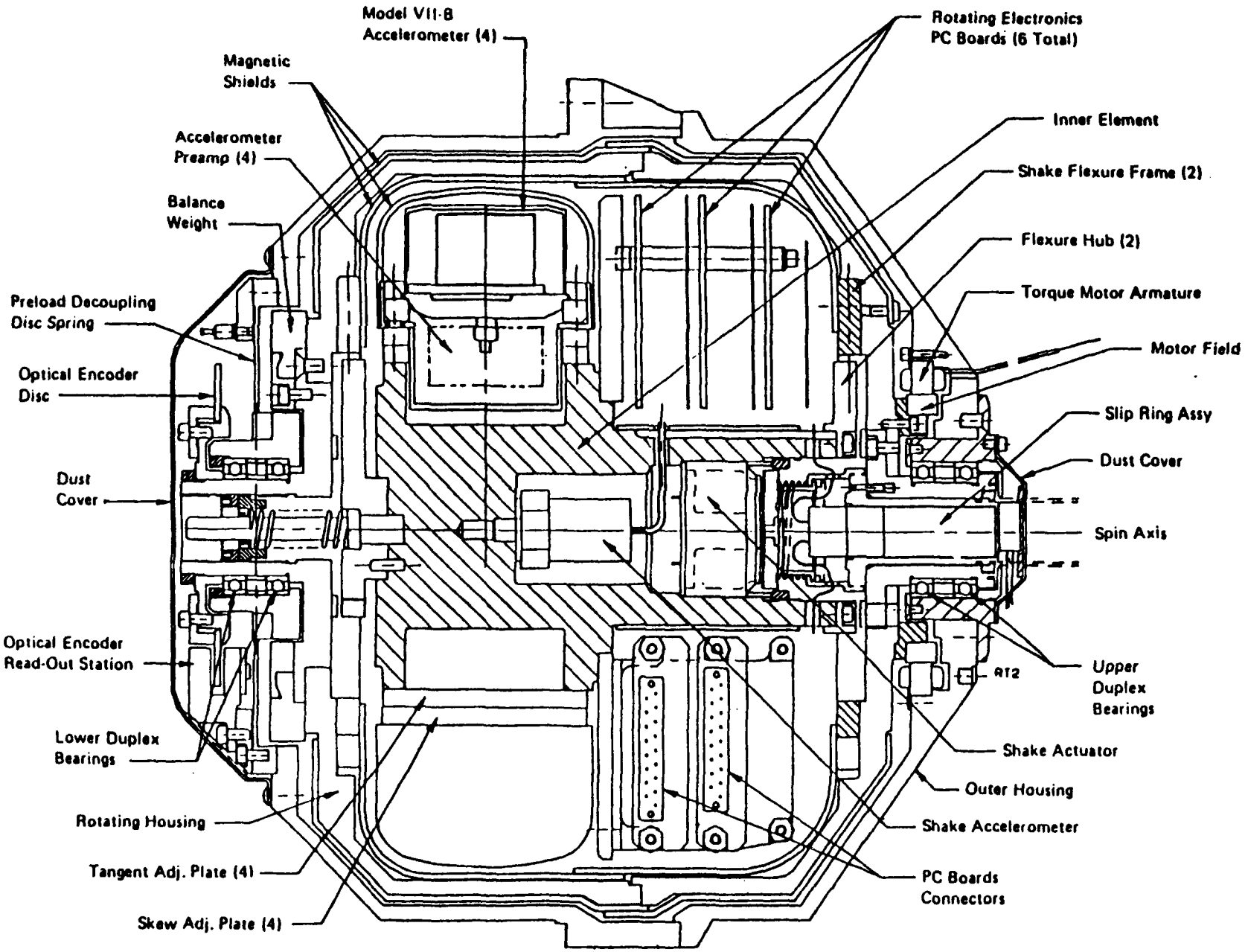

GRAVITY GRADIOMETER INSTRUMENT

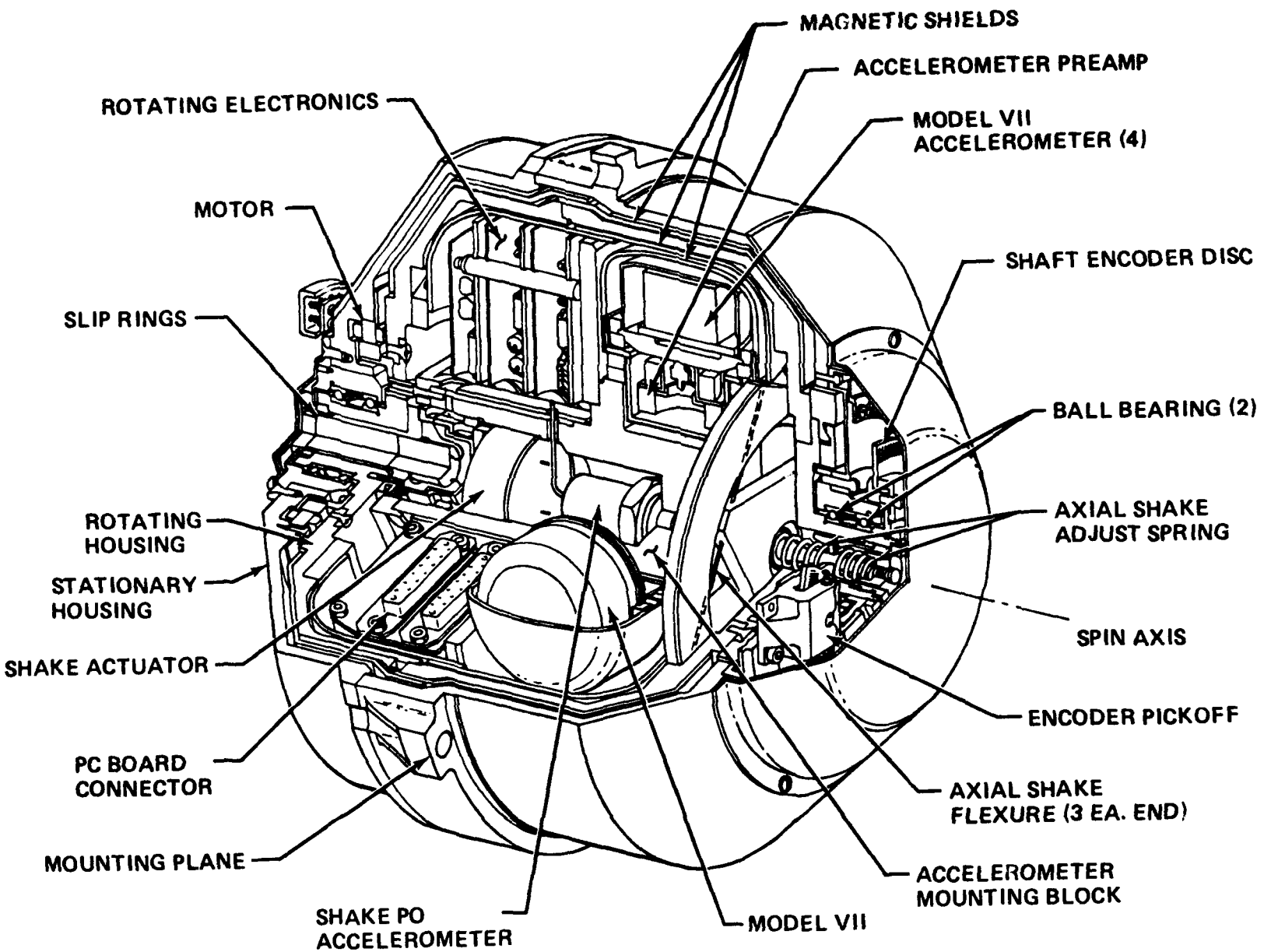

HORIZONTAL g ⊥ TO SA EXPERIENCED BY GGI WITH SA IN PLANE OF TRACKS DURING TURNS

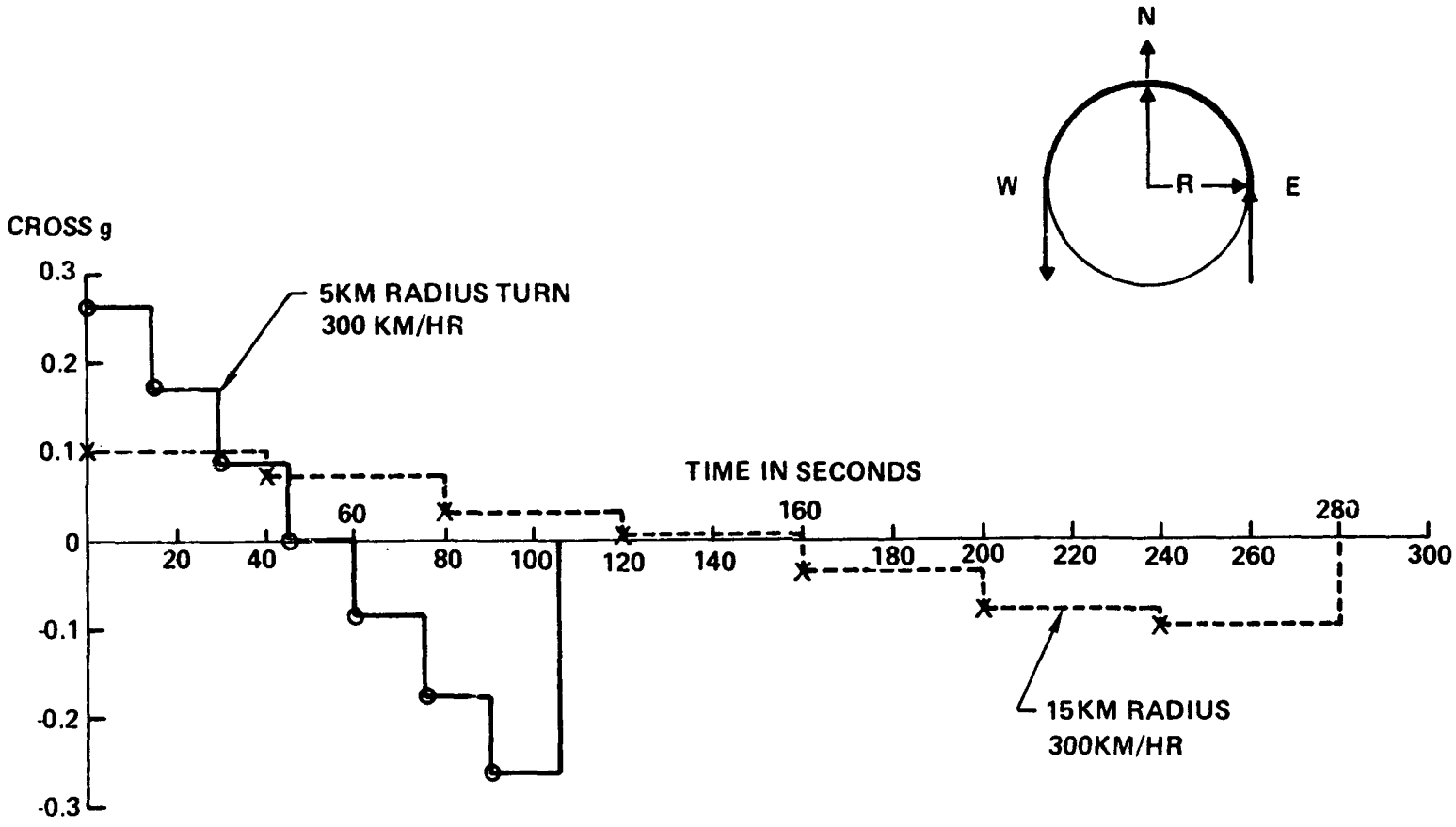

NO MEASURABLE CHANGE IN GGI OUTPUT
AFTER SIMULATED CROSS g ON LEITZ HEAD

GRAVITY SENSOR SYSTEM (GSS)

OPERATIONAL SYSTEM

GSS FSD PROGRAM OVERVIEW

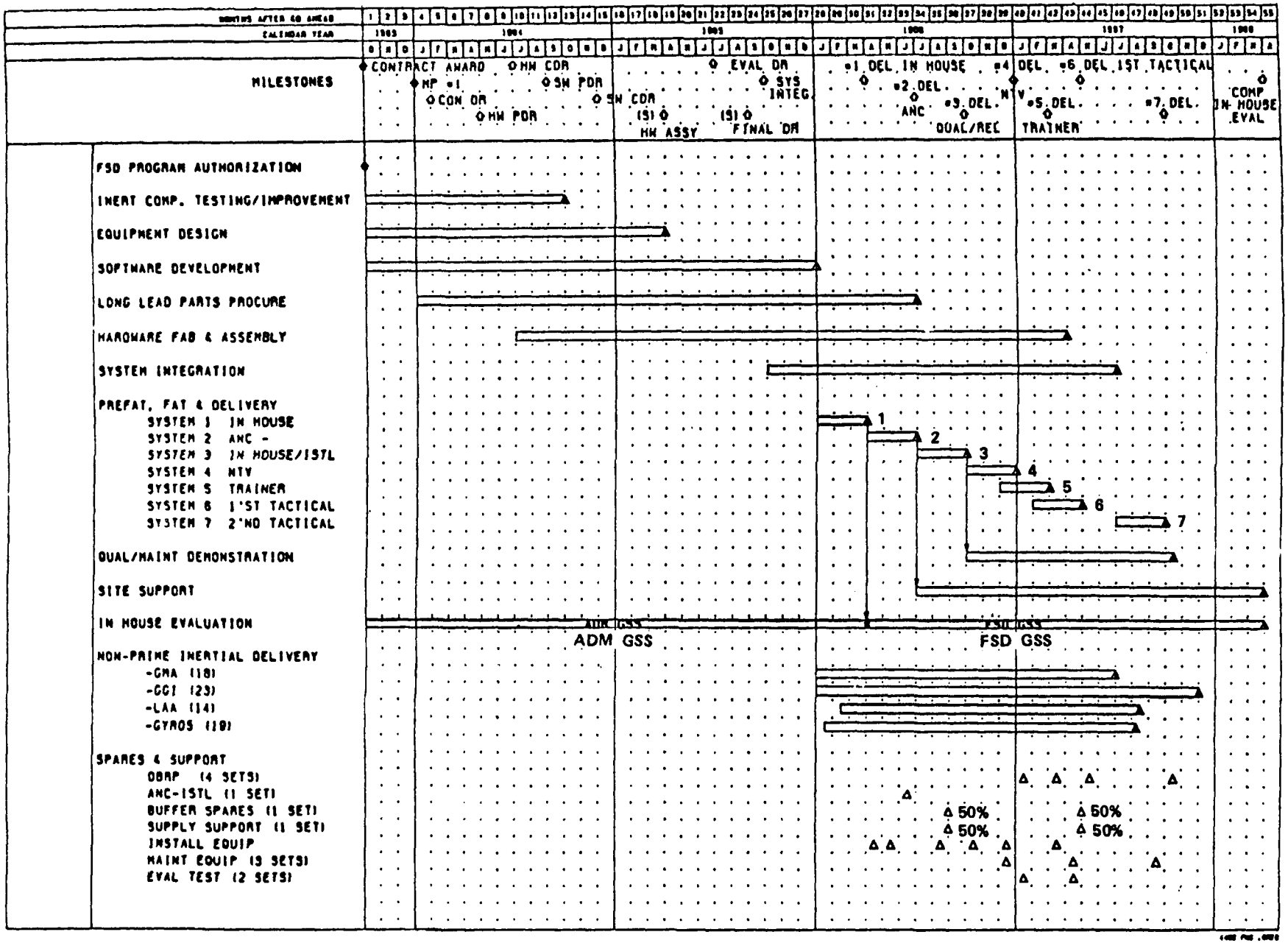

GSS FSD FUNCTIONAL BLOCK DIAGRAM

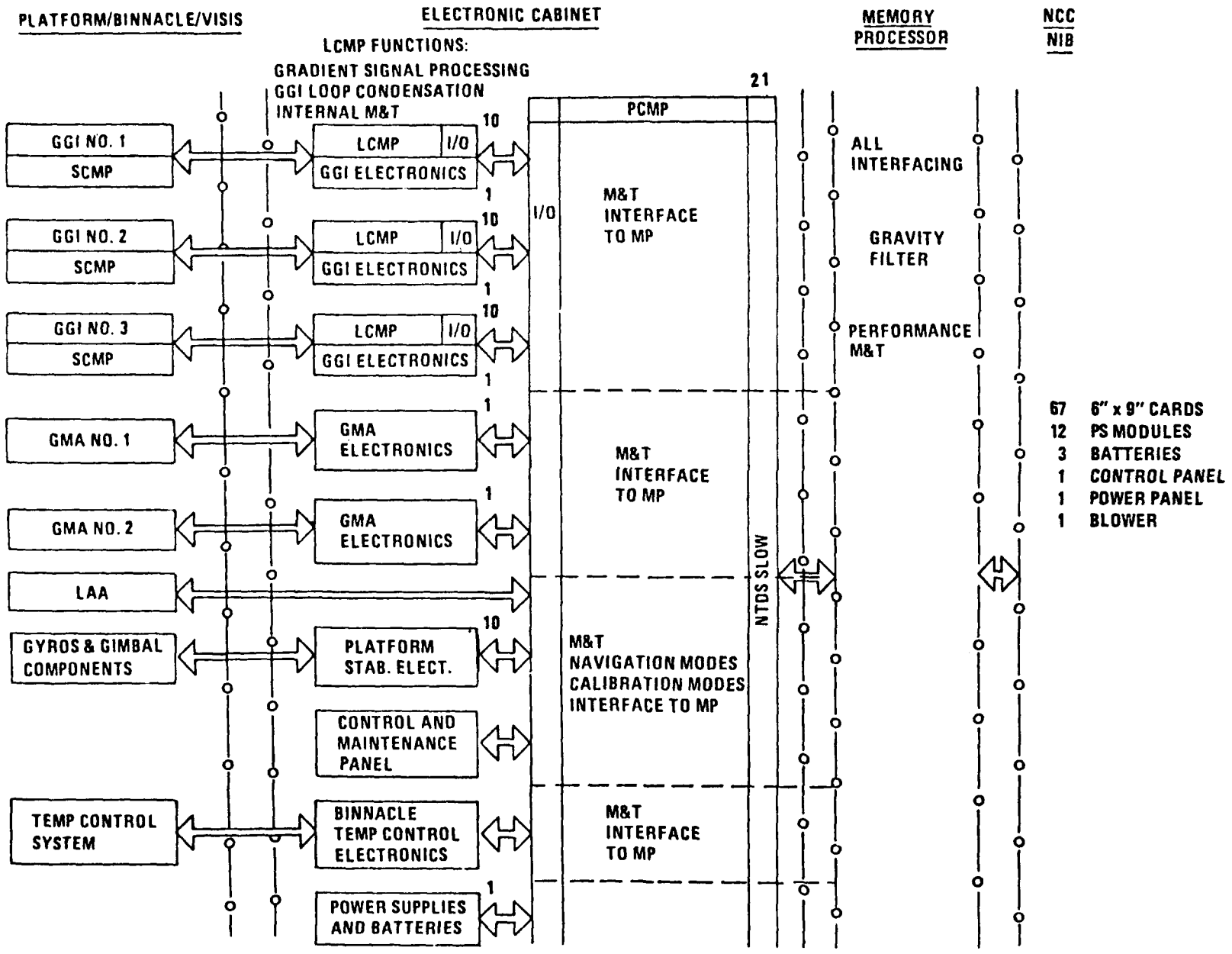

GEC CONCEPTUAL DESIGN

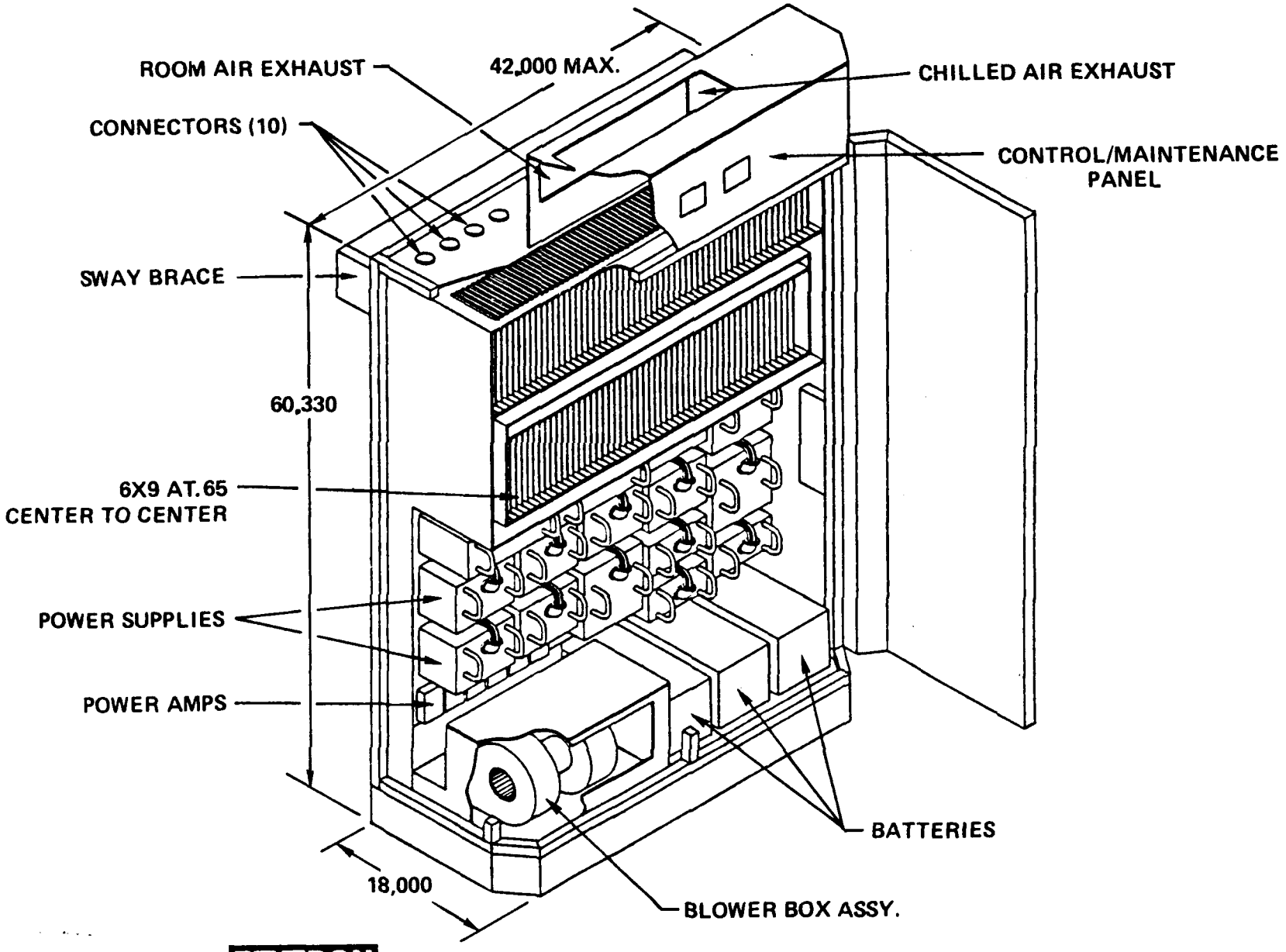

Bell Aerospace TEXTRON

GSS ADM TO GSS OS DELTAS

	GSS ADM	GSS FSD	RATIONALE
GMS's	0	2	ADDITIONAL GRAVITY FIELD INFORMATION
VSIS FREQUENCY RESPONSE	9 Hz	5 Hz	SHOCK ISOLATION
PLATFORM WIRING	POINT TO POINT COST REDUCTION	WIRE HARNESSES	COMPLEXITY AND COST REDUCTION
MICROPROCESSORS (LCMP's)	TI 9900	MOTOROLA 68000	HI-REL COMPONENT
PLATFORM CONTROL	VAX 11/780	MOTOROLA 68000	IMPROVED PARTIONING WITH MP
MAINTAINABILITY/ TESTABILITY	MANUAL ONLY	AUTOMATIC FAULT DETECTION AND ISOLATION	MINIMIZE SAILOR INTERVENTION
ELECTRONIC CABINETS	2	1	SPACE AND COMPLEXITY REDUCTION
ELECTRONIC BOARD SIZE	SEMS	6 IN. x 9 IN.	M&T REQ.
GGI SLIP RING MAINTENANCE INTERVAL	3000 HOURS	MORE THAN 20,000 HOURS	MAINTAINABILITY IMPROVEMENT
HANDBOOK (TASK ANALYSIS)	ENG. LEVEL	GJ-12-1793A	FOR OPERATION BY SAILOR'S
BATTERY BACK-UP	NONE	YES	TEMPORARY PRIME POWER OUTLINE

BASIC FAULT ISOLATION EFFECTIVENESS GOALS

- 95% Probability of On-Line Fault Detection
- 98% Probability of Off-Line Fault Detection
- 95% Probability of Fault Isolation on First Pull

FUNCTIONAL STRATEGY/INSTRUMENTATION FOR M/T

- PCMP Provides Central Control for Fault Isolation M/T
- Full Function or Functions on Cards for Efficient M/T
- Individual GGI or GMA Instruments and Associated Electronics Can be Taken Off-Line and Fault Isolation Performed Thereon While GSS Remains On-Line
- Complete Confidence Test of Each Board and Component on Turn On

B-507U

COMPARISON OF AT-SEA GRADIOMETER TEST RESULTS WITH AN INDEPENDENT GRAVITY GRADIENT REFERENCE

Presented At

TWELFTH MOVING BASE GRAVITY GRADIOMETER CONFERENCE
UNITED STATES AIR FORCE ACADEMY

14-15 February 1984

Dynamics Research Corporation
60 Concord Street
Wilmington, Massachusetts 01887

ABSTRACT

COMPARISON OF AT-SEA GRADIOMETER TEST RESULTS WITH AN INDEPENDENT GRAVITY GRADIENT REFERENCE

Donald O. Benson, Jr., Alan H. Zorn, and Bernard J. Regenauer
Dynamics Research Corporation
60 Concord Street
Wilmington, Massachusetts 01887

At-sea demonstration and testing of the Bell Gravity Gradiometer near coastal regions is desirable to allow access of engineering personnel for equipment grooming and maintenance, and to obtain reasonable signal-to-noise ratios since large deflections and gradients occur near many coastal regions (Ref. 1). Reference gravity maps in these regions either do not exist, do not have sufficient accuracy when derived from satellite altimetry or are extremely time consuming to survey using gravimetric methods.

This presentation discusses the generation of a gravity gradient reference off the north coast of Puerto Rico and subsequent comparison of Gravity Gradiometer gradients with the reference. The gradient reference was derived using position differences between an accurate marine inertial system and an accurate geodetic position reference, Autotape. Similar techniques have been used for vertical deflections over land but, in contrast, require frequent stopping for gyro recalibration (Ref. 2). Feasibility of the at-sea survey technique was established using covariance error analysis. Subsequently a test plan was developed to acquire data for map development, and the survey was performed with equipment onboard the USNS Vanguard. Returns over the same paths and crossing paths during the survey allow separation of time varying gyro and accelerometer errors from position varying gradients and deflections when the survey data is processed. The analysis and data processing include local geodetic constraints on the gradients to satisfy conditions of the earth's gravitational potential (Ref. 3).

The survey paths were repeated on a later at-sea test with the Bell Gravity Gradiometer onboard. Gravity gradients from the gradiometer compare remarkably well with the independent gravity gradient reference along the survey paths.

References

1. Dehlinger, P., Marine Gravity, Elsevier Scientific Publishing Co., New York, 1978.

2. "Proceedings of the Second International Symposium on Inertial Technology for Surveying and Geodesy," Banff, Canada, June 1-5, 1981.

3. Heiskanen, W. A. and Moritz, H., Physical Geodesy, W. H. Freeman & Co., San Francisco, 1967.

COMPARISON OF AT-SEA GRADIOMETER TEST RESULTS WITH AN INDEPENDENT GRAVITY GRADIENT REFERENCE

OVERVIEW

PART I: DEVELOPMENT OF AN INDEPENDENT GRAVITY GRADIENT REFERENCE

PART II: COMPARISON OF AT-SEA GRADIOMETER TEST RESULTS WITH REFERENCE

DEVELOPMENT OF AN INDEPENDENT GRAVITY GRADIENT REFERENCE

OVERVIEW - PART I

- BACKGROUND AND THEORY
- FEASIBILITY ANALYSIS LEADING TO A TEST PLAN
- THE TEST PLAN

DEVELOPMENT OF AN INDEPENDENT GRAVITY GRADIENT REFERENCE

BACKGROUND AND THEORY

- METHOD BASED ON DIFFERENCES BETWEEN HIGHLY ACCURATE ESGM INERTIAL NAVIGATION SYSTEM (INS) OUTPUTS AND GEODETIC POSITION REFERENCE (AUTOTAPE)
  - Vertical Deflections Cause INS Position and Velocity Errors
  - If INS Position Errors are Measured Then Vertical Deflections (and Their Gradients) Can Be Determined:

Measurement: $Z = P_{INS} - P_{REF}$

But: $P_{INS} = P_{TRUE} + \delta P_{INS}$

$P_{REF} = P_{TRUE} + \delta P_{REF}$

Then: $Z = \delta P_{INS} - \delta P_{REF}$

- THIS METHOD ALSO CALLED DIRECT RECOVERY TECHNIQUE (DRT) IS NOT NEW
- TECHNIQUES USED TO ELIMINATE ERROR SOURCES AND PROCESS THE DATA ARE NEW

BACKGROUND AND THEORY

- PROBLEMS THAT MUST BE SOLVED FOR EFFECTIVE USE OF DRT
  - Other Error Sources Also Cause INS Position and Velocity Errors

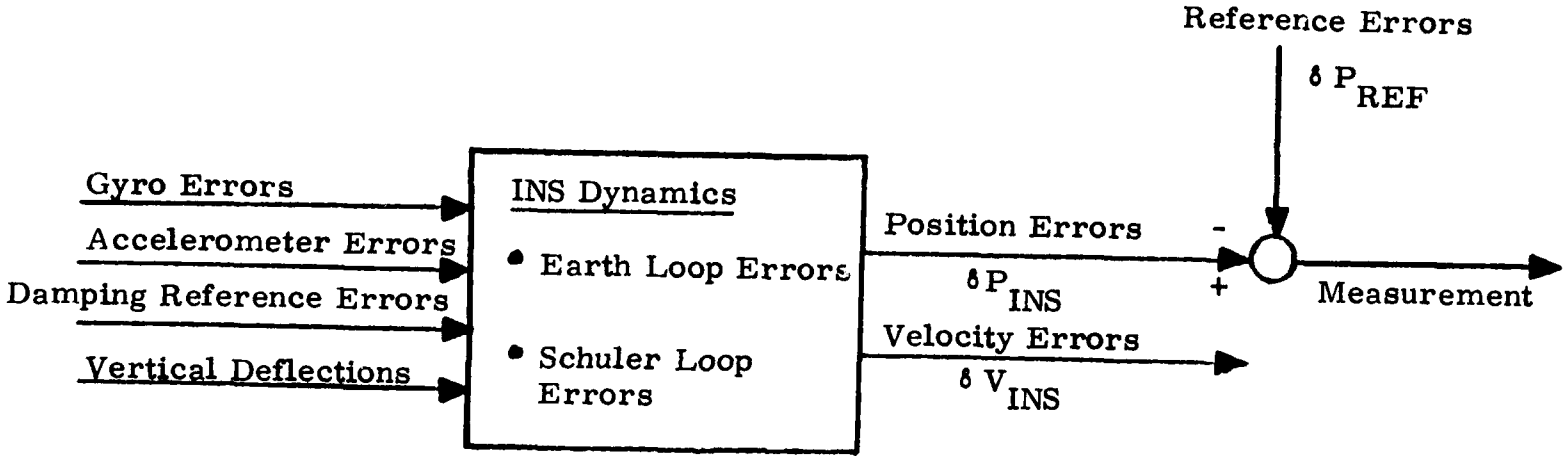

  - INS Dynamics Must be Taken Into Account

BACKGROUND AND THEORY

- ELIMINATION AND MINIMIZATION OF ERROR SOURCES
  - Gyro Errors Cause Psi (ψ) Angle Earth Loop Errors to Oscillate and Build Up With Time
    - Dockside calibration reduces magnitude of gyro errors
    - Buildup of ψ errors slow with long-term stability of ESGM system
  - Accelerometer Errors Cause Schuler Loop Errors
    - Dockside calibration also reduces accelerometer errors
    - Calibration coefficients stable in ESGM system
  - Damping Reference Errors Also Cause Schuler Loop Errors
    - Error source substantially eliminated by running free inertial during survey
  - Position Reference Errors Can Not Be Distinguished From Vertical Deflections
    - Error source virtually eliminated by using highly accurate Autotape reference
  - Residual Errors Still Remain
    - Further reduction achieved by returning over same path
    - Gravity Gradients are function of position while remaining errors are functions of time

BACKGROUND AND THEORY

- INS DYNAMICS AND STRUCTURE OF RESIDUAL ERRORS TAKEN INTO ACCOUNT BY MODELLING AS LINEAR DYNAMIC SYSTEM

- DATA PROCESSING BASED ON KALMAN FILTER/SMOOTHER ALGORITHMS

FEASIBILITY ANALYSIS LEADING TO A TEST PLAN

TRADE-OFF OF DOCKSIDE CALIBRATION TIME

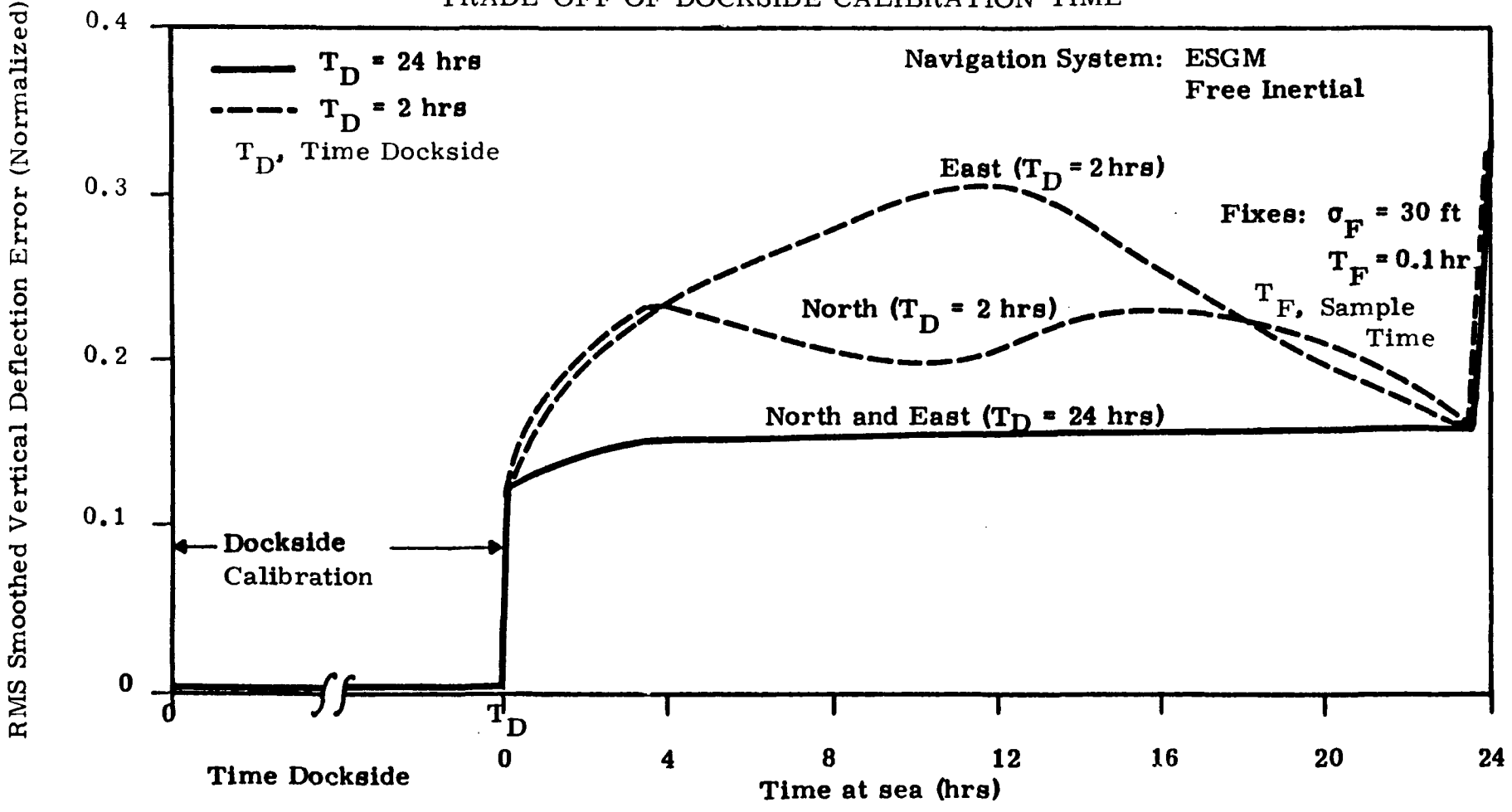

FEASIBILITY ANALYSIS LEADING TO A TEST PLAN

TRADE-OFF OF DATA RATES

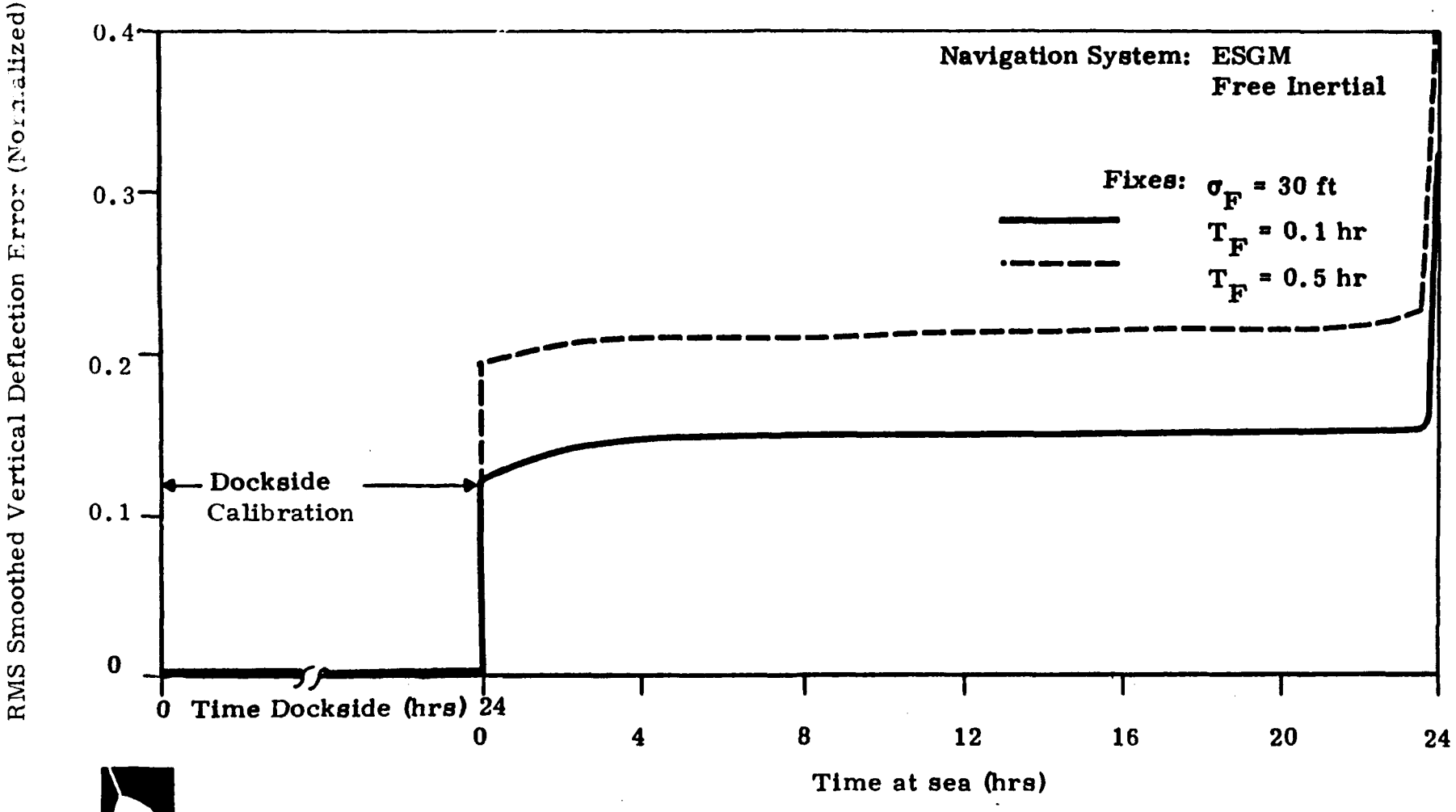

DEVELOPMENT OF AN INDEPENDENT GRAVITY GRADIENT REFERENCE

FEASIBILITY ANALYSIS LEADING TO A TEST PLAN

TRADE-OFF OF EQUIPMENT CONFIGURATIONS - NEED ESGM

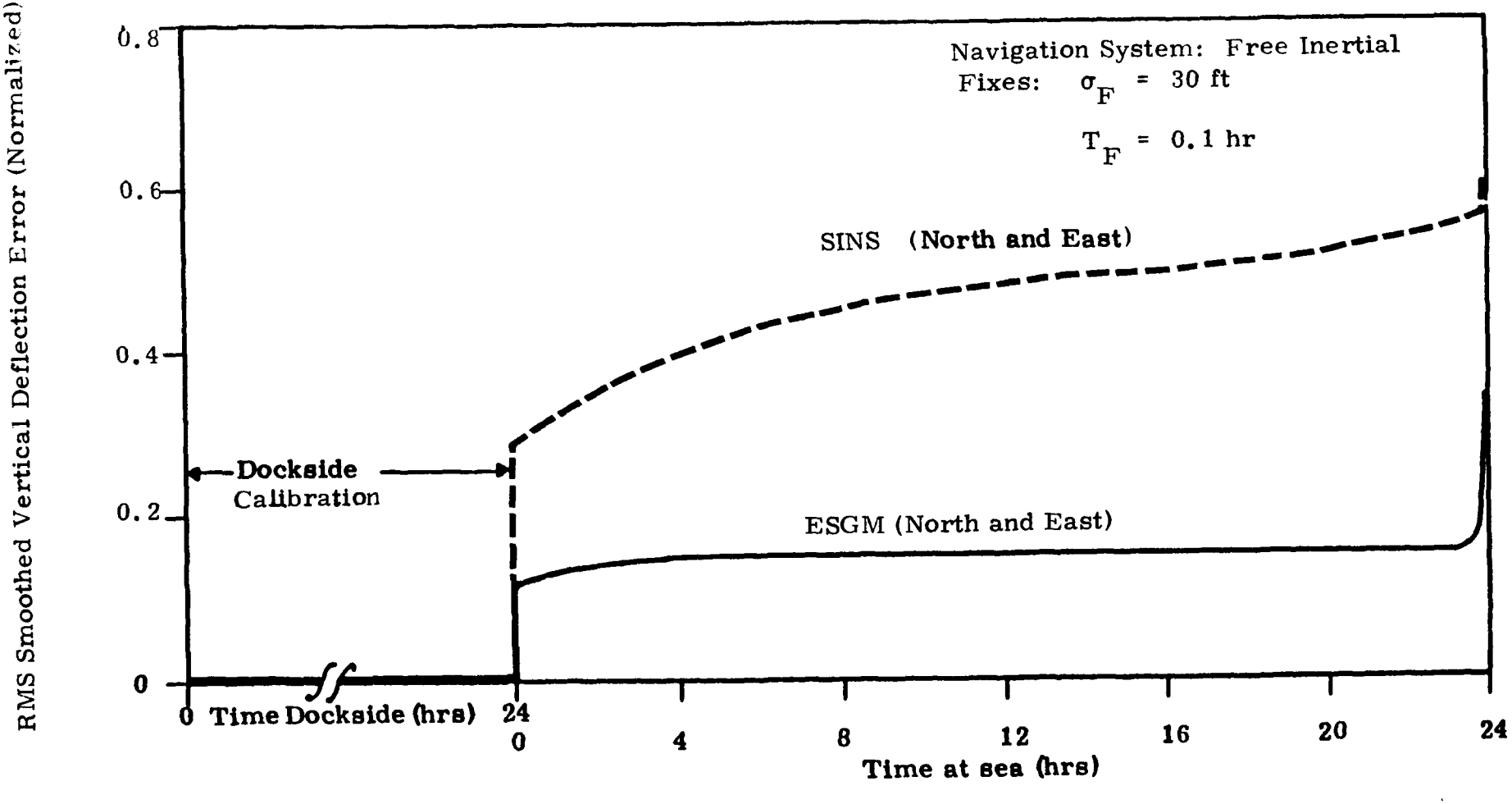

DRC

THE TEST PLAN

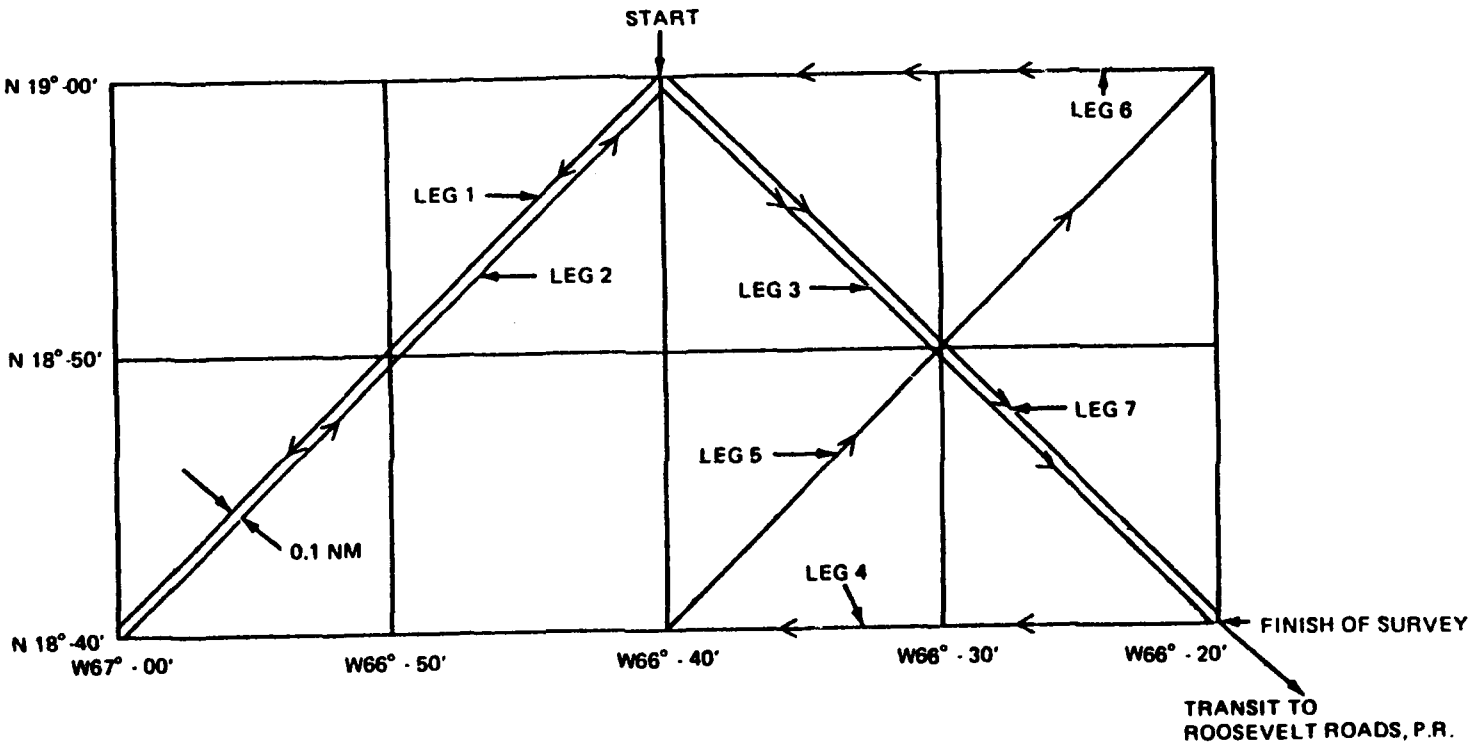

- ESGM Free Inertial During Survey
- One Sample Per Second Data Rate
- Return and Crossing Paths Included in Survey Pattern
- Survey Track Spacing Determined From Bottom Depth Profile
- Dockside Time For Calibration 30 Hours

COMPARISON OF AT-SEA GRADIOMETER TEST RESULTS WITH REFERENCE

OVERVIEW - PART II

- GRADIOMETER CONFIGURATION AND MODE OF OPERATION
- GRADIOMETER DATA REDUCTION
- RESULTS

COMPARISON OF AT-SEA GRADIOMETER TEST RESULTS WITH REFERENCE

GRADIOMETER CONFIGURATION AND MODE OF OPERATION

- BELL AEROSPACE GRAVITY SENSOR SYSTEM (GSS) ADVANCED DEVELOPMENT MODEL (ADM)

- THREE GRAVITY GRADIOMETER INSTRUMENTS (GGI) ARRANGED IN UMBRELLA CONFIGURATION - EACH GGI MEASURES TWO COMPONENTS OF GRAVITY GRADIENT

- GGIs CAROUSELLED ABOUT VERTICAL AT ω_C = 500 DEG/HR

GRADIOMETER DATA REDUCTION

- REFERENCE NOT USED IN ANY WAY TO AID IN PROCESSING
- 2-MINUTE AVERAGES
- CORRECTIONS MADE FOR
  - Factory Scale Factor
  - Ship and Gimbal Self-Gradients
  - Angular Acceleration Gradient
- BIAS AND RAMP OF GGI DETERMINED FROM COARSE AT-SEA CALIBRATION
- IN COMPUTING GRAVITY GRADIENT TENSOR ELEMENTS FROM GGI OUTPUTS, REDUNDANT MEASUREMENTS RESOLVED USING LEAST SQUARES

COMPARISON OF AT-SEA GRADIOMETER TEST RESULTS WITH REFERENCE

Γ_{NE}

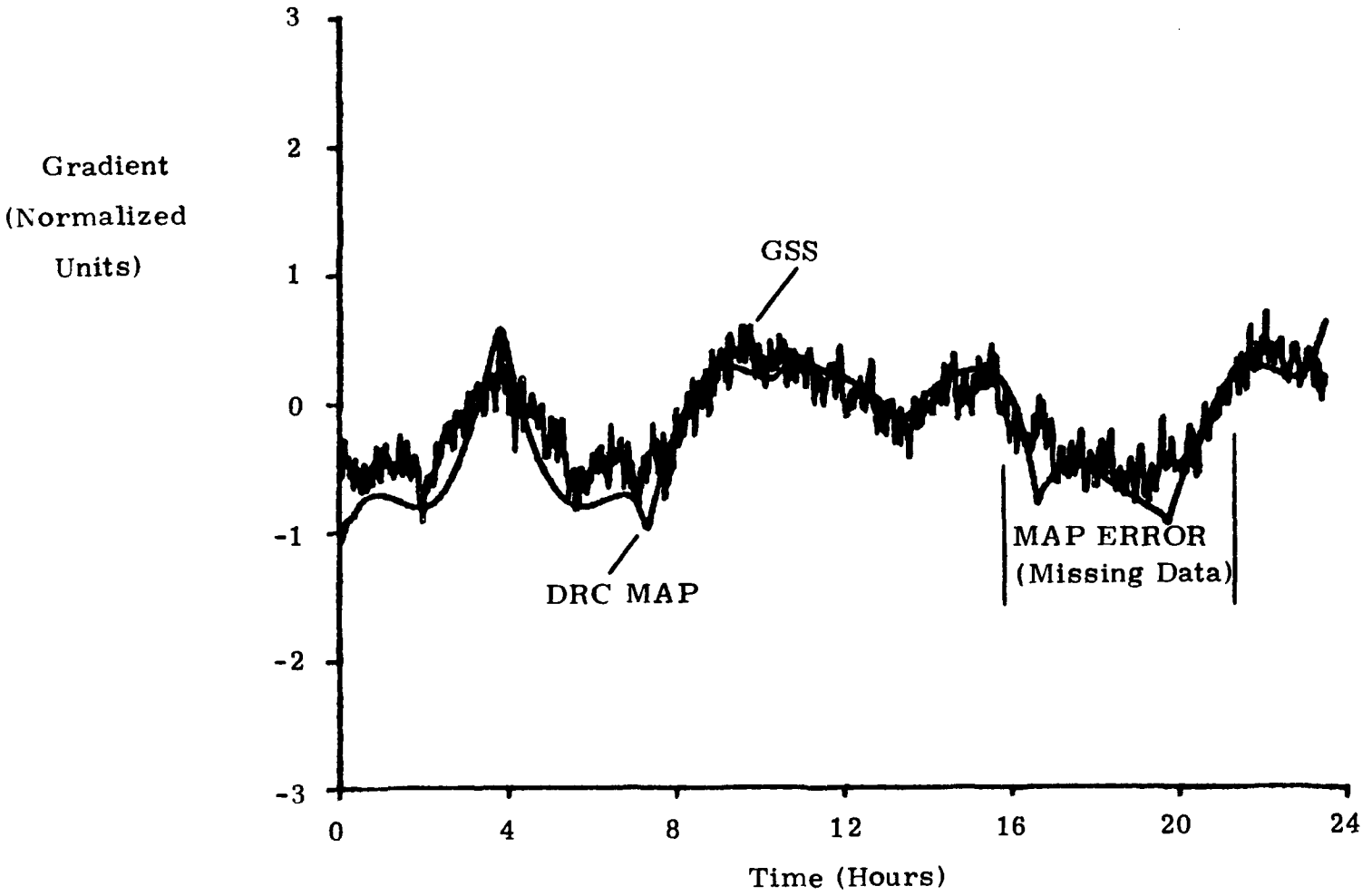

- GSS BIAS AND LF ERRORS ARE MODULATED BY 2 ω_C IN Γ_{NE}

COMPARISON OF AT-SEA GRADIOMETER TEST RESULTS WITH REFERENCE

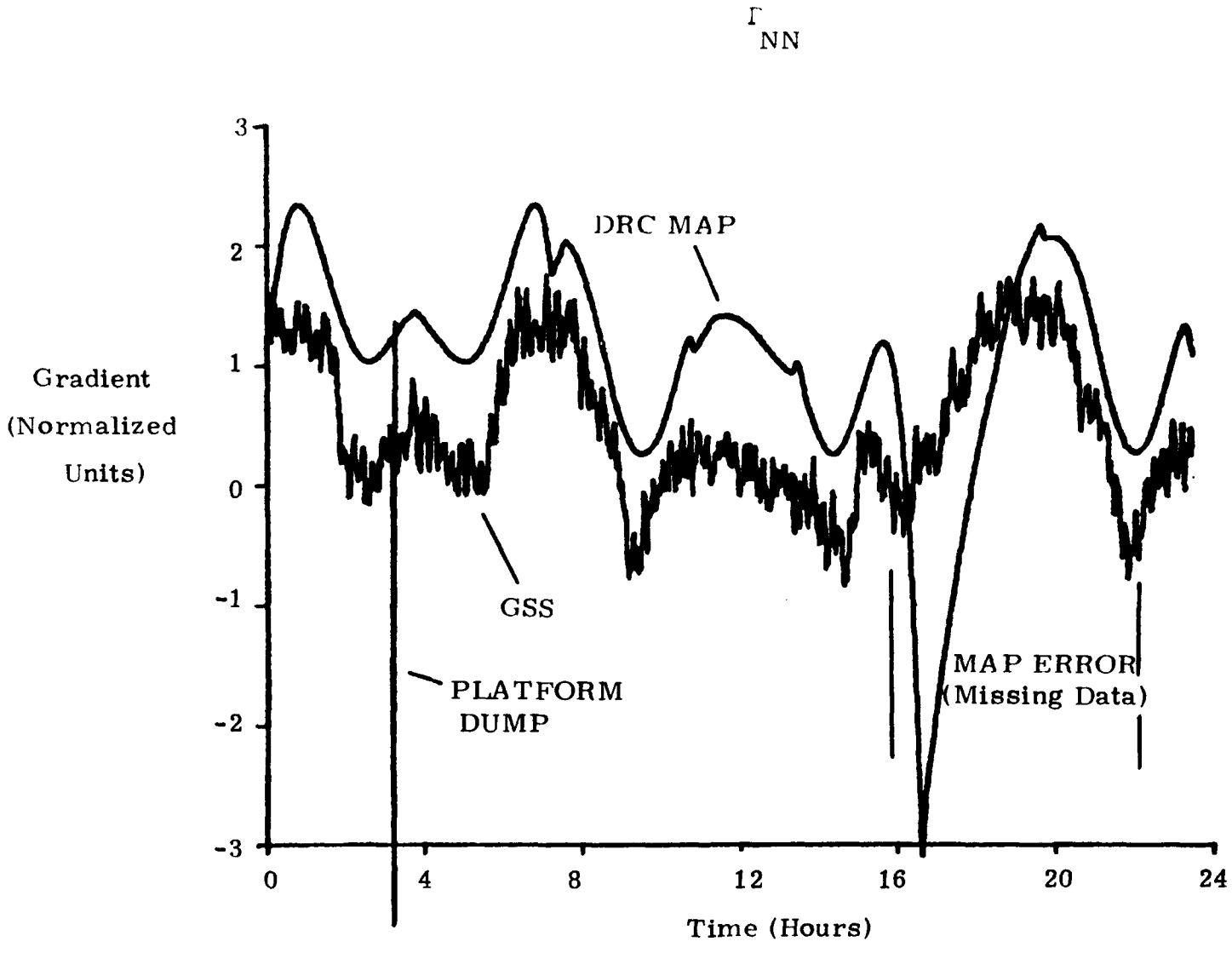

- CONSTANT DIFFERENCE ATTRIBUTABLE TO THE UNMODULATED COMPONENT OF GSS BIAS

COMPARISON OF AT-SEA GRADIOMETER TEST RESULTS WITH REFERENCE

Γ_{EE}

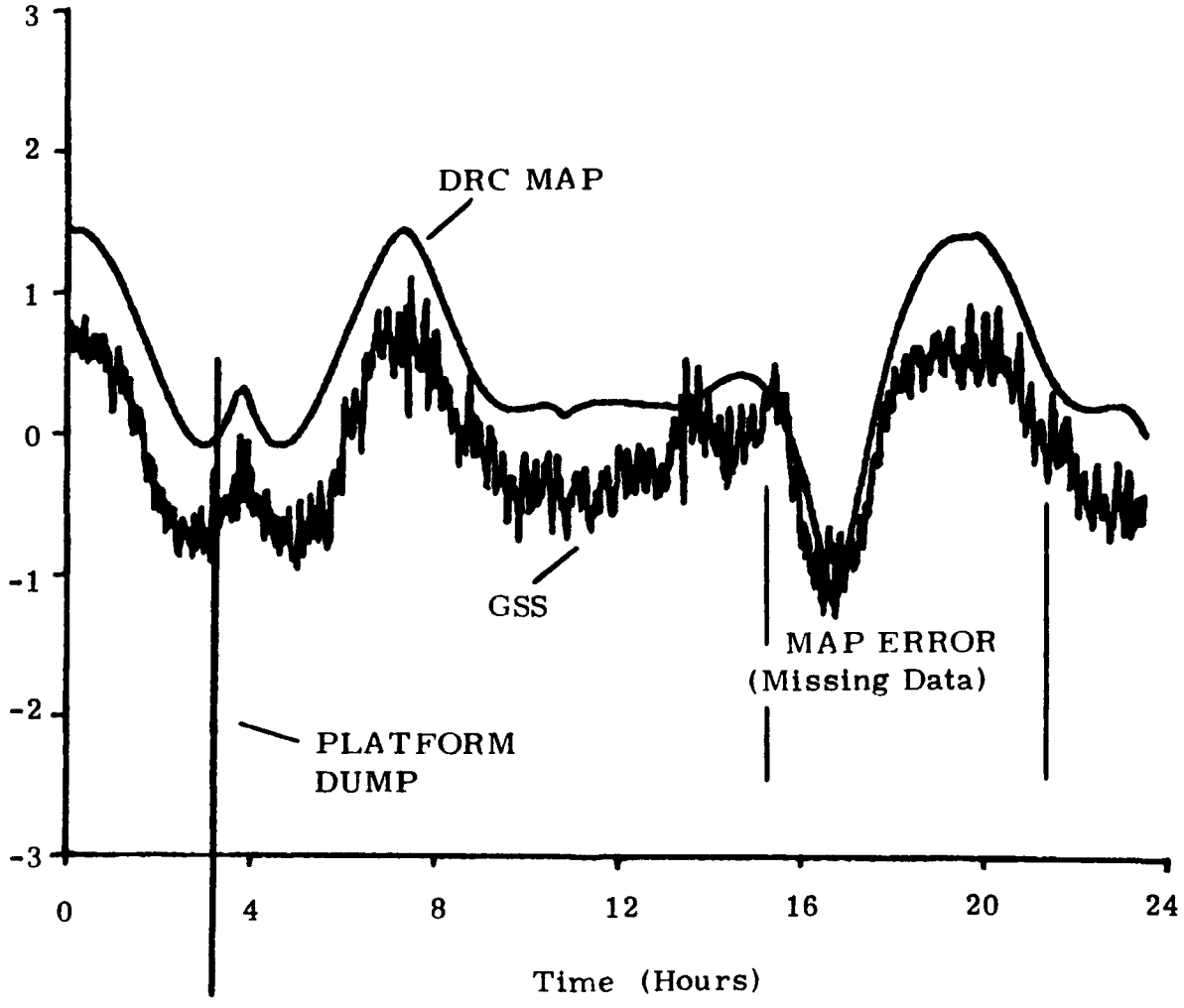

- CONSTANT DIFFERENCE IN Γ_{FF} SAME AS THAT IN Γ_{NN}

$(\Gamma_{NN} - \Gamma_{EE})/2$

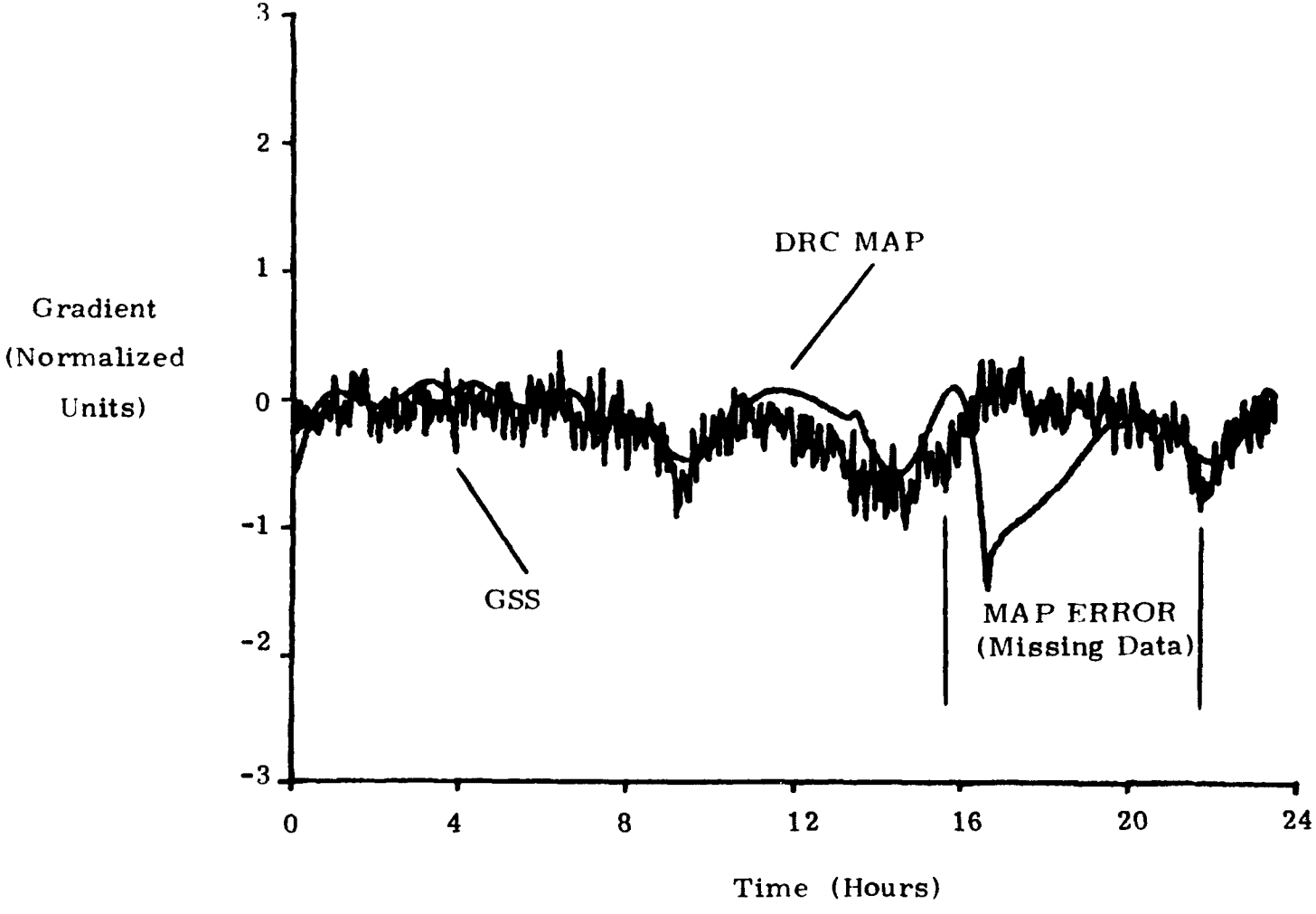

- JUST AS IN Γ_{NE}, GSS BIAS AND LF ERRORS ARE MODULATED BY 2 ω_C – HENCE NO CONSTANT DIFFERENCE

CONCLUSIONS

- FIRST SUCCESSFUL TEST OF GSS AGAINST TOTALLY INDEPENDENT REFERENCE

- DIRECT RECOVERY TECHNIQUE IMPLEMENTED ON MOVING BASE A VIABLE ALTERNATIVE TO GRAVIMETRIC AND SATELLITE SURVEY METHODS NEAR COASTAL REGIONS

- EXCELLENT COMPARISON SUBSTANTIATES BOTH MAP QUALITY AND BELL GRADIOMETER PERFORMANCE

SP-4423-6

CURRENT AIRBORNE GGSS PERFORMANCE EXPECTATIONS AND ERROR ALLOCATIONS

14-15 February 1984

Prepared for:

TWELFTH MOVING BASE GRAVITY GRADIOMETER REVIEW
United States Air Force Academy
Colorado

THE ANALYTIC SCIENCES CORPORATION
One Jacob Way
Reading, Massachusetts 01867

A-5368

CURRENT AIRBORNE GGSS PERFORMANCE EXPECTATIONS AND ERROR ALLOCATIONS

TASC
THE ANALYTIC SCIENCES CORPORATION

OVERVIEW

A-536J

- REVIEW OF TEST/SURVEY GEOMETRY AND GOALS
- DISCUSSION OF ERROR SOURCES
- GGSS SENSITIVITY TO VARIATIONS IN FREQUENCY CONTENT OF GRAVITY FIELD
- CONTRIBUTIONS OF EACH CLASS OF ERRORS
- SENSITIVITY TO SURVEY ALTITUDE
- CONCLUSIONS

TASC
THE ANALYTIC SCIENCES CORPORATION

NOMINAL AIRBORNE GGSS* TEST SCENARIO

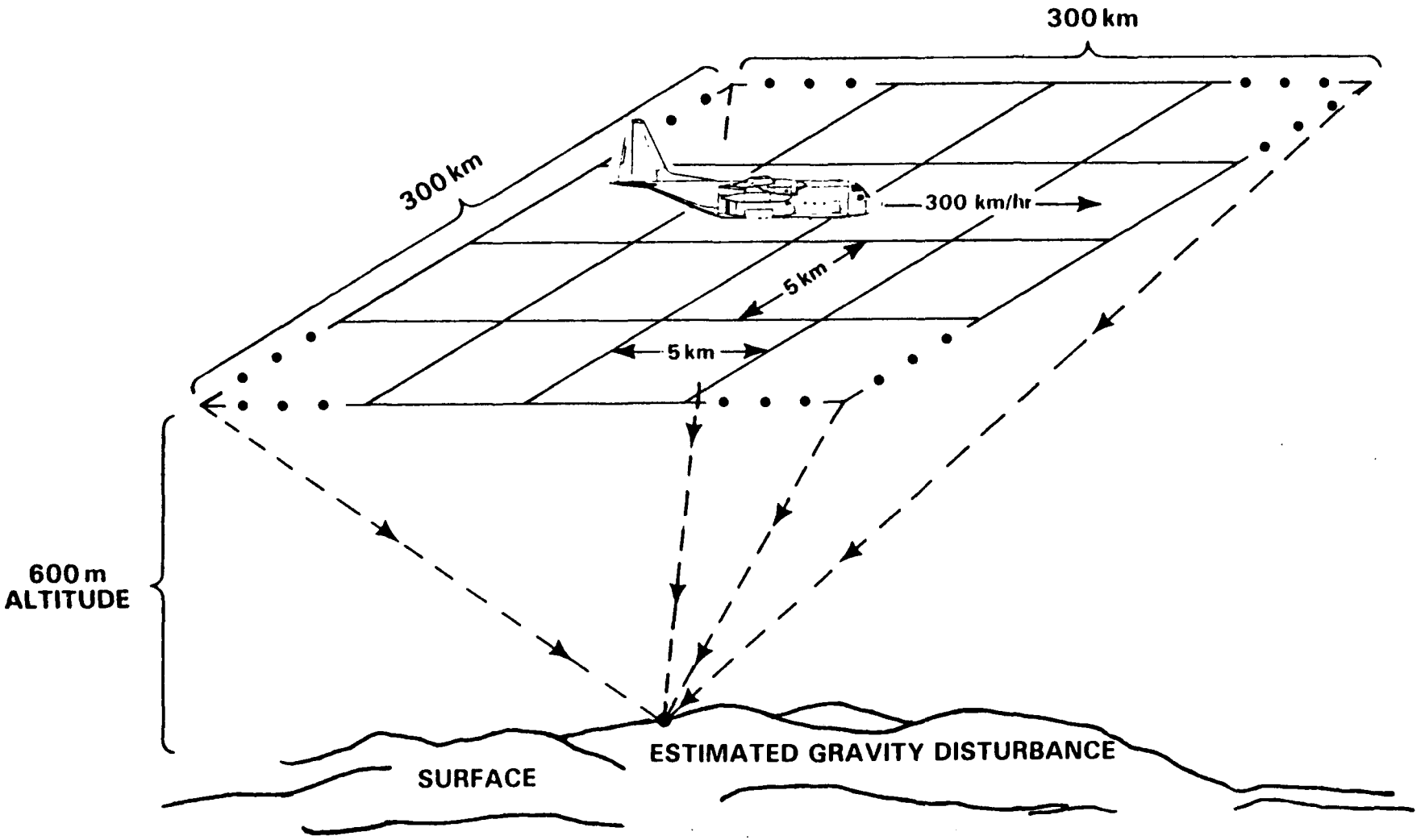

*GRAVITY GRADIOMETER SURVEY SYSTEM.

TASC
THE ANALYTIC SCIENCES CORPORATION

PERFORMANCE SPECIFICATIONS AND GOALS

A 5370

ERRORS IN HIGH FREQUENCY PORTION OF RECOVERED GRAVITY DISTURBANCE VECTOR AT THE SURFACE

- GGSS PERFORMANCE IS SPECIFIED AT GRAVITY WAVELENGTHS OF 500 km AND SHORTER
- LONG WAVELENGTH GGSS RECOVERY IS NOT SPECIFIED BUT WILL BE UTILIZED DURING SURVEY OPERATIONS
- rms DEFLECTION ERROR (PER AXIS) $\leq$ 0.18 $\widehat{sec}$
- rms VERTICAL DISTURBANCE ERROR $\leq$ 0.9 mgal

OVERALL GOAL FOR RECOVERY OF ENTIRE GRAVITY DISTURBANCE (ALL WAVELENGTHS)

- COMBINE GRADIOMETER DATA WITH EXISTING/FUTURE LONG WAVELENGTH GRAVITY MEASUREMENTS
- rms DEFLECTION ERROR (PER AXIS) $\leq$ 0.2 $\widehat{sec}$
- rms VERTICAL DISTURBANCE ERROR $\leq$ 1.0 mgal

TASC
THE ANALYTIC SCIENCES CORPORATION

KEY ERROR SOURCE CATEGORIES

A-5371

- GRADIOMETER SYSTEM NOISE
- SAMPLING EFFECTS
- DOWNWARD CONTINUATION
- LIMITED DATA EXTENT

TASC
THE ANALYTIC SCIENCES CORPORATION

GGSS-RELATED ERRORS—GRADIOMETER SYSTEM NOISE

A-1780

- GRAVITY GRADIOMETER INSTRUMENT (GGI) SELF-GENERATED NOISE
- ENVIRONMENTAL SENSITIVITIES
  - LINEAR AND ANGULAR ACCELERATIONS
  - TEMPERATURE FLUCTUATIONS
  - MAGNETIC FIELDS
  - PRESSURE SENSITIVITY
- NAVIGATION, ATTITUDE AND ATTITUDE RATE (JITTER) CONTROL
- GIMBAL AND VEHICLE SELF-GRADIENT COMPENSATION

TASC
THE ANALYTIC SCIENCES CORPORATION

SURVEY LIMITATIONS

A-1781

- SAMPLING EFFECTS

  ALIASING - ERROR DUE TO MISRECOGNITION OF HIGH-FREQUENCY* COMPONENTS

  HIGH-FREQUENCY TRUNCATION - ERROR RESULTING FROM FAILURE TO OBSERVE HIGH-FREQUENCY* COMPONENTS

  BOTH ACT ALONG-TRACK AS WELL AS CROSS-TRACK

- DOWNWARD CONTINUATION - ERROR DUE TO LOSS OF SHORT WAVELENGTH PORTION OF GRAVITY GRADIENT SIGNAL BECAUSE OF ATTENUATION WITH ALTITUDE

- LIMITED DATA EXTENT - ERROR ASSOCIATED WITH LOSS OF LONG WAVELENGTH PORTION OF GRAVITY GRADIENT SIGNAL BECAUSE FAR FIELD IS NOT OBSERVED

*BEYOND ONE-HALF OF THE SAMPLING FREQUENCY

TASC
THE ANALYTIC SCIENCES CORPORATION

NOMINAL PARAMETERS FOR SURVEY SIMULATION

- GRADIOMETER NOISE MODEL

  $1.7 \times 10^{-4}/f^{1.6} + 55.0\ E^2/Hz$, DOUBLE-SIDED

  $1.06 \times 10^{-3}/\omega^{1.6} + 17.5\ E^2/rad/sec$, SINGLE-SIDED

- BASELINE SURVEY OPERATING CONDITIONS

  SPEED - 300 km/hr
  ALTITUDE - 600 m
  TRACK SPACING - 5 km
  AZIMUTHS - BIDIRECTIONAL (EAST-WEST, NORTH-SOUTH)

- GGSS-UNIQUE PARAMETERS

  CUTOFF WAVELENGTH - 500 km
  ASSUMED SAMPLING INTERVAL (AVERAGING TIME) - 10 sec

TASC
THE ANALYTIC SCIENCES CORPORATION

ESTIMATION OF FINITE EXTENT EFFECTS

A-1682

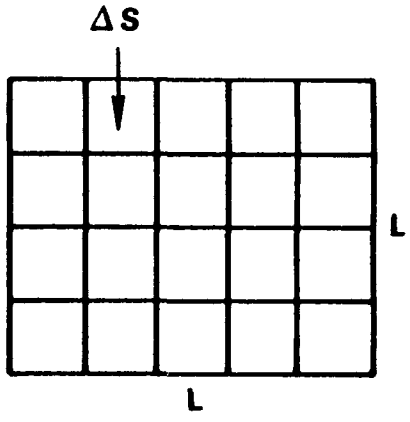

- OPTIMAL ERROR COVARIANCE EQUATIONS: $C_{ee} = C_{xx} - C_{xz}C_{zz}^{-1}C_{zx}$
  (COLLOCATION SOLUTION IMPLEMENTED USING GEOFAST ALGORITHM)
- PARALLEL TRACKS IN ORTHOGONAL DIRECTIONS
  DATA DIMENSION L × L
  TRACK SPACING ΔS (km)
- MEASUREMENTS OF T_{zz} AT ZERO ALTITUDE
- ALIASING DUE TO FINITE TRACK SPACING REMOVED BY TRUNCATING HIGH FREQUENCY MODEL CONTRIBUTIONS (WAVELENGTHS LESS THAN 2 ΔS)
- GRADIOMETER MEASUREMENT NOISE SET TO ZERO
- RESULTS EVALUATE EFFECT OF SURVEY EXTENT ONLY

TASC
THE ANALYTIC SCIENCES CORPORATION

VERTICAL DISTURBANCE RECOVERY vs DATA EXTENT

- WORLDWIDE ATTENUATED WHITE NOISE GRAVITY MODEL WITH WAVELENGTHS >500 km REMOVED
- 10 km TRACK SPACING WITH COMPENSATION FOR ALIASING
- RMS ERROR AT CENTER OF DATA REGION
- COMPUTER TIME REQUIRED TO IMPROVE NUMERICAL ACCURACY BOUND IS UNECONOMICAL
- LOWER BOUND ESTABLISHED BY ANALYSIS OF AVAILABLE PRECISION
- RESULT AT 620 km EQUIVALENT TO INVERTING COVARIANCE MATRIX WITH 3844^2 ELEMENTS (CORRESPONDING TO 62^2 DATA POINTS)

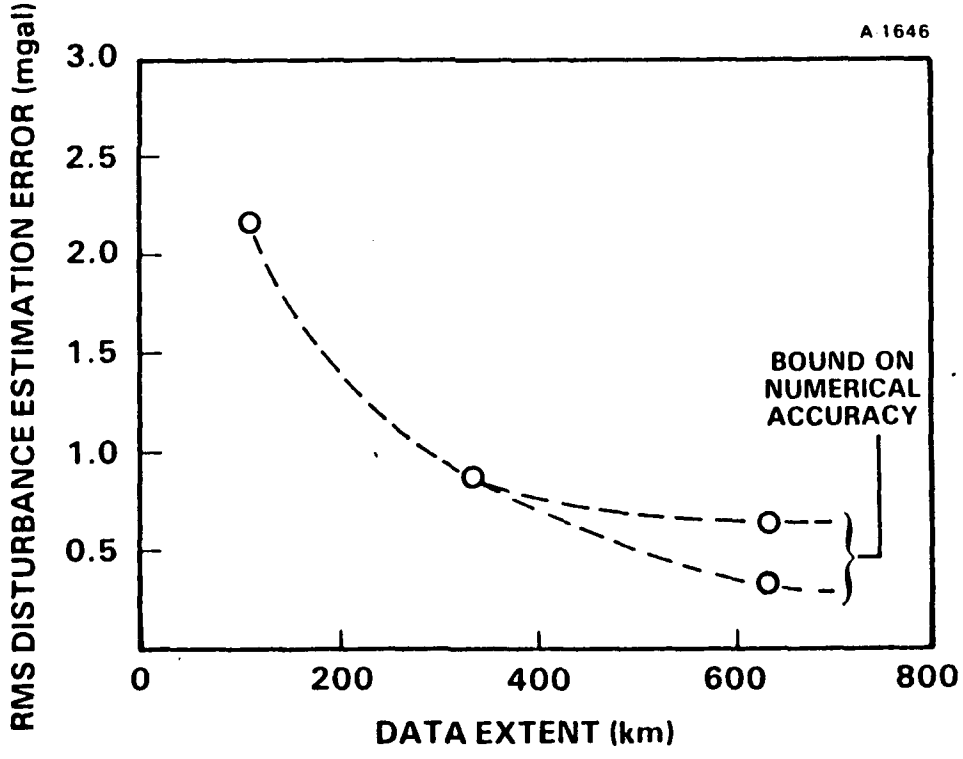

TASC
THE ANALYTIC SCIENCES CORPORATION

SENSITIVITY OF GGSS SHORT-WAVELENGTH* RECOVERY TO GRAVITY FIELD MODEL FOR NOMINAL SURVEY CONDITIONS

A-1779

GRAVITY FIELD MODEL	rms SURVEY ERROR		ERROR AS A PERCENT OF rms GGSS SPECIFICATION	
	DEFLECTION OF THE VERTICAL† ($\widehat{sec}$)	VERTICAL GRAVITY DISTURBANCE‡ (mgal)	DEFLECTION OF THE VERTICAL	VERTICAL GRAVITY DISTURBANCE
ATTENUATED WHITE NOISE-APPROPRIATE FOR GRAVITATIONALLY SMOOTH AREAS	0.085	0.57	47%	63%
BASELINE - "TYPICAL" TERRAIN	0.096	0.66	53%	73%
ACTIVE - UNUSUALLY RUGGED TERRAIN	0.133	0.89	74%	99%

*WAVELENGTHS SHORTER THAN 500 km

†GGSS SPECIFICATION = 0.18 $\widehat{sec}$ rms

‡GGSS SPECIFICATION = 0.9 mgal

TASC
THE ANALYTIC SCIENCES CORPORATION

METHODOLOGY FOR COMPUTING INDIVIDUAL ERROR CONTRIBUTIONS AND SENSITIVITIES

A 1782

- COMPUTE NOMINAL rms RECOVERY ERROR (ALL ERROR SOURCES INCLUDED) - $\sigma_{1\ldots N}$
- COMPUTE rms RECOVERY ERROR IF i^{th} ERROR SOURCE ABSENT - $\sigma_{1\ldots i-1,i+1\ldots N}$
- COMPUTE rms CONTRIBUTION OF i^{th} ERROR SOURCE - $\sqrt{\sigma^2_{1\ldots N} - \sigma^2_{1\ldots i-1,i+1\ldots N}} = \sigma_i$
- COMPUTE PERCENT CONTRIBUTION OF i^{th} ERROR SOURCE TO TOTAL VARIANCE -

$$\text{PERCENT CONTRIBUTION} = 100 \times \sigma_i^2 / \sum_{i=1}^{N} \sigma_i^2$$

- COMPUTE CHANGE IN RECOVERY ERROR VARIANCE ASSOCIATED WITH A UNIT IMPROVEMENT IN NOMINAL ERROR VARIANCE LEVEL OR NOMINAL PARAMETER VALUE OF i^{th} ERROR SOURCE -

$$\frac{\partial\left(\sigma^2_{1\ldots N}\right)}{\partial m_i}$$

TASC
THE ANALYTIC SCIENCES CORPORATION

PRELIMINARY BUDGET VALUES FOR GGSS SURVEY ERROR SOURCES

A 1783

ERROR SOURCE (i)	NOMINAL QUANTITY AND VALUE (m_i)	PERCENTAGE OF ERROR VARIANCE CONTRIBUTED BY i^{th} SOURCE	ERROR SENSITIVITY $\frac{\partial\left(\sigma^2_{1\ldots N}\right)}{\partial m_i}$
GRADIOMETER SYSTEM NOISE	WHITE & RED NOISE $55 + 1.7/f^{1.6}$ E^2/Hz*	34%	6.5
SAMPLING EFFECTS	TRACK SEPARATION - 5 km	12%	9.2
DOWNWARD CONTINUATION	SURVEY ALTITUDE - 600 m	5%	1.7
LIMITED DATA EXTENT	BLOCK SIDE DIMENSION - 500 km	49%†	1.9†

*$17.5 + 10^{-3}/\omega^{1.6}$ E^2/rad/sec (SINGLE-SIDED)
†RESULTS BASED ON USE OF ACTIVE AND BASELINE MODELS

- rms ERROR IF SOURCES ARE TAKEN TO BE INDEPENDENT - 0.72 mgal
- ACTUAL rms ERROR WITH ALL SOURCES ACTING - 0.66 mgal (vs 0.9 mgal SPECIFICATION)
- rms ERROR IF SURVEY WERE GLOBAL - 0.43 mgal
- BASELINE GRAVITY MODEL, WAVELENGTHS LONGER THAN 500 km EXCLUDED

TASC

SENSITIVITY OF rms VERTICAL DISTURBANCE RECOVERY ERROR TO SURVEY ALTITUDE

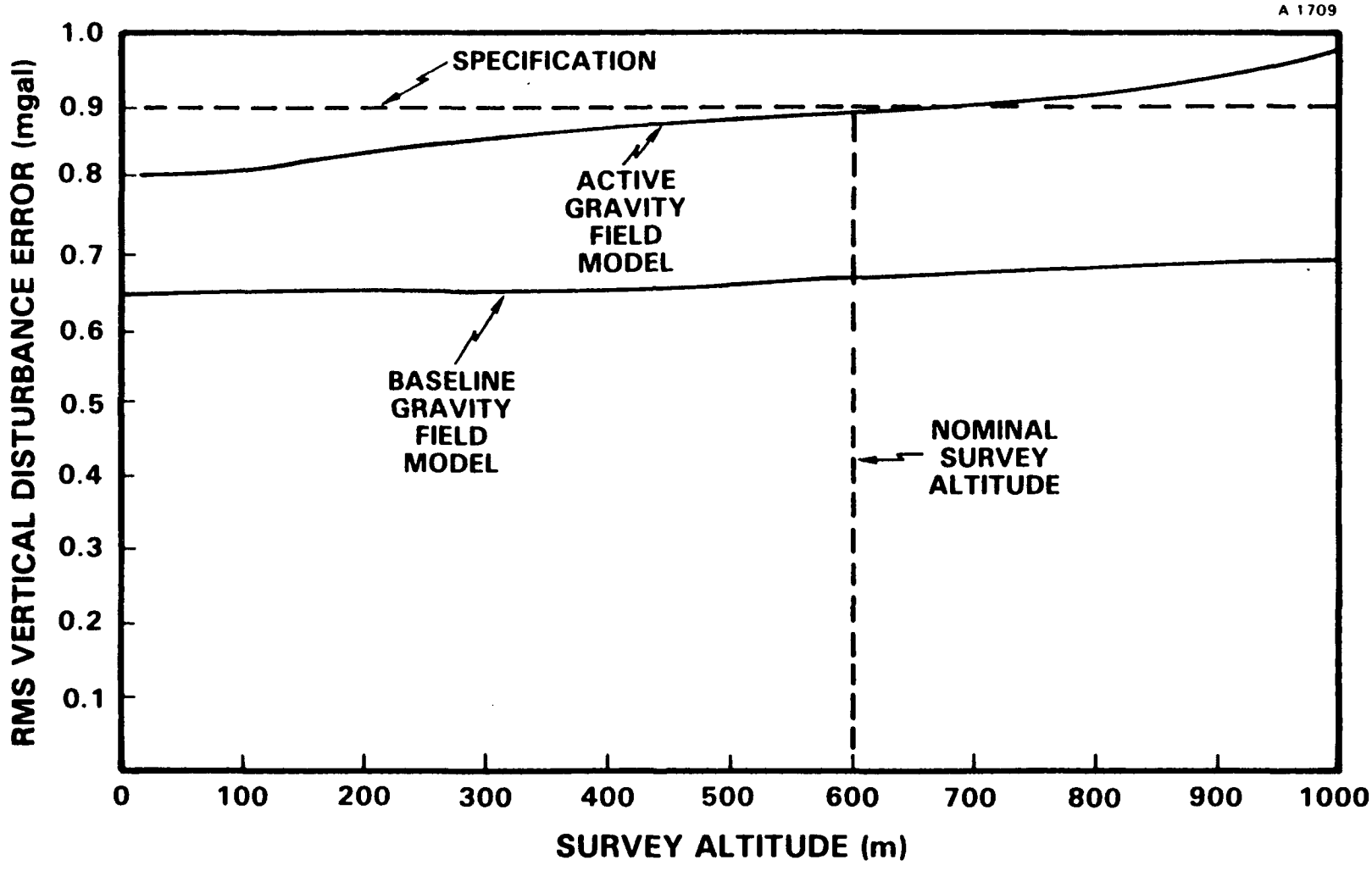

TASC
THE ANALYTIC SCIENCES CORPORATION

PRELIMINARY BUDGET VALUES FOR GGSS SURVEY ERROR SOURCES

A-1785

ERROR SOURCE (i)	NOMINAL QUANTITY AND VALUE (m_i)	PERCENTAGE OF ERROR VARIANCE CONTRIBUTED BY i^{th} SOURCE	ERROR SENSITIVITY $\frac{\partial(\sigma^2_{1\ldots N})}{\partial m_i}$
GRADIOMETER SYSTEM NOISE	WHITE & RED NOISE $55 + 1.7/f^{1.6}$ E^2/Hz*	38%	6.2
SAMPLING EFFECTS	TRACK SEPARATION - 5 km	7%	6.7
DOWNWARD CONTINUATION	SURVEY ALTITUDE - 1000 m	10%	4.4
LIMITED DATA EXTENT	BLOCK SIDE DIMENSION - 500 km	45%†	1.8†

*$17.5 + 10^{-3}/\omega^{1.6}$ E^2/rad/sec (SINGLE-SIDED)
†RESULTS BASED ON USE OF ACTIVE AND BASELINE MODELS

- rms ERROR IF SOURCES ARE TAKEN TO BE INDEPENDENT - 0.74 mgal
- ACTUAL rms ERROR WITH ALL SOURCES ACTING - 0.69 mgal (vs 0.9 mgal SPECIFICATION)
- rms ERROR IF SURVEY WERE GLOBAL - 0.47 mgal
- BASELINE GRAVITY MODEL, WAVELENGTHS LONGER THAN 500 km EXCLUDED

TASC

CONCLUSIONS

A-5372

- SPECIFIED GGSS PERFORMANCE IS OBTAINABLE IF SURVEY PARAMETERS CAN BE MAINTAINED NEAR BASELINE VALUES
- ULTIMATE REFINEMENT OF ERROR BUDGET REQUIRES GRAVITY MODELS TUNED TO TEST AREA
- LONG WAVELENGTH DATA CAPABILITY OF GRADIOMETER WILL NOT BE DEMONSTRATED DURING TEST BECAUSE OF 300 × 300 km DATA LIMITATION
- HOWEVER, TEST RESULTS WILL PERMIT HIGH CONFIDENCE EXTRAPOLATIONS FROM MEASURED PERFORMANCE AT SHORT WAVELENGTHS TO SPECIFIED CAPABILITIES AT ALL WAVELENGTHS LESS THAN 500 km
- COMPARISON WITH POINT TRUTH MEASUREMENTS WILL REQUIRE ACCOUNTING FOR LONG WAVELENGTH COMPONENT (>500 km) OF THE GRAVITY DISTURBANCE VECTOR
- DMAAC one deg × one deg MEAN ANOMALY (OR DISTURBANCE) DATA BASE IS WELL-SUITED TO PROVIDE THE LONG WAVELENGTH SUPPLEMENT

TASC
THE ANALYTIC SCIENCES CORPORATION

EFFICIENT PROCESSING OF GRADIOMETER OUTPUTS USING A KALMAN FILTER

FEBRUARY 14-15, 1984

Bell Aerospace TEXTRON
Division of Textron Inc.

- MOTIVATION
- MARKOVIAN STRAIGHT TRACK GRAVITY MODEL
- KALMAN FILTER DESCRIPTION
- MAPPING PROBLEM
- KALMAN SMOOTHING RESULTS
- MASCON SYNTHETIC GRAVITY FIELD
- SIMULATION RESULTS
- FUTURE WORK

MOTIVATION

- GRADIOMETER MEASURES HIGH FREQUENCY COMPONENT OF FIELD SO MUST BE SAMPLED AT A HIGH RATE

- FIVE INDEPENDENT COMPONENTS OF SECOND ORDER TENSOR

⇒ REQUIREMENT FOR DATA COMPRESSION TECHNIQUES USING A RECURSIVE FILTER/SMOOTHER

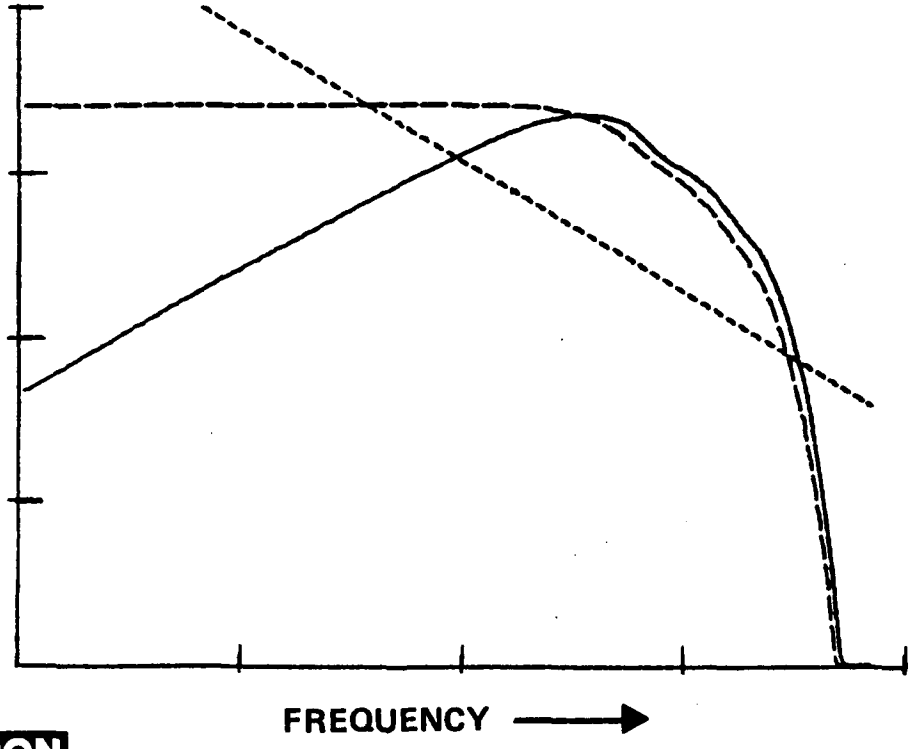

MARKOVIAN (STATE SPACE) STRAIGHT LINE GRAVITY MODEL

SELF CONSISTANT GRAVITY MODEL $C(N\Delta\tau)$

STATE SPACE APPROXIMATION $\Phi(\Delta\tau)$, Q

$$\epsilon = \sum_{N} \left\| C(N\Delta\tau) - C(0) \left[\Phi(\Delta\tau)^{N} \right]^{T} \right\|^{2}$$

$$Q = C(0) - \Phi(\Delta\tau)\, C(0)\, \Phi(\Delta\tau)^{T}$$

$$\Phi(\Delta\tau) = C(\Delta\tau)\, C(\tau)^{-1}$$

COMPARISON OF STAG AND STATE SPACE CORRELATIONS
(NORMALIZED CORRELATION VS NORMALIZED DISTANCE)

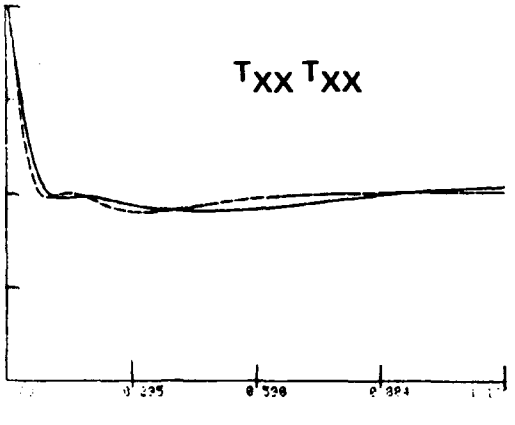

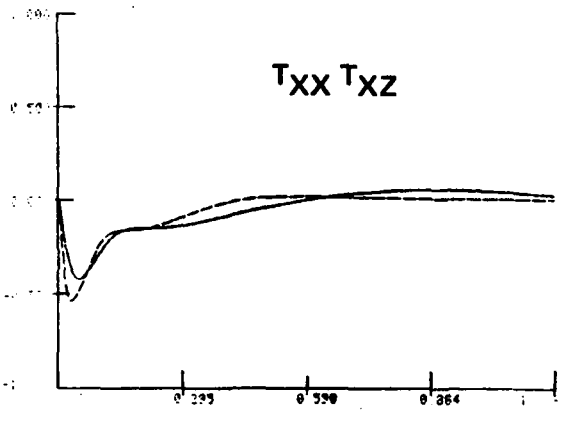

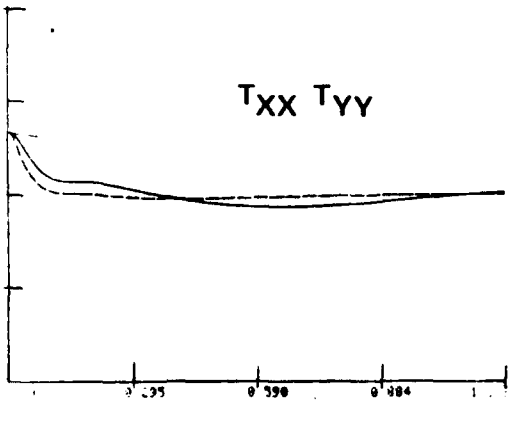

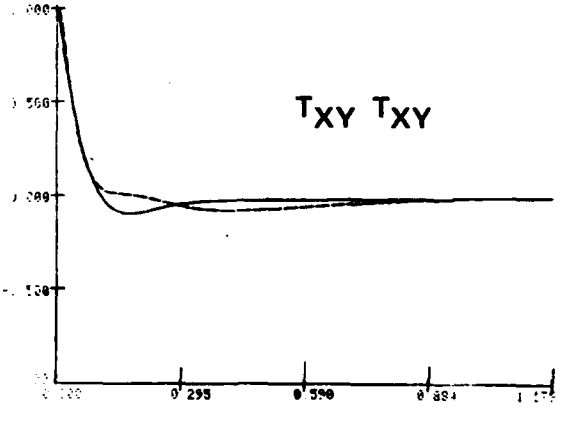

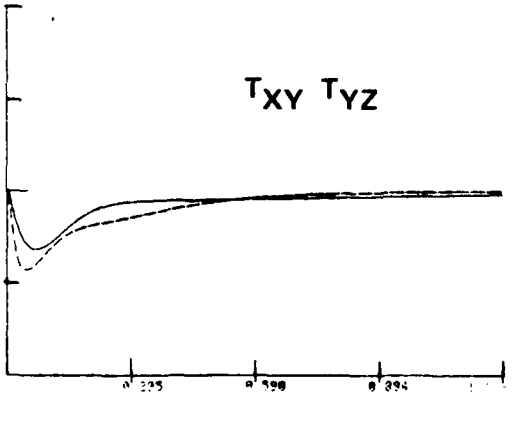

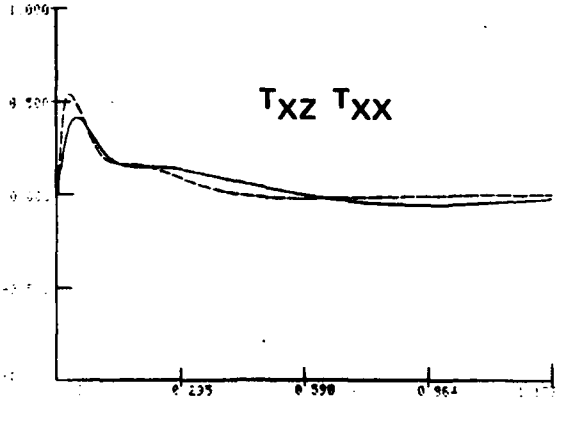

COMPARISON OF STAG AND STATE SPACE CORRELATIONS
(NORMALIZED CORRELATION VS DISTANCE)

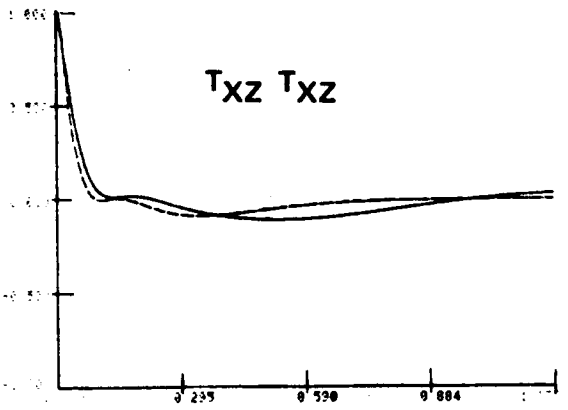

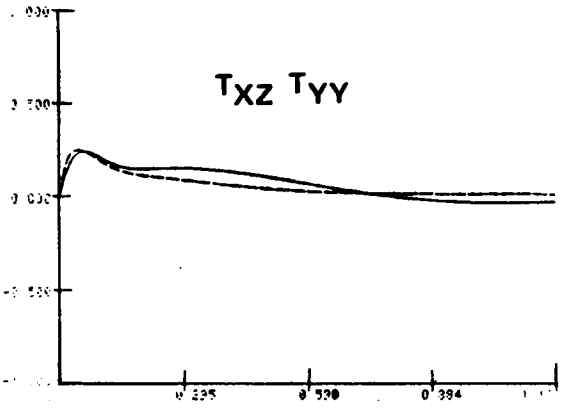

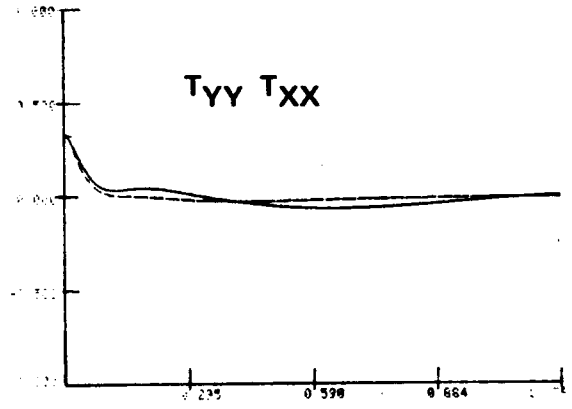

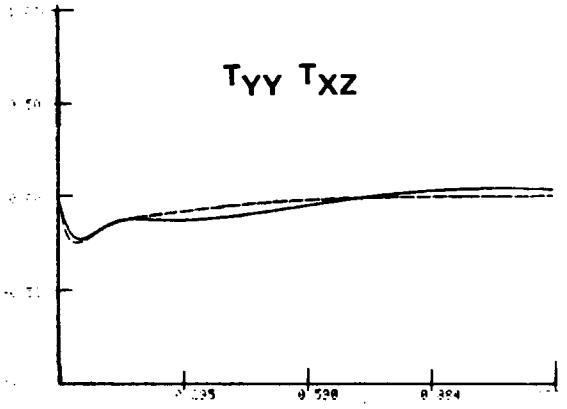

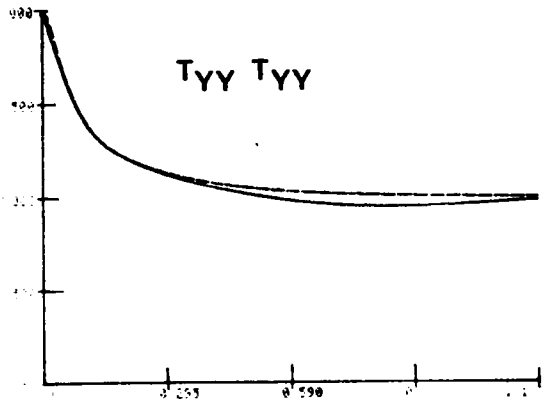

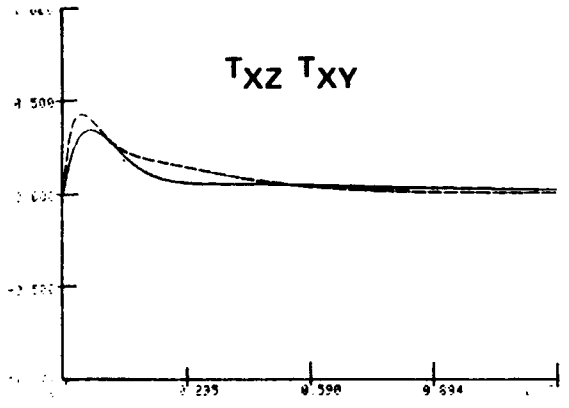

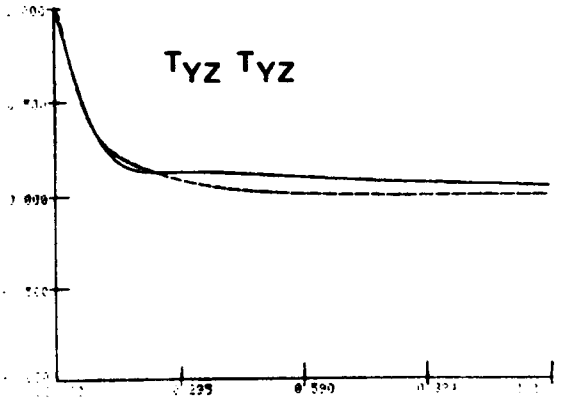

COMPARISON OF STAG AND STATE SPACE CORRELATIONS
(NORMALIZED CORRELATION VS DISTANCE)

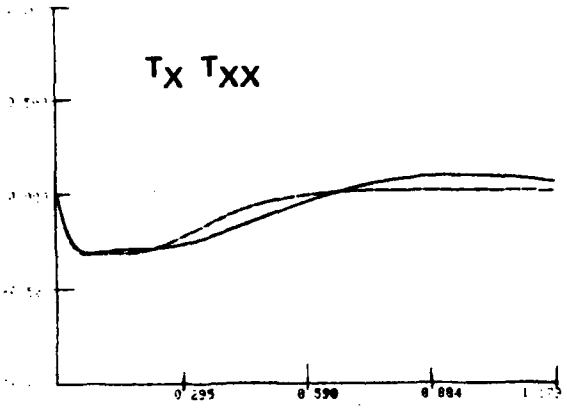

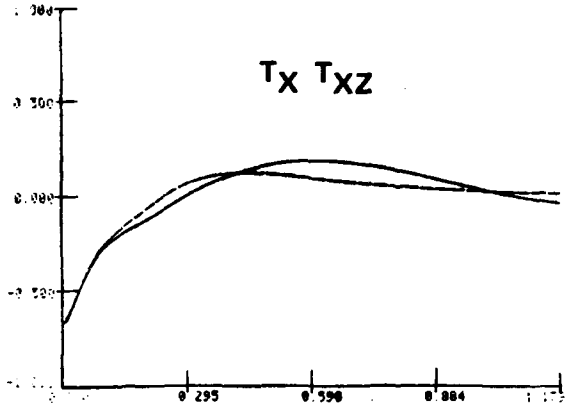

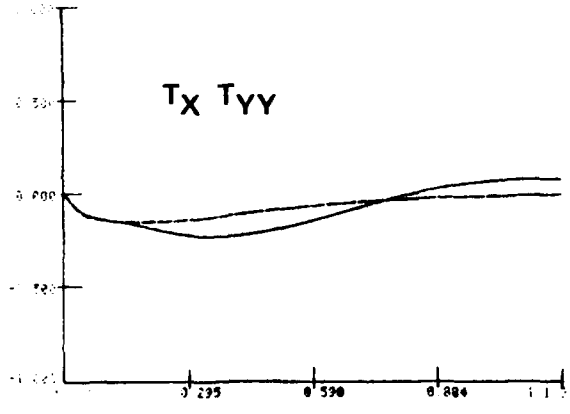

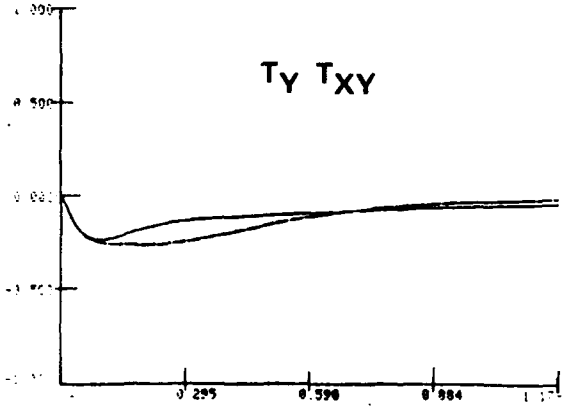

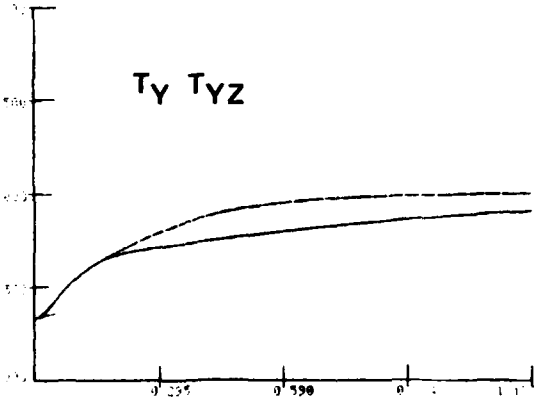

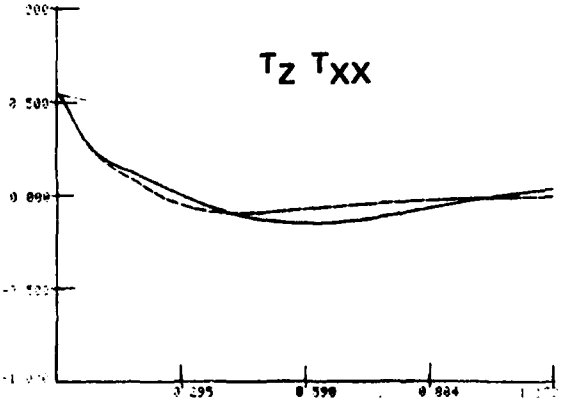

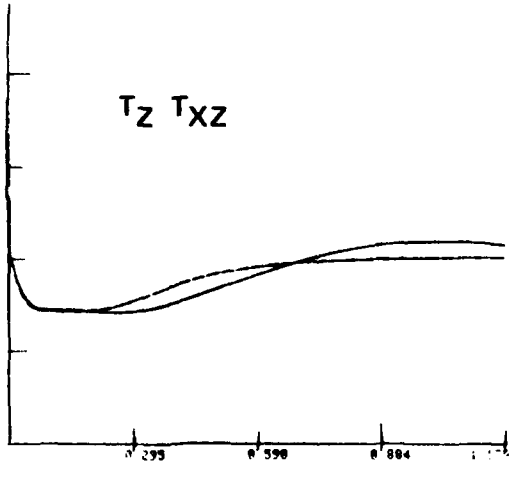

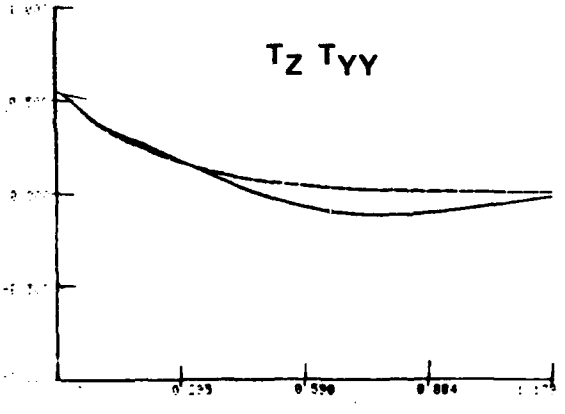

COMPARISON OF STAG AND STATE SPACE CORRELATIONS
(NORMALIZED CORRELATION VS DISTANCE)

$T_X\ T_X$

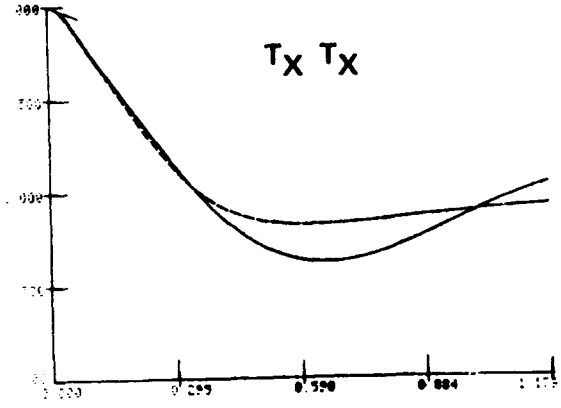

$T_X\ T_Z$

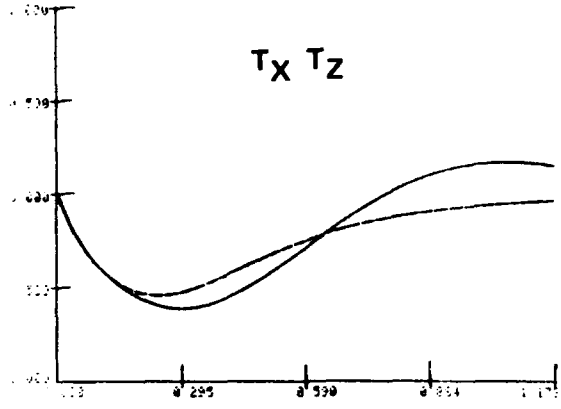

$T_Y\ T_Y$

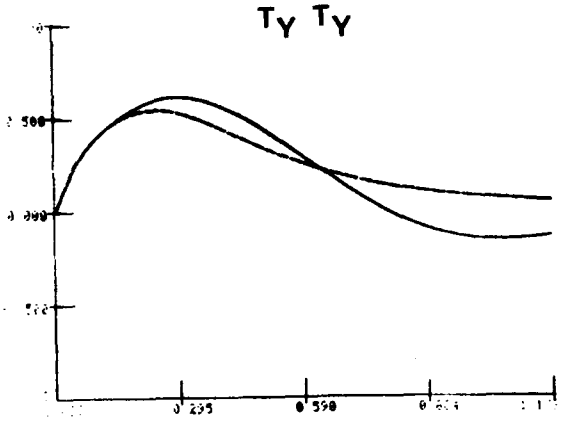

$T_Z\ T_X$

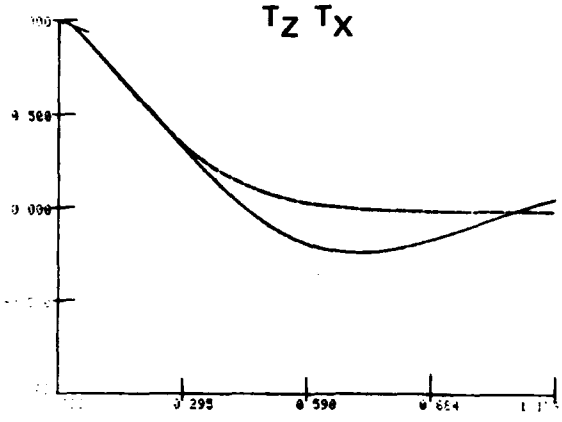

$T_Z\ T_Z$

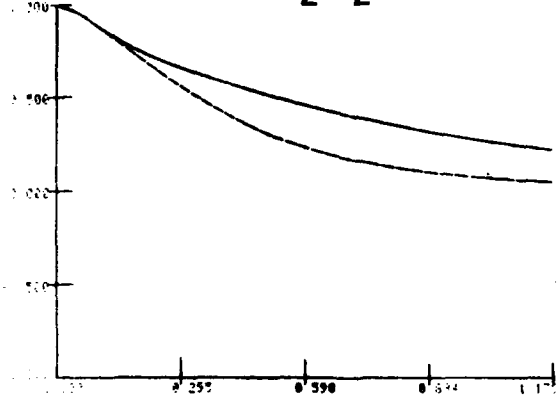

SIGNAL AND NOISE MODELS

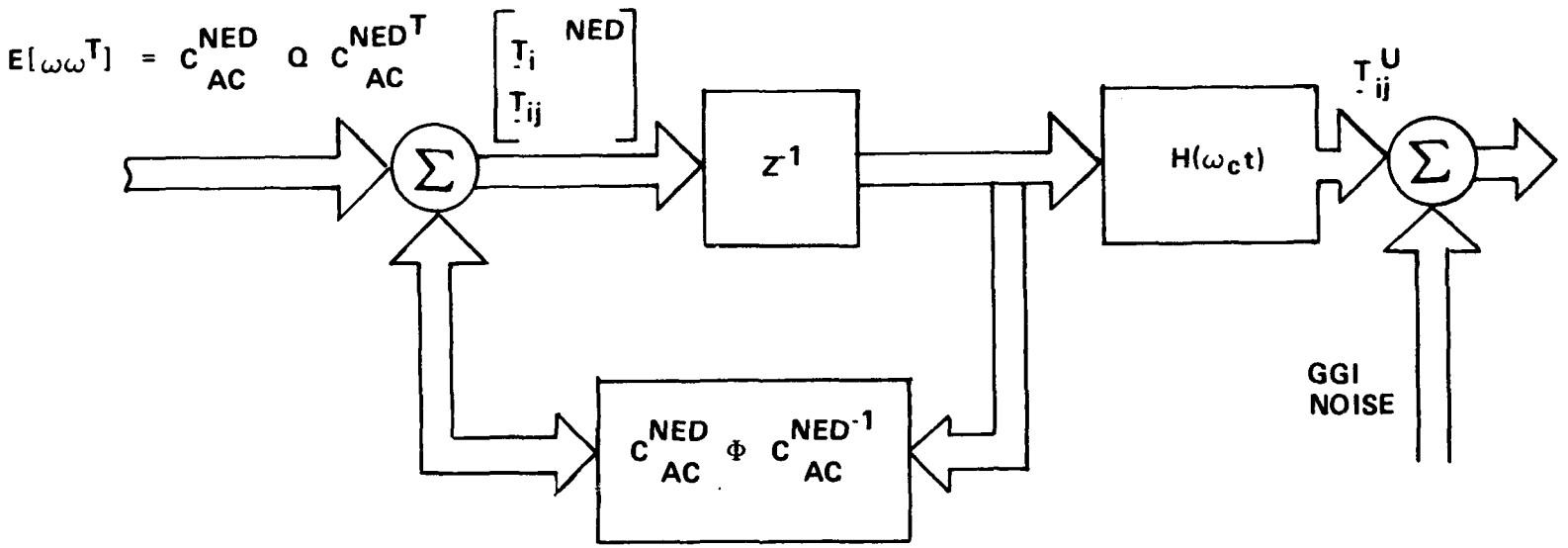

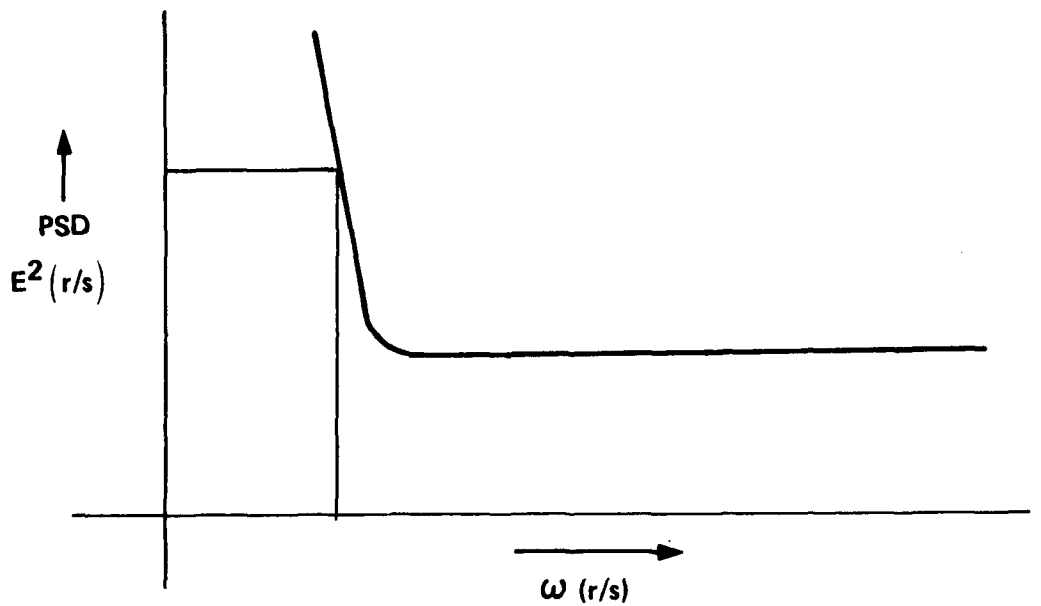

GGI NOISE MODEL

COMPARISON OF FIXED POINT SMOOTHING AND LEAST SQUARES COLOCATION RESULTS

(300 KM TRACK, GRADIENTS PROCESSED EVERY 5 KM, GGI 5E SIGMA WHITE NOISE MODEL, STAG NORTH ATLANTIC)

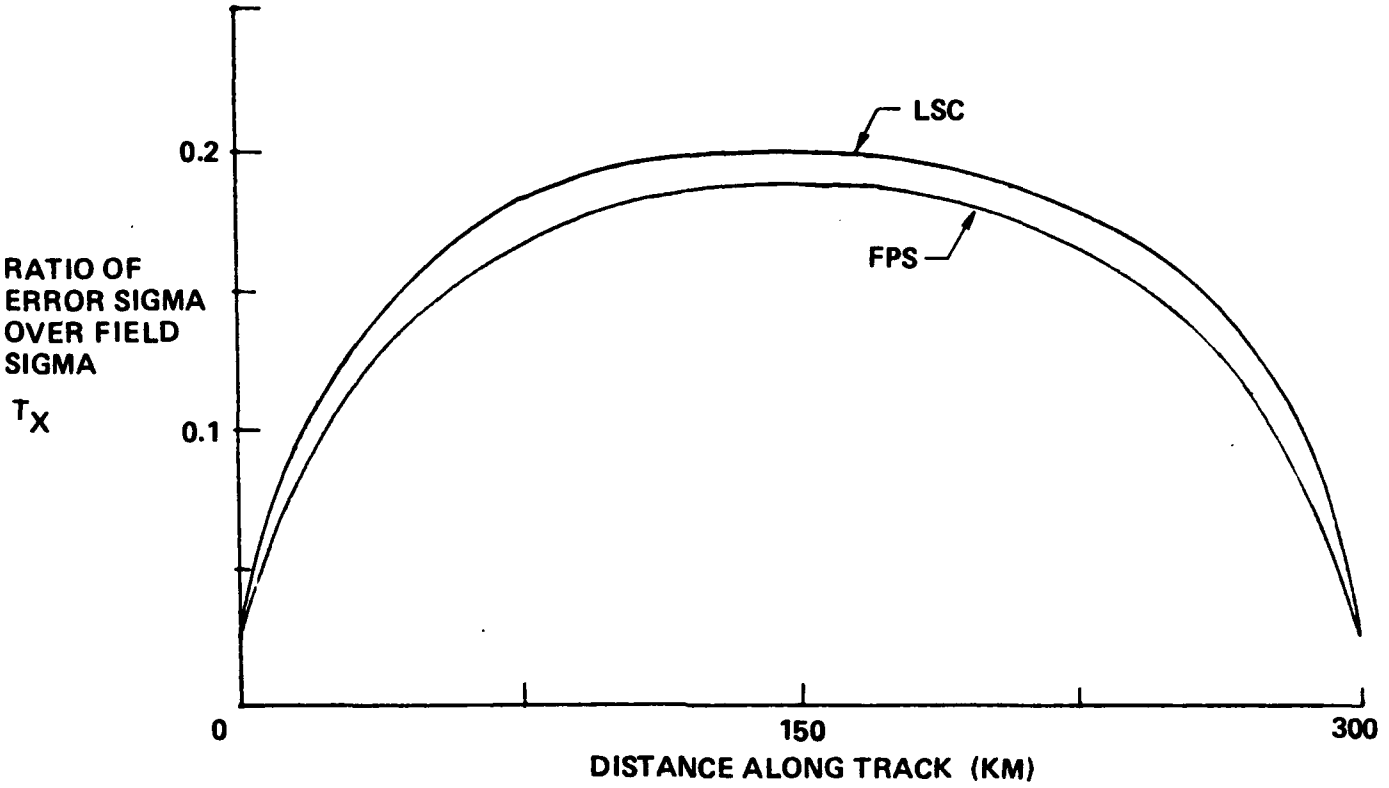

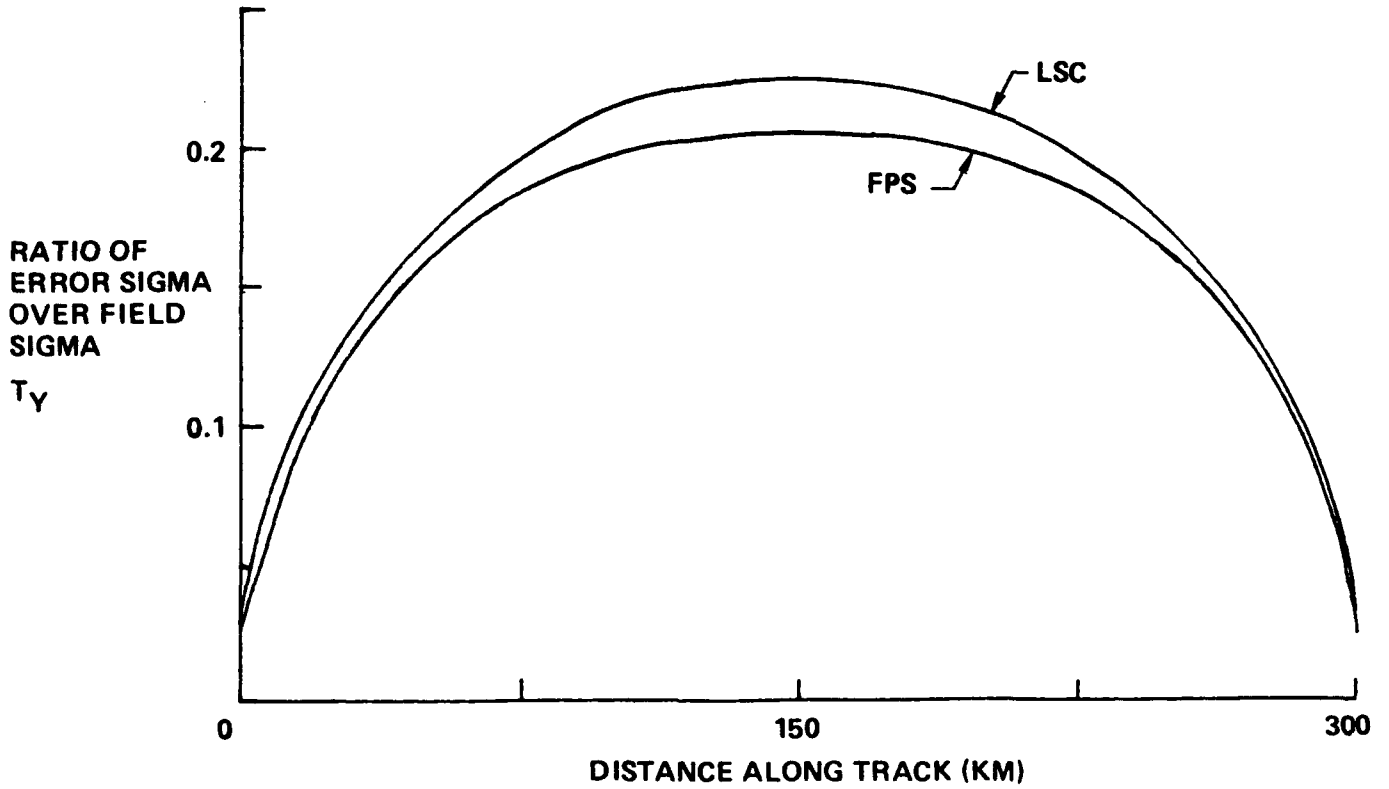

APPLICATION OF KALMAN SMOOTHER TO GRAVITY MAPPING PROBLEM

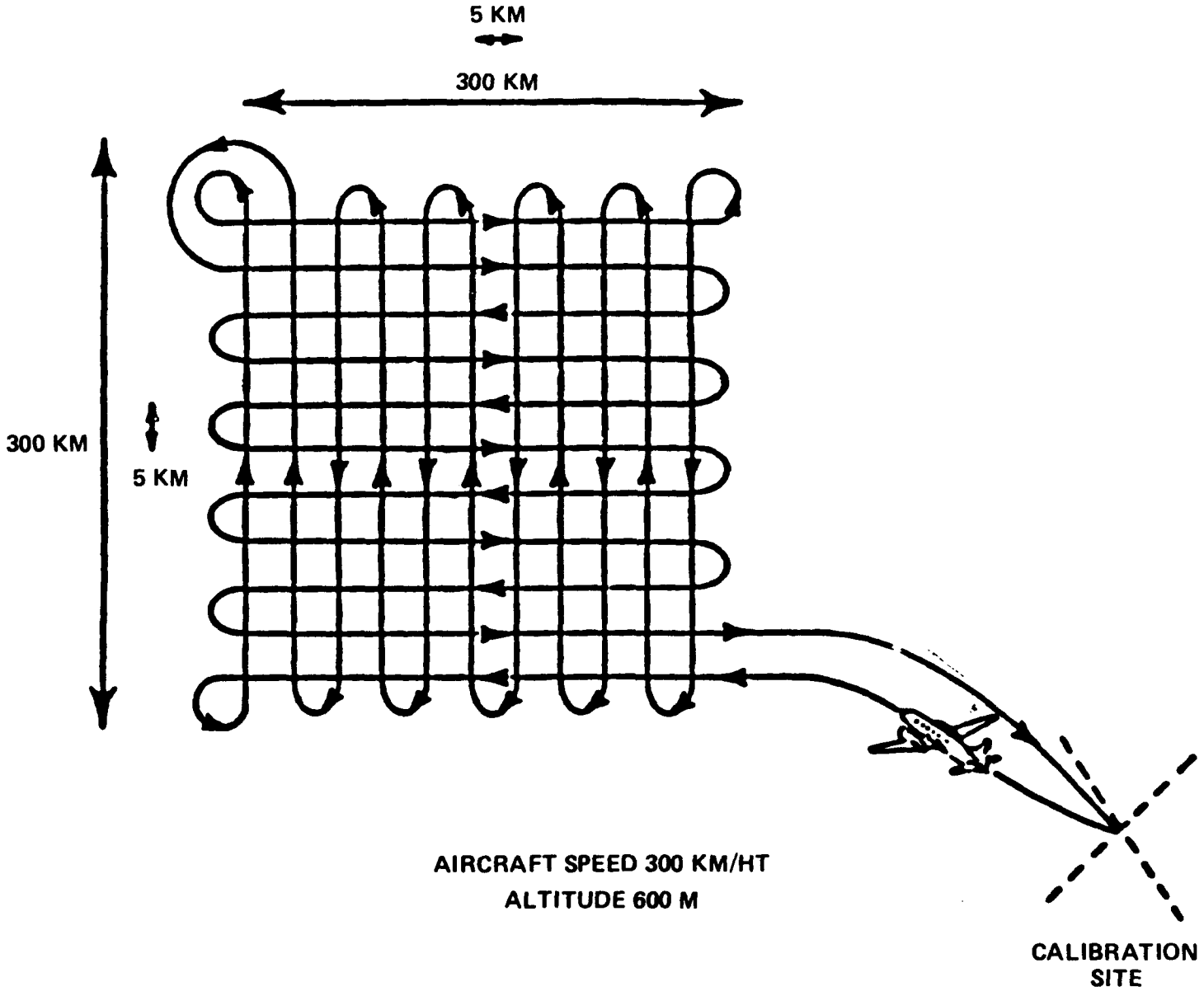

RATIO OF ERROR SIGMA OVER FIELD SIGMA VS DISTANCE ALONG TRACK SHOWING EFFECT OF USING GGI SAMPLING DISTANCES OF 5 KM, 2.5 KM, 1 KM AND 1/6 KM

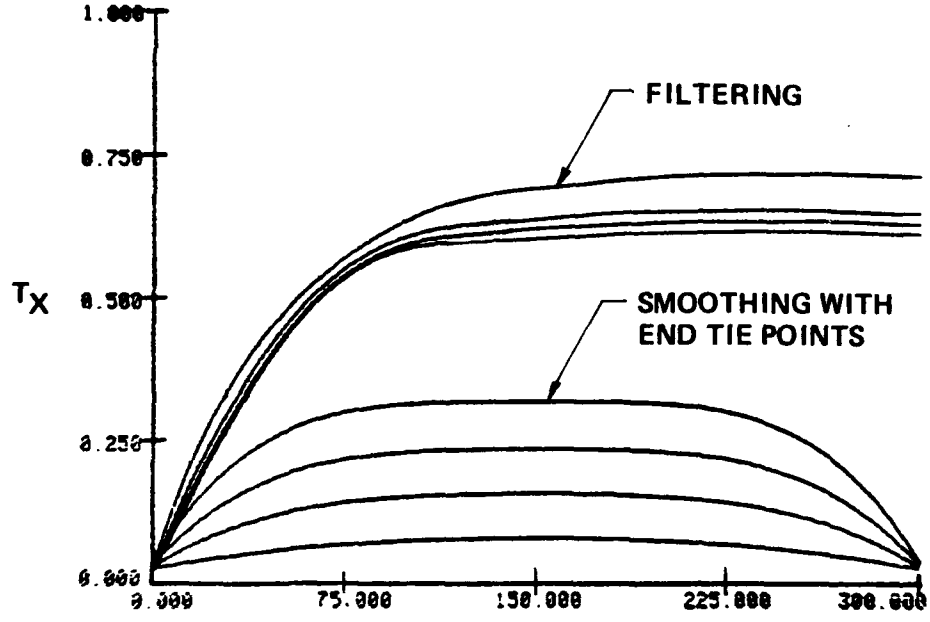

LOW INSTRUMENT NOISE CASE

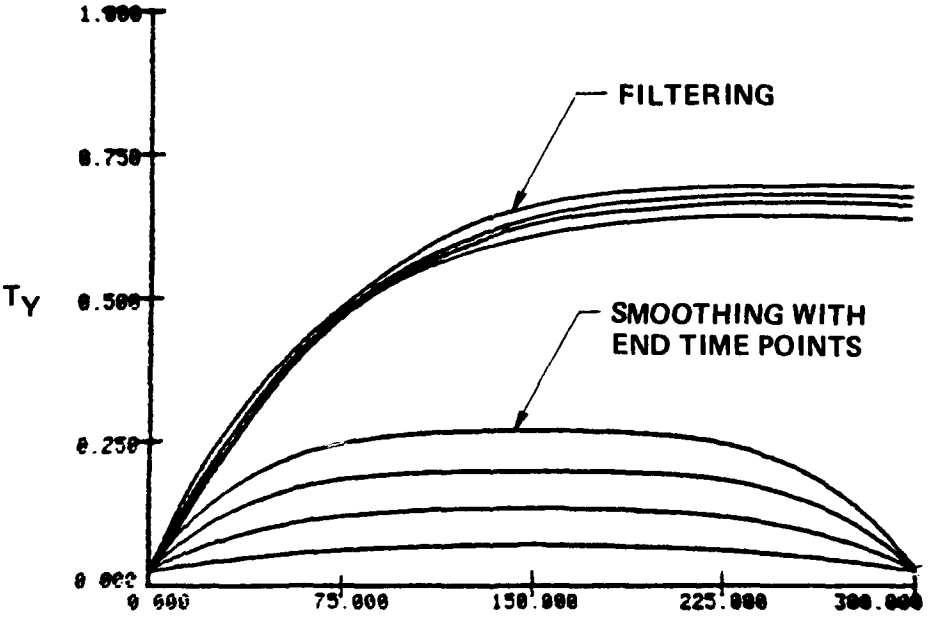

RATIO OF ERROR SIGMA OVER FIELD SIGMA VS DISTANCE ALONG TRACK SHOWING EFFECT OF USING GGI SAMPLING DISTANCES OF 5 KM, 2.5KM, 1 KM AND 1/6 KM

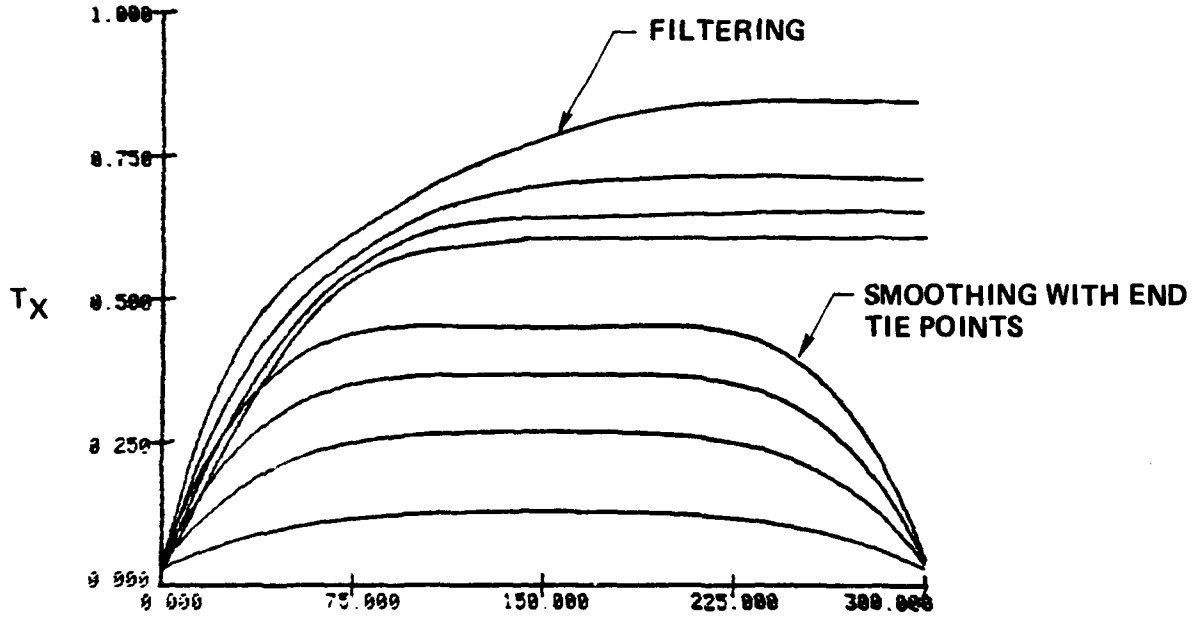

HIGH INSTRUMENT NOISE CASE

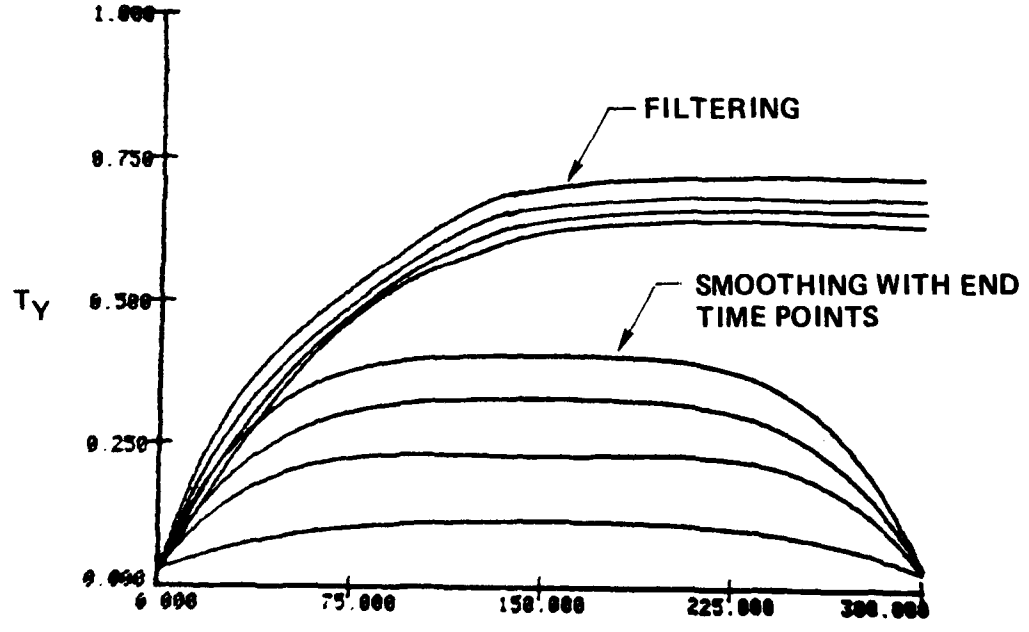

MASCON SYNTHETIC GRAVITY FIELD

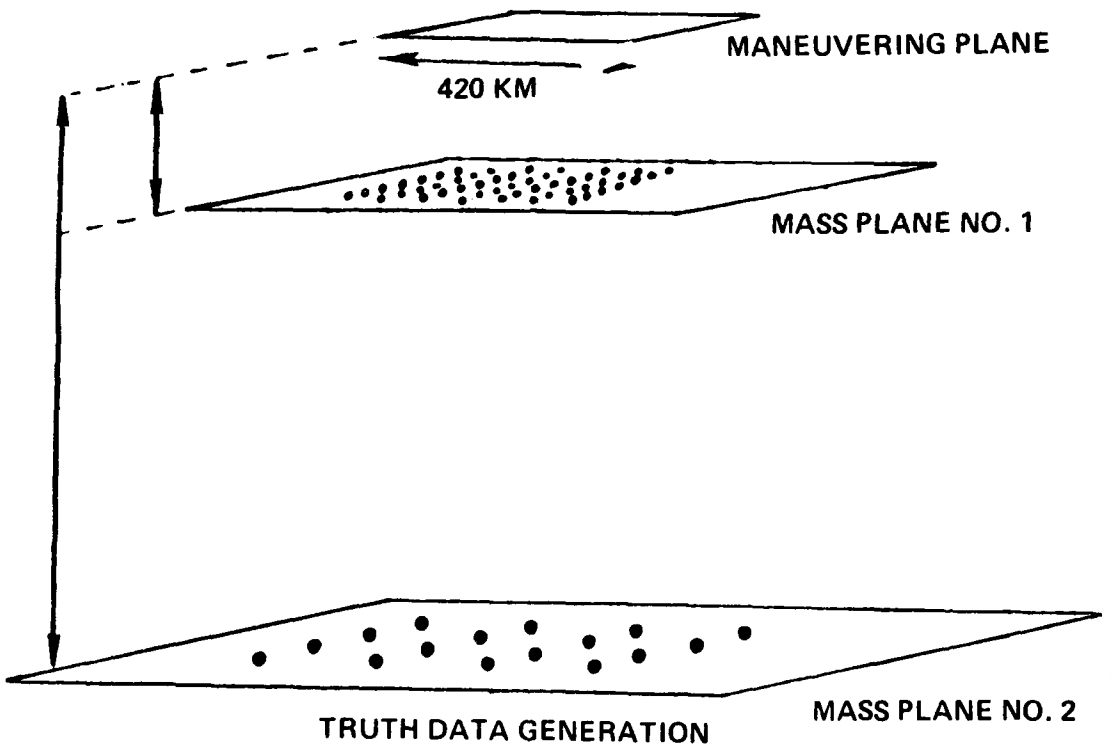

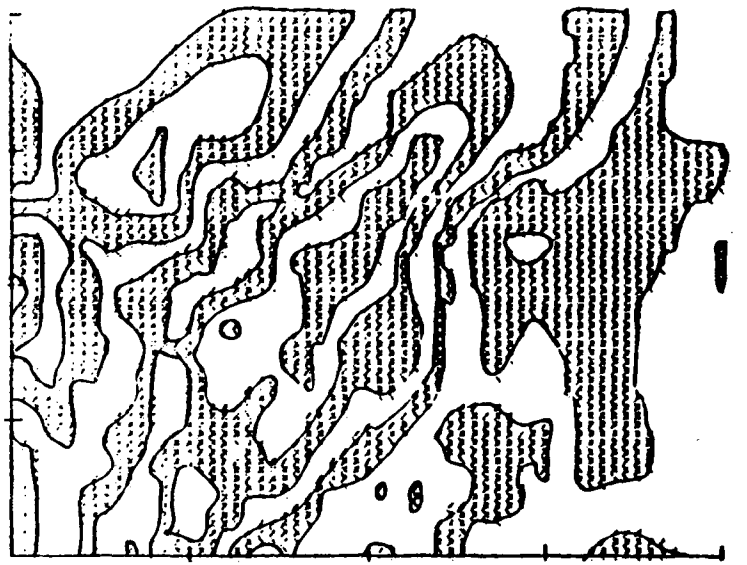

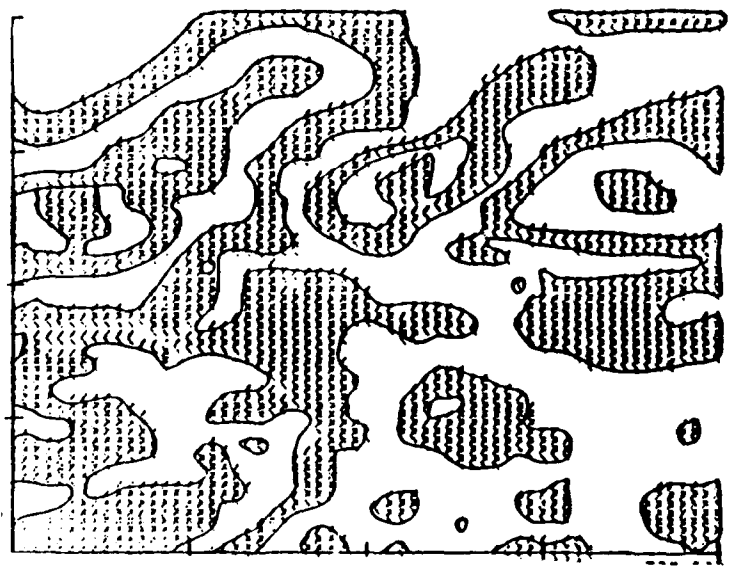

VERY LOW NOISE SIMULATION

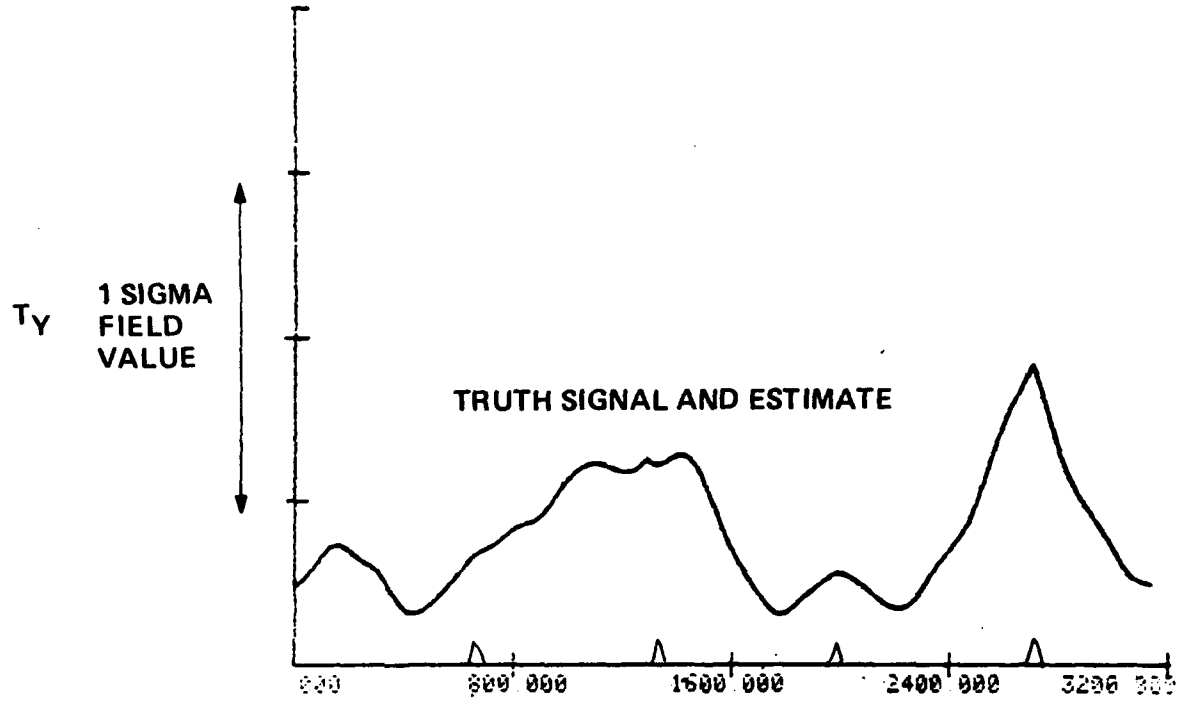

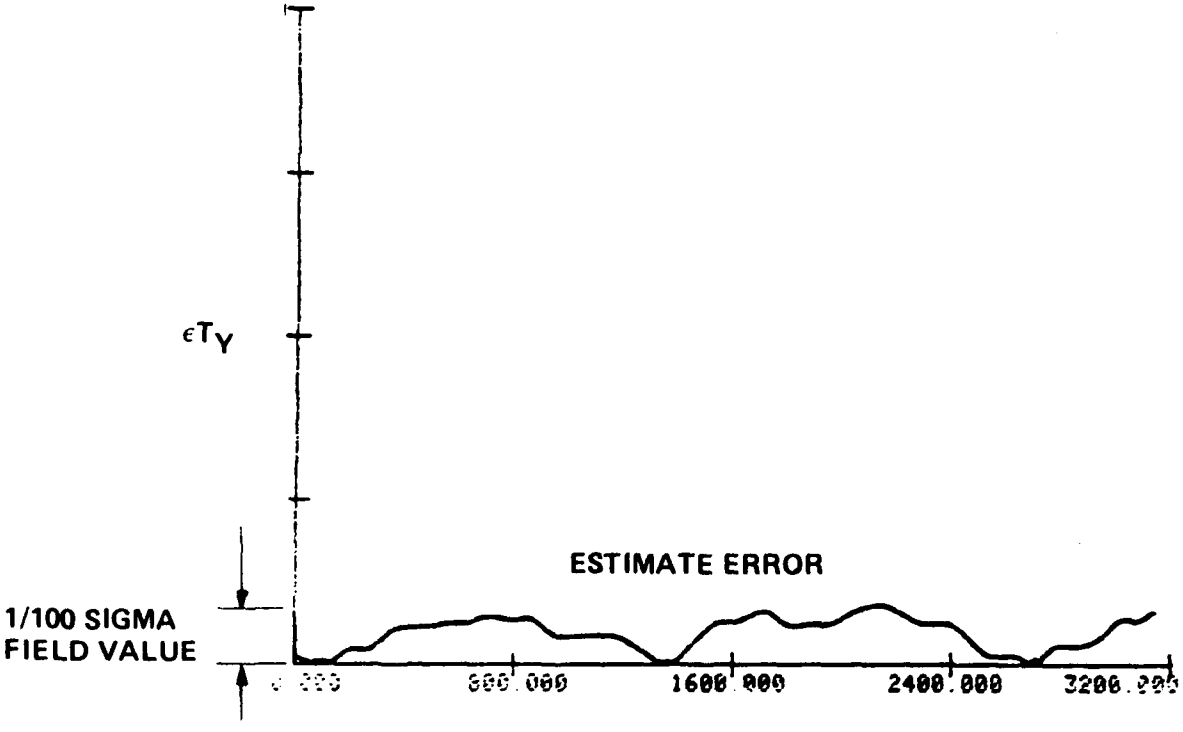

VERY LOW NOISE SIMULATION

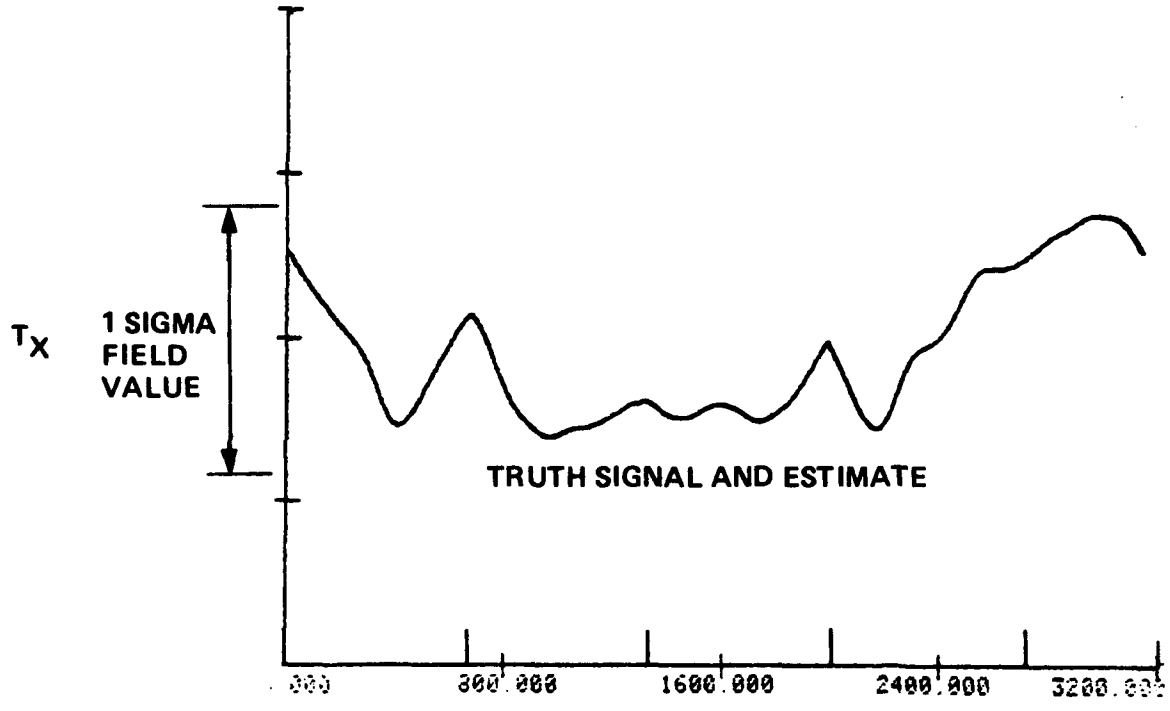

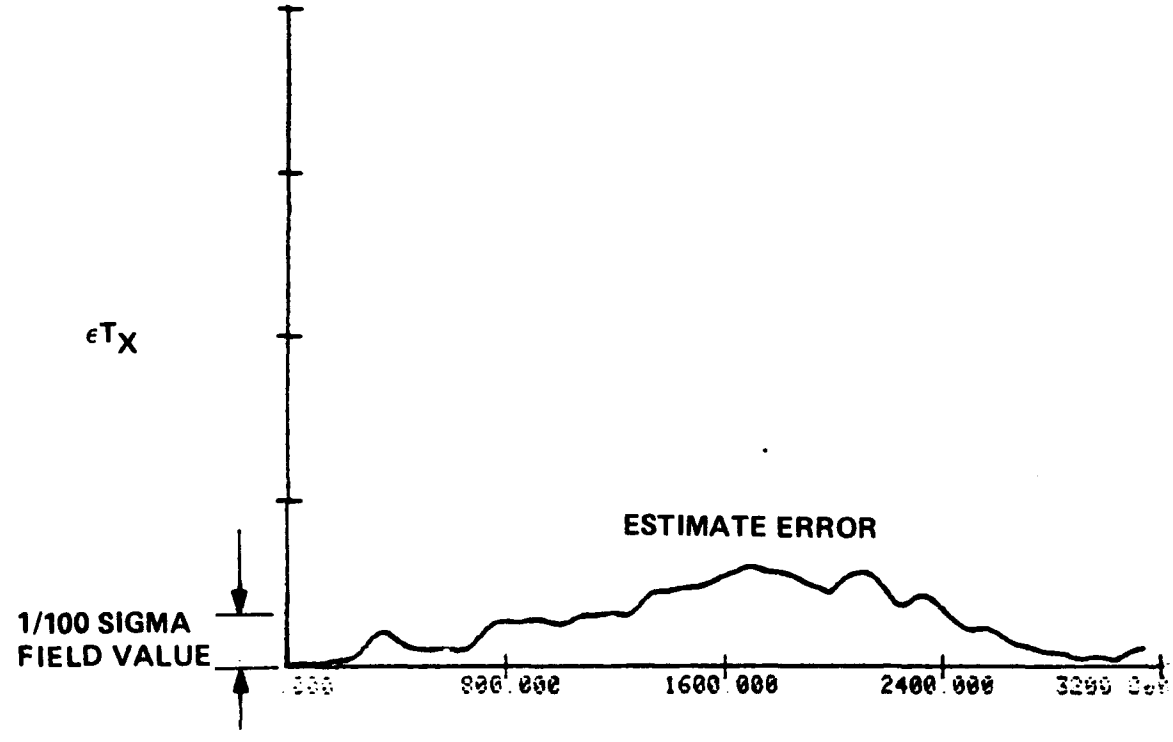

REALISTIC NOISE SIMULATION

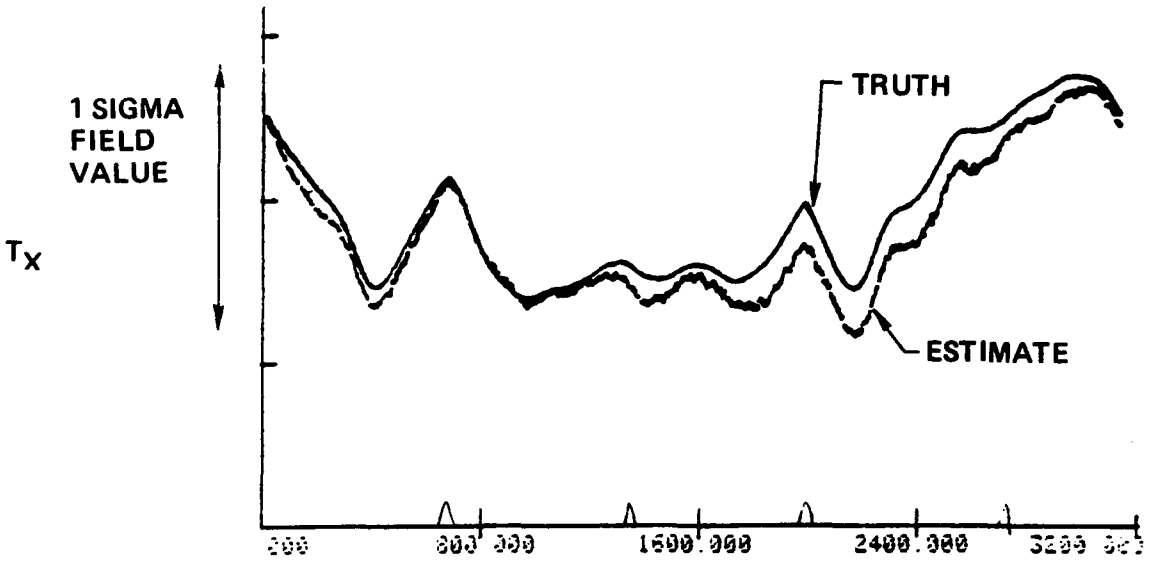

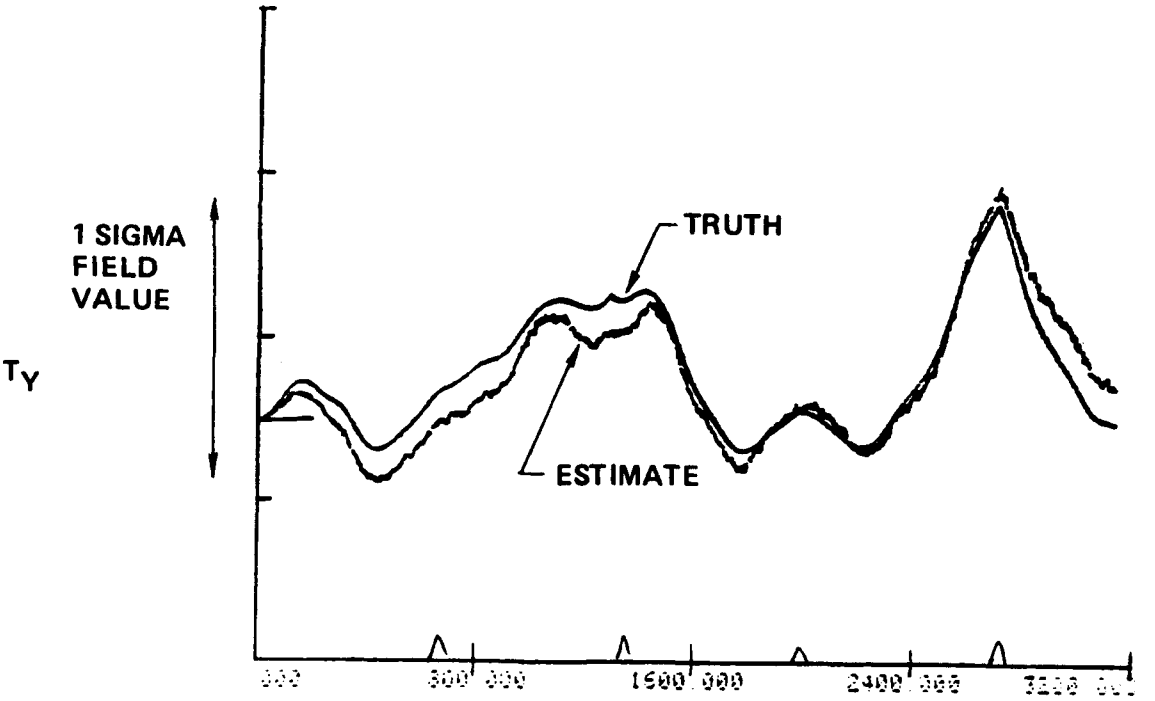

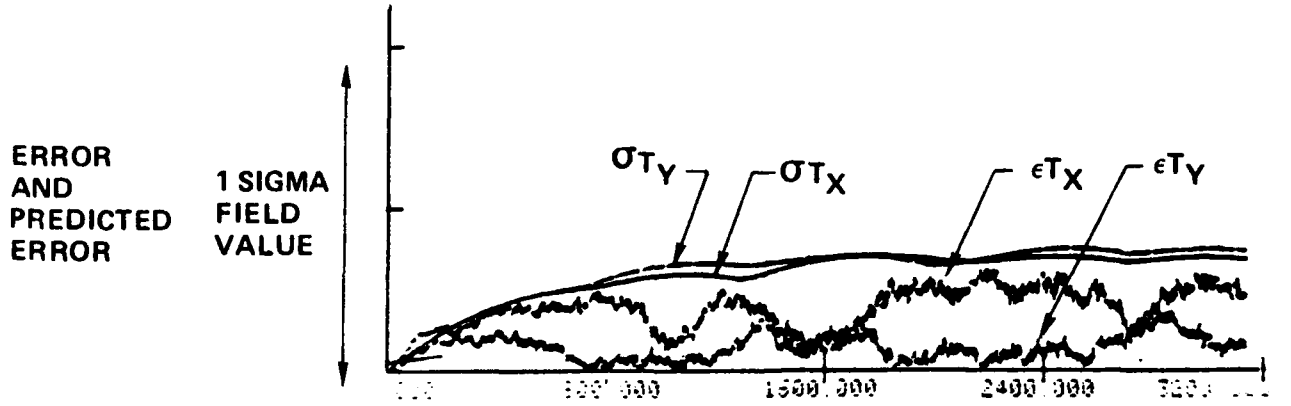

VELOCITY ERROR AND VELOCITY ERROR ESTIMATE

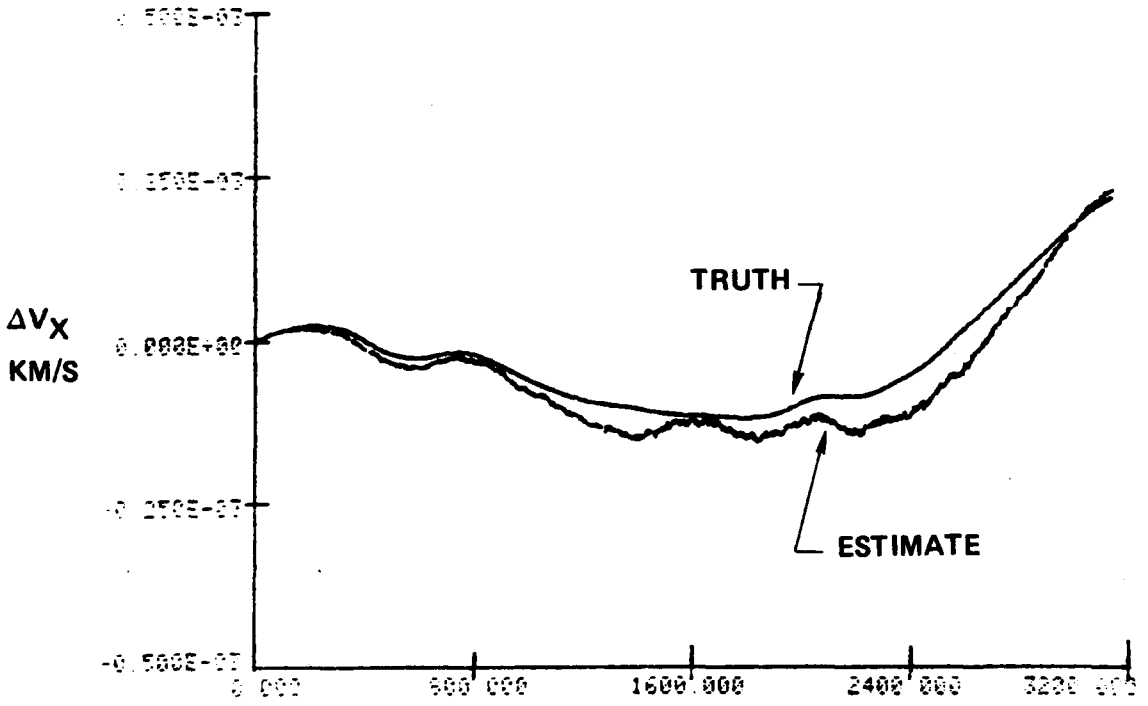

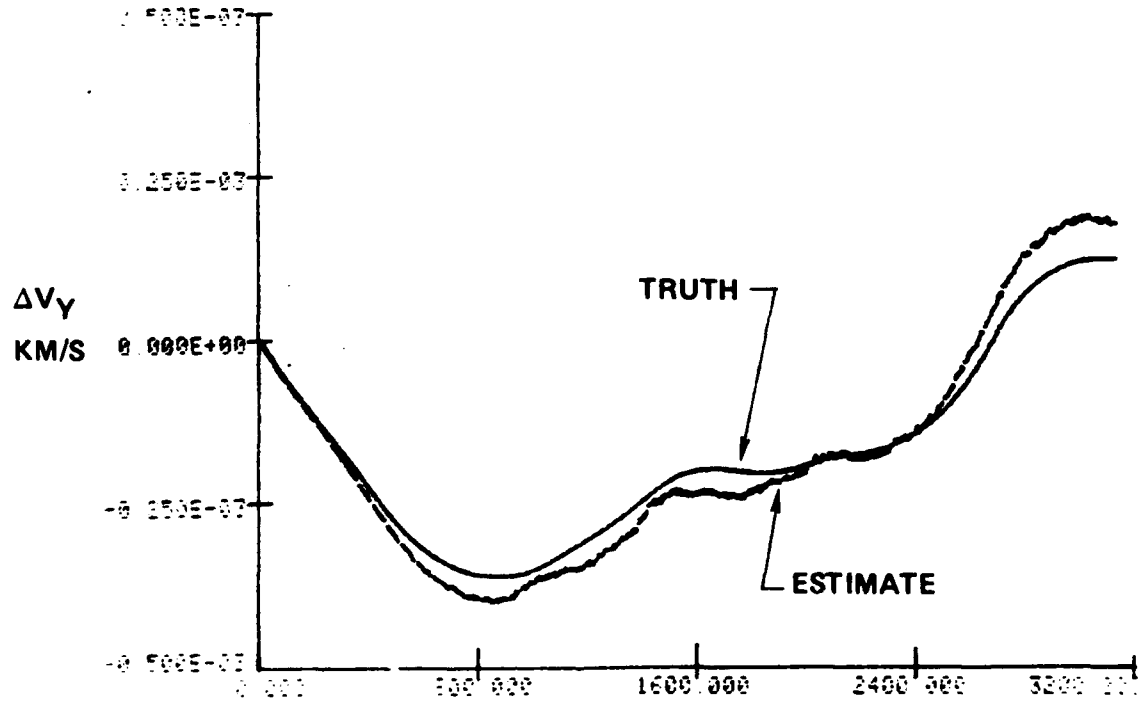

CONCLUSIONS

- STATE SPACE STRAIGHT LINE GRAVITY SHAPING FILTER WORKS WELL
  - CLOSE AGREEMENT BETWEEN LEAST SQUARES COLOCATION AND KALMAN SMOOTHER
  - CONSISTANT SIMULATION RESULTS USING MASCON SYNTHETIC FIELD
- STRAIGHT LINE FILTER WORKS WELL AROUND TURNS
- VELOCITY ESTIMATION WORKS WELL
- KALMAN SMOOTHER COULD BE USED AS BASIS FOR GRAVITY MAPPING DATA REDUCTION
- ENVIRONMENTAL SENSITIVIES AND LOW FREQUENCY DATA BASE COULD EASILY BE INCORPORATED IN KALMAN FILTER

FUTURE WORK

- DEVELOP A GRAVITY SURVEY DATA REDUCTION SCHEME BASED ON KALMAN SMOOTHER.
- USE MASCON SYNTHETIC FIELD EXTENSIVELY TO TEST DIFFERENT SURVEY SCHEMES AND SURVEY DATA REDUCTION ALGORITHMS.

SP-4423-7

ONGOING TASC WORK ON GGSS POST-TEST DATA PROCESSING ALGORITHM DEVELOPMENT

14-15 February 1984

Prepared for:

TWELFTH MOVING BASE GRAVITY GRADIOMETER REVIEW
United States Air Force Academy
Colorado

THE ANALYTIC SCIENCES CORPORATION
One Jacob Way
Reading, Massachusetts 01867

ONGOING TASC WORK ON GGSS POST-TEST DATA PROCESSING ALGORITHM DEVELOPMENT

TASC

OVERVIEW

- BACKGROUND ON GGSS POST-TEST/SURVEY DATA PROCESSING ISSUES
- PREFILTER DESIGN CONSIDERATIONS
- TWO ALTERNATIVE ESTIMATION APPROACHES
  - SEQUENTIAL COMPLEMENTARY FILTER
  - OPTIMIZED TEMPLATE ALGORITHM
- SUMMARY AND CURRENT STATUS

TASC

BACKGROUND

- INHERENT 16Hz SAMPLING RATE GENERATES 8×10^6 GRADIENT TENSOR MEASUREMENTS OVER A 320 km × 320 km TEST AREA WHEN TRAVERSED ACCORDING TO NOMINAL* SURVEY PROCEDURE
- TOTAL NUMBER OF DATA ITEMS INVOLVED IN SOLUTION FOR SINGLE ESTIMATE OF GRAVITY DISTURBANCE IS 5×10^7
- FORTUNATELY MUCH OF THIS DATA IS REDUNDANT
- REDUNDANCY MOTIVATES PREFILTER TO SUPPRESS NOISE, MINIMIZE ALIASING AND ESTABLISH GRID
- RESULT IS CONCENTRATION OF INFORMATION INTO FEWER GRADIENT DATA ITEMS
- GRAVITY DISTURBANCE VECTOR IS ESTIMATED FROM PREFILTERED GRADIENTS

*BIDIRECTIONAL SURVEY AT 300 km/hr, 5 km TRACK SPACING

TASC

SENSITIVITY OF BASELINE SURVEY TO PREFILTER TIME CONSTANT

A 1645

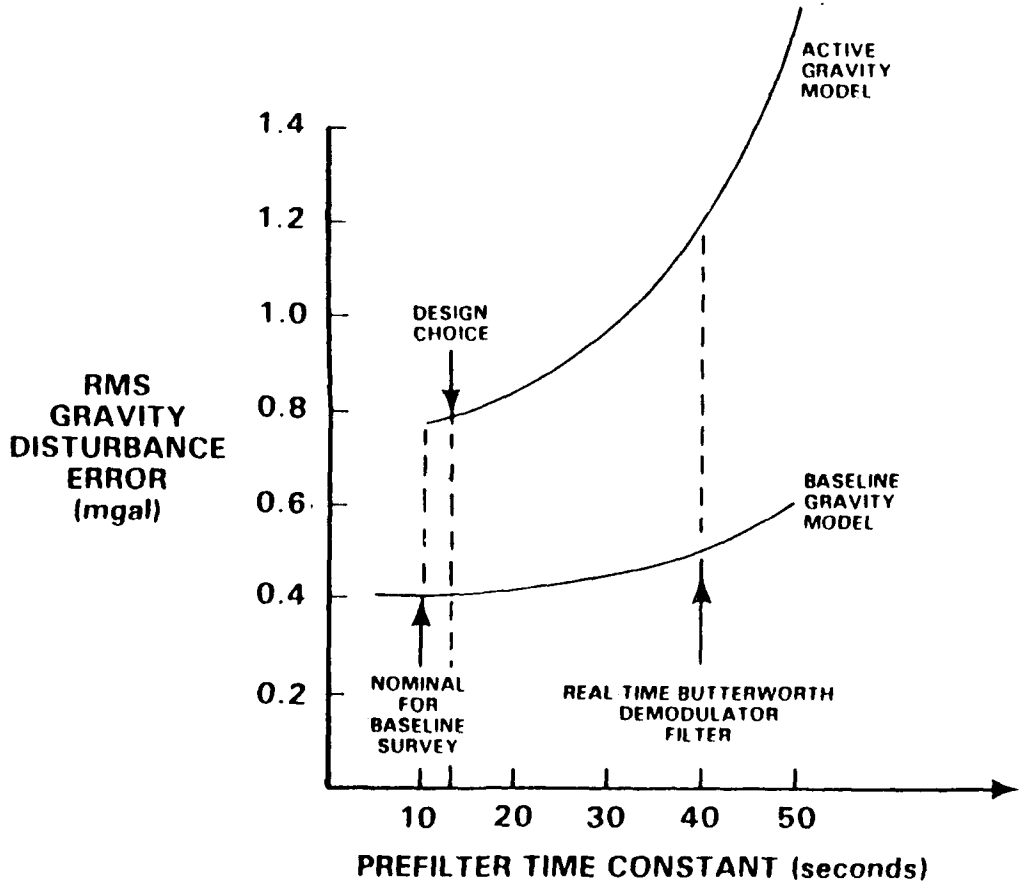

- NOMIMAL SURVEY PARAMETERS AND INSTRUMENT NOISE
- OPTIMAL PROCESSING OF ALL GRADIENT ELEMENTS
- INFINITE EXTENT
- SAMPLING INTERVAL CHOSEN TO BE SAME AS PREFILTER TIME CONSTANT
- DESIGN CHOICE OF 12 SECOND PREFILTER TIME REDUCES TOTAL NUMBER OF GRADIENT DATA POINTS TO 2.5×10^5
- FURTHER FACTOR OF 2 OR 3 POSSIBLE IF TEST/SURVEY AREA IS KNOWN TO BE "NOT ACTIVE"

TASC

IMPLICATIONS OF DATA QUANTITY AFTER PREFILTERING

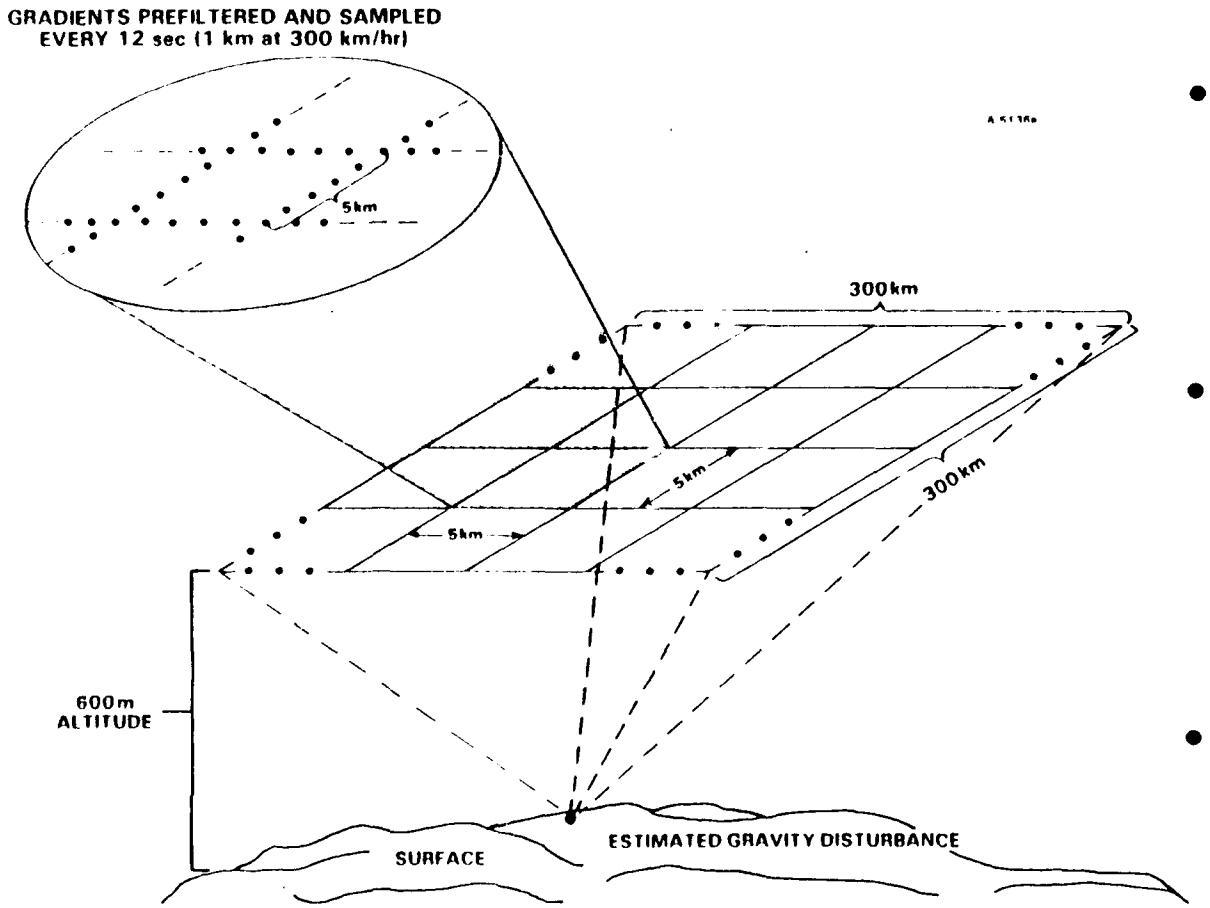

- CLASSICAL OPTIMAL ESTIMATION USING ALL 2.5×10^5 DATA POINTS WOULD ENTAIL COVARIANCE MATRICES WITH OVER 10^{10} ELEMENTS

- ESTIMATE ABOVE IGNORES CONSIDERATION OF SUPPLEMENTAL LONG WAVELENGTH DATA (e.g. ONE DEGREE × ONE DEGREE MEAN ANOMALIES)

- MOTIVATES SUBOPTIMAL APPROACHES WHICH ADD NEGLIGIBLE (0.1-0.2 MGAL) RMS ESTIMATION ERROR

TASC

TWO ALTERNATIVE ESTIMATION APPROACHES

- BOTH TAKE ADVANTAGE OF GRIDDED DATA STRUCTURE

- EACH USES REFERENCE FIELD WHICH INCLUDES WAVELENGTHS NOT MEASURED ACCURATELY BY GRADIOMETER, e.g. WAVELENGTHS > 500 km (~DEGREE AND ORDER =45)

- SEQUENTIAL COMPLEMENTARY FILTER METHOD IS OPTIMAL AT EACH STAGE
  - UTILIZES HIGH DATA DENSITY NEAR CENTER, LOWER AT EDGES
  - EXPLOITS BLOCK TOEPLITZ COVARIANCE MATRIX STRUCTURE THROUGH GEOFAST ALGORITHM
  - SOMEWHAT INVOLVED "BOOKKEEPING"

- OPTIMIZED TEMPLATE ALGORITHM IS BASED ON DECREASING RESOLUTION REQUIREMENTS IN DISTANT ZONES
  - TEMPLATE CONSTRUCTED TO MINIMIZE COVARIANCE MATRIX SIZE
  - APPROACH FORCES GOOD NUMERICAL CONDITIONING
  - ARBITRARY TEMPLATE GEOMETRY REQUIRES NUMERICAL OPTIMIZATION DURING DESIGN
  - ATTRACTIVENESS IS SIMPLICITY OF APPLICATION

TASC

SEQUENTIAL COMPLEMENTARY FILTER APPROACH

PARTITION GRAVITY DISTURBANCE BY BANDWIDTH

$$\delta g = \delta g_1 + \delta g_2 + \delta g_3$$

SELECT BANDS IN COMPLEMENTARY MANNER

$$\delta g_1 = \frac{1}{A_1} \iint_{A_1} \delta g \, dA$$ LARGE AREA AVERAGE (S_1)

$$\delta g_2 = \frac{1}{A_2} \iint_{A_2} \delta g \, dA - \delta g_1$$ INTERMEDIATE AREA AVERAGE (S_2)

$$\delta g_3 = \delta g - \delta g_1 - \delta g_2$$ CENTRAL ZONE POINT DATA (S_3)

ESTIMATE EACH BAND SEPARATELY USING APPROPRIATE AVERAGES AND EXTENTS OF MEASURED GRADIENTS, e.g.

$\delta \hat{g}_i = K\underline{Z}$ where

$\underline{Z}$ ARE GRADIENT MEASUREMENT AVERAGES

K ARE THE OPTIMAL COVARIANCE-DETERMINED ESTIMATION "GAINS"

TASC

SPACE AND FREQUENCY DOMAIN REPRESENTATIONS OF SEQUENTIAL COMPLEMENTARY FILTER ALGORITHM

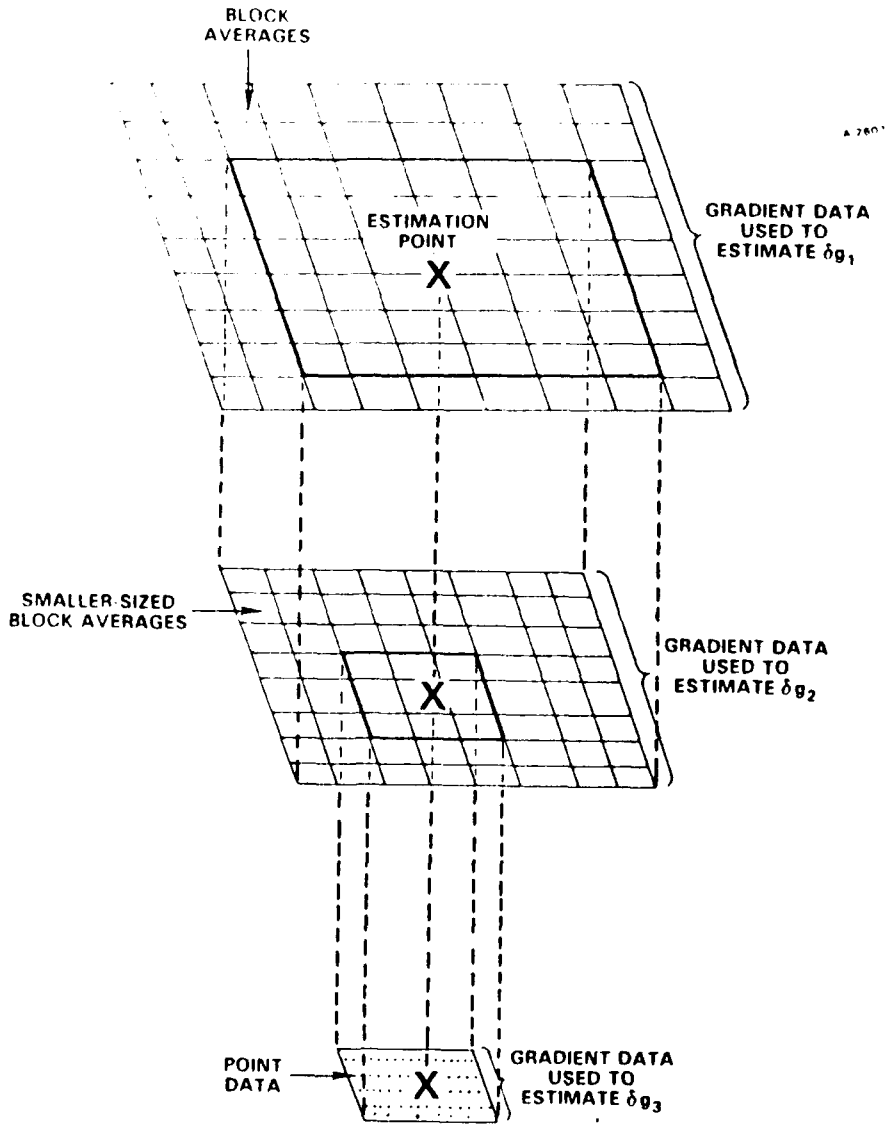

REGIONAL SUBDIVISIONS

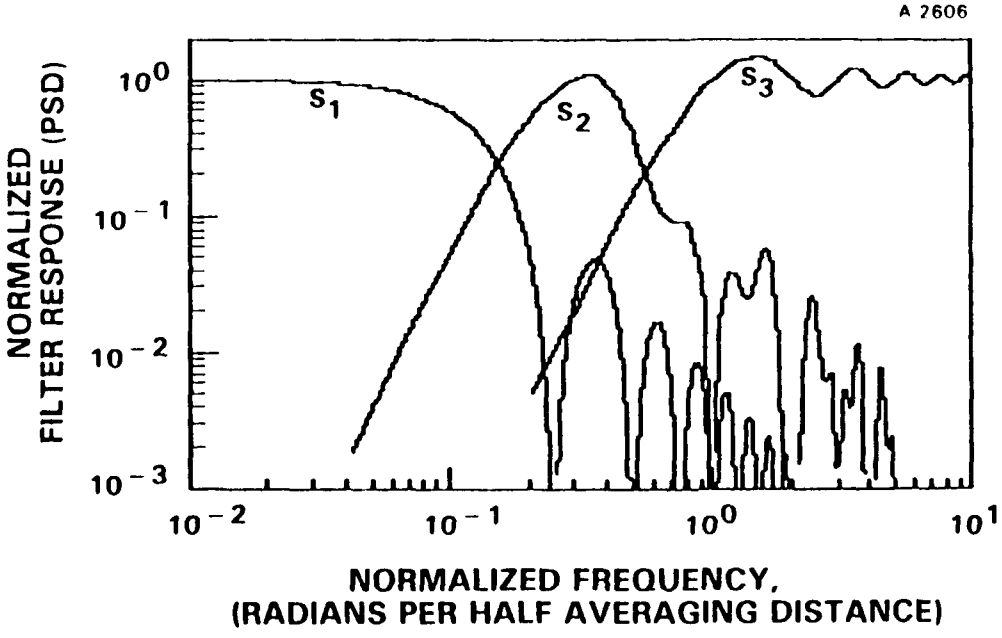

FILTER RESPONSE

TASC

FIRST-LOOK AT REGION SIZES AND DATA ENSEMBLES

	ALGORITHM STAGE		
	1	2	3
QUANTITY ESTIMATED	δg_1	δg_2	δg_3
SPECTRAL REGION	S_1	S_2	S_3
INPUT QUANTITIES	ONE deg × ONE deg MEAN ANOMALIES* 120km × 120km MEAN GRADIENTS (6)	30km × 30km RESIDUAL MEAN GRADIENTS (6) WITH 120km × 120km MEAN GRADIENTS REMOVED	RESIDUAL POINT GRADIENTS (6) WITH 30km × 30km RESIDUAL MEAN GRADIENTS REMOVED
ESTIMATION REGION SIZE	360km × 360km†	300km × 300km	80km × 80km
WORST CASE NUMBER OF INPUT DATA	49 MEAN ANOMALIES 54 MEAN GRADIENTS	3600 MEAN GRADIENTS	14,790 POINT GRADIENTS
SIZE OF EQUIVALENT COVARIANCE MATRIX INVERSE	103 × 103	3600 × 3600	14,790 × 14,790‡
EFFECTIVE RANGE OF FILTER (BETWEEN HALF POWER POINTS)	REFERENCE FIELD CUTOFF FREQUENCY<f<0.0083cy/km	0.0083cy/km <f<0.033cy/km	0.033cy/km<f< GRAVITY DISTURBANCE FIELD CUTOFF FREQUENCY

*PLUS SURROUNDING "APRON" OF ADDITIONAL ONE DEGREE MEAN ANOMALY DATA POINTS, e.g. 40 ADDITIONAL POINTS TO EXTEND COVERED AREA TO 600km × 600km

†SIZE CHOSEN FOR ILLUSTRATIVE CONVENIENCE (COMPATIBLE WITH ONE DEGREE MEAN ANOMALY DATA)

‡BENCHMARK GEOFAST TEST CASE INVOLVING 16,384 GRADIENT DATA POINTS REQUIRED 5.2 HRS ON VAX 11/780 (INCLUDING COVARIANCE GENERATION PHASE)

TASC

OPTIMIZED TEMPLATE ALGORITHM

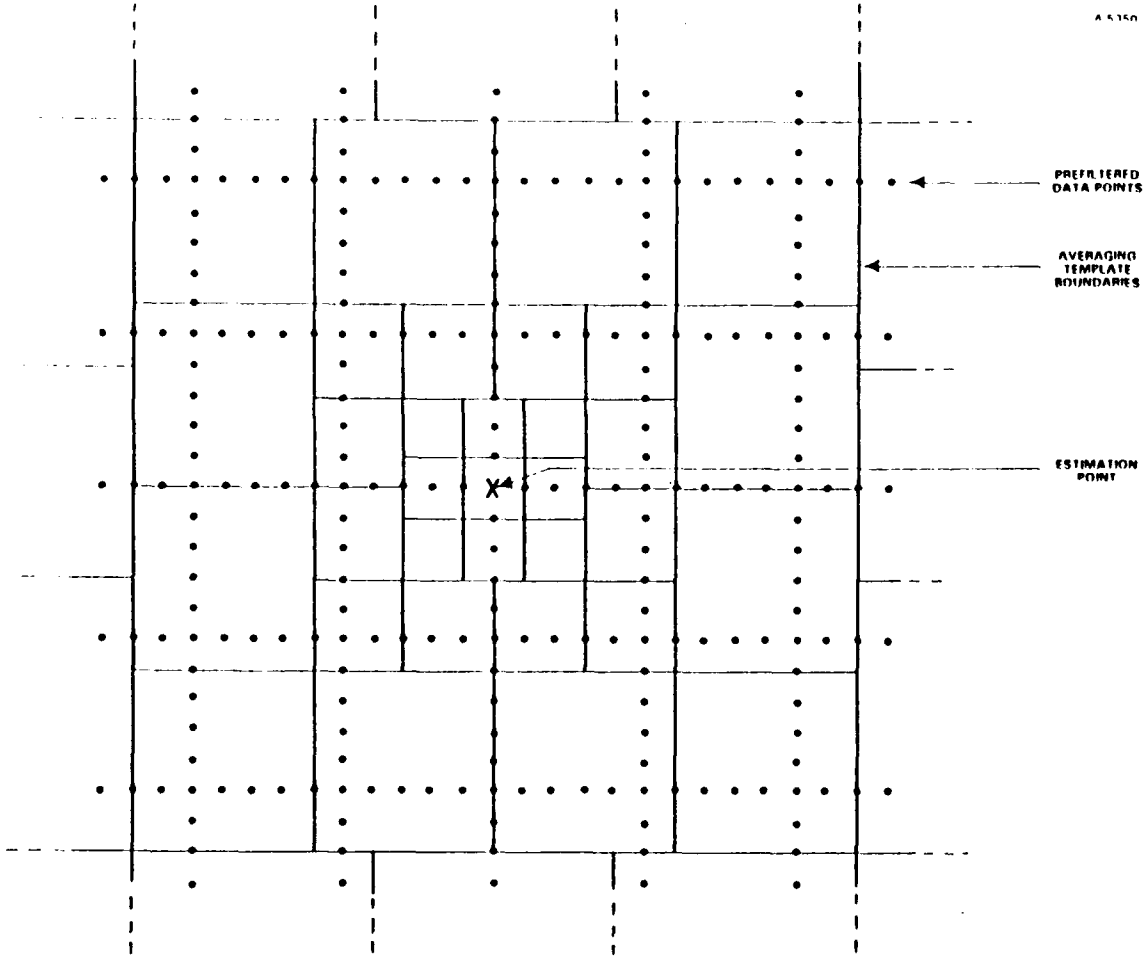

- GRADIENTS ARE AVERAGED OVER RECTANGULAR REGIONS WHICH INCREASE IN SIZE AS DISTANCE FROM ESTIMATION POINT INCREASES
- SHAPE OF REGIONS IS THEORETICALLY ARBITRARY BUT PRACTICALLY LIMITED BY NEED TO AVOID 4-FOLD INTEGRAL QUADRATURES TO COMPUTE COVARIANCE FUNCTIONS
- DIFFERENT TEMPLATE USED FOR ONE deg × ONE deg MEAN ANOMALY DATA

TASC

FEASIBILITY STUDY USING T_{zz} TO ESTIMATE NUMBER OF TEMPLATE CELLS REQUIRED

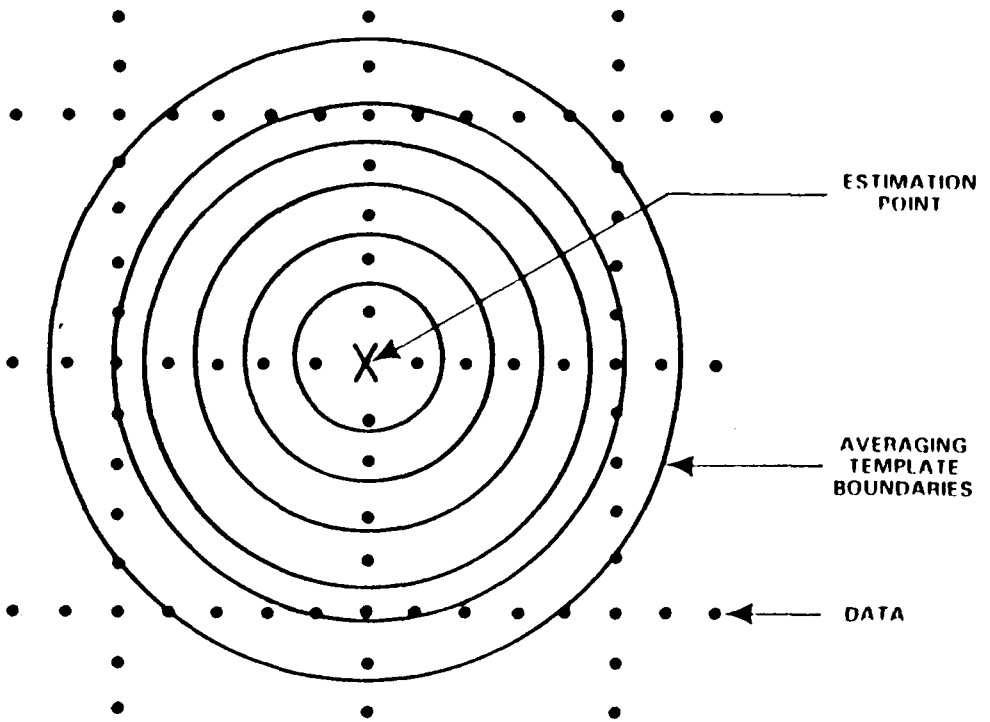

- STUDY CASE TAKES ADVANTAGE OF CIRCULAR SYMMETRY ASSOCIATED WITH ESTIMATING δg_z FROM T_{zz} MEASUREMENTS TO SOLVE AVERAGING INTEGRALS SEMI-ANALYTICALLY
- MEASUREMENTS ARE AVERAGED OVER EACH ZONE
- RADII OF SUCCESSIVE ANNULI INCREASE BY APPROXIMATELY 25% UNTIL 320 km × 320 km REGION IS INCLUDED
- LONG WAVELENGTH DATA IS SIMULATED BY ESTIMATING POINT GRAVITY DISTURBANCES LESS A ONE deg × ONE deg MEAN, e.g. ESTIMATE = $\delta g_{\text{POINT}} - \delta\bar{g}_{\text{ONE deg}}$

TASC

ESTIMATION ERROR USING 18 ZONES SCALED TO NOMINAL TEST/SURVEY CONDITIONS (ATTENUATED WHITE NOISE GRAVITY MODEL)

GGSS NOISE POWER SPECTRUM (E^2/Hz-DOUBLE SIDED)	(E^2/rad/sec-SINGLE SIDED)	RMS ESTIMATION ERROR *(MGAL)
0	0	0.13
20	6.4	0.27
40	12.7	0.29
80	25.5	0.32

- SUCCESS WITH 18 ANNULI AND OTHER STUDIES INDICATE THAT APPROXIMATELY 72 WELL-CHOSEN TEMPLATE REGIONS WILL SUFFICE
- IF SAME TEMPLATE IS USED FOR ALL 6 GRADIENTS, RESULT WOULD BE 452 DATA ITEMS
- ONGOING STUDIES SUGGEST CONSIDERABLE PROMISE FOR FURTHER DATA REDUCTION IN NUMBER OF REQUIRED TEMPLATE SUBDIVISIONS

*QUANTITY ESTIMATED IS POINT VERTICAL DISTURBANCE WITH ONE deg × ONE deg MEAN REMOVED

TASC

OVERVIEW OF AIRBORNE GRAVITY AND COMPARISON OF GRAVITY AND GRADIENT ANOMALIES*

Sigmund Hammer
University of Wisconsin, Madison, WI 53706

William R. Gumert
Carson Geoscience Co., Perkasie, PA 18944

ABSTRACT

The topic is introduced by a very brief history of gravity measurements in a moving vehicle. The Carson Helicopter Gravity Measuring System (HGMS) is then described. HGMS has been operational about four years and observes an average of 5000 km of line data per month with a probable error of the order of 1 mgal and anomaly resolution limit of about 3 km. Survey altitude, as specified, can vary from low terrain clearance up to about 14,000 ft (4300 m) above sea level and over any type of terrain including environmentally restricted areas such as the Wildlife Reserve in Alaska.

The magnitudes and rates of attenuation with altitude of gradient and gravity anomalies are then compared. It is pertinent to emphasize that the rate of attenuation of all components of the gravity gradient is the same for a given type of anomaly. The gradient attenuates with altitude an order of magnitude faster than the corresponding gravity anomaly.

As a conclusion the question is raised: to accomplish the basic objectives of this Conference, what is the best way to proceed? (a) Concentrate efforts on the development of theory and instrumentation for gravity gradiometry; or (b) Undertake a world-wide gravity mapping program with the rapid and precise HGMS which is now available.

---

*Prepared for presentation at: Twelfth Moving Base Gravity Gradiometry Review, U.S. Air Force Academy, Colorado Springs, CO, February 14-15, 1984

OVERVIEW OF AIRBORNE GRAVITY AND COMPARISON OF GRAVITY AND GRADIENT ANOMALIES

Sigmund Hammer and William R. Gumert

INTRODUCTION

So far as I know there are, as yet, no published field data from functional gravity gradiometers. Our overview, therefore, will assess the present state of gravity observations leading up to the present Helicopter Gravity Measuring System (HGMS). This gravity overview may provide some useful background for evaluating the comparative potential usefulness of airborne gravity versus airborne gradiometer measurements for this symposium.

First a very brief history of gravity measurements in a moving vehicle. The first measurements of gravity in a moving vehicle were accomplished 55 years ago by Vening-Meinesz in a submerged submarine using special three-pendulum apparatus. His spectacular results over the Indonesian Islands Arc-Trench system were early precursors of the subduction phenomenon which is a major element in today's plate tectonics theory. Shipborne gravity surveys with modern high-precision gravimeters began 40 years ago and continue today on a commercial scale.

Airborne gravity measurements have been under investigation since about 1958. Tests in fixed-wing aircraft have yielded enough encouragement to justify continuation but satisfactory results have not been achieved up to now. Successful commercial gravity surveys, using specially stabilized helicopters, have been operational since 1979. High frequency anomalies, applicable to petroleum exploration, are being mapped at requested altitudes from low terrain clearance to more than 14,000 feet (4300 m). Since HGMS is quite new it may be useful to present a very brief explanation of the operation.

HELICOPTER GRAVITY MEASURING SYSTEM (HGMS)

The helicopter measurements are made in a large especially stabilized Sikorski S-61. The first slide shows the helicopter in flight. Gravity is

SLIDE #1: Carson helicopter in flight

measured by a LaCoste-Romberg sea-air meter on a greatly improved stable platform at the center of gravity in the helicopter. It may be of interest to point out that the helicopter has been modified so that the center of gravity does not shift as thousands of pounds of fuel are consumed. Total field magnetic field data are recorded simultaneously by a trailed proton precession magnetometer. Terrain clearance is recorded by narrow beam laser. All data are recorded digitally each second. Flying is done at night to minimize air turbulence. Flight speed is normally 50 knots but can be specified for the purpose at hand up to 100 knots (185 km/hr).

The procedure which brought success was to fly a more or less square grid of intersecting lines as illustrated on slide 2. In this project the

SLIDE #2: Flight pattern

line spacing was 3,300 feet (1 km) and flight altitude 1000 feet (305 m). The area is a marshy jungle of extremely difficult access on the ground. Note that north-south flights are avoided to improve the Eötvös corrections.

THE ATTENUATION PROBLEM

The principal elements in the operation are well illustrated in a demonstration survey over two well-known salt domes in the Texas Gulf Coast (Car-

SLIDE #3: Gulf Coast survey

son, 1981). The survey consisted of 20 lines, spaced one-half statute mile (0.805 km), within the area bordered by dashed lines as shown on Figure 3. The contoured results clearly define the airborne gravity anomalies on the two salt domes in the shaded areas. The contour interval is 1/2 mgal.

A comparison with ground data is illustrated on Figure 4. The salt domes

SLIDE #4: Profile results

are sketched at the bottom of the figure. Note the exaggerated vertical scale on the domes - the caprock is very shallow. Conventional ground gravity data along the location of the flight line across the centers of the dome are shown by the central profile. These data were kindly provided by interested oil companies, but not until after completion of the HGMS project. The gravity profile measured in flight is the solid curve at the top of the figure. Upward continuation of the ground data, without filtering, are shown by the dotted curve (.....). For comparison with the helicopter measurements the upward continued ground data were then smoothed by the 60-second filter which removes high frequency motional acceleration effects in the HGMS observations (-----). The differences between the airborne and filtered ground data nowhere exceed 1 mgal. However, it is obvious that the sharp, positive caprock anomalies are strongly attenuated. This will be examined below.

A simulated, quantitative analysis of the anomaly attenuation is illustrated in Figure 5. This salt dome is comparable to the Big Hill and High

SLIDE #5: Simulated analysis

Island domes and is generally typical of salt domes with shallow caprock in the Gulf Coast, U.S.A. The density contrasts were taken from Nettleton (1976; Figure 8-14). The calculated gravity anomalies, with and without caprock, at ground level and at "flight elevation" of 1000 feet (305 m), are plotted in solid lines. The attenuation of the caprock anomaly is moderate. However, for comparison with HGMS gravity measurements the "upward continued" ground data must also be filtered. The filter used by Carson had a time-width of 60 seconds and its width is directly proportional to flight speed. If the filter width is equal to or larger than the width of the anomaly the smoothing will be great. On the other hand, if the filter width is less than the width of the anomaly the smoothing will be small. Thus, we see on slide 5 that an assumed flight speed of 50 knots* greatly attenuates the sharp caprock anomaly and spreads it over almost the entire anomaly (xxxxx). For an assumed flight speed of 25 knots, however, the filter width is only half as wide and the attenuation effect for a caprock anomaly of this magnitude is very much less (.....).

If high frequency, sharp anomalies are of interest, slow flight speed is indicated. The flight speed for the 1981 demonstration survey was too fast to record the complete caprock anomalies but the evidence of shallow positive influence within the well-defined salt dome minima in Figure 3 are clearly recognizable to an experienced observer.

Gravity gradient measurements, as mentioned at the beginning, are beyond the scope of this study. This completes the overview portion of our paper.

---

*Filter width approximately equal to the width of the caprock anomaly.

COMPARISON OF GRAVITY AND GRADIENT ANOMALIES

We turn now to the comparative study of gravity and gradient anomalies. Gravity and gradient anomalies are quite different in both magnitude and behavior in space. Figure 6 compares gravity and several gradient components

SLIDE #6: Gravity gradient comparison

from a horizontal cylinder of infinite length at increasing altitudes. In the present context, the point of interest on this figure is that the gradients, which are seen to have comparable magnitude at ground level, attenuate with altitude an order of magnitude faster than the gravity anomalies. This figure is from an early paper (Hammer, 1971) which analyzed the behavior of gradients from a theoretical point of view.

Figure 7 is plotted on a semi-log scale and compares the rate of attenuation with altitude of the gravity and vertical gradient anomalies for a spherical mass. Gravity is shown by solid curves and right ordinate scale; vertical

SLIDE #7: Gravity and vertical gradient for a spherical mass

gradient by dashed curves and left ordinate. Three sets of curves represent different depths (D) of the anomalous mass. For all cases the gravity anomaly at ground level $\Delta g(D)$ is 10 mgal.

If we assign resolution limits to the gradient and gravity measurements, these curves define the maximum altitude at which the anomalies can be detected. For example, on the first set of curves (with 100 m depth to the center of mass) the magnitude of the gradient anomaly drops below one (1) EÖtvÖs unit above altitude 1200 m; the gravity anomaly drops below one (1) milligal above altitude 300 m. The other two sets of curves show data for greater depths and indicate higher limiting altitudes.

As mentioned, this represents a gravity anomaly at ground level of 10 mgal. For larger (or smaller) gravity anomalies the ordinate magnitudes are to be multiplied by the ratio.

Figure 8 shows a similar analysis for a two-dimensional gravity anomaly

SLIDE #8: Gravity and vertical gradient for a horizontal cylinder

for a horizontal cylinder of infinite length. The limiting altitudes of detection for this case are considerably larger. The maximum altitudes at which the gradient and gravity anomalies in Figures 7 and 8 are detectable ($\Delta g \geqslant 1$ mgal, $V_{zz} \geqslant 1E°$) are listed in Table 1.

TABLE 1: Maximum Altitudes for Anomaly Detection

	Sphere		Cylinder	
D meters	Gravity meters	Gradient meters	Gravity meters	Gradient meters
100	316	1260	1000	3162
500	1581	3684	5000	7071
2000	6325	9283	20000	14145

This analysis suggests that lower flight altitude is advantageous for gravity measurements. This may be unfavorable for fixed-wing gravity operations. Jordan (1978) has shown that low flight altitudes have other advantages as well.

This completes the technical portion of our paper.

PRESENT STATUS

Finally, it may be of interest to point out that very extensive coverage of HGMS surveys has been accomplished in the past four years (Hammer, 1983). Nearly 200,000 km of gravity line data have been observed in 20 survey areas, 16 of which were overseas and 4 were in the United States and Alaska. The normal production speed is 50 knots, but any speed up to 100 knots (185 km/hr) is possible. The probable error of the data is of the order of 1 mgal and the anomaly resolution limit is of the order of 3 km. The helicopter is capable of flights at altitudes up to 14,000 feet (4300 m) above any type of terrain and environmentally sensitive access. Duration of flights is up to 7 hours. Normal output per month is about 3,000 miles (5000 km) of line data.

A very large project, which has been in progress for some time now, is outlined on Figure 9. If you would like to escape this cold winter weather

SLIDE #9: Bahamas project

in the sunny Bahamas you might like to get involved with this project.

CONCLUSION

In conclusion: the basic purpose of this paper is to emphasize to this group that the anomaly attenuation of gravity gradient components is an order of magnitude greater than of the corresponding gravity anomalies.

Finally, I would like to pose a fundamental dilemma. The question is: To achieve the basic objectives of this symposium what is the best way to proceed?

(a) Should we continue the long-range development of the theory and instrumentation of the gradient measurements; or

(b) Undertake a world-wide gravity mapping program with the precise and rapid HGMS which is now available?

*****FINIS*****

REFERENCES

Carson Geoscience Co., 1981, "Airborne Gravity - Gulf Coast 1981". Company brochure, Perkasie, Pennsylvania 18944.

Hammer, S., 1971, "Vertical attenuation of anomalies in airborne gravimetry". Geophysics, vol. 36, p. 867-877.

Hammer, S., 1983, "Airborne gravity is here!". Geophyiscs, vol. 48, p. 213-223.

Jordan, S.K., 1978, "Moving-base gravity gradiometer surveys and interpretation". Geophysics, vol. 43, p. 94-101.

Nettleton, L.L., 1976, Gravity and Magnetics in Oil Prospecting. McGraw-Hill Book Co.

FIGURE CAPTIONS

Figure 1

Photograph of Carson HGMS in flight. Note trailing magnetometer at lower right.

Figure 2

Flight pattern of HGMS survey. Line spacing 1 km, flight altitude 1000 ft (305 m), and flight speed 50 knots.

Figure 3

Demonstration gravity survey in 1981 over known salt domes in Texas Gulf Coast. Flight elevation 1000 ft (305 m), flight speed 45 knots, and contour interval 1/2 mgal.

Figure 4

Profile comparison of HGMS and conventional ground gravity data from demonstration survey in Figure 3.

Figure 5

Analysis and comparison of simulated HGMS and conventional ground gravity data relative to data in Figure 4.

Figure 6

Theoretical comparison of magnitude and attenuation of all gradient components and gravity anomaly for a horizontal cylinder of infinite length.

Figure 7

Comparative attenuation of gravity and vertical gradient anomalies over a spherical mass. Note semilog ordinate which indicates that gradients attenuate an order of magnitude faster than gravity. See also Table 1 in the text.

Figure 8

Same as Figure 7 but for a two-dimensional mass - a horizontal cylinder of infinite length.

Figure 9

Layout of HGMS gravity survey now in progress in the Bahamas.

Figure 10 (extra)

Attenuation of airborne terrain correction simulated by an assembly of two-dimensional mass elements.

:anm

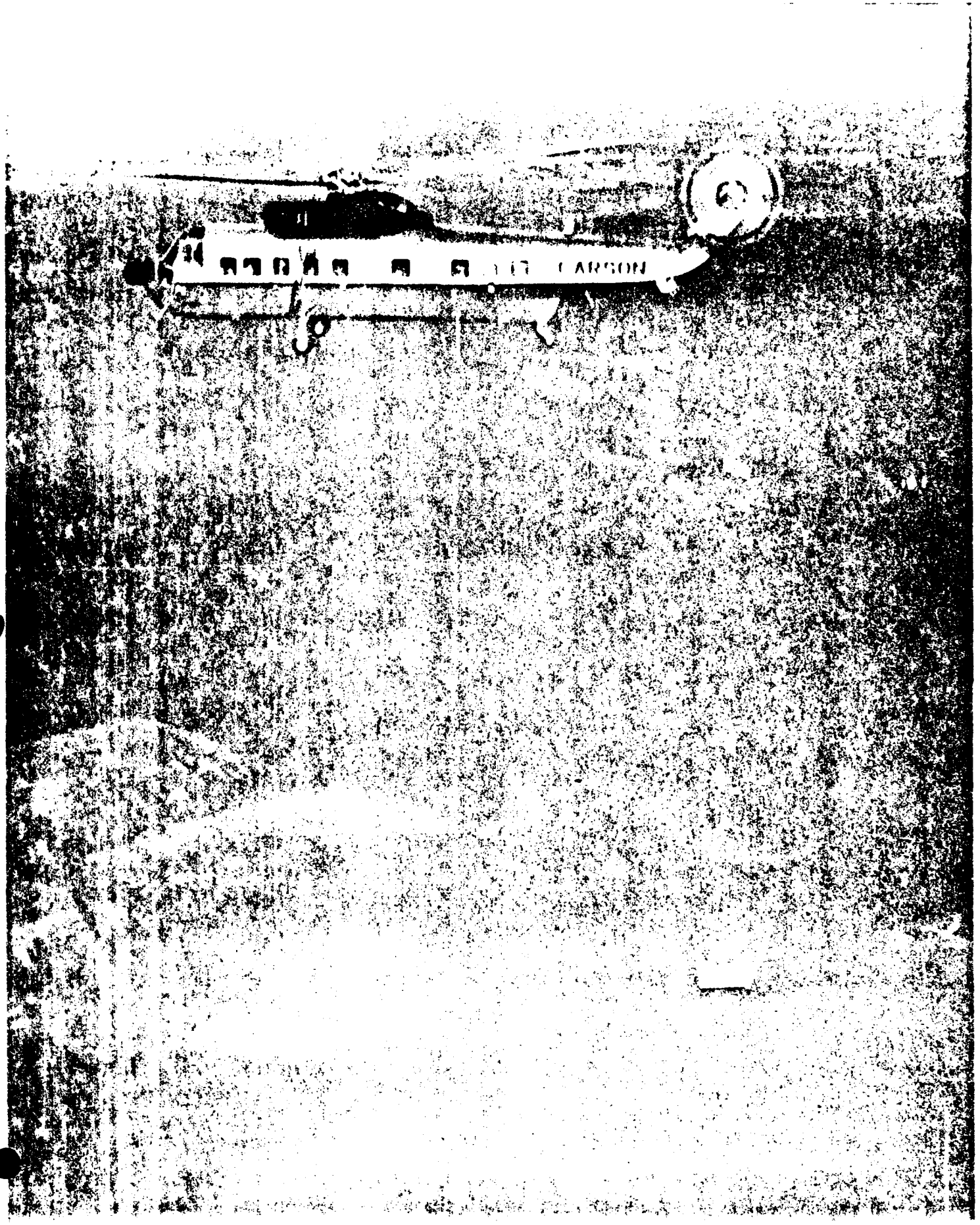

FIG 1 HAMMER & GUMERT

FIG 2 HAMMER & GUMERT 110

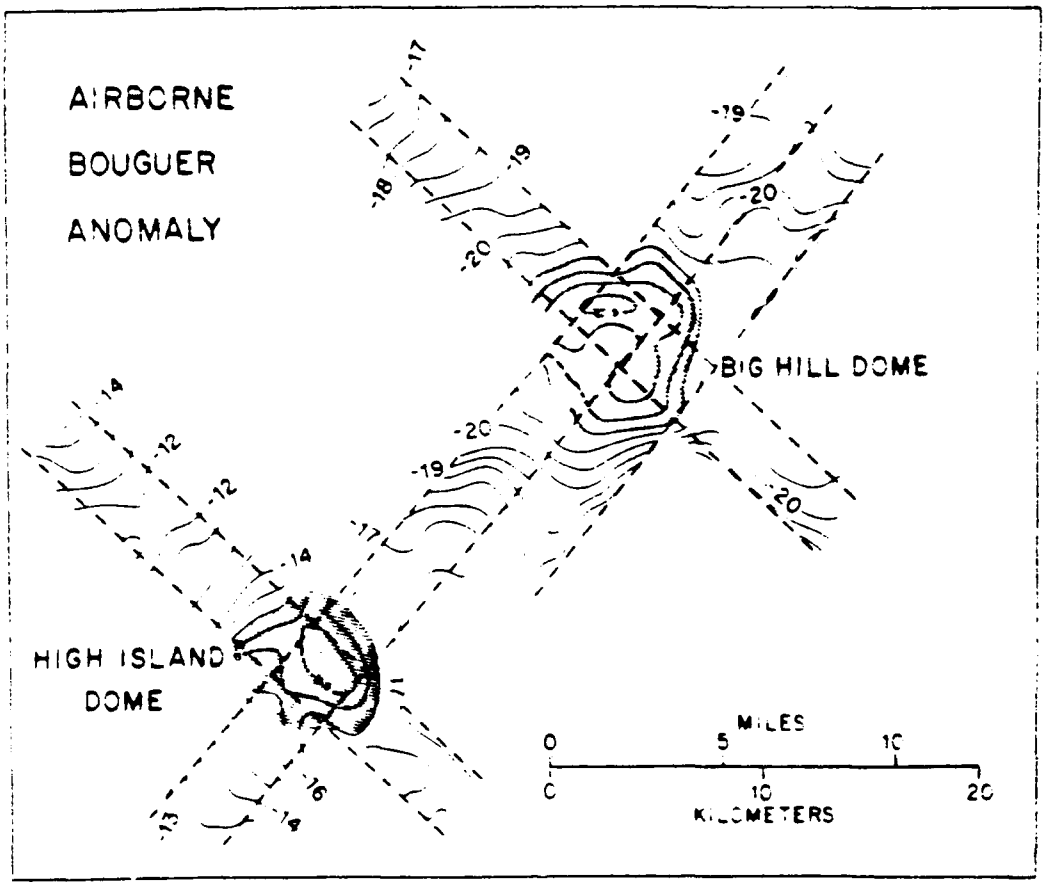

FIG 3 HAMMER & GUMERT

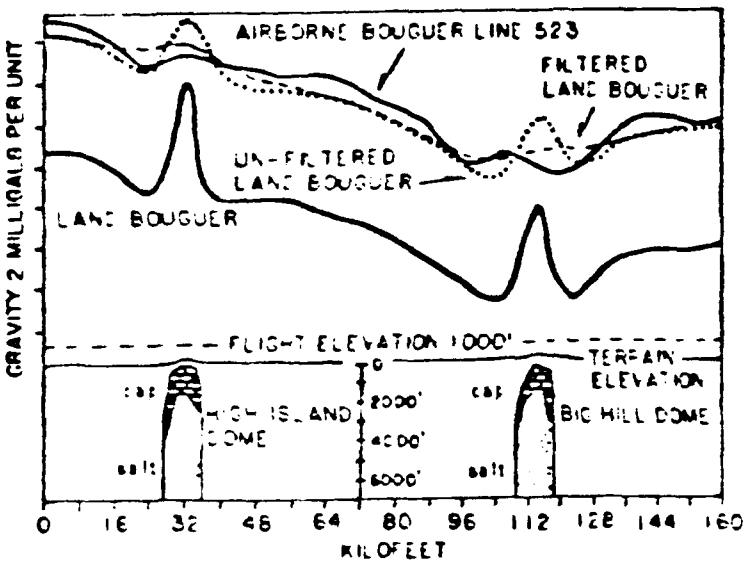

FIG. 4 HAMMER & GUMERT

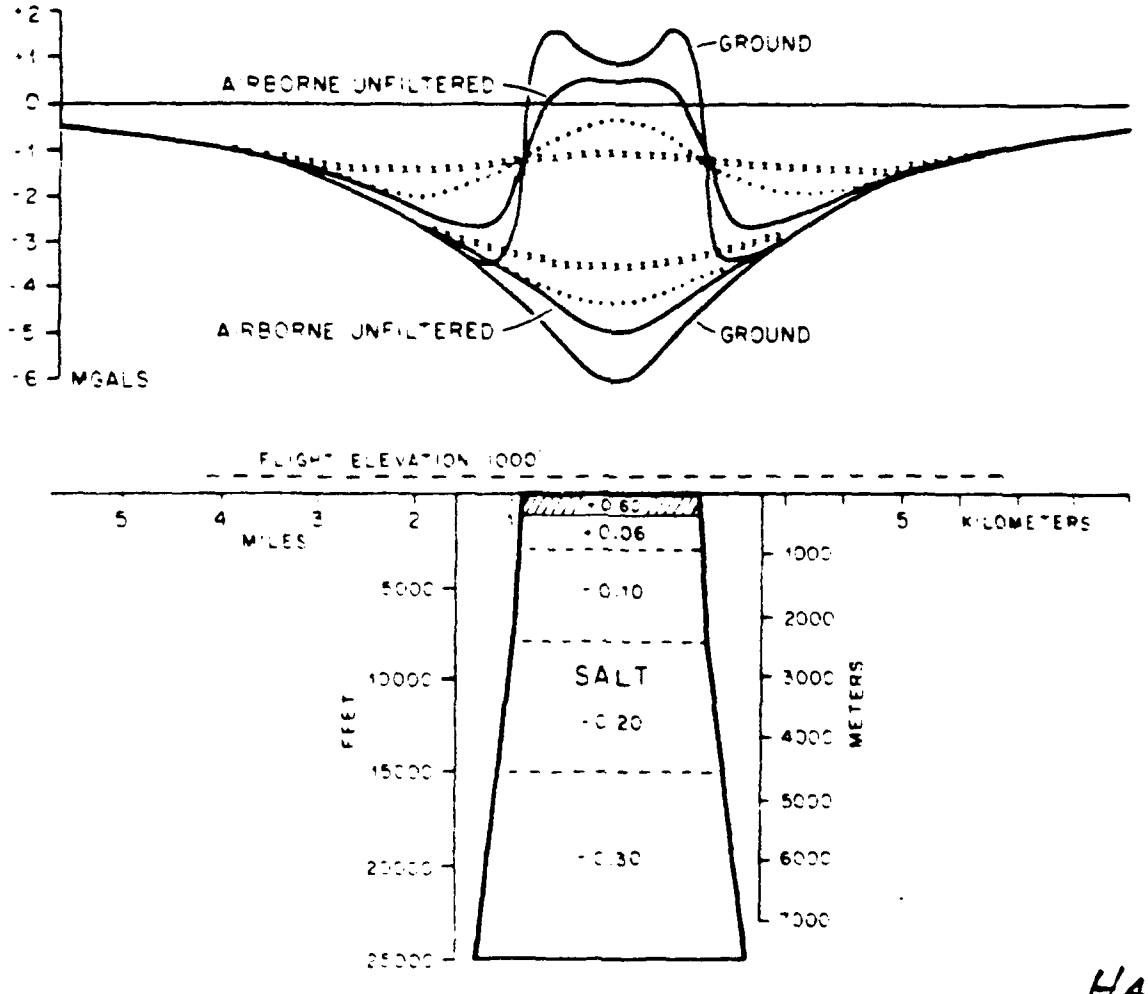

FIG 5 HAMMER & GUMERT

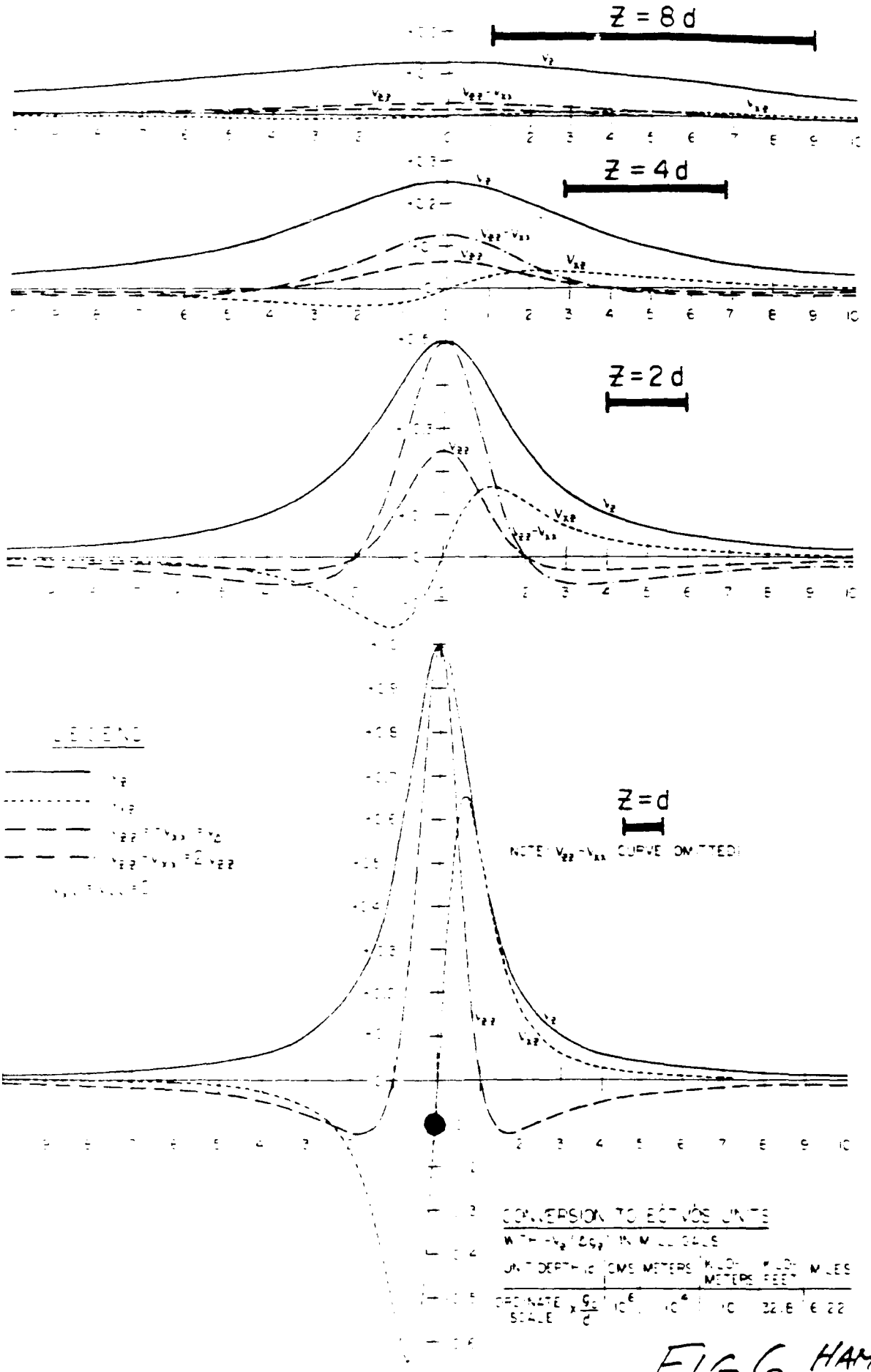

FIG 6 HAMMER & GUMERT

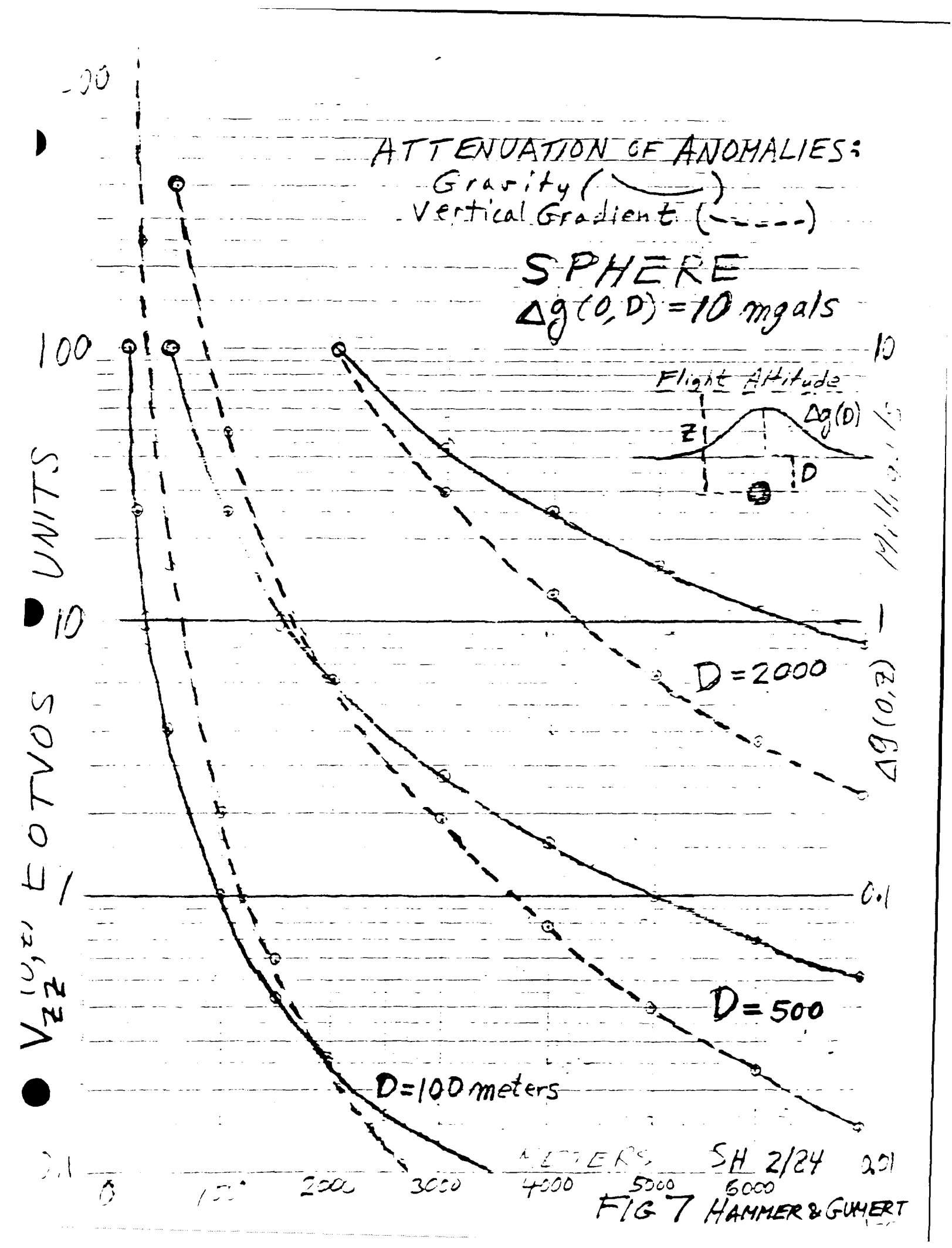

SH 2/24

FIG 7 HAMMER & GUMERT

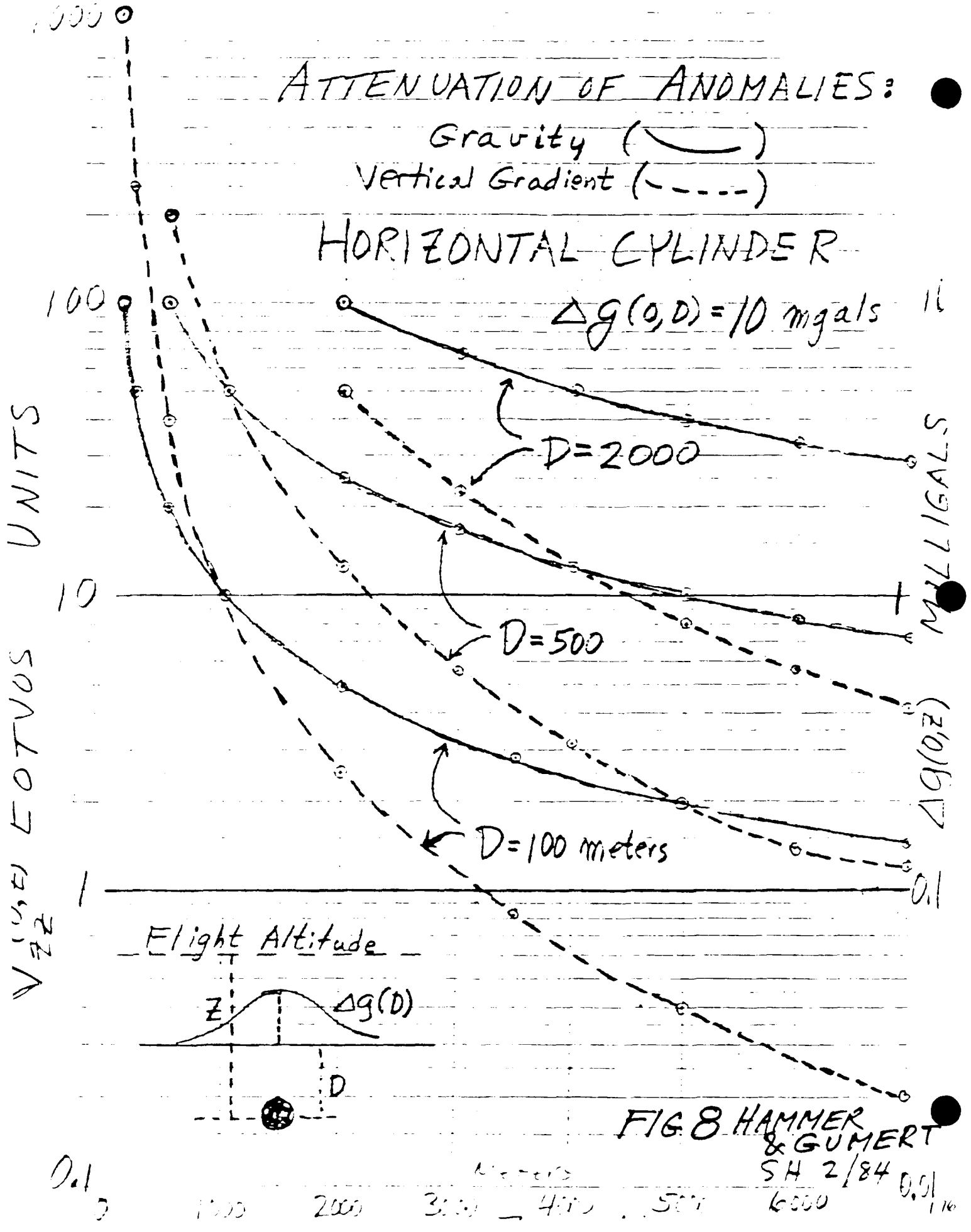
ATTENUATION OF ANOMALIES:
Gravity (——)
Vertical Gradient (- - - -)
HORIZONTAL CYLINDER
Δg(0,D) = 10 mgals
D=2000
D=500
D=100 meters
100
10
1
0.1
0.01
EOTVOS UNITS
MILLIGALS
Δg(0,z)
Flight Altitude
z
Δg(D)
D
FIG 8 HAMMER & GUMERT
SH 2/84
2000
6000

THE COMMONWEALTH OF THE BAHAMAS

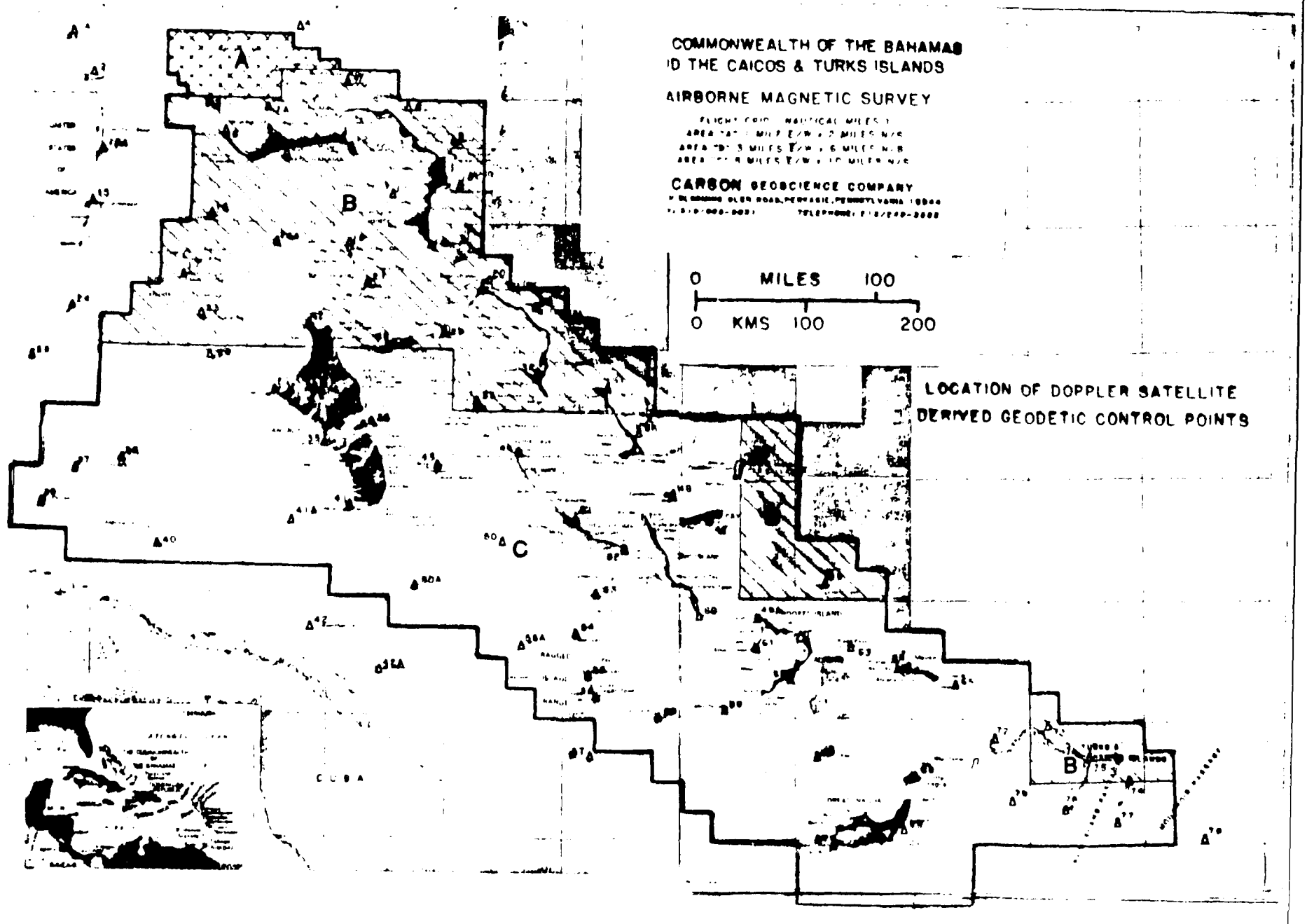

FIG 9 HAMMER & SUMERT

RE-LOOKING AT MASCONS FOR REPRESENTING GRAVITY SURVEY DATA

J. V. BREAKWELL (STANFORD U.)

ABSTRACT: THE REPRESENTATION OF THE HIGHER HARMONIC PART OF THE EARTH'S GRAVITY FIELD BY A FINITE GRID OF MASCONS IN TWO LAYERS, ONE AT THE EARTH'S SURFACE AND ONE AT THE BOTTOM OF THE EARTH'S CRUST, LEADS TO AN ERROR IN THE GRAVITY COMPONENTS AT ALTITUDE (IN ADDITION TO THE ERROR FROM THE ESTIMATION OF DENSITY FLUCTUATIONS IN THE TWO LAYERS). THESE ERRORS ARE EXAMINED FOR VARIOUS RATIOS OF GRID SIZE TO ~~SATELLITE~~ GRADIOMETER ALTITUDE.

Table 3 $\sigma_{\Delta g(z)}$ *(m gal)* **From Truncation**

ℓ_1 \ z (km)	180	240	300
180	.043	.0069	.0011
135	.19	.048	.012
90	.78	.28	.11

8,100 $J_{\ell m}$'s

$$\sigma^2_{\Delta g(z)} = \frac{1}{4\pi^2} \iint_{|\vec{\omega}| \geq \ell_1 / R_\oplus} \text{A-PRIORI } \Phi_{g(z)}(\vec{\omega})\, d\omega_x\, d\omega_y$$

Table 4 $\sigma_{\Delta g(z)}$ *(m gal)* **From Mascon Model Error With Optimal Scalar Averaging** $\mathbf{B}(\omega)$

Δ(km) \ z (km)	180	240	300
110	.050	.0080	.0013
165	.30	.11	.031
220	1.10	.37	.14

Table 5 $\sigma_{\Delta g(z)}$ *(m gal)* **From Mascon Model Error With Optimal Matrix Averaging**

Δ(km) \ z (km)	180	240	300
110	.0088	.00068	.000052
165	.13	.024	.0045
220	.42	.12	.034

$$\begin{pmatrix} (\rho_1)_{AV} \\ (\rho_2)_{AV} \end{pmatrix} = \underset{2\times 2}{B(\vec{\omega})} \begin{pmatrix} \rho_1 \\ \rho_2 \end{pmatrix}$$

SOME LOW ALTITUDE RESULTS

$\sigma_{\Delta g(\Sigma)}^{(\text{mgal})}$ FROM MASCON MODEL ERROR

	Σ (km)	Δ (km)	$\sigma_{\Delta g(\Sigma)}$
1 LAYER	10	5	$.52 \times 10^{-3}$
1 LAYER	"	$5\sqrt{2}$	$.28 \times 10^{-5}$
2 LAYERS	"	5	$.63 \times 10^{-9}$

(OPTIMAL MATRIX AVERAGING)

Table 1 $\sigma_{\Delta g(z)}$ (m *gal*) **From Estimation Error**

ASSUME 1 INDEP. MEAS. EVERY 8 SEC FOR 6 MONTHS

σ_W \ z (km)	180	240	300
0.1E	0.19	0.15	0.14
0.01E	0.022	0.018	0.017

Table 2a $\sigma_{\Delta g(z)}$ (m *gal*) **From Mascon Model Error**

Δ/z \ z (km)	180	240	300
0.2	0.027	0.027	0.026
0.025	0.044	0.041	0.037
0.33	0.077	0.068	0.15
0.5	0.16	0.15	0.15

Table 2b $\sigma_{\Delta g(z)}$ (m *gal*) **From Mascon Model Error**

Δ (km) \ z (km)	180	240	300
110	0.23	0.12	0.075
165	0.76	0.33	0.20
220	2.1	0.71	0.38

37,000 MASCONS

(90 LOCAL ??)

$$\mu_0(\vec{\omega}) = \frac{2\pi\gamma}{\omega}\left\{ \rho_1(\vec{\omega}) + e^{-H\omega}\, \rho_2(\vec{\omega}) \right\}$$

$$\rho_{i_{AV}}(\vec{\omega}) = B(\vec{\omega})\, \rho_i(\vec{\omega}) ,$$

WHERE $$B(\vec{\omega}) = \frac{\sin\left(\frac{\omega_x \Delta}{2}\right) \sin\left(\frac{\omega_y \Delta}{2}\right)}{\left(\frac{\omega_x \Delta}{2}\right)\left(\frac{\omega_y \Delta}{2}\right)}$$

SOME USEFUL FORMULAE

POTENTIAL: $U(z,\vec{\omega}) = e^{-z\omega} U_0(\vec{\omega})$

GRAVITY: $g(z,\vec{\omega}) = -U_z = \omega e^{-z\omega} U_0(\vec{\omega})$

$\Rightarrow$ A-PRIORI SPECTRUM OF $g(z)$:

$$\Phi_{g(z)}(\vec{\omega}) = \omega^2 e^{-2z\omega} \Phi_{U_0}(\vec{\omega})$$

Φ_{U_0} ← HELLER, ✓ TSCHERNING-RAPP, KAULA

VERTICAL GRADIOMETER: $g_{zz}(z,\vec{\omega}) = -\omega^2 e^{-z\omega} U_0(\vec{\omega})$

$\Rightarrow$
- SIGNAL SPECTRUM: $\omega^4 e^{-2z\omega} \Phi_{U_0}(\vec{\omega})$
- NOISE SPECTRUM: $\sigma_W^2 \cdot (\text{AREA} / \text{INDEP. MEAS.})$

WHAT IS ERROR IN $g(\vec{z})$ DUE TO MASCON SPACING?

($\vec{z}$: ALTITUDE)

$$\sigma^2_{\Delta g(z)} = \frac{1}{4\pi^2} \iint_{|\vec{\omega}| \geq l_0/R_\oplus} \phi_{\Delta g(z)}(\vec{\omega})\, d\omega_x\, d\omega_y$$

[e.g. $l_0 \doteq 10$]

$$\phi_{\Delta g(z)}(\vec{\omega}) = \frac{\text{A-PRIORI } \phi_{g(z)}(\vec{\omega})}{1 + \frac{\text{SIGNAL}}{\text{NOISE}}(\vec{\omega})}$$

$$+ \frac{\text{SIGNAL/NOISE}}{1 + \text{SIGNAL/NOISE}} \cdot \Big\{ \text{ALIASING OF A-PRIORI } \phi_{g^*(z)}$$

$$+ \text{A-PRIORI } \phi_{[g^*(z) - g(z)]} \Big\}$$

WHERE $g^*(z)$ = GRAVITY FROM AVERAGED DENSITIES

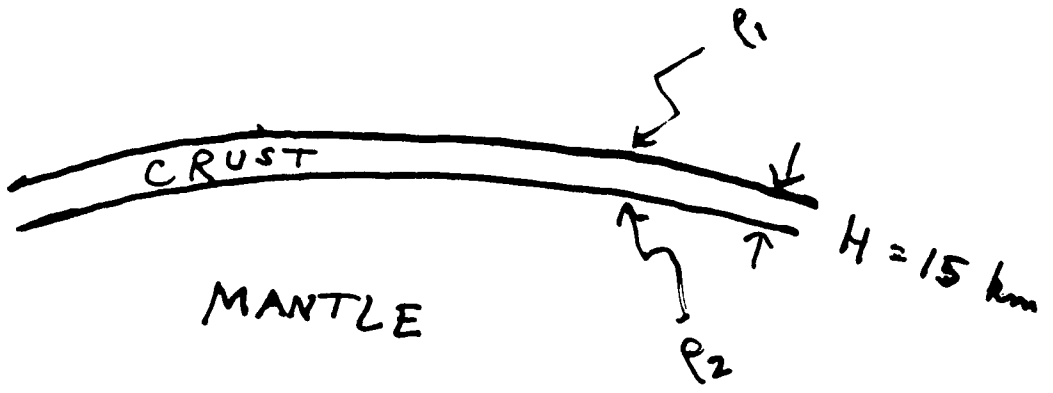

CORE

JEFFREYS' ELASTIC COMPENSATION:

(FOURIER TRANSF.) $\rho_2(\vec{\omega}) = -\rho_1(\vec{\omega}) / (1 + \omega^4 d^4)$

$\omega = |\vec{\omega}| = \sqrt{\omega_x^2 + \omega_y^2}$, $d = 48$ km

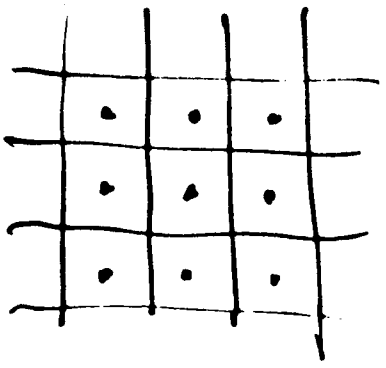

2 LAYERS OF MASCONS : $i = 1, 2$

$M^{(i)}_{nm}$ AT CENTER OF SQUARE $\Delta \times \Delta$

$M^{(i)}_{nm} = \Delta^2 \cdot \{$ ESTIMATED $(\rho_i)_{AV.}$ OVER SQUARE

RE-LOOKING AT MASCONS FOR REPRESENTING GRAVITY SURVEY DATA

J. V. BREAKWELL (STANFORD U.)

ABSTRACT: THE REPRESENTATION OF THE HIGHER HARMONIC PART OF THE EARTH'S GRAVITY FIELD BY A FINITE GRID OF MASCONS IN TWO LAYERS, ONE AT THE EARTH'S SURFACE AND ONE AT THE BOTTOM OF THE EARTH'S CRUST, LEADS TO AN ERROR IN THE GRAVITY COMPONENTS AT ALTITUDE (IN ADDITION TO THE ERROR FROM THE ESTIMATION OF DENSITY FLUCTUATIONS IN THE TWO LAYERS). THE ERRORS ARE EXAMINED FOR VARIOUS RATIOS OF GRID SIZE TO ~~SATELLITE~~ GRADIOMETER ALTITUDE.

Table 3 $\sigma_{\Delta g(z)}$ (m gal) From Truncation

ℓ_1 \ z (km)	180	240	300
180	.043	.0069	.0011
135	.19	.048	.012
90	.78	.28	.11

$8,100$ $J_{\ell m}$'s

$$\sigma^2_{\Delta g(z)} = \frac{1}{4\pi} \iint_{|\vec{\omega}| \geq \ell_1 / R_\oplus} \text{A-PRIORI } \Phi_{g(z)}(\vec{\omega})\, d\omega_x\, d\omega_y$$

Table 4 $\sigma_{\Delta g(z)}$ (m gal) From Mascon Model Error With Optimal Scalar Averaging $B(\omega)$

Δ(km) \ z (km)	180	240	300
110	.050	.0080	.0013
165	.30	.11	.031
220	1.10	.37	.14

Table 5 $\sigma_{\Delta g(z)}$ (m gal) From Mascon Model Error With Optimal Matrix Averaging

Δ(km) \ z (km)	180	240	300
110	.0088	.00068	.000052
165	.13	.024	.0045
220	.42	.12	.034

$$\begin{pmatrix} (\rho_1)_{AV} \\ (\rho_2)_{AV} \end{pmatrix} = \underset{2\times 2}{B(\vec{\omega})} \begin{pmatrix} \rho_1 \\ \rho_2 \end{pmatrix}$$

SOME LOW ALTITUDE RESULTS

$\sigma_{\Delta g(z)}^{(\text{mgal})}$ FROM MASCON MODEL ERROR

	z (km)	Δ (km)	$\sigma_{\Delta g(z)}$
1 LAYER	10	5	$.52 \times 10^{-3}$
1 LAYER	"	$5\sqrt{2}$	$.28 \times 10^{-5}$
2 LAYERS	"	5	$.63 \times 10^{-9}$

(OPTIMAL MATRIX AVERAGING)

Table 1 $\sigma_{\Delta g(z)}$ (m *gal*) From Estimation Error

ASSUME 1 INDEP. MEAS. EVERY 8 SEC FOR 6 MONTHS

σ_W \ z (km)	180	240	300
0.1E	0.19	0.15	0.14
0.01E	0.022	0.018	0.017

Table 2a $\sigma_{\Delta g(z)}$ (m *gal*) From Mascon Model Error

Δ/z \ z (km)	180	240	300
0.2	0.027	0.027	0.026
0.025	0.044	0.041	0.037
0.33	0.077	0.068	0.15
0.5	0.16	0.15	0.15

Table 2b $\sigma_{\Delta g(z)}$ (m *gal*) From Mascon Model Error

Δ (km) \ z (km)	180	240	300
110	0.23	0.12	0.075
165	0.78	0.33	0.20
220	2.1	0.71	0.38

37,000 MASCONS

(90 LOCAL ??)

$$U_0(\vec{\omega}) = \frac{2\pi\gamma}{\omega}\left\{ \rho_1(\vec{\omega}) + e^{-H\omega}\, \rho_2(\vec{\omega})\right\}$$

$$\rho_{i_{AV}}(\vec{\omega}) = B(\vec{\omega})\, \rho_i(\vec{\omega}) ,$$

WHERE $$B(\vec{\omega}) = \frac{\sin\left(\frac{\omega_x \Delta}{2}\right) \sin\left(\frac{\omega_y \Delta}{2}\right)}{\left(\frac{\omega_x \Delta}{2}\right)\left(\frac{\omega_y \Delta}{2}\right)}$$

SOME USEFUL FORMULAE

POTENTIAL: $U(z,\vec{\omega}) = e^{-z\omega} U_0(\vec{\omega})$

GRAVITY: $g(z,\vec{\omega}) = -U_z = \omega e^{-z\omega} U_0(\vec{\omega})$

$\Rightarrow$ A-PRIORI SPECTRUM OF $g(z)$:

$$\Phi_{g(z)}(\vec{\omega}) = \omega^2 e^{-2z\omega} \Phi_{U_0}(\vec{\omega})$$

Φ_{U_0}: ✓ TSCHERNING-RAPP > KAULA
HELLER >

VERTICAL GRADIOMETER: $g_z(z,\vec{\omega}) = -\omega^2 e^{-z\omega} U_0(\vec{\omega})$

$\Rightarrow$
- SIGNAL SPECTRUM: $\omega^4 e^{-2z\omega} \Phi_{U_0}(\vec{\omega})$
- NOISE SPECTRUM: $\sigma_W^2 \cdot$ (AREA / INDEP. MEAS.)

WHAT IS ERROR IN $g(z)$ (z: ALTITUDE) DUE TO MASCON SPACING?

$$\sigma^2_{\Delta g(z)} = \frac{1}{4\pi^2} \iint_{|\vec{\omega}| \geq l_0/R_\oplus} \phi_{\Delta g(z)}(\vec{\omega})\, d\omega_x\, d\omega_y$$

[e.g. $l_0 \doteq 10$]

$$\phi_{\Delta g(z)}(\vec{\omega}) = \frac{\text{A-PRIORI } \phi_{g(z)}(\vec{\omega})}{1 + \frac{\text{SIGNAL}}{\text{NOISE}}(\vec{\omega})}$$

$$+ \frac{\text{SIGNAL/NOISE}}{1 + \text{SIGNAL/NOISE}} \cdot \Big\{ \text{ALIASING OF A-PRIORI } \phi_{g^*(z)}$$

$$+ \text{A-PRIORI } \phi_{[g^*(z) - g(z)]} \Big\}$$

WHERE $g^*(z)$ = GRAVITY FROM AVERAGED DENSITIES

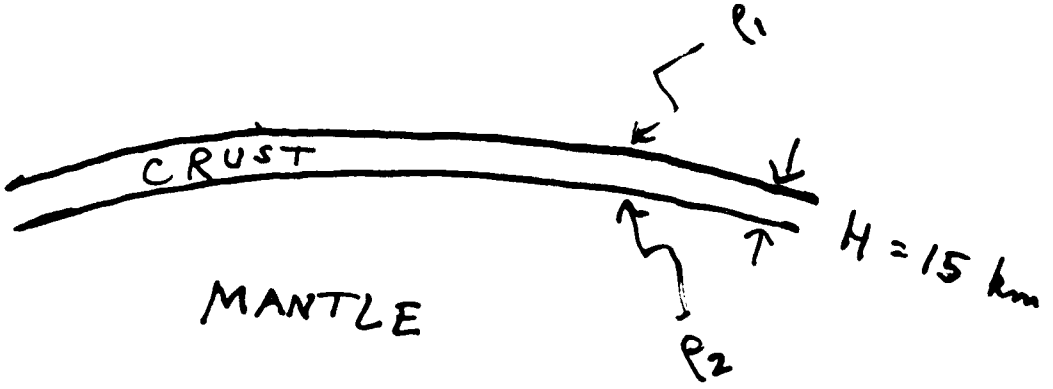

CORE

JEFFREYS' ELASTIC COMPENSATION:

(FOURIER TRANSF.) $\rho_2(\vec{\omega}) = -\rho_1(\vec{\omega})/(1+\omega^4 d^4)$

$\omega = |\vec{\omega}| = \sqrt{\omega_x^2 + \omega_y^2}$, $d = 48$ km

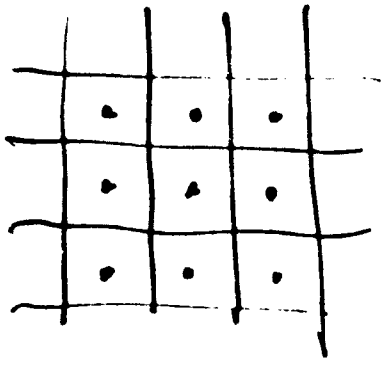

2 LAYERS OF MASCONS : $i = 1, 2$

$M^{(i)}_{nm}$ AT CENTER OF SQUARE $\Delta \times \Delta$

$M^{(i)}_{nm} = \Delta^2 \cdot \{$ ESTIMATED $(\rho_i)_{AV.}$ OVER SQUARE

RE-LOOKING AT MASCONS FOR REPRESENTING GRAVITY SURVEY DATA

J. V. BREAKWELL (STANFORD U.)

ABSTRACT: THE REPRESENTATION OF THE HIGHER HARMONIC PART OF THE EARTH'S GRAVITY FIELD BY A FINITE GRID OF MASCONS IN TWO LAYERS, ONE AT THE EARTH'S SURFACE AND ONE AT THE BOTTOM OF THE EARTH'S CRUST, LEADS TO AN ERROR IN THE GRAVITY COMPONENTS AT ALTITUDE (IN ADDITION TO THE ERROR FROM THE ESTIMATION OF DENSITY FLUCTUATIONS IN THE TWO LAYERS). THESE ERRORS ARE EXAMINED FOR VARIOUS RATIOS OF GRID SIZE TO ~~SATELLITE~~ GRADIOMETER ALTITUDE.

Table 3 $\sigma_{\Delta g(z)}$ *(m gal)* **From Truncation**

l_1 \ z (km)	180	240	300
180	.043	.0069	.0011
135	.19	.048	.012
90	.78	.28	.11

8,100 J_{lm}'s

$$\sigma^2_{\Delta g(z)} = \frac{1}{4\pi} \iint_{|\vec{\omega}| \geq l_1/R_\oplus} \text{A-PRIORI}\ \Phi_{g(z)}(\vec{\omega})\, d\omega_x\, d\omega_y$$

Table 4 $\sigma_{\Delta g(z)}$ *(m gal)* **From Mascon Model Error With Optimal Scalar Averaging** $\mathcal{B}(\omega)$

Δ(km) \ z (km)	180	240	300
110	.050	.0080	.0013
165	.39	.11	.031
220	1.10	.37	.14

Table 5 $\sigma_{\Delta g(z)}$ *(m gal)* **From Mascon Model Error With Optimal Matrix Averaging**

Δ(km) \ z (km)	180	240	300
110	.0088	.00068	.000052
165	.13	.024	.0045
220	.42	.12	.034

$$\begin{pmatrix} (\rho_1)_{AV} \\ (\rho_2)_{AV} \end{pmatrix} = \overset{2\times 2}{B(\vec{\omega})} \begin{pmatrix} \rho_1 \\ \rho_2 \end{pmatrix}$$

SOME LOW ALTITUDE RESULTS

$\sigma_{\Delta g(z)}^{(\text{mgal})}$ FROM MASCON MODEL ERROR

	z (km)	Δ (km)	$\sigma_{\Delta g(z)}$
1 LAYER	10	5	$.52 \times 10^{-3}$
1 LAYER		$5\sqrt{2}$	$.28 \times 10^{-5}$
2 LAYERS	"	5	$.63 \times 10^{-7}$

(OPTIMAL MATRIX AVERAGING)

Table 1 $\sigma_{\Delta g(z)}$ (m gal) From Estimation Error

ASSUME 1 INDEP. MEAS. EVERY 8 SEC FOR 6 MONTHS

σ_W \ z (km)	180	240	300
0.1E	0.19	0.15	0.14
0.01E	0.022	0.018	0.017

Table 2a $\sigma_{\Delta g(z)}$ (m gal) From Mascon Model Error

Δ/z \ z (km)	180	240	300
0.2	0.027	0.027	0.026
0.025	0.044	0.041	0.037
0.33	0.077	0.068	0.15
0.5	0.16	0.15	0.15

Table 2b $\sigma_{\Delta g(z)}$ (m gal) From Mascon Model Error

Δ(km) \ z (km)	180	240	300
110	0.23	0.12	0.075
165	0.76	0.33	0.20
220	2.1	0.71	0.38

37,000 MASCONS

(90 LOCAL ??)

$$U_0(\vec{\omega}) = \frac{2\pi\gamma}{\omega}\left\{ \rho_1(\vec{\omega}) + e^{-H\omega}\, \rho_2(\vec{\omega})\right\}$$

$$\rho_{i_{AV}}(\vec{\omega}) = B(\vec{\omega})\, \rho_i(\vec{\omega}) ,$$

WHERE $$B(\vec{\omega}) = \frac{\sin\left(\frac{\omega_x \Delta}{2}\right) \sin\left(\frac{\omega_y \Delta}{2}\right)}{\left(\frac{\omega_x \Delta}{2}\right)\left(\frac{\omega_y \Delta}{2}\right)}$$

SOME USEFUL FORMULAE

POTENTIAL: $U(z,\vec{\omega}) = e^{-z\omega} U_0(\vec{\omega})$

GRAVITY: $g(z,\vec{\omega}) = -U_z = \omega e^{-z\omega} U_0(\vec{\omega})$

$\Rightarrow$ A-PRIORI SPECTRUM OF $g(z)$:

$$\Phi_{g(z)}(\vec{\omega}) = \omega^2 e^{-2z\omega} \Phi_{U_0}(\vec{\omega})$$

Φ_{U_0} ✓ HELLER, TSCHERNING-RAPP, KAULA

VERTICAL GRADIOMETER: $g_z(z,\vec{\omega}) = -\omega^2 e^{-z\omega} U_0(\vec{\omega})$

$\Rightarrow$
- SIGNAL SPECTRUM: $\omega^4 e^{-2z\omega} \Phi_{U_0}(\vec{\omega})$
- NOISE SPECTRUM: $\sigma_W^2 \cdot$ (AREA / INDEP. MEAS.)

WHAT IS ERROR IN $g(z)$ DUE TO MASCON SPACING

(z = ALTITUDE)

$$\sigma^2_{\Delta g(z)} = \frac{1}{4\pi^2} \iint_{|\vec{\omega}| \geq l_0/R_\oplus} \phi_{\Delta g(z)}(\vec{\omega})\, d\omega_x\, d\omega_y$$

[e.g. $l_0 \doteq 10$]

$$\phi_{\Delta g(z)}(\vec{\omega}) = \frac{\text{A-PRIORI } \phi_{g(z)}(\vec{\omega})}{1 + \frac{\text{SIGNAL}}{\text{NOISE}}(\vec{\omega})}$$

$$+ \frac{\text{SIGNAL/NOISE}}{1 + \text{SIGNAL/NOISE}} \cdot \Big\{ \text{ALIASING OF A-PRIORI } \phi_{g^*(z)}$$

$$+ \text{A-PRIORI } \phi_{[g^*(z) - g(z)]} \Big\}$$

WHERE $g^*(z)$ = GRAVITY FROM AVERAGED DENSITIES

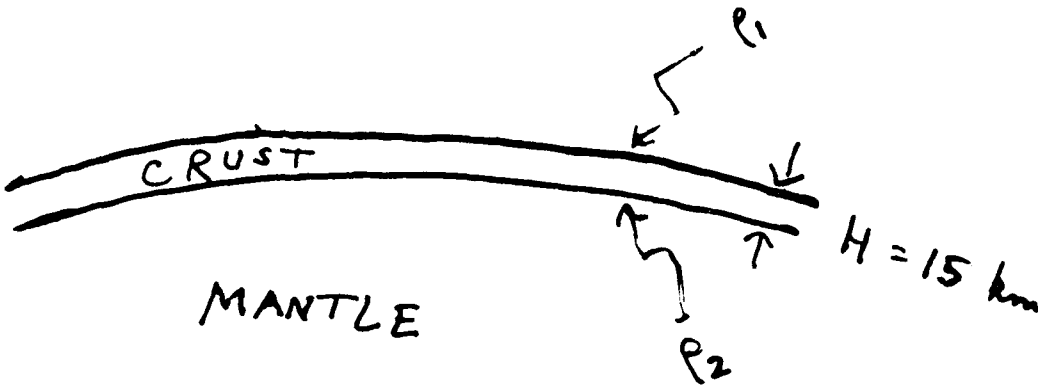

CORE

JEFFREYS' ELASTIC COMPENSATION:

(FOURIER TRANSF.) $\rho_2(\vec{\omega}) = -\rho_1(\vec{\omega}) / (1 + \omega^4 d^4)$

$\omega = |\vec{\omega}| = \sqrt{\omega_x^2 + \omega_y^2}$, $d = 48$ km

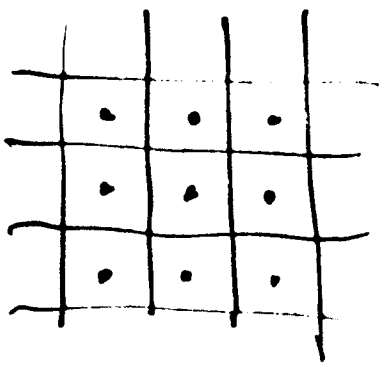

2 LAYERS OF MASCONS : $i = 1, 2$

$M^{(i)}_{nm}$ AT CENTER OF SQUARE $\Delta \times \Delta$

$M^{(i)}_{nm} = \Delta^2 \cdot \{$ ESTIMATED $\rho_i)_{AV.}$ OVER SQUARE

B-506U

INTEGRAL FORMULAS RELATING GRAVITY GRADIENTS TO VERTICAL DEFLECTIONS

Presented At

TWELFTH MOVING BASE GRAVITY GRADIOMETER CONFERENCE
UNITED STATES AIR FORCE ACADEMY

14-15 February 1984

Dynamics Research Corporation
60 Concord Street
Wilmington, Massachusetts 01887

ABSTRACT

INTEGRAL FORMULAS RELATING GRAVITY GRADIENTS TO VERTICAL DEFLECTIONS

ALAN H. ZORN
Dynamics Research Corporation
60 Concord Street
Wilmington, Massachusetts 01887

A number of integral formulas relating gravity gradients to vertical deflections are presented. The formulas are derived from standard geodesy theory and are similar to the Stokes' and Vening-Meinesz integral formulas. The deterministic formulas provide a physical explanation of certain properties common to various self-consistent stochastic gravity models. For example, the high degree of correlation between the gravity gradient, T_{xz}, and the vertical deflection, T_x, in most gravity models can be physically justified based on a deterministic integral formula. The integral formulas may lead to insight into the construction of gradiometer filters to estimate vertical deflections which are insensitive to stochastic gravity models. Implementation considerations involving discretization and truncation of the integral formulas are explored using surface gravity data over the Blake Escarpment.

OBJECTIVE

- TO EXTEND THE STOKES' AND VENING MEINESZ INTEGRAL FORMULAS TO GRAVITY GRADIENT
- TO INVESTIGATE PRACTICAL CONSIDERATIONS OF IMPLEMENTATION
- TO DISCUSS VERTICAL DEFLECTION SURVEY APPLICATIONS AND GRAVITY GRADIENT TEST REFERENCE METHODS

SOME DEFINITIONS

- N = GEOIDAL HEIGHT
- T = ANOMALOUS POTENTIAL (BRUNS FORMULA GIVES GEOIDAL HEIGHT AS $N = T/g_o$)
- Δg = GRAVITY ANOMALY
- $\xi = -\frac{\partial N}{\partial x}$ AND $\eta = -\frac{\partial N}{\partial y}$ ARE VERTICAL DEFLECTIONS $(x - y - z = N - E - D)$ AND ARE PROPORTIONAL TO T_x AND T_y RESPECTIVELY
- $\begin{bmatrix} T_{xx} & T_{xy} & T_{xz} \\ T_{yx} & T_{yy} & T_{yz} \\ T_{zx} & T_{zy} & T_{zz} \end{bmatrix}$ = ANOMOLOUS GRAVITY GRADIENT TENSOR

ASSUMPTIONS AND APPROXIMATIONS

- ANOMALOUS POTENTIAL T (x, y, z) IS A HARMONIC FIELD. THAT IS,

$$\frac{\partial^2 T}{\partial x^2} + \frac{\partial^2 T}{\partial y^2} + \frac{\partial^2 T}{\partial z^2} = 0$$

- FLAT - EARTH APPROXIMATION

- $\Delta g \cong T_z$ (FUNDAMENTAL EQUATION OF PHYSICAL GEODESY IS $\Delta g = T_z - 2 (g_o/r) N$)

STOKES' FORMULA

- SHAPE OF THE EARTH CAN BE FOUND FROM GRAVITY ANOMALY MEASUREMENTS:

$$N(x, y) = \frac{1}{2\pi g_o} \int_{-\infty}^{\infty}\int_{-\infty}^{\infty} \frac{\Delta g(u, v)}{[(x-u)^2 + (y-v)^2]^{1/2}}\, du\, dv$$

- USING BRUNS FORMULA $N = T/g_o$ AND THE APPROXIMATION $\Delta g \cong T_z$,

$$T(x, y) = \frac{1}{2\pi} \int_{-\infty}^{\infty}\int_{-\infty}^{\infty} \frac{T_z(u, v)}{[(x-u)^2 + (y-v)^2]^{1/2}}\, du\, dv$$

- STOKES' FORMULA HOLDS FOR ANY HARMONIC FUNCTION. CAN REPLACE T WITH T_x, T_y, OR T_z TO OBTAIN STOKES' FORMULAS FOR THE GRADIENTS:

$$T_x(x, y) = \frac{1}{2\pi} \int_{-\infty}^{\infty}\int_{-\infty}^{\infty} \frac{T_{xz}(u, v)}{[(x-u)^2 + (y-v)^2]^{1/2}}\, du\, dv$$

$$T_y(x, y) = \frac{1}{2\pi} \int_{-\infty}^{\infty}\int_{-\infty}^{\infty} \frac{T_{yz}(u, v)}{[(x-u)^2 + (y-v)^2]^{1/2}}\, du\, dv$$

$$T_z(x, y) = \frac{1}{2\pi} \int_{-\infty}^{\infty}\int_{-\infty}^{\infty} \frac{T_{zz}(u, v)}{[(x-u)^2 + (y-v)^2]^{1/2}}\, du\, dv$$

FORMULAS OF VENING MEINESZ

- DEFLECTIONS OF THE VERTICAL CAN ALSO BE FOUND FROM GRAVITY ANOMALY MEASUREMENTS:

$$\xi(x, y) = \frac{1}{2\pi g_o} \int_{-\infty}^{\infty} \int_{-\infty}^{\infty} \frac{(x-u)\,\Delta g(u, v)}{[(x-u)^2 + (y-v)^2]^{3/2}}\, du\, dv$$

$$\eta(x, y) = \frac{1}{2\pi g_o} \int_{-\infty}^{\infty} \int_{-\infty}^{\infty} \frac{(y-v)\,\Delta g(u, v)}{[(x-u)^2 + (y-v)^2]^{3/2}}\, du\, dv$$

- LEADS TO:

$$T_x(x, y) = -\frac{1}{2\pi} \int_{-\infty}^{\infty} \int_{-\infty}^{\infty} \frac{(x-u)\,T_z(u, v)}{[(x-u)^2 + (y-v)^2]^{3/2}}\, du\, dv$$

$$T_y(x, y) = -\frac{1}{2\pi} \int_{-\infty}^{\infty} \int_{-\infty}^{\infty} \frac{(y-v)\,T_z(u, v)}{[(x-u)^2 + (y-u)^2]^{3/2}}\, du\, dv$$

- HOLDS FOR ANY HARMONIC FUNCTION. CAN REPLACE T WITH T_x, T_y, OR T_z TO GET GRADIENT FORMULAS OF VENING MEINESZ:

$T_{xx} \leftarrow T_{xz}$ $\qquad$ $T_{xy} \leftarrow T_{xz}$

$T_{xy} \leftarrow T_{yz}$ $\qquad$ $T_{yy} \leftarrow T_{yz}$

$T_{xz} \leftarrow T_{zz}$ $\qquad$ $T_{yz} \leftarrow T_{zz}$

RELATIONSHIPS BETWEEN GRAVIMETRIC QUANTITIES

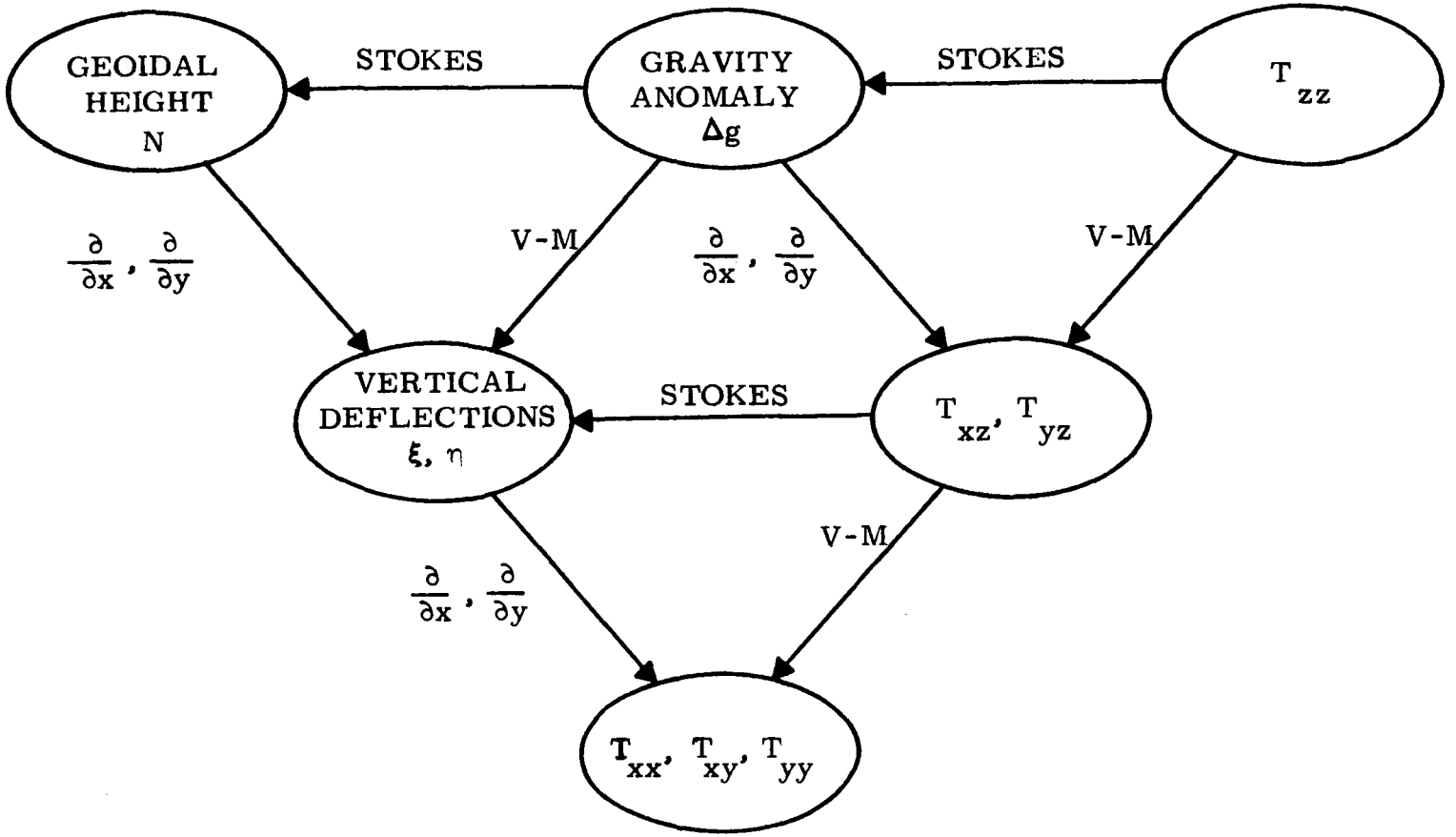

- TRANSFORMATIONS OPERATE IN THE LEVEL x-y PLANE ONLY

USES OF THE GRADIENT INTEGRAL FORMULAS

- CONSTRUCTION OF VERTICAL DEFLECTION MAPS FROM GRADIOMETER SURVEYS
- CONSTRUCTION OF GRAVITY GRADIENT TEST REFERENCE FROM GRADIOMETER SURVEY
- GRAVITY FILTER DESIGN (OFFERS DETERMINISTIC APPROACH OR HELPS IN DESIGN OF GRAVITY MODEL INSENSITIVE STOCHASTIC FILTER)

RECOVERY OF VERTICAL DEFLECTIONS FROM GRADIENT

- TRANSFORM STOKES' FORMULA FOR THE GRADIENTS TO POLAR COORDINATES:

$$T_x(x, y) = \frac{1}{2\pi} \int_{-\infty}^{\infty} \int_{-\infty}^{\infty} \frac{T_{xz}(u, v)}{[(x-u)^2 + (y-v)^2]^{1/2}} \, du \, dv$$

$$= \frac{1}{2\pi} \int_0^{\infty} \int_0^{2\pi} \frac{T_{xz}(x - r\cos\theta, y - r\sin\theta)}{r} \, r \, d\theta \, dr$$

$$= \int_0^{\infty} \left\{ \frac{1}{2\pi} \int_0^{2\pi} T_{xz}(x - r\cos\theta, y - r\sin\theta) \, d\theta \right\} dr$$

$$= \int_0^{\infty} \overline{T_{xz}} \, dr$$

$\overline{T_{xz}}$ = AVERAGE VALUE OF T_{xz} ON CIRCLE CENTERED AT (x, y) OF RADIUS r

- AT FIRST GLANCE, INTEGRAL UNBOUNDED. HOWEVER, INTEGRAL CONVERGES FOR "HIGH" FREQUENCIES

RESULTS BASED ON BLAKE ESCARPMENT DATA

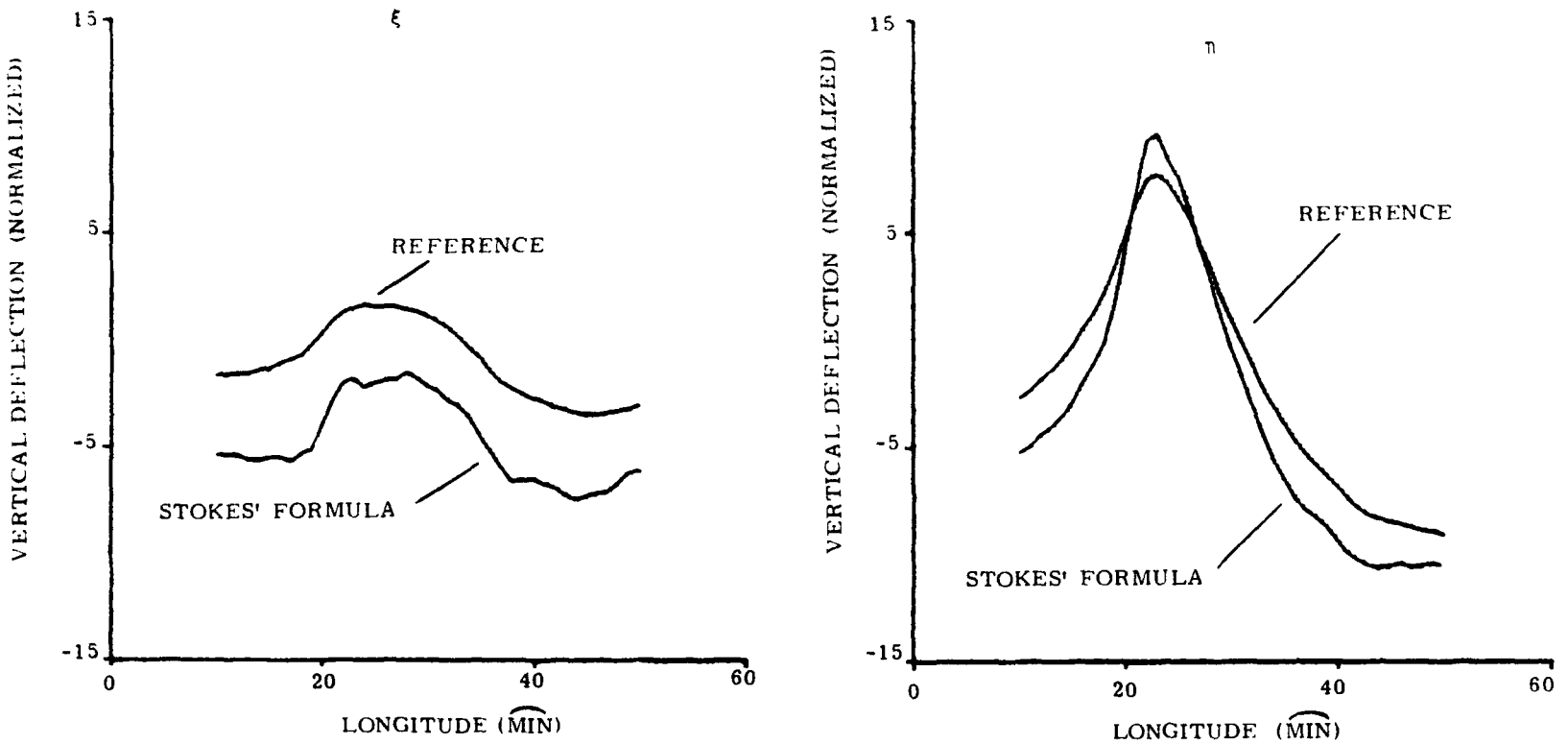

- GRADIENT MAP CONSTRUCTED FROM REFERENCE MAP (ANOMALIES AND VERTICAL DEFLECTIONS) USING BICUBIC SPLINE DIFFERENTIATION
- STOKES' FORMULA DISCRETIZED ON 1 $\widehat{\text{MIN}}$ GRID AND TRUNCATED AT 40 NM

ERRORS IN USING STOKES' INTEGRAL FORMULA

- DISCRETIZATION OF INTEGRAL (MINOR ON 1 $\overset{\frown}{\text{MIN}}$ GRID)
- TRUNCATION OF INTEGRAL (MAJOR) - ERROR DEPENDS ON FREQUENCY OF GRAVITY
- CONSISTENCY OF DATA OR GRADIOMETER MEASUREMENT ERROR (DEPENDING ON SOURCE OF REFERENCE)

TRUNCATION ERRORS

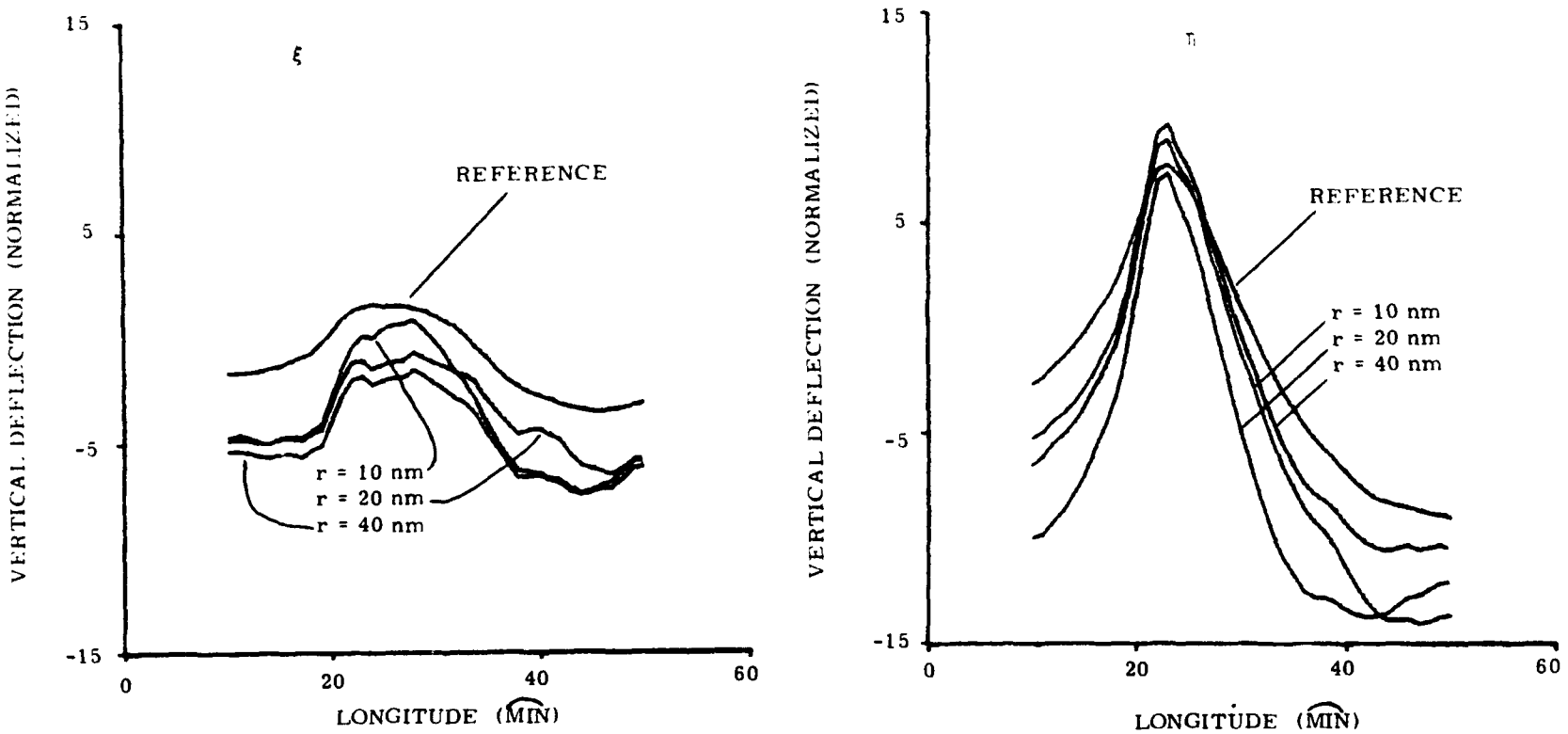

- r IS RADIUS OF CIRCLE BOUNDING REGION OF INTEGRATION

MORE ON TRUNCATION ERRORS

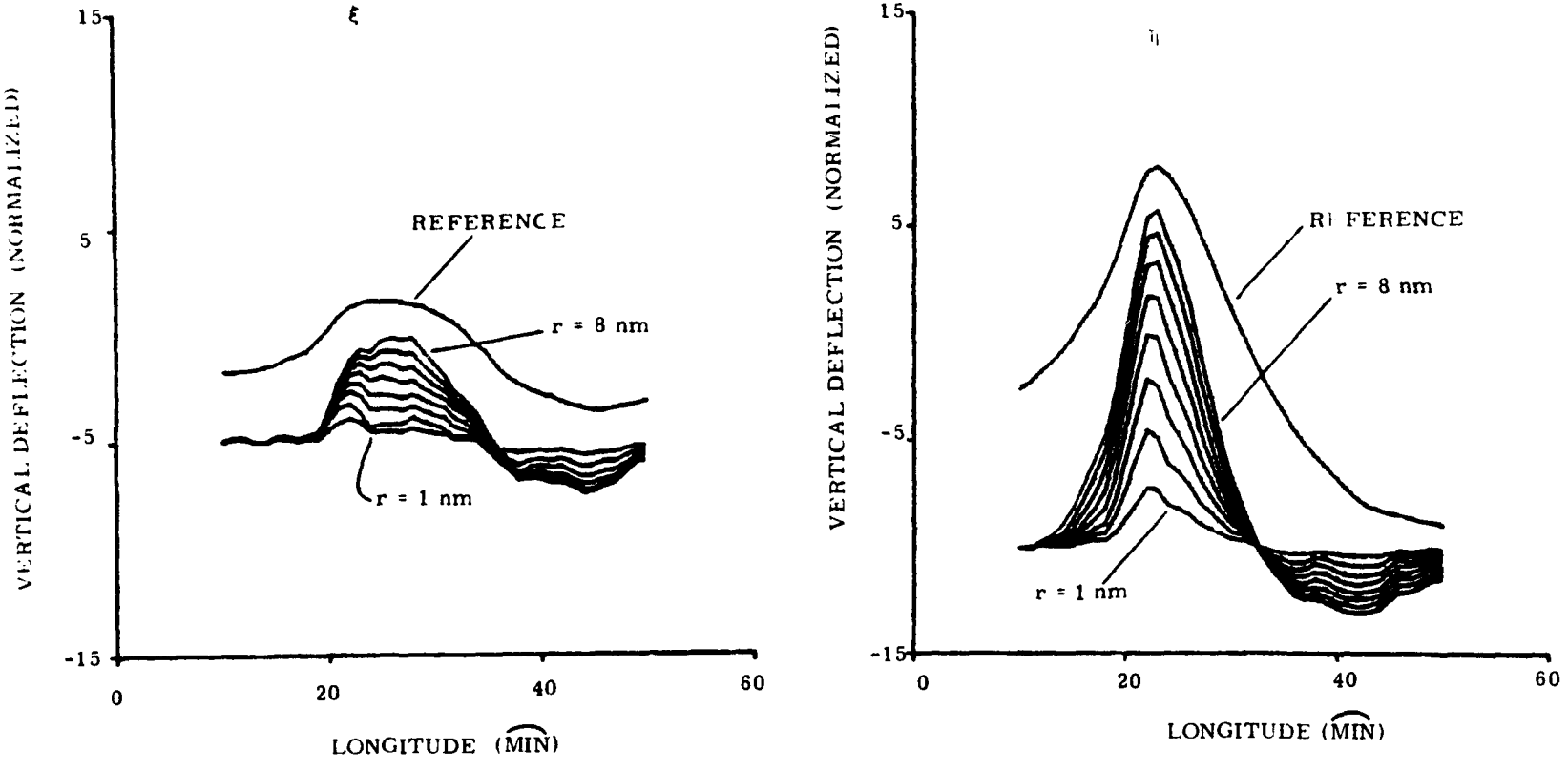

- RADIUS VARIED THROUGH r = 1, 2, . . . , 8 NM
- FOR SMALL RADII, STOKES' INTEGRAL FORMULA APPROXIMATES ξ AND η AS PROPORTIONAL TO A SMOOTHED VALUE OF T_{xz} AND T_{yz}, RESPECTIVELY

CORRELATIONS BETWEEN VERTICAL DEFLECTIONS AND GRAVITY GRADIENTS

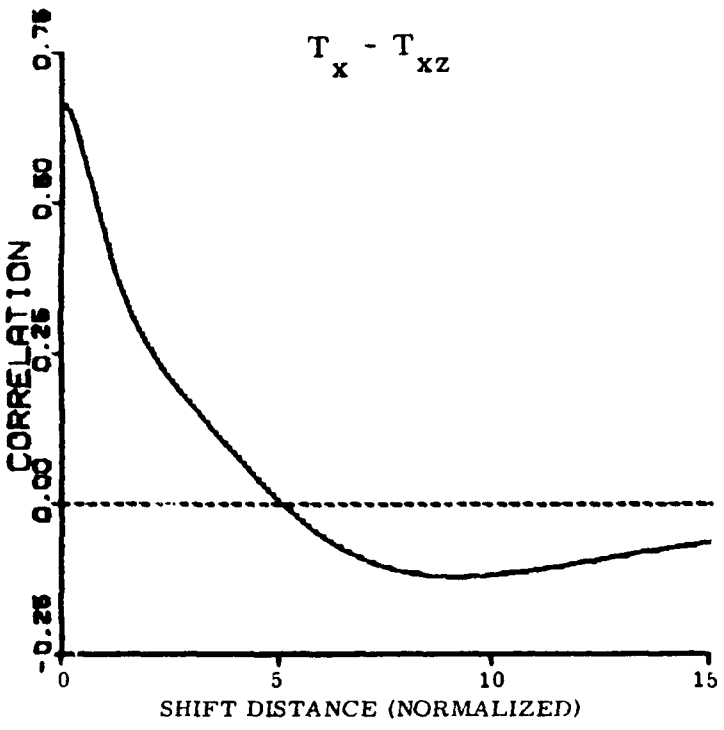

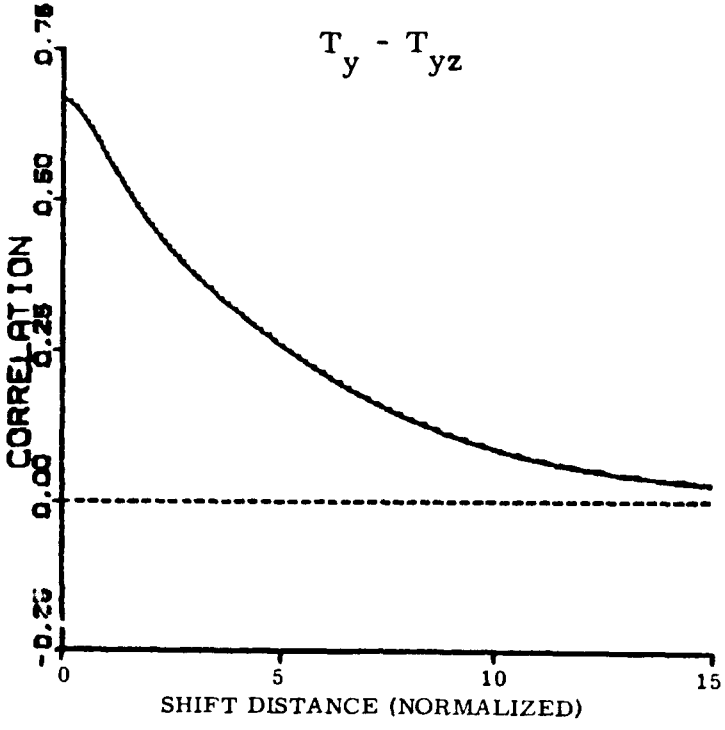

- 3-TERM STAG MODEL
- x = ALONG TRACK, y = CROSS TRACK, z = DOWN
- LARGE CORRELATION AT ZERO SHIFT BETWEEN T_x AND T_{xz} IS DUE TO THE DETERMINISTIC RELATIONSHIP BROUGHT OUT IN STOKES' FORMULAS FOR THE GRADIENTS

SUMMARY AND CONCLUSIONS

- VERTICAL DEFLECTION MAPS CAN BE CONSTRUCTED FROM GRADIOMETER SURVEY USING STOKES' FORMULA.

- STOKES' AND VENING MEINESZ FORMULAS (AND OTHERS) CAN BE USED TO GENERATE A GRADIENT REFERENCE FOR THE TEST AND CALIBRATION OF GRADIOMETERS.

- THE DETERMINISTIC RELATIONSHIP GIVEN BY STOKES' FORMULA FOR THE GRADIENTS (EG. - T_x IS SPATIAL INTEGRAL OF T_{xz}) EXPLAINS THE HIGH CORRELATION BETWEEN T_x AND T_{xz} AT ZERO SHIFT IN STOCHASTIC GRAVITY MODELS.

- SUPPORTS THE CONTENTION THAT ALL GRADIENT COMPONENTS (NOT JUST THE LEVEL GRADIENTS T_{xx}, T_{xy}, AND T_{yy}) PROVIDE USEFUL VERTICAL DEFLECTION INFORMATION.

REAL-TIME VERTICAL DEFLECTION ESTIMATION USING GRADIENT DATA

Presented at

TWELFTH MOVING BASE GRAVITY GRADIOMETER CONFERENCE
UNITED STATES AIR FORCE ACADEMY

14 - 15 February 1984

Presented by

W. Feldman
Sperry Corporation
Electronic Systems
Great Neck, New York 11020

and

B. Epstein
Strategic Systems Project Office
Department of the Navy
Great Neck, New York 11020

SYNOPSIS

REAL-TIME VERTICAL DEFLECTION ESTIMATION USING GRADIENT DATA

WALTER K. FELDMAN
Sperry Corporation/Electronic Systems
Great Neck, New York 11020

and

BERNARD EPSTEIN
Strategic Systems Project Office
Department of the Navy
Great Neck, New York 11020

Techniques/algorithms for making real-time estimates of vertical deflections from gravity gradient measurements are discussed. First, techniques/algorithms used to condition sensor data for effects of high-frequency noise, pressure sensitivity, self-gradients, bias/trend, and carouselling are outlined. Plots of typical gradient data before and after preprocessing are shown to illustrate the effectiveness of the preprocessing. Second, a batch filter formulation for estimating deflections from gradient and SEASAT map data is illustrated. Finally, filter results are demonstrated by plots of filter estimates of vertical deflection vs. reference values for several ship tracks.

REAL-TIME VERTICAL DEFLECTION ESTIMATION USING GRADIENT DATA

TWELFTH MOVING BASE GRAVITY
GRADIOMETER CONFERENCE
UNITED STATES AIR FORCE ACADEMY

14 - 15 February 1984

Presented by

SPERRY CORPORATION
ELECTRONIC SYSTEMS
GREAT NECK, NEW YORK 11020

AND

STRATEGIC SYSTEMS PROJECT OFFICE
DEPARTMENT OF THE NAVY
GREAT NECK, NEW YORK 11020

ac

OVERVIEW

- PART I: PREPROCESSING TECHNIQUE USED
- PART II: BATCH FILTER FORMULATION
- PART III: FILTER RESULTS
- PART IV: SUMMARY PROCESSING FIGURE

OVERVIEW: PART I

- GRADIOMETER SYSTEM (BACKGROUND)
- PROCESSING AT THE INSTRUMENT LEVEL
- PROCESSING IN NED COORDINATES
- GRADIENT PLOTS

GRADIOMETER SYSTEM DATA PREPROCESSING

- GRADIOMETER SYSTEM (BACKGROUND)
  - 3 GGIs ARRAYED IN AN "UMBRELLA" COORDINATE CONFIGURATION (120^0 APART) RESIDING ON A LOCAL-LEVEL PLATFORM (LLP)
  - THE LLP IS ROTATED ABOUT THE VERTICAL AXIS AT A CONSTANT RATE
  - EACH GGI HAS TWO OUTPUTS CONTAINING THE GRADIENTS IN THE PLANE PERPENDICULAR TO ITS SPIN AXIS
    - INLINE(P): DIFFERENCE OF TWO PRINCIPAL GRADIENTS
    - CROSS(X): CROSS-GRADIENT
  - THE OUTPUTS OF AN ERROR FREE GRADIOMETER IN INSTRUMENT COORDINATES ARE RELATED TO THE LOCAL-LEVEL GRADIENT COORDINATES (NORTH, EAST, DOWN (N/E/D)) BY THE TRANSFORMATIONS INDICATED IN FIGURE 1

GRADIOMETER PREPROCESSING (CONT)

FIGURE 1. RELATIONSHIP OF INSTRUMENT SENSOR OUTPUTS TO N/E/D GRADIENTS

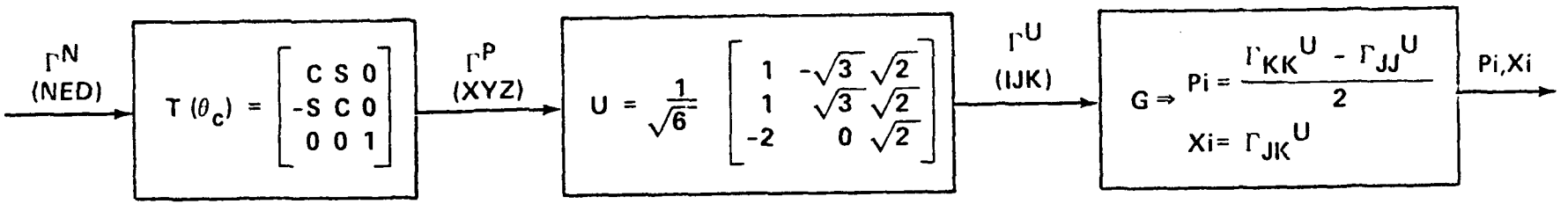

WHERE:

Γ^N	=	GRADIENTS IN NED COORDINATES
Γ^P	=	GRADIENTS IN ROTATING LLP COORDINATES
Γ^U	=	GRADIENTS IN UMBRELLA COORDINATES
X, Y, Z	=	LLP COORDINATE AXES (Z DOWN)
I, J, K	=	UMBRELLA COORDINATE AXES
θ_c	=	CAROUSEL ANGLE (ZERO WHEN X AND N COINCIDE)

GRADIOMETER PREPROCESSING (CONT)

- DATA PROCESSING PERFORMED AT THE INSTRUMENT LEVEL
  - EDITED GGI DATA
    - DELETED BAD DATA
    - AVERAGED GGI OUTPUTS FOR NOISE/BANDWIDTH REDUCTION
  - COMPENSATED KNOWN ERROR SOURCES
    - SELF-GRADIENTS OF SHIP AND GSS
      - HEADING MINUS CAROUSEL ANGLE DEPENDENT
        - COEFFICIENTS OBTAINED BY PROCESSING CALIBRATION RUNS
    - PRESSURE
      - SENSITIVITY COEFFICIENT MULTIPLIED BY MEASURED PRESSURE VARIATIONS
    - CAROUSELLING EFFECTS (CENTRIFUGAL GRADIENTS)
      - INTERACTION BETWEEN CAROUSELLING AND EARTH'S ROTATION
    - VELOCITY EFFECTS
      - CORIOLIS TERM DUE TO INTERACTION OF CAROUSELLING AND SHIP'S VELOCITY
  - REMOVED REFERENCE ELLIPSOID
    - EFFECTS OF EARTH'S ROTATION AND EARTH MASS
  - TRANSFORMED GGI OUTPUTS INTO NED COORDINATES FOR FURTHER PROCESSING

125

GRADIOMETER PREPROCESSING (CONT)

- DATA PROCESSING IN NED COORDINATES
  - EFFECTS OF GGI RESIDUAL ERRORS
    - GGI INSTRUMENT ERRORS CAUSE MODULATED ERRORS ABOUT TWICE AND ONCE CAROUSELLING FREQUENCY (Ω) (OSCILLATIONS IN HORIZONTAL (Γ_{NN}, Γ_{NE}, Γ_{EE}) AND VERTICAL (Γ_{ED}, Γ_{ND}) GRADIENTS, RESPECTIVELY)
    - PRINCIPAL GRADIENTS (Γ_{NN}, Γ_{EE}) CONTAIN UNMODULATED ERRORS IN ADDITION TO THE 2 ΩOSCILLATION
      - BIAS AND RAMP ERRORS APPEAR IN NED GRADIENTS
    - CROSS GRADIENTS (Γ_{NE}, Γ_{ED}, Γ_{ND}) DO NOT CONTAIN ANY UNMODULATED ERRORS
      - NO BIAS OR RAMP IN NED
  - NED ERROR EQUATIONS THAT ARE DUE TO GGI RESIDUAL ERRORS ARE SUMMARIZED IN TABLE 1

GRADIOMETER PREPROCESSING (CONT)

TABLE 1. NED ERRORS DUE TO INSTRUMENT ERRORS

$$3\delta\Gamma_{NN} = -(\delta X_1 + \delta X_2 + \delta X_3) + \left[\frac{1}{\sqrt{3}}(\delta P_2 + \delta P_3 - 2\delta P_1) + \sqrt{3}(\delta X_2 - \delta X_3)\right] \text{SIN } 2\theta_c$$

$$+ \left[(\delta P_2 - \delta P_3) + (2\delta X_1 - \delta X_2 - \delta X_3)\right] \text{COS } 2\theta_c$$

$$3\delta\Gamma_{NE} = \left[(\delta P_2 - \delta P_3) + (2\delta X_1 - \delta X_2 - \delta X_3)\right] \text{SIN } 2\theta_c - \left[\frac{1}{\sqrt{3}}(\delta P_2 + \delta P_3 - 2\delta P_1) + \sqrt{3}(\delta X_2 - \delta X_3)\right] \text{COS } 2\theta_c$$

$$3\delta\Gamma_{ND} = \left[\sqrt{\frac{2}{3}}(\delta P_2 + \delta P_3 - 2\delta P_1) + \sqrt{\frac{3}{2}}(\delta X_3 - \delta X_2)\right] \text{SIN } \theta_c + \left[\sqrt{2}(\delta P_3 - \delta P_2) + \frac{1}{\sqrt{2}}(2\delta X_1 - \delta X_2 - \delta X_3)\right] \text{COS } \theta_c$$

- δP_i, δX_i ARE ERRORS IN GGI OUTPUTS, θ_c = CAROUSEL ANGLE
- $\delta\Gamma$'S ARE ERRORS IN NED GRADIENTS
- $\delta\Gamma_{EE}$ SIMILAR TO $\delta\Gamma_{NN}$, $\delta\Gamma_{ED}$ SIMILAR TO $\delta\Gamma_{ND}$

221

GRADIOMETER PREPROCESSING (CONT)

- DATA PROCESSING IN NED COORDINATES (CONT)
  - FIXED INTERVAL SLIDING LEAST-SQUARES FIT (LSF) ALGORITHM USED TO REDUCE BOTH NOISE (AVERAGING), 1Ω, AND 2Ω OSCILLATIONS (Ω = CAROUSELLING RATE)

	LSF MODELS*
$\Gamma_{NN}, \Gamma_{NE}, \Gamma_{EE}$	$A + Bt + C \cos 2\Omega t + D \sin 2\Omega t$
Γ_{ED}, Γ_{ND}	$E + Ft + G \cos \Omega t + H \sin \Omega t$

*t = time, 'A' TO 'H' LSF PARAMETERS

  - OUTPUT OF THE LSF ALGORITHM CONSISTS OF BIAS AND RAMP (A,B,E, AND F TERMS) FROM THE ABOVE MODELS WHICH ARE INPUTS TO BATCH FILTER
  - STUDIES/DATA PROCESSING RESULTS HAVE INDICATED THAT BATCH FILTER CAN EFFECTIVELY PROCESS DATA WITH OSCILLATIONS PRESENT (IF ERRORS MODELLED CORRECTLY)
    - AVERAGING STILL RECOMMENDED IN NED FRAME FOR NOISE REDUCTION
    - REMOVAL OF OSCILLATIONS DESIRABLE
      - PROVIDES ANOMALOUS GRADIENTS DIRECTLY
      - PROVIDES ESTIMATION OF RESIDUAL NOISE FOR MONITORING

GRADIOMETER PREPROCESSING (CONT)

- DATA PROCESSING IN NED COORDINATES (CONT)
  - IF VD MAP IS AVAILABLE ALONG THE SHIP'S TRACK, THE PRINCIPAL GRADIENT BIAS AND RAMP ERRORS CAN ALSO BE REDUCED VIA A RECURSIVE FIT
    - EXTRAPOLATE PRINCIPAL GRADIENTS FROM VD MAP (VIA 16-POINT LAGRANGIAN INTERPOLATOR)
    - FIT THE DIFFERENCE BETWEEN THE GGI DERIVED GRADIENTS AND THE EXTRAPOLATED VD-MAP GRADIENTS WITH A BIAS PLUS RAMP MODEL
  - HOWEVER, ANALYSIS/RESULTS INDICATE NEGLIGIBLE DETERIORATION IN VD ESTIMATION IF THE BIAS/RAMP ARE NOT REMOVED (BUT MODELED IN FILTER)
- SAMPLES OF GRADIENTS BEFORE AND AFTER PREPROCESSING ARE SHOWN IN FIGURE 2, A, B, AND C

FIGURE 2A NORTH-NORTH AND EAST-EAST GRADIENTS BEFORE AND AFTER PREPROCESSING

Γ_{NN}

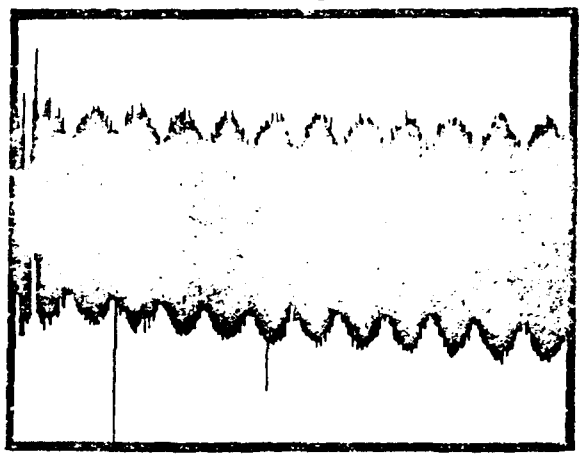

Γ_{EE}

Γ_{NN}

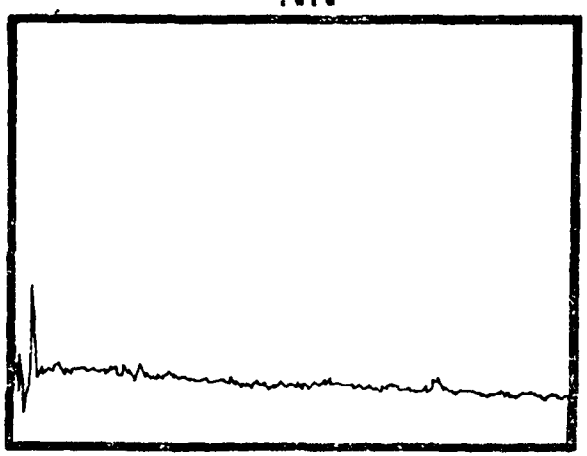

Γ_{EE}

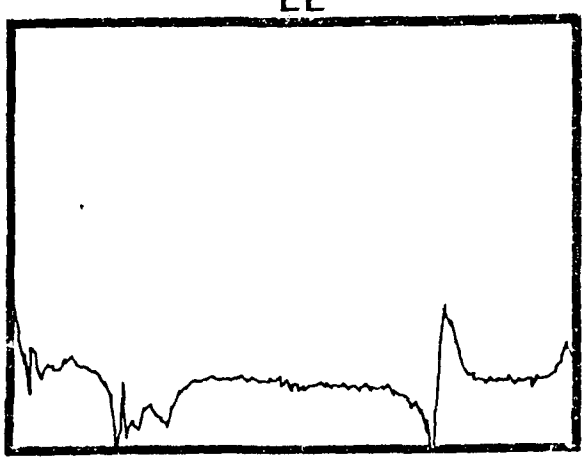

FIGURE 2B NORTH-DOWN AND EAST-DOWN GRADIENTS BEFORE AND AFTER PREPROCESSING

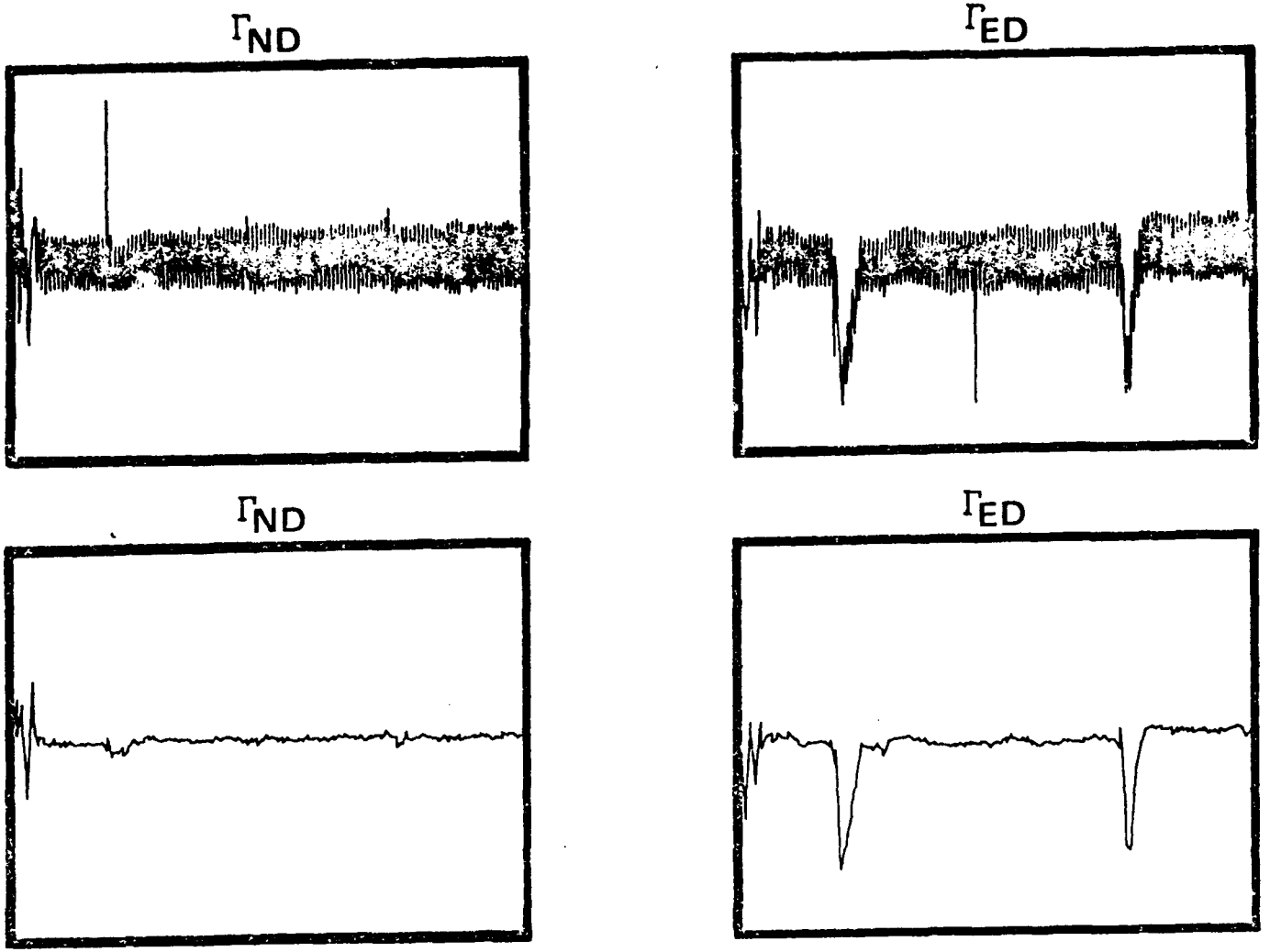

FIGURE 2C NORTH-EAST GRADIENTS BEFORE AND AFTER PREPROCESSING

Γ_{NE}

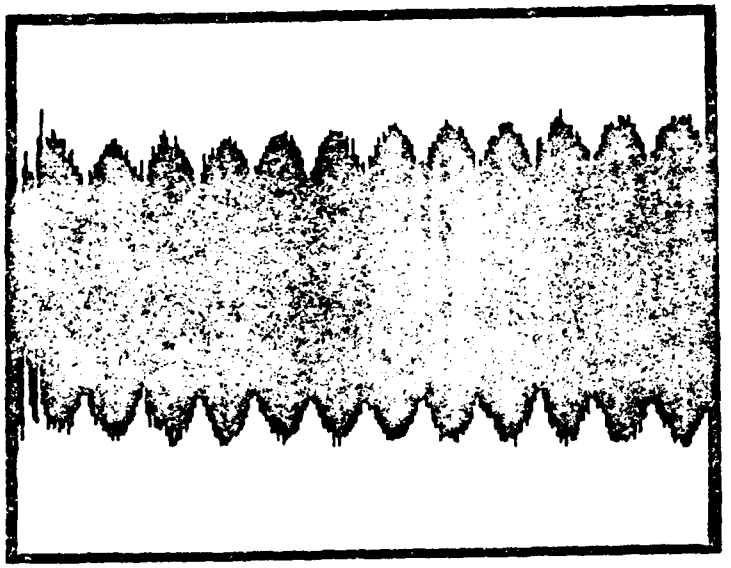

Γ_{NE}

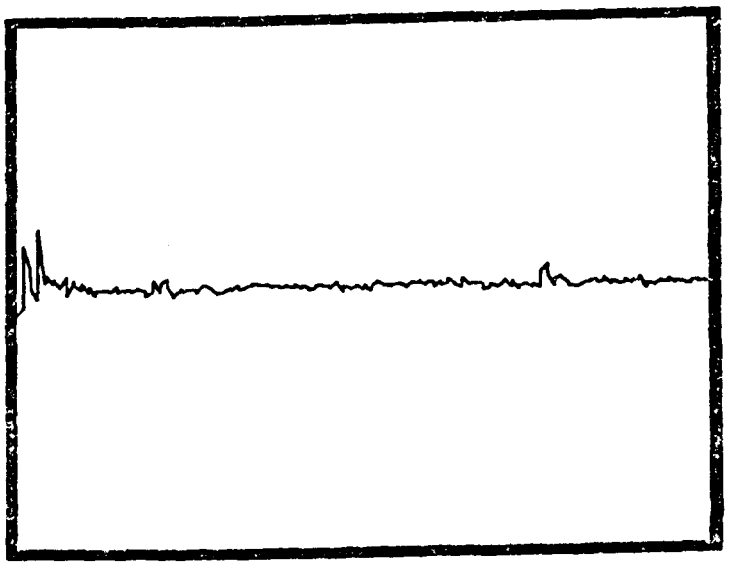

OVERVIEW: PART II

- FILTER FUNDAMENTALS
- FILTER DESIGN
- STAG GRAVITY FIELD MODEL
- NOISE MODELS
- TYPICAL FILTER OPERATION

BATCH FILTER FUNDAMENTALS

- NON-RECURSIVE ALTERNATIVE TO A KALMAN FILTER—WHICH HAS NOT PROVED CAPABLE OF ESTIMATING VD ALONG A MANEUVERING TRACK
- COMPUTES VD ESTIMATES THAT ARE OPTIMAL IN A MINIMUM VARIANCE OR LEAST-SQUARES SENSE, USING A FINITE NUMBER OF GGI MEASUREMENTS AND VD MAP VALUES
  - VD MAP AIDS FILTER ESTIMATION BY PROVIDING LOW-FREQUENCY INFORMATION
- GIVEN A MEASUREMENT VECTOR, [G], A TWO-DIMENSIONAL VD ESTIMATE VECTOR, $[\hat{g}]$, FOR A GIVEN POINT IS COMPUTED BY:

$$[\hat{g}] = [b]^T [G]$$

  WHERE [b] IS AN ARBITRARY GAIN MATRIX

- A MINIMUM-VARIANCE ESTIMATE IS OBTAINED WITH THE OPTIMAL GAIN MATRIX:

$$[b_o] = [P_{GG}]^{-1} [E_{Gg}]$$

  WHERE $[P_{GG}]$ IS THE COVARIANCE MATRIX OF THE MEASUREMENT VECTOR, $E[\,[G]\,[G]^T]$

  AND $[E_{Gg}]$ IS THE COVARIANCE MATRIX OF THE MEASUREMENT AND TRUE VD VECTORS, $E[\,[G]\,[g]^T]$

BATCH FILTER DESIGN

- INPUT MEASUREMENTS
  - SETS OF FIVE ANOMALOUS GRAVITY GRADIENT MEASUREMENTS IN NED COORDINATES: Γ_{NN}, Γ_{EE}, Γ_{NE}, Γ_{ND}, Γ_{ED}
  - SETS OF TWO-AXIS VD MAP VALUES: $g_{MAP\ N}$, $g_{MAP\ E}$
- FUNCTIONAL STEPS
  - COMPUTE COVARIANCE ELEMENTS OF THE $[P_{GG}]$ AND $[E_{Gg}]$ MATRICES
  - SOLVE FOR $[b_o]$
    - CHOLESKY DECOMPOSITION OF $[P_{GG}]$ USED TO AVOID EXPLICIT INVERSION OF LARGE MATRIX
  - CALCULATE $[\hat{g}]$

BATCH FILTER COVARIANCES — STAG MODEL

- THE SPERRY THREE-DIMENSIONAL ALGEBRAIC GRAVITY (STAG) MODEL IS USED FOR THE AUTO-CORRELATION FUNCTION (ACF) OF THE GRAVITY DISTURBING (ANOMALOUS) POTENTIAL. THE MODEL IS:
  - ISOTROPIC
  - STATIONARY
  - SELF-CONSISTENT
  - UPWARD CONTINUOUS
  - A GOOD FIT TO REAL DATA

THE FORM OF THE STAG MODEL FOR THE ANOMALOUS POTENTIAL ACF IS: $\phi_{TT}(r, \hat{h}) = \sigma_T^2 \sum_{k=1}^{n} a_k \dfrac{D_k/D_k^*}{\left(1 + \dfrac{r^2}{D_k^{*2}}\right)^{1/2}}$

r = RADIAL DISTANCE ON SURFACE

$\hat{h}$ = SUM OF ALTITUDES

$D_k^* = D_k + \hat{h}$

$\sum_{k=1}^{n} a_k = 1$

σ_T^2, a_k, D_K CHOSEN TO FIT REAL DATA

BATCH FILTER COVARIANCES — STAG MODEL (CONT)

- SINCE THE FILTER STATES CAN EACH BE DEFINED IN FORMS OF ANOMALOUS POTENTIAL DERIVATIVES (E.G., $\Gamma_{NN} = \frac{\partial^2 T}{\partial N^2}$), THE FILTER COVARIANCES ARE EXPRESSED AS DERIVATIVES OF THE STAG MODEL, E.G.,

$$\phi_{\Gamma_{NN}, \Gamma_{EE}} = \phi_{\frac{\partial^2 T}{\partial N^2}, \frac{\partial^2 T}{\partial E^2}} = \frac{\partial^4 \phi_{TT}}{\partial^2 N \, \partial^2 E}$$

BATCH FILTER COVARIANCES - NOISE MODELS

- EACH OF THE 6 GGI OUTPUTS HAS INDEPENDENT ERRORS, MODELED AS:
  - RANDOM BIAS ERROR
  - LONG AND SHORT PERIOD MARKOV ERRORS
  - RAMP ERROR FROM TURN-ON
  - EXPONENTIAL ERROR (FROM TURN-ON)
  - PRESSURE SENSITIVITY
- RESIDUALS (ERRORS) OF SHIP SELF-GRADIENTS ARE REPRESENTED AS RANDOM BIASES IN THE SHIP-COORDINATE FRAME
- VD MAP ERRORS ARE REPRESENTED AS WHITE NOISE

TYPICAL BATCH FILTER OPERATION

- 15 SETS OF NED-FRAME GRADIENTS MEASUREMENTS ARE ACCUMULATED ALONG SHIP'S TRACK
- 7 X 7 MAP GRID IS SELECTED AND VD VALUES READ
- $[P_{GG}]$ AND $[E_{Gg}]$ COVARIANCE MATRIX ELEMENTS ARE CALCULATED
- OPTIMAL GAIN MATRIX AND THE VD ESTIMATE VECTOR ARE COMPUTED.
- NEW VD ESTIMATES AT SMALL TIME INCREMENTS GENERATED BY CALCULATING $[E_{Gg}]$ COVARIANCE AND OBTAINING NEW SOLUTIONS FROM THE ORIGINAL $[P_{GG}]$ MATRIX
- WHEN A NEW SET OF GRADIENT MEASUREMENTS IS AVAILABLE, IT REPLACES THE STALEST SET. THE MAP GRID IS UPDATED IF NECESSARY, AND THE $[P_{GG}]$ COVARIANCES FOR THE AFFECTED FILTER STATES ARE RE-CALCULATED. THE NEW $[E_{Gg}]$ MATRIX IS CALCULATED AND SOLUTIONS PROCEED

2384

PART III: FILTER RESULTS

- FIGURES 3A AND 3B SHOW BATCH FILTER PERFORMANCE FOR TWO TRACKS
  - GRADIOMETER DATA TAKEN ABOARD NAVIGATION TEST VEHICLE (NTV; USNS VANGUARD) (WHILE MANEUVERING)
  - FILTER PROCESSING PERFORMED AT SPERRY (SIMULATED REAL-TIME OPERATION); SIMILAR ANALYSIS/PROCESSING DONE BY OTHERS (E.G., TASC, DRC, NADC, RI)
    - SEASAT ALTIMETRY DERIVED VD MAP USED TO AID FILTER
    - GRAVIMETRICALLY DERIVED VD MAP USED AS REFERENCE

FIGURE 3A VD FILTER RESULTS-TRACK 1

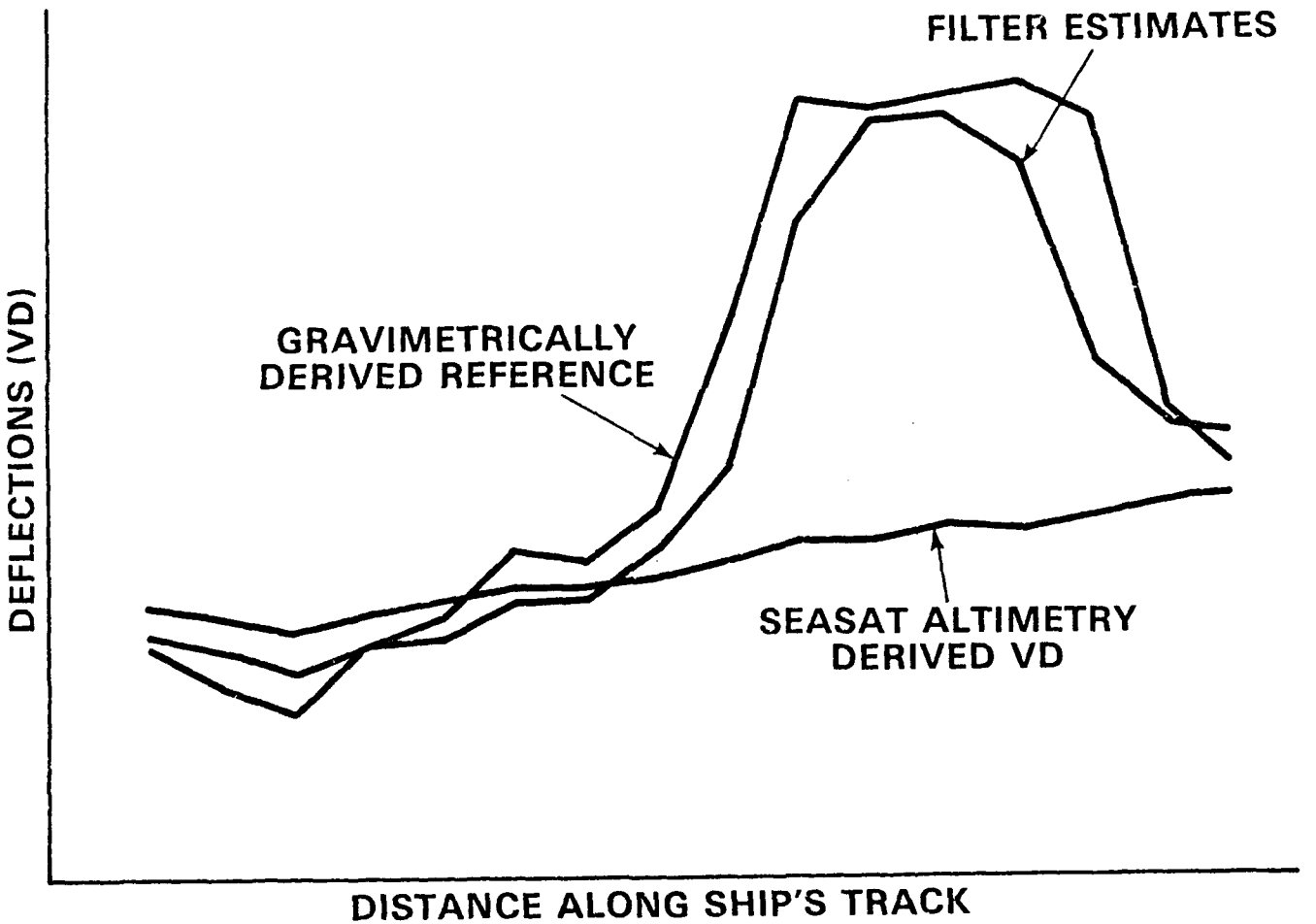

FIGURE 3B VD FILTER RESULTS-TRACK 2

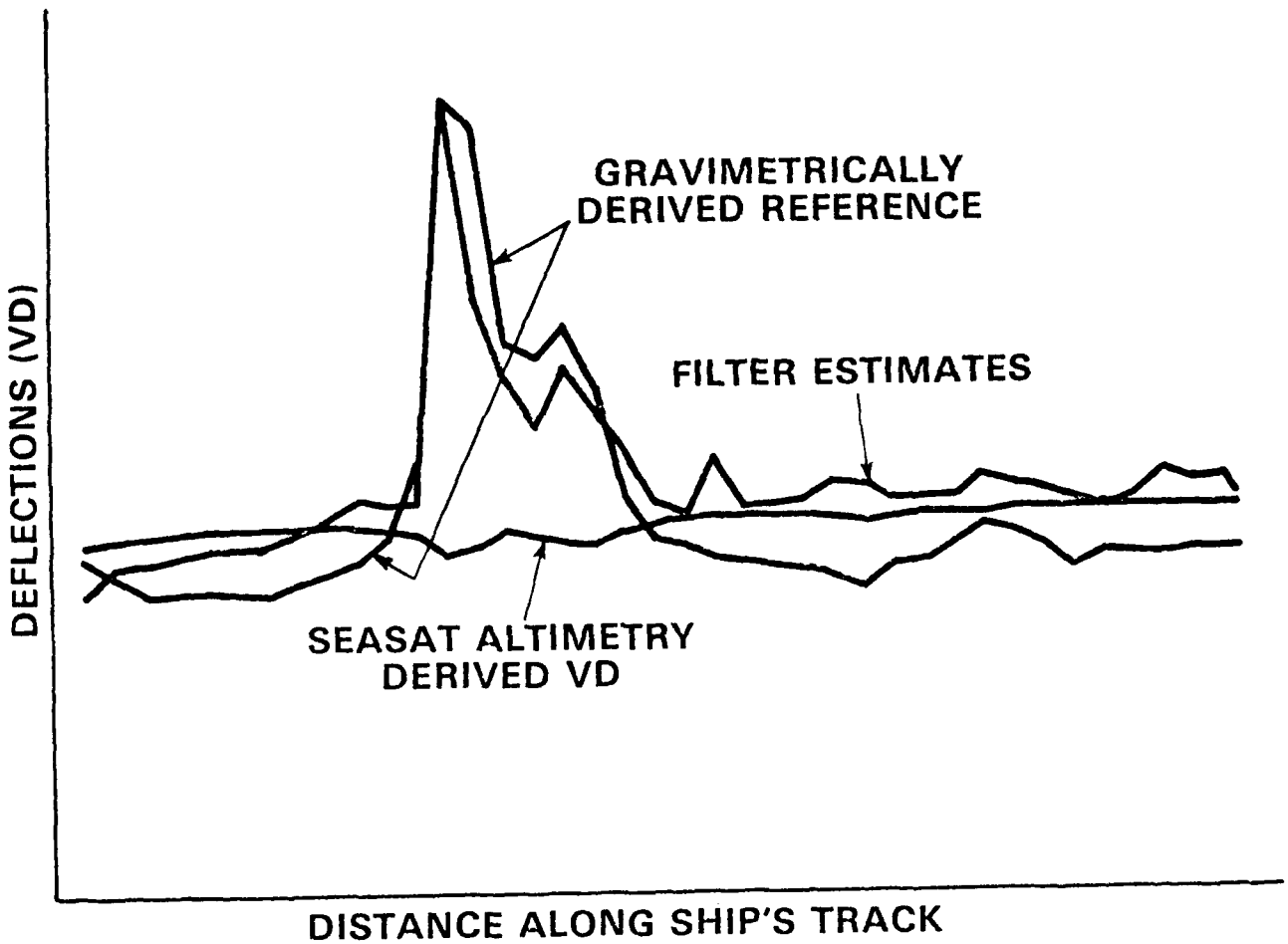

PART IV

- FIGURE 4 SUMMARIZES REAL-TIME PROCESSING ALGORITHMS FOR ESTIMATING DEFLECTIONS FROM GSS/MAP MEASUREMENTS

FIGURE 4 ALGORITHMS FOR REAL-TIME VD ESTIMATION

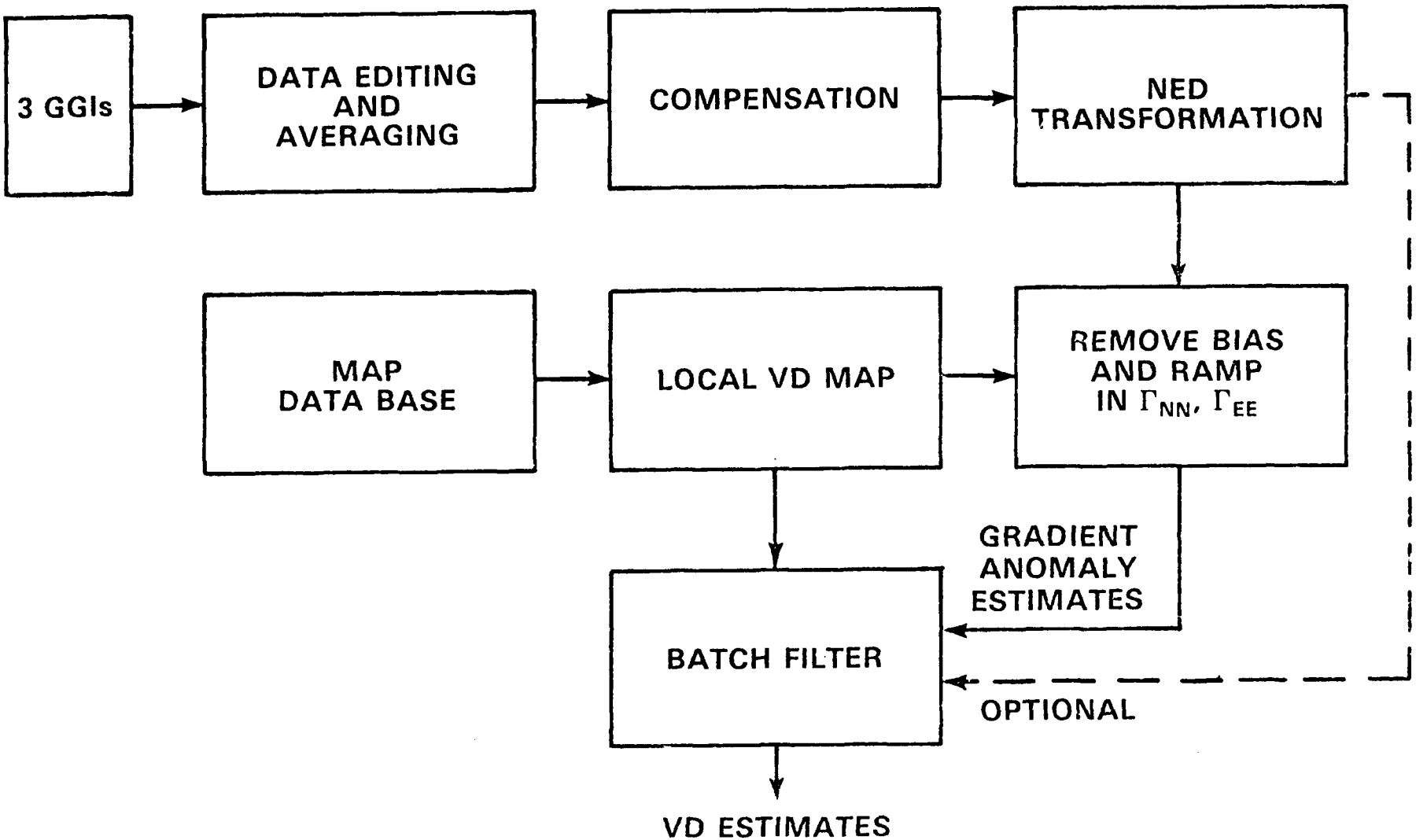

TUNNEL DETECTION

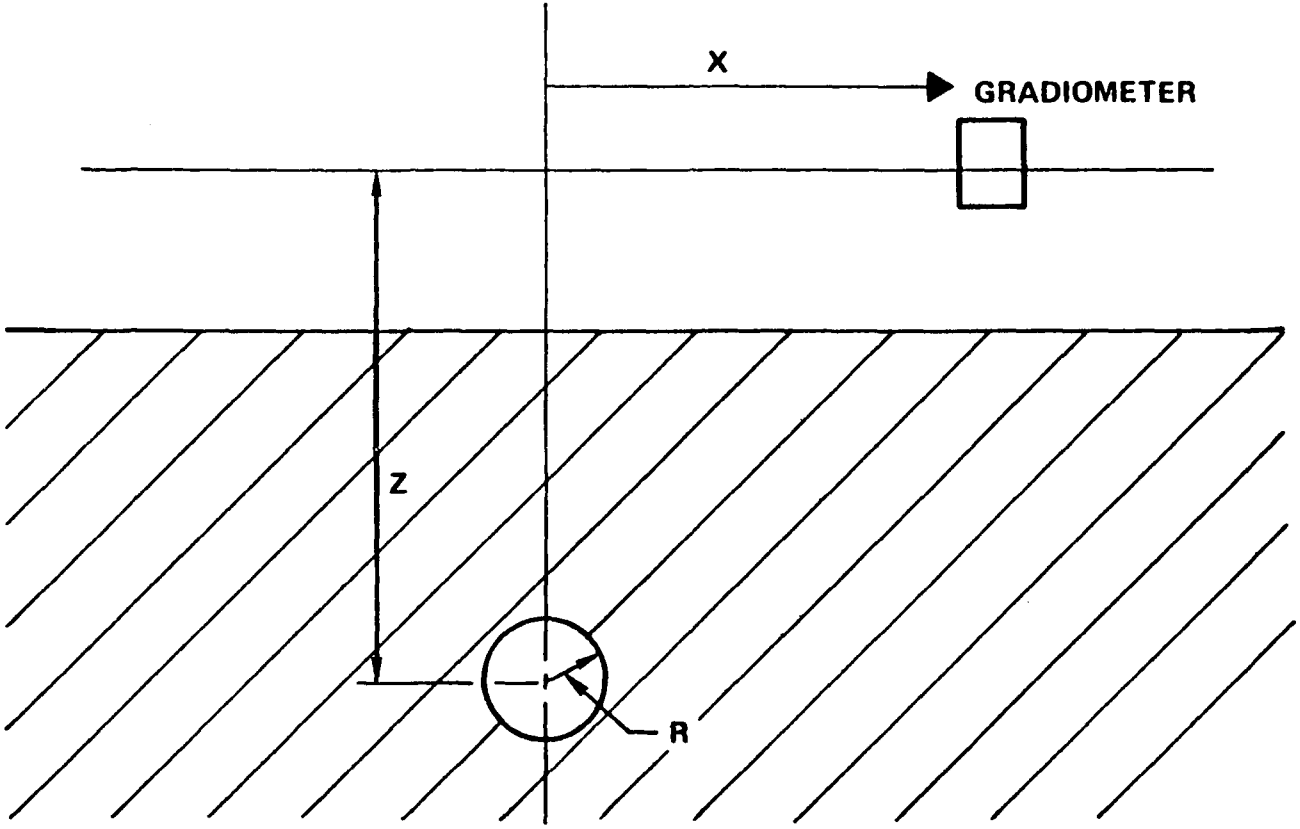

$$T_{ij} = \frac{2k\rho_L}{(X^2+Z^2)^2}\begin{pmatrix} Z^2-X^2 & 0 & 2XZ \\ 0 & 0 & 0 \\ 2XZ & 0 & -(Z^2-X^2) \end{pmatrix}$$

SUBST

$$\alpha = \frac{X}{Z}$$

$$k = 6.673\times10^{-8}\ \frac{cm^3}{gm\ sec^2}$$

$$\rho_L = \pi R^2 \rho_V$$

$$T_{ij} = \frac{419\rho_V}{(Z/R)^2}\begin{pmatrix} \frac{1-\alpha^2}{(1+\alpha^2)^2} & 0 & \frac{2\alpha}{(1+\alpha^2)^2} \\ 0 & 0 & 0 \\ \frac{2}{(1+\alpha^2)^2} & 0 & \frac{-(1-\alpha^2)}{(1+\alpha^2)^2} \end{pmatrix} \quad E$$

GRADIENTS DUE TO TUNNEL

Y GGI

$$I = \frac{419\rho_V}{(Z/R)^2} \quad \frac{1-\alpha^2}{(1+\alpha^2)^2}$$

$$C = \frac{419\rho_V}{(Z/R)^2} \quad \frac{2\alpha}{(1+\alpha^2)^2}$$

X GGI

$$I = -\frac{1}{2} \frac{419\rho_V}{(Z/R)^2}$$

$$C = 0$$

Z GGI

$$I = \frac{1}{2} \frac{419\rho_V}{(Z/R)^2} \quad \frac{1-\alpha^2}{(1+\alpha^2)^2}$$

$$C = 0$$

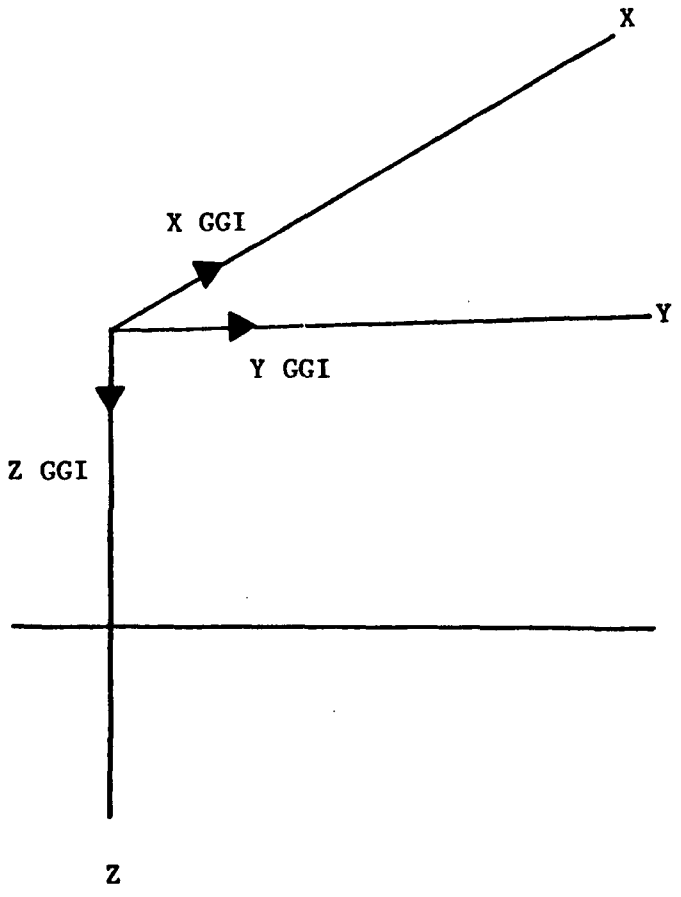

6 GRADIOMETER OUTPUTS

TWO OUTPUTS OF Y GGI

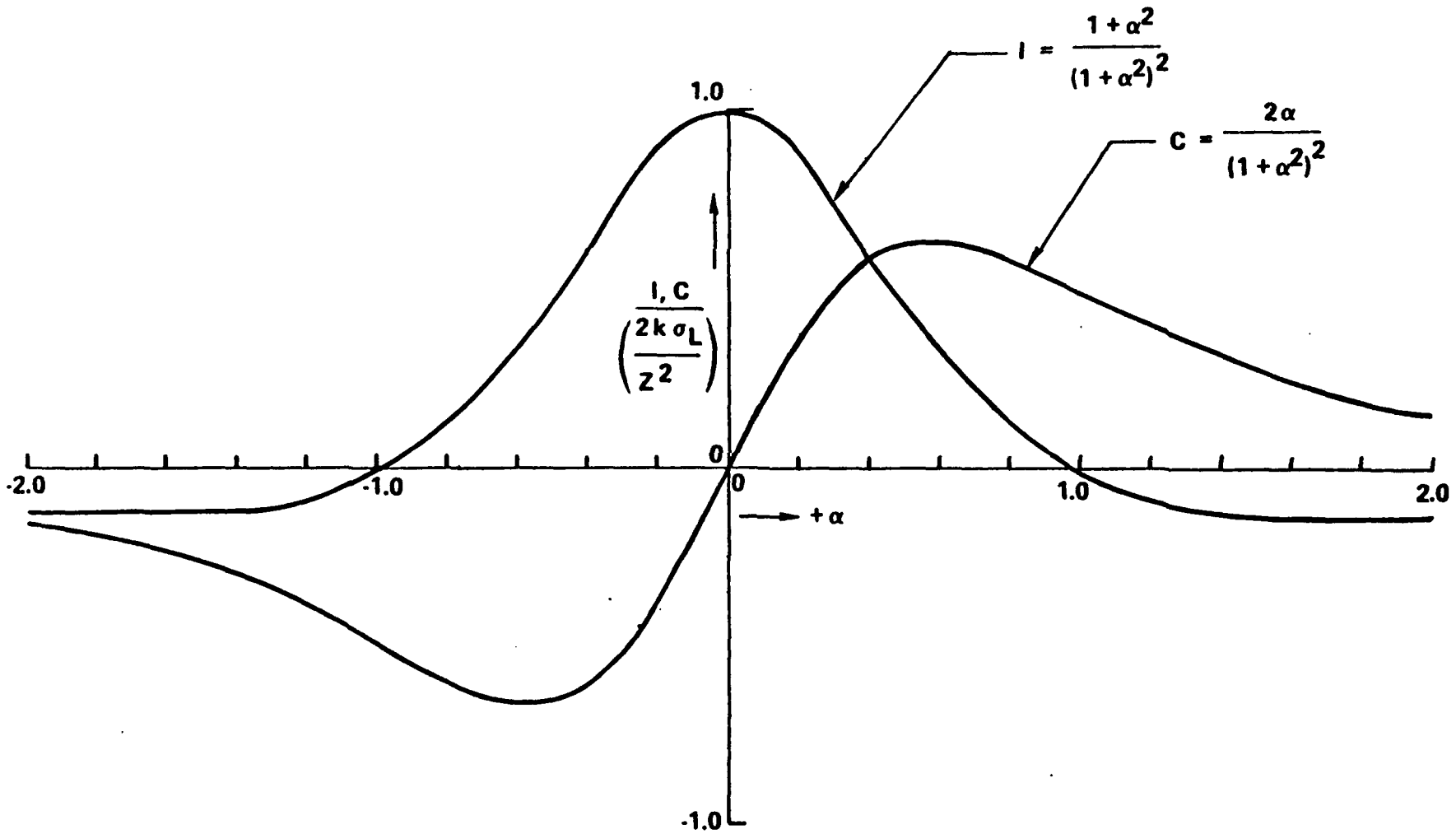

TWO PROBLEMS

1) DETECT A NEW TUNNEL

2) DETECT AN OLD TUNNEL

MULTI TRACK SURVEY

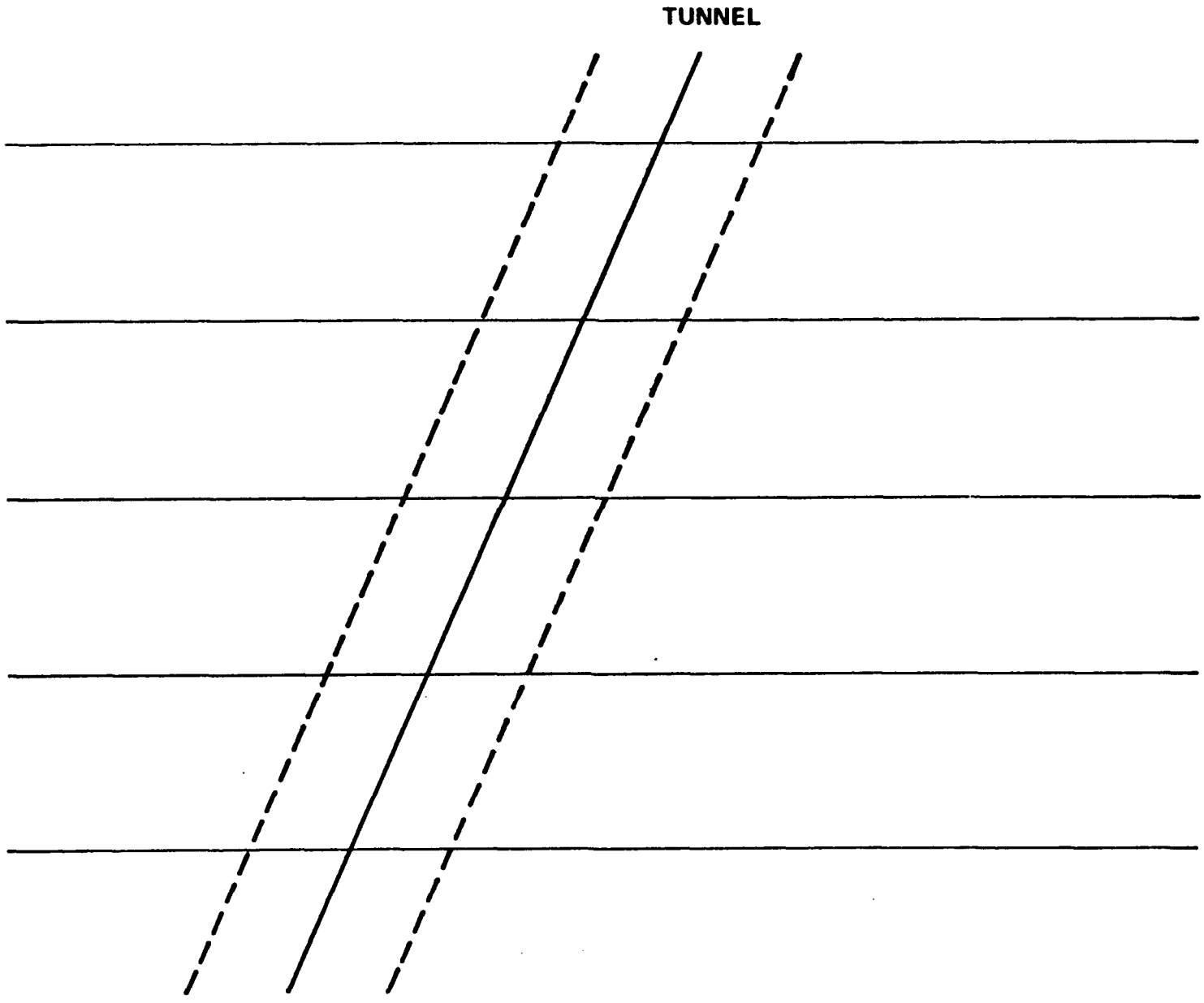

$$\text{P-P SIGNAL} = 1.3\,\frac{419\rho_V}{(Z/R)^2} = \frac{545\rho_V}{(Z/R)^2}$$

HIGH FREQUENCY NOISE FLOOR 10 $E^2/r/s$.

$$\sigma^2_{T/POINT} = \left[10\,\frac{E^2}{r/s}\right]\left[V\,\frac{m}{s}\right]\left[\frac{2\pi r}{(2)(V)m}\right] = 10\pi = 31.4\ E^2/MEAS$$

$$\sigma^2_{T/PASS} = \frac{10(\pi)}{(PTS/PASS)} = \frac{10\pi}{4Z/(V)(1\ SEC)} = \frac{10\pi V}{4Z}\ E^2/PASS$$

$$\sigma^2_{T/N\ PASSES} = \frac{10\pi V}{4Z\ N_p}$$

$$\frac{SIGNAL}{NOISE} = 1 \rightarrow \frac{545\rho_V}{(Z/R)^2} = \frac{10\pi V}{4ZN_p}$$

$$\frac{R^2 545\rho_V}{Z} = \frac{10\pi V}{4N_p}$$

$$Z = \frac{4N_p 545\rho_V R^2}{10\pi V} = \frac{69.4\rho_V N_p R^2}{V}$$

LAND VEHICLE SURVEY

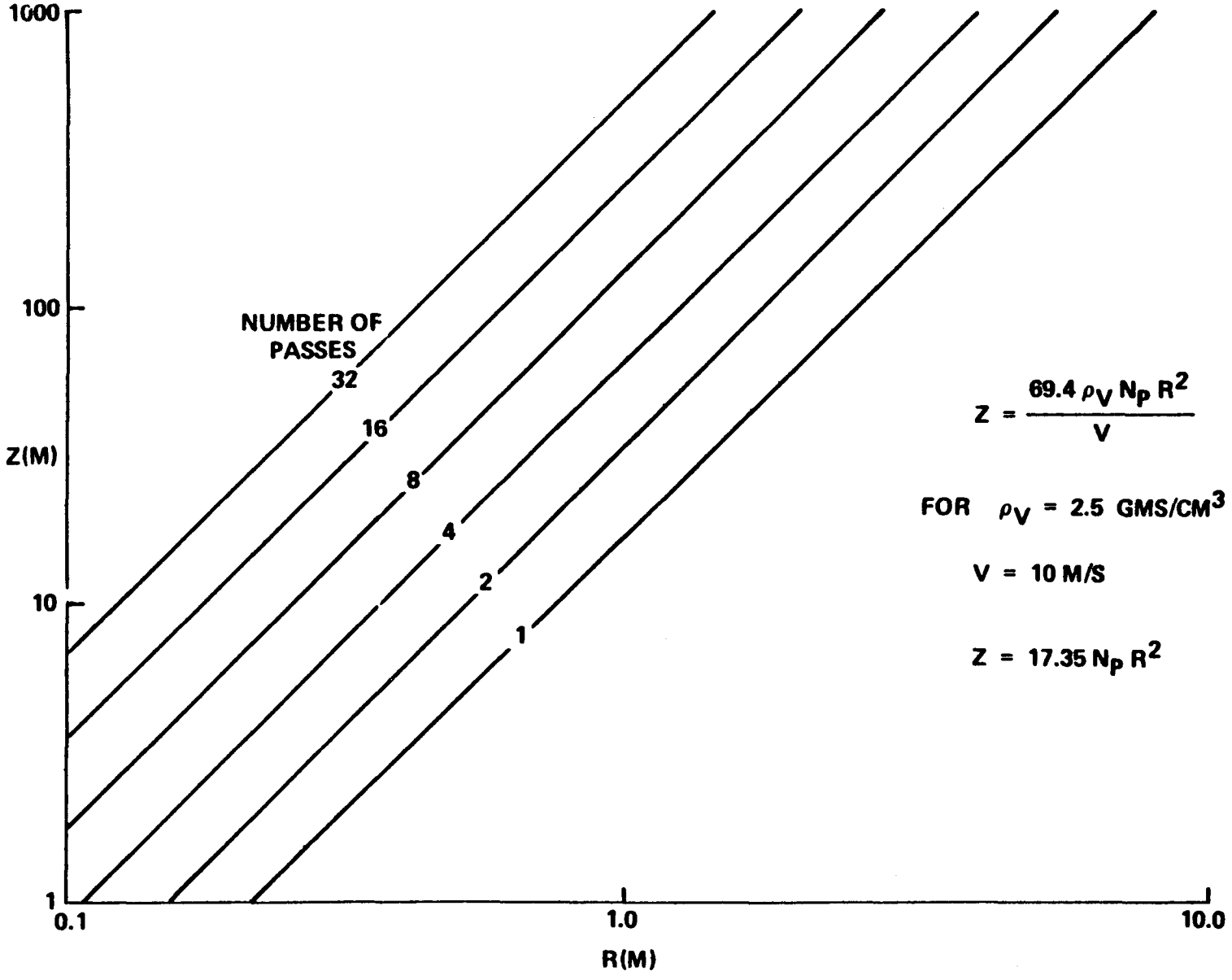

HELICOPTER SURVEY

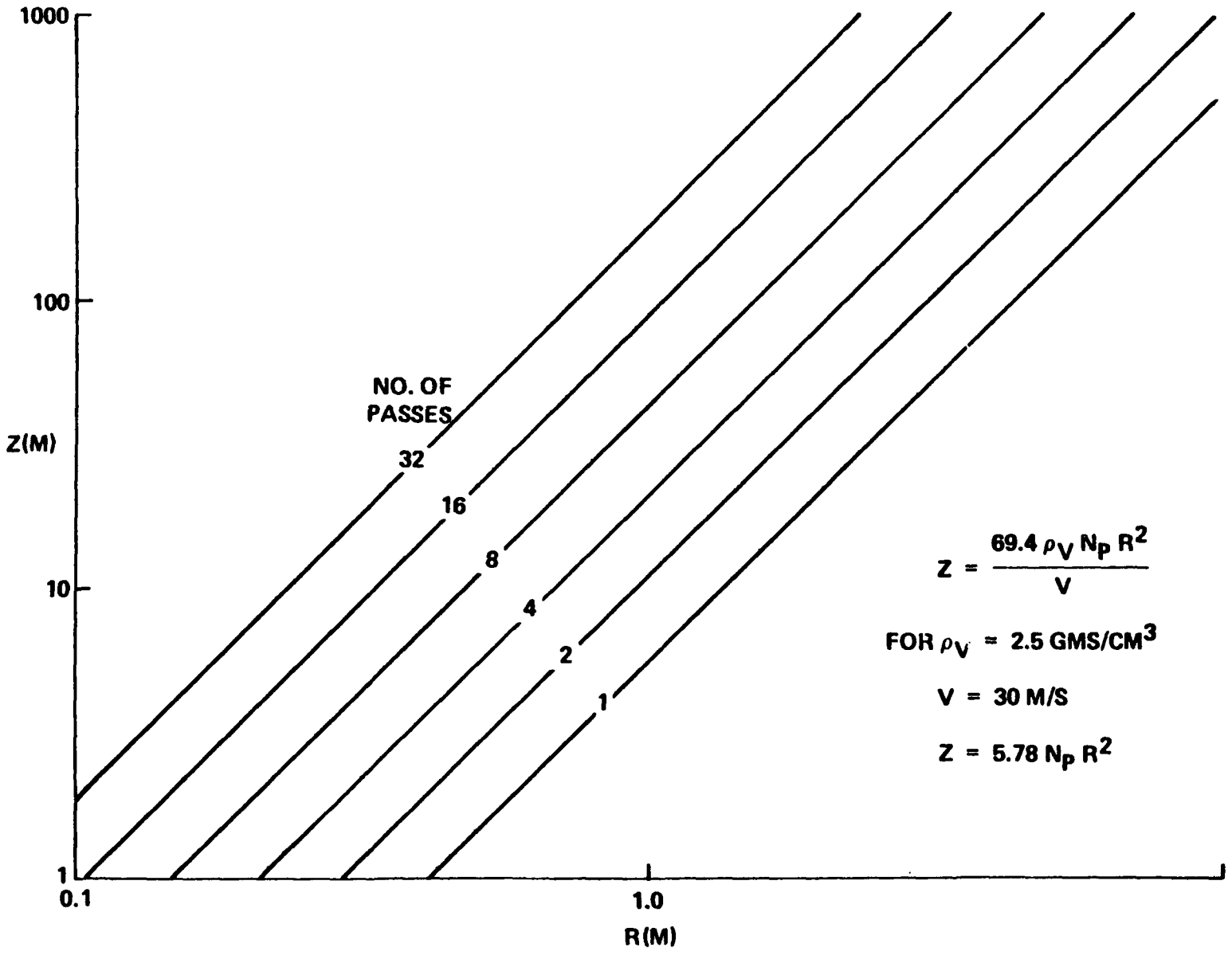

Bell Aerospace TEXTRON

OLD TUNNEL DETECTION

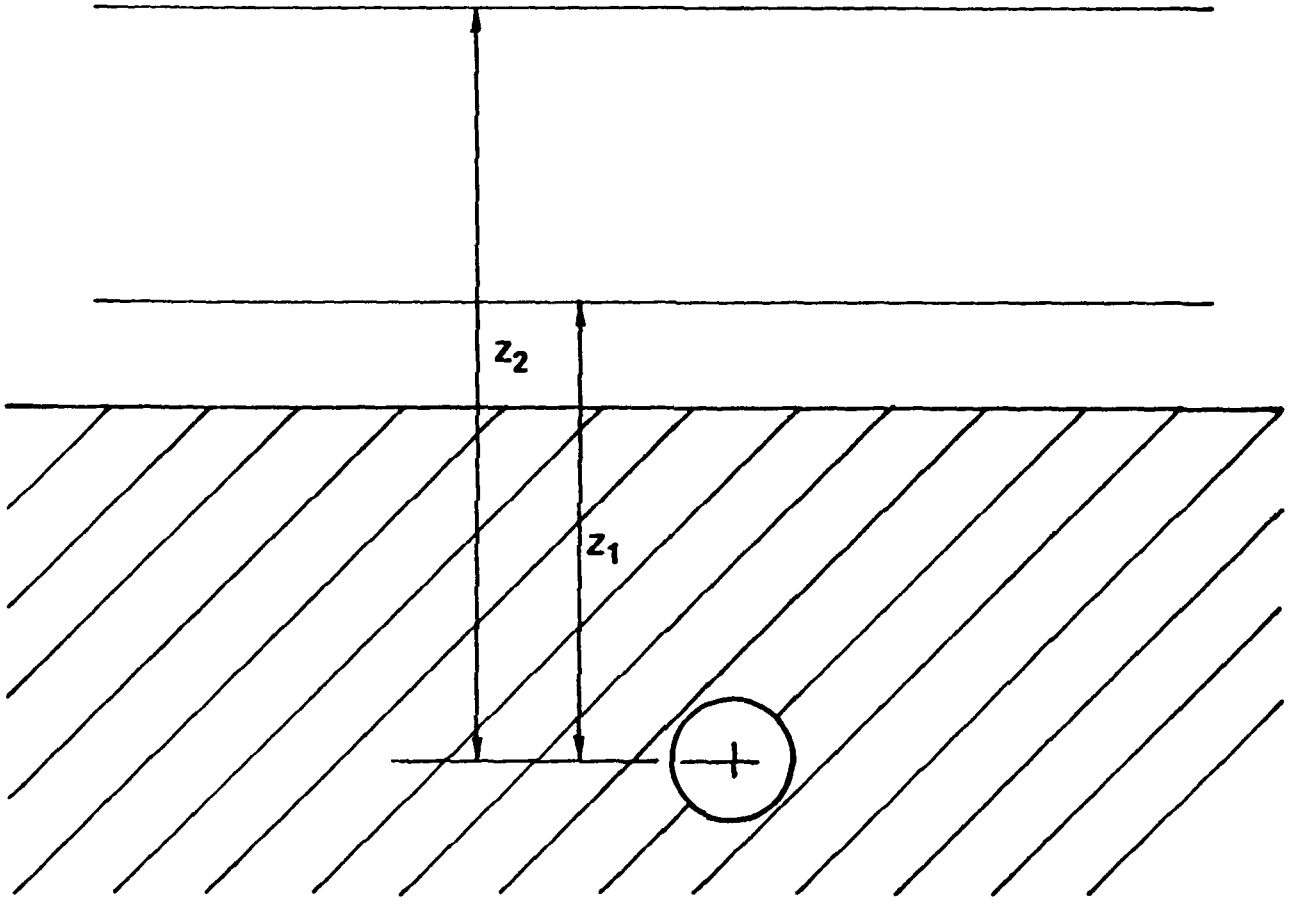

OLD TUNNEL DETECTION

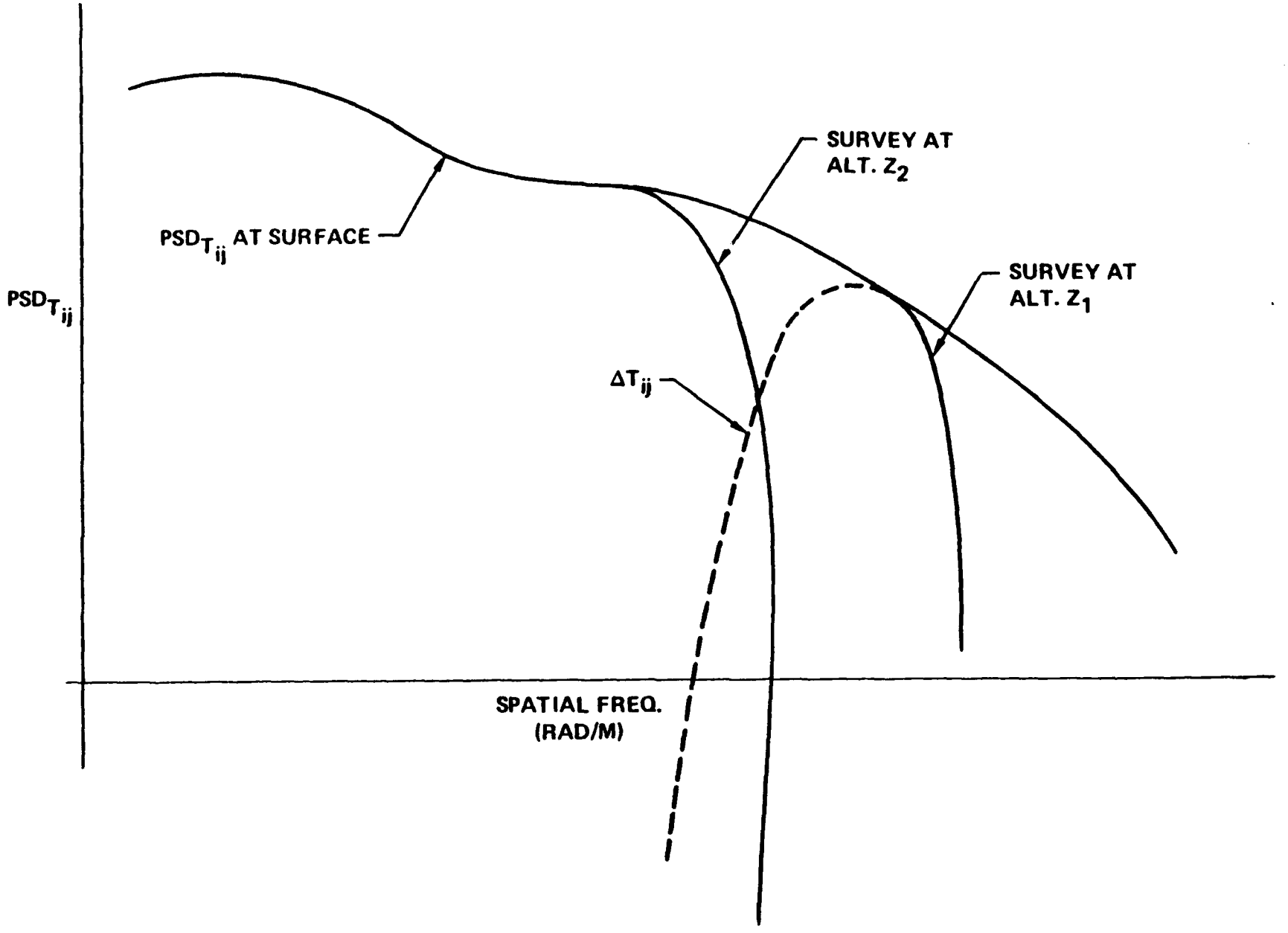

Bell Aerospace TEXTRON

OLD TUNNEL DETECTION

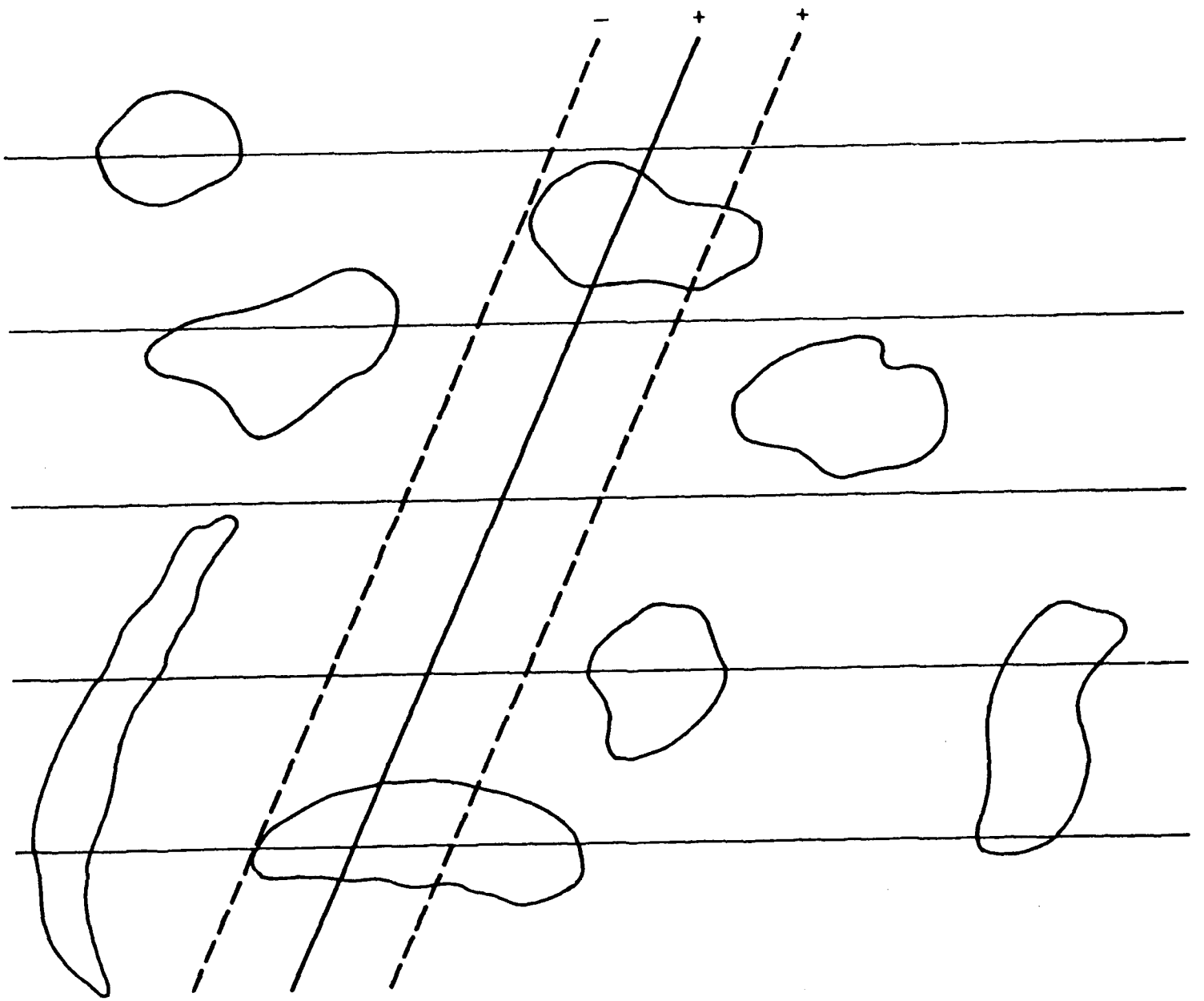

INTERPRETATION OF OLD TUNNEL DATA

- COMPUTE AND SUBTRACT TERRAIN COMPONENT OF FIELD
- IDENTIFY ALL "TUNNEL LIKE" SIGNATURES
- USE ADDITIONAL AVAILABLE DATA TO CLASSIFY
  (ROAD, STREAM, TUNNEL, FAULT, ETC.)
- COLLECT ADDITIONAL DATA TO RESOLVE QUESTIONABLE INTERPRETATIONS
  (MORE PASSES, BORE HOLE GRADIOMETER, SEISMIC, RESISTIVITY,
  BORE HOLE CAMERA, ETC.)

PREPRINT

A SIMPLIFICATION OF THE LEAST SQUARES DETERMINATION OF THE GRAVITY FIELD FROM LOW-LOW SATELLITE TRACKING DATA UTILIZING AN OPERATOR REPRESENTATION OF THE RANGE OBSERVABLE

V. Reinhardt
Bendix Field Engineering Corporation, Columbia, Maryland 21045

February 1984

ABSTRACT

One of the purposes of NASA/Goddard Space Flight Center's proposed Geopotential Research Mission is to map the gravity field of the Earth to 1-2 mgal in 41,253 1 degree x 1 degree blocks using range rate tracking data between two polar low orbiting satellites in the same orbit. Because there are 41,253 blocks in the gravity map, it takes, in general, at least 9.4×10^{13} real floating point operations (flop) to solve the least square fit (LSQF) matrix equation used to determine the gravity potential from the tracking data. In this paper, by studying the symmetry of an operator which generates the range rate acceleration between the satellites from the along track gravity field, it is shown that the LSQF cross correlation matrix (T-matrix) formed from a complex spherical harmonic ($Y_{\ell m}$) expansion of the gravity potential is, in the circular orbit infinite trajectory length approximation, diagonal in m. Further, for the actual mission, an iterative method which utilizes the inverse of the m-diagonal portion of the T-matrix, is shown to produce the 32758 coefficients of the $Y_{\ell m}$ model of the gravity potential to 64 bit precision in less than 1×10^{12} flop. A second iterative method is shown to produce an approximate covariance matrix for the coefficients in less than another 5×10^{11} flop. This paper also demonstrates a method which eliminates the problem of aliasing when attempting to solve the full problem sequentially, first, by solving for the approximate trajectories of the satellites with a reduced model of the gravity field, and then, by solving for a full model of the gravity field using the approximate trajectories.

1. INTRODUCTION

One of the purposes of Goddard Space Flight Center's (GSFC) proposed Geopotential Research Mission (GRM) (Smith, et. al., 1982) is to map the gravity field of the Earth to 1-2 mgal in 41,253 1 degree x 1 degree blocks using range rate tracking data between two polar low orbiting satellites in the same orbit (low-low range rate tracking). Using worst case analysis, both GSFC and the Johns Hopkins University Applied Physics Laboratory (APL), which has performed much of the design and study work for the proposed mission, have concluded that the data analysis required to turn the range rate data into the gravity map will consume very large amounts of computer time even on the fastest computers that exist today (Weiffenbach, 1983; vonBun, 1983). One of the most time consuming parts of the data analysis is in solving the least square fit (LSQF) matrix equation used to determine the gravity potential from

the tracking data because of the 41,253 blocks in the gravity map. It is later shown that the solution of this equation using Gaussian elimination techniques (See Section 5 and Appendix B.) will take, in general, at least 9.4×10^{13} real floating point operations (flop).

By examining the symmetry of an operator which generates the range acceleration from the along track gravity field, this paper demonstrates that the LSQF cross correlation matrix (T-matrix) formed from a complex spherical harmonic ($Y_{\ell m}$) expansion of the gravity potential is, in the circular orbit infinite trajectory length approximation, diagonal in m Further, for the actual mission, an iterative method which utilizes the inverse of the m-diagonal portion of the T-matrix, is shown to produce the 32758 coefficients of the $Y_{\ell m}$ model of the gravity potential in less than 1×10^{12} flop. A second iterative method is shown to produce an approximate covariance matrix for the coefficients in less than another 5×10^{11} flop.

This paper also demonstrates a method which eliminates the problem of aliasing when attempting to solve the full problem sequentially by solving for the approximate trajectories of the satellites, and then, first, by solving for the full gravity potential using the approximate trajectories.

2. GRM GRAVITY FIELD NORMAL EQUATIONS

As shown in Figure 1, the 2 GRM satellites will be launched in the same 160 Km polar nearly circular orbit with an along track separation of about 300 Km (Smith, et. al., 1982). On board navigation and control systems effectively make the motion of both satellites drag free so changes in satellite motion for times longer than a few seconds are solely due to the gravity field of the Earth (Ibid.). Thus, the motion of each satellite can be described by:

$$\ddot{\vec{r}}_i = -\vec{\nabla} V(r_i, t) \tag{2.1}$$

where $\vec{r}_i$, satellite i's center of mass position, and $\vec{\nabla}$, the gradient, are in units of R_h, the average orbital radius. The coordinate system for this equation is an approximately inertial geocentric system, so the gravity potential of the Earth, V, is a function of time due to the Earth's rotation. From this point on, the time dependence of V will not be explicitly written.

To determine the Earth's gravity field, GRM will use the observable p, the magnitude of the range vector between the center of mass of the satellites given by:

$$\vec{p} = \vec{r}_2 - \vec{r}_1 . \tag{2.2}$$

Since the satellites are in the same nearly circular orbit and p is small compared with the circumference of the orbit, p is essentially the along track component of $\vec{r}_2 - \vec{r}_1$. Thus we can write:

$$\ddot{p}(t) = - \nabla_s V(r_2) + \nabla_s V(r_1) \tag{2.3}$$

where ∇_s is the component of the gradient along $d\vec{s}$, the differential along track vector from satellite 1 to 2 in units of R_h. We can rewrite this

in a more compact form using a position difference operator, $P(\vec{\rho})$, defined by:

$$P(\vec{\rho})f(\vec{r}) = f(\vec{r}+\vec{\rho}) - f(\vec{r}). \tag{2.4}$$

Using this operator, (2.3) becomes a normal equation for $\ddot{\rho}$ in terms of V and the operator P:

$$\ddot{\rho}(t) = - P \nabla_s V(r) \tag{2.5}$$

where P will be implicitly $P(\vec{\rho})$ unless the functional dependence is otherwise specified. A normal equation for $\dot{\rho}$, the range rate observable, can be generated from (2.5) by integrating the equation.

3. CIRCULAR ORBIT APPROXIMATION

If we assume that the orbit is circular, (2.5) can be written in a form which will prove extremely useful later.

In a polar coordinate system, (r, θ, ϕ), whose north polar axis coincides with the North Pole of the Earth, the along track diferential coordinate, $d\vec{s}$, is parallel to the θ coordinate. If the descending node of the orbit, ϕ_n is 0 deg - 180 deg, $ds = d\theta$. If the descending node of the orbit is 180 deg - 360 deg, $ds = -d\theta$. Thus, since r =1 at the orbit height:

$$\nabla_s = \pm \frac{\partial}{\partial \theta} \tag{3.1}$$

where the plus or minus depends on the value of ϕ_n as given above.

Using (3.1) and integrating (2.5) with respect to t, we obtain an explicit form for the normal equation for $\dot{\rho}$ in the circular orbit approximation given by:

$$\dot{\rho}(t) = - PV/v \tag{3.2}$$

where v is the satellite orbital speed. To obtain (3.2), we have used the fact that:

$$dt = ds/v = \pm d\theta/v \tag{3.3}$$

and that P commutes with the integration.

We can also derive an explicit operator expression for P by considering the properties of the displacement operator, D, defined by:

$$D(\vec{\rho})f(\vec{r}) = f(\vec{r}+\vec{\rho}). \tag{3.4}$$

To derive the properties of D, first consider the operator for a differential displacement. (This is a standard derivation found in many texts, i.e., Tinkham, 1964; Messiah, 1966.) For a differential displacement in the along track direction, $d\vec{s}$, D is given by:

$$D(d\vec{s})f(\vec{r}) = d\vec{s}\cdot\vec{\nabla} f(\vec{r}) + f(\vec{r}), \tag{3.5}$$

so:

$$D(d\vec{s}) = 1 + ds\nabla_s. \tag{3.6}$$

If we can assume all the $d\vec{s}$ are along the direction of $\vec{p}$ (This true for $p \ll 1$, the case here.), then we can write $p = nds$. Thus $D(p)$ can be written as $(D(ds))^n$ yielding:

$$D(\vec{p}) = \lim_{n\to\infty} (1 + p\nabla_s/n)^n = e^{p\nabla_s} \tag{3.7}$$

Using (3.1), we obtain:

$$D(\vec{p}) = e^{\pm p\frac{\partial}{\partial\theta}}. \tag{3.8}$$

(If p were not small, in the above expression, p would have to be replaced by the arc length between the end points of p.)

But P can be written as:

$$P(\vec{p}) = D(\vec{p}) - 1. \tag{3.9}$$

Therefore:

$$P(\vec{p}) = e^{\pm p\frac{\partial}{\partial\theta}} - 1. \tag{3.10}$$

4. SEQUENTIAL LEAST SQUARES FITTING

The standard technique of deriving V from (2.5) or (3.2) using the range rate data is to represent V by a set of known basis functions times unknown coefficients and to use least squares fitting techniques to determine the coefficients and the trajectory, $\vec{r}(t)$. Since our primary concern is V and not $\vec{r}(t)$, one can attempt to solve the full problem sequentially, first, by solving for the approximate trajectories of the satellites with a reduced model of the gravity field, and second, by solving for a full model of the gravity field using the approximate trajectories. Let us consider the consequences of using this approach.

For this discussion, let our normal equation be represented as:

$$\dot{p}(t) = \sum_i a_i P f_i(\vec{r}) + \sum_i (b_i + c_i) P g_i(\vec{r}) \tag{4.1}$$

where we want to determine the cofficients a_i and $b_i + c_i$ given range rate data taken over some unknown trajectory $\vec{r}(t)$ and the known sets of functions f_i and g_i. Assume also that, through least squares fitting over the same trajectory, possibly using ancilliary data, we have found a solution:

$$\dot{p}_0(t) = \sum_i b_i P g_i(\vec{r}_0) \tag{4.2}$$

which has yielded the values b_i and the approximate orbit vector $\vec{r}_0(t)$. (The fit may involve each satellite individually and may use a priori b_i's.) Defining $\Delta p = p - p_0$ and subtracting (4.2) from (4.1), yields:

$$\Delta\dot{p}(t) = \sum_i a_i P f_i(\vec{r}) + \sum_i (b_i+c_i) P g_i(\vec{r}) - \sum_i b_i P g_i(\vec{r}_o). \qquad (4.3)$$

Further assume that the functions $f_i(\vec{r})$ and $g_i(\vec{r})$ can be approximated by $f_i(\vec{r}_o)$ and $g_i(\vec{r}_o)$. (f and g don't change appreciably over the distance $|\vec{r}-\vec{r}_o|$.) This turns (4.3) into:

$$\Delta\dot{p}(t) = \sum_i a_i P f_i(\vec{r}_o) + \sum_i c_i P g_i(\vec{r}_o) \qquad (4.4)$$

It is necessary to include the set of c-coefficients in the problem because the coefficients of the g-fuctions derived from a least square fit of (4.1) will not, in general, be the same as the the coefficients derived from a least squares fit which doesn't include the f-functions; to obtain the least squares condition without the f-functions, the g-function must alias the effects described by the f-function through alteration of the b-cofficients from the "true" value obtained if the full least squares fit were performed. (This is also true if a priori b-coefficients used in the 1st fit, were determined from past fits.) Thus by including the the c- coefficients and the g-functions in a second least squares fit on (4.4), we can correct our original b-coefficients to obtain better values and we can ensure that the previous fit does not cause aliasing problems in the a-coefficients. Since the coefficients of the g-functions are being refit, the only importance of the first fit is to produce a good $\vec{r}_o(t)$.

If we were interested in a further refinement in the trajactory, we could apply the approach used to obtain (4.4) to generate an expression for a correction to the trajectory given by:

$$\ddot{\vec{r}}(t) = -\sum_i a_i \vec{\nabla}(v f_i(\vec{r}_o)) - \sum_i (b_i+c_i)\vec{\nabla}(v g_i(\vec{r}_o)) \qquad (4.5)$$

This expression could be integrated twice to generate a better estimate of $\vec{r}(t)$ after the a_i's , b_i's, and c_i's were determined. This better $\vec{r}(t)$ could then be used to obtain an improved data set for generating $\Delta p(t)$ which in turn could be used to obtain improved a_i and c_i values, etc. Thus (4.4) and (4.5) can be used together in an iterative chain to refine the results obtained before iteration.

4.2 USING LEAST SQUARE FITTING TO DETERMINE THE GRAVITY FIELD

If we now assume the g-functions are to be part of the f-functions and set $\Delta\dot{p} = y$, we can write (4.4) in the general form:

$$y(t) = \sum_i a_i P f_i(\vec{r}_o) \qquad (4.6)$$

Let us allow the fit functions and the coefficients to be complex even though y is real. (This will lead to simpler notation later.) The sum of the squares or χ^2 is then given by:

$$\chi^2 = \int_{\vec{r}_o} ds\, w'(\vec{r}_o)\left(y-\sum_i a_i^* P f_i^*(\vec{r}_o)\right)\left(y-\sum_i a_i P f_i(\vec{r}_o)\right) \qquad (4.7)$$

where $w'(\vec{r}_o)$ is a weighting factor to be determined later and where the integration is over the trajectory, $\vec{r}_o$.

If the elapsed time for the trajectory is long compared with 24 hours, the rotation period of the Earth, the trajectory will pass over or nearly over every point on Earth with a probability which is only function of θ (infinite trajectory limit). (The orbit period of the satellite must also not be an exact harmonic of the Earth's rotation period, the case here.) In the infinite trajectory limit, the orbit also passes over each point an equal number of times with $ds=+d\theta$ and $ds=-d\theta$. In this limit and assuming the circular orbit approximation, (4.7) thus becomes:

$$\chi^2 = \sum_{\pm} \int d\Omega\, w(\Omega)\left(y-\sum_i a_i^* P f_i^*(\Omega)\right)\left(y-\sum_i a_i P f_i(\Omega)\right) \tag{4.8}$$

where we have replaced the integral over the trajectory with a sum over the two possible directions of ds in P of an integral over a geostationary spherical surface of radius R_h times an orbit density function absorbed into $w(\Omega)$. In (4.8), notice that y is now a function of $\vec{r}$, not t, and the implicit t dependence in V has disappeared. y must now be interepreted as the average value of $\dot{p}$ over the earth fixed point (θ,ϕ). The new weighting function $w(\Omega)$ is given in terms of the old one by:

$$w(\Omega)=n(\theta)w'(\vec{r}_o) \tag{4.9}$$

where $n(\theta)$ is the density of trajectory points over the Earth region (θ,ϕ) given by:

$$n(\theta) = Nrev/(\pi \sin\theta) \tag{4.10}$$

where Nrev is the number of revolutions in the trajectory. (4.8) is not a practical χ^2 for performing the actual least square fit, but will be useful for the theoretical analysis of the least square fit problem to follow.

From (4.8), least square fit equations can be developed in the usual way (Wolberg, 1967) by taking the derivatives of χ^2 with respect to the a-coefficients. This results in the following matrix equation:

$$L = TA \tag{4.11}$$

where:

$$A_i = a_i^* \tag{4.12}$$

$$L_i = (1/2)\sum_{\pm}\int d\Omega w y P f_i(\theta,\phi) \tag{4.13}$$

$$T_{ij} = (1/2)\sum_{\pm}\int d\Omega w P^* f_j^* P f_i \tag{4.14}$$

L and A are column vectors and T is a hermetian matrix whose inverse provides the solution:

$$A = T^{-1}L \tag{4.15}$$

The covariance matrix $C_{ij} = \langle \delta A_i \delta A_j^* \rangle$ (<..> is an ensemble average) is given by:

$$C = T^{-1}\chi^2/F \tag{4.16}$$

where δA_i is the deviation of A_i from the "true" value and

where F is the number of degrees of freedom, the number of independent measurements minus the number of a-coefficients. We can determine χ^2 by expanding (4.8) and using (4.15) to yield:

$$\chi^2 = \bar{y^2} - A^+L = \bar{y^2} - L^+A \qquad (4.17)$$

where $A^+L = \sum_i A_i^* L_i$, etc, and where:

$$\bar{y^2} = \tfrac{1}{2}\Sigma \int w(\theta)\ y^2 d\Omega \qquad (4.18)$$
$$\pm$$

If the χ^2 of (4.7) is used instead of that of (4.8), the equations remain the same except that the sum plus integral over the spherical surface goes back to an integral over the trajectory and w is replaced by w'

5. SOLVING THE MATRIX EQUATIONS

THE SCALE OF THE OVERALL PROBLEM

The basic GRM gravity data analysis problem is to find the orbit approximation, $\vec{r}(t)$, to solve the matrix equation (4.11) in terms of functions at the orbit height, and to analytically extend the solution at orbit height to the geoid. The analytic extension problem can be solved without large computations by using basis functions for V which are solutions to Laplace's equation. We will not concern ourselves with the orbit computation problem here. We will concern ourselves here with the remaining problem, the solution of the matrix equation.

There are two aspects of the matrix problem, forming the matrix elements and inverting T. The size of these tasks are determined by the number of basis functions, N, and the number of range rate data points collected, n. N is determined by the number of blocks in the gravity map. In a coordinate lattice which minimizes the number of blocks (regular square spherical shell lattice), the 1 degree resolution requirement of GRM (Smith, et. al., 1983) translates into 41,253 such blocks. If localized functions are used to make the map, one function to a map block, then there will be 41,253 basis functions. If complex spherical harmonics, $Y_{\ell m}$, are used to the point where one half wavelength of the function (π/ℓ) equals the block size, there will be spherical harmonics to order ℓ_m=180 and there will be $((\ell_m+1)^2-3)$=32758 real basis functions. For a 6 month mission with 1 data point per 4 seconds (Ibid.), n is 3.9×10^6.

Inverting an NxN matrix using Gaussian elimination techniques requires approximately $(4/3)N^3$ real floating point operations (flop) (See Appendix B.) and requires access to the matrix elements N times. Use of caching techniques as planned by GSFC in the proposed mission (Weiffenbach, 1983) and as described by others (Duff, 1981) can reduce the number of of disk accesses to the point where a large processor can run at 10 to 20 percent of full processing speed (Briggs, 1984). This means that with a Cyborg type computer, one can plan on having 10-20 Mflop/s of effective speed (Ibid.). Using this number for the processing speed and 41,253 for N, we obtain that 9.4×10^{13} flops and 1300-2600 hrs of computing time required for inversion of T.

Forming the matrix elements for the matrix equation is dominated by the calculation of T. Naively approaching the problem, it would seem that there are on the order of $nxN^2 = 7x10$ flop required to calculate the elements of T, based on calculating $N^2/2$ basis functions for n data points. Even at 80 Mflop, this would require 23,000 hrs to compute the elements. However, since the basis functions only change for lengths on the order of a block size, one does not have to calculate the basis functions for each point. APL has developed a scheme to do this in approximately 5000 hrs of computer time (Weiffenbach, 1980). The problem of calculating the matrix elements, though clearly the dominant problem, will not be addressed here.

One approach to finding a way of reducing the computation time associated with inverting T is to investigate the symmetries and near symmetries associated with the P operator and various sets of basis functions to see if the matrix can be broken down or approximately broken down into several irreduceable submatrices (diagonal blocks of submatrices) of lower dimensionality (Tinkham, 1964). These can be inverted with less computation time because the number of operations goes as such a high power (N^3) of the dimensionality.

If a symmetry is only approximate, it will create small terms instead of zeros off the irreduceable submatrices. If a residual matrix equation is created by operating on the original matrix equation, TA = L, with the inverse of the approximately irreproduceable submatrices of T, it is shown in Appendix B that the residual equation can be solved iteratively if the residual T-matrix is diagonally dominant. If this is the case, Appendix B also shows that the residual equation can be solved for A iteratively in less than $1x10^{12}$ flop (Appendix B.4) and that an approximate T^{-1} for determining the covariance can be generated in another $5x10^{11}$ flop (Appendix B.6).

Investigations by the author using the form of the P operator derived in Section 3 were carried out using point anomaly basis functions and spherical harmonic basis functions. The point anomaly functions were generated from the gravity field of point masses at the center of square spherical shell lattice blocks at a depth below the surface equal to the width of the block. The T-matrix generated from these anomaly functions was highly diagonal but unfortunately was not diagonally dominant. Also unfortunate was the lack of correlation in the large off diagonal terms (nearest neighbors) which may cause back-filling problems (See Appendix B.1.). (This is an essential feature of trying to index a two-dimensional surface with a one dimensional matrix index - most nearest neighbors are not nearest in index number.) To show that the matrix does or does not have back-filling problems will require further investigation.

The investigation using spherical harmonic basis functions proved so successful in demonstrating that there is an approximate symmetry which will greatly reduce the computation time required for inverting T that only this approach will be presented here. The next section presents the approach based on these functions.

6. CONSEQUENCES OF USING SPHERICAL HARMONIC BASIS FUNCTIONS

Let us consider the consequences of using spherical harmonics as the basis functions for V. To simplify writing the equations and for other reasons which shall become apparent later in this section, let us use the complex spherical harmonics, $Y_{\ell m}(\theta,\phi)$, with complex coefficients $a_{\ell m}$ rather than the real spherical harmonics, $R_{\ell m}(\theta,\phi)$ and $S_{\ell m}(\theta,\phi)$ used normally in Geodesy (Heisman and Moritz, 1967). In terms of $Y_{\ell m}$, a solution to Laplace's equation valid in all regions outside a sphere of any radius is given by (Jackson, 1962):

$$V(r,\theta,\phi) = v\sum_{\ell=0}^{\infty}\sum_{m=-\ell}^{\ell}\frac{a_{\ell m}}{r^{\ell+1}}\,Y_{\ell m}(\theta,\phi) \tag{6.1}$$

where we have normalized the coefficients so:

$$f(1,\theta,\phi) = \frac{V}{v} = \sum_{\ell=0}^{\infty}\sum_{m=-\ell}^{\ell} a_{\ell m}\,Y_{\ell m}(\theta,\phi) \tag{6.2}$$

$Y_{\ell m}$ is given by (Messiah, 1966, Vol. 1, Appendix B):

$$Y_{\ell m}(\theta,\phi) = (-1)^m\left[\frac{(2\ell+1)(\ell-m)!}{4\pi(\ell+m)!}\right]^{\frac{1}{2}} P_{\ell m}(\cos\theta)\,e^{im\phi} \tag{6.3}$$

where $P_{\ell m}$ is the associated Legendre polynomial of order (ℓ,m) given by the following for positive m (Ibid.):

$$P_{\ell m}(x) = (1-x^2)^{\frac{1}{2}m}\,\frac{d^{\ell+m}}{dx^{\ell+m}}\,(x^2-1)^{\ell} \tag{6.4}$$

For negative m, the $P_{\ell m}$ are defined by (Ibid.):

$$Y_{\ell,-m} = (-1)^m\,Y^*_{\ell m} \tag{6.5}$$

As defined here, the $Y_{\ell m}$ are orthonormal with respect to integrations on a unit sphere (Ibid.).

For a spherical harmonic basis, in the circular orbit approximation, the T-matrix elements become:

$$T_{\ell'm'\ell m} = \tfrac{1}{2}\sum_{\pm}\int P^*Y^*_{\ell m}\;P\;Y_{\ell' m}w(\theta)\,d\Omega \tag{6.6}$$

where we have put a restriction on $w(\Omega)$ that it be only a function of θ. Normally, the weighting function in terms of the trajectory integral, $w'(\vec{r}_d)$, will be a constant; since p is approximately the same everywhere along the trajectory, we expect the range rate data collected all along the trajectory to have about the same noise content. This means that normally $w(\Omega)$ is proportional to $n(\theta)$, so the restriction is normally satisfied. In the next paragraph, we will show that this restriction, along with the properties of P in the circular orbit approximation, are instrumental in simplifying the inversion of the T-matrix.

The expression for the P operator in the circular orbit approximation, (3.10), is written in terms of the operator $\partial/\partial\theta$. Since P has no ϕ dependence, it does not effect the functional dependence of the $Y_{\ell m}$'s with respect to ϕ ($e^{im\phi}$). Thus, since we assumed $w(\Omega)$ is only a function of θ, the matrix elements will be zero if m is not equal to m' because the integral of $e^{im\phi}$ over 360 degrees is zero unless m=m', regardless of the θ behavior. In other words, the T-matrix is diagonal in m. For a given m, there are only $Y_{\ell m}$'s with with $\ell \geq |m|$, so each $T_{\ell m \ell' m}$ is non-zero only for $\ell \geq |m|$ and $\ell' \geq |m|$.

The fact that the T-matrix is diagonal in m greatly reduces the number of computer operations required to invert the T-matrix. If we subgroup the indices by m first rather than by ℓ first, we can form the T-matrix into $2\ell_m+1$ diagonal m submatrices. ($\ell_m = 180$ is the maximum value $|m|$ can have.) Each m submatrix for $m \geq 1$ has $(\ell_m - |m|+1)^2$ complex elements ($(2\ell_m+1)$ elements for m=0). Summing for $m = -\ell_m$ to ℓ_m the approximately $(16/3)(\ell_m - |m|+1)^3$ real operations required to invert each submatrix, we find that only approximately $(8/3)\ell_m^4 = 2.8\times10^9$ flop are needed to invert the full matrix. Also of impact on the computation time is the fact that the largest submatrix (m=0) only requires 260642 real words for storing the matrix elements (and only 64800 words for the next largest, etc.), so we can load each submatrix to be inverted wholly into core memory on a large machine. This means the machine can run at virtually full speed to invert the matrix. So assuming an 80 Mflop/s computation rate and a 1 Mbyte/s disc transfer rate, one can invert the matrix in 66 seconds.

To aid in further investigations of this approach, it would be useful to be able to calculate the matrix elements of T in the circular orbit approximation. Appendix A shows how to generate closed formulas for the matrix elements without actually performing the integrations. It shows that the operator P in the circular orbit approximation can be written in terms of the quantum mechanical angular momentum operators, L_+ and L_- (Messiah, 1966), which have well known properties when acting on $Y_{\ell m}$ and yield linear combinations of other $Y_{\ell m}$'s. It also shows that the orbit density function in the circular orbit approximation times $Y_{\ell m}$ can be expressed as linear combinations of other $Y_{\ell m}$'s. Together these properties, along with the orthonormal property of the $Y_{\ell m}$'s, allow $T_{\ell m \ell' m'}$ to be written in terms of sums over coefficients which are functions of ℓ, m, ℓ', m', and p.

7. WILL AN ITERATIVE INVERSION OF THE RESIDUAL T-MATRIX CONVERGE?

We showed for (A) a circular orbit polar orbit, (3) $w(r) = w(\theta)$, and (C) the infinite trajectory limit that the T-matrix can be inverted fast because it is diagonal in m. In Appendix B, it is shown that the actual matrix equation, TA = L, can be solved iteratively for A (Appendix B.4) and for an approximate covariance (Appendix B.6) if the residual T-matrix formed by operating on T with the inverse of the diagonal-m portion of T is diagonally dominant (Appendices B.3 and B.5). Let us examine the violations of the assumptions (A), (B), and (C) that will occur in the actual planned mission to see if the diagonal dominance criterion is satisfied or not.

In the infinite trajectory limit, for the diagonalization in m to be violated there must be some ϕ dependence in P, $w(\vec{r})$, or ∇s (See equation2.5.). A small eccentricity in the orbit would not cause problems because this only causes mixing of the radial and θ coordinates. A deviation of the orbit from a polar one causes mixing of the ϕ coordinate into the $p\cdot\vec{\nabla}$ argument of P and into ∇s, but in a way which doesn't effect the diagonalization as follows. The ϕ dependent part of $p\cdot\vec{\nabla}$ can be written as, and the ϕ dependent part of ∇s is proportional to:

$$(p\cdot\vec{\nabla})_\phi = \pm p_\phi(\theta)(1/\sin\theta)\ \frac{\partial}{\partial\phi} \qquad (7.1)$$

where $p_\phi(\theta)$ functionally describes the orbit with θ as the independent variable and where the $\pm$ is for the 2 possible directions of ds at the point (θ, ϕ). Since $\frac{\partial}{\partial\phi}e^{im\phi} = ime^{im\phi}$, this term does not change the orthogonality of the $Y_{\ell m}$'s, so the matrix elements off diagonal in m remain zero. Also a deviation of the orbit from a polar one does not cause $w(\vec{r})$ to become a function of ϕ since the density remains axially symmetric regardless of the orbit in the infinite trajectory limit. Therefore, a deviation of the orbit from a polar one does not produce terms off diagonal in m in the infinite trajectory limit.

The finiteness of the actual data, however, can introduce ϕ dependence into $w(\vec{r})$. As stated previously, this effect goes to zero in the limit of an infinite trajectory length since the phase relationship between the rotation of the Earth and the rotation of the spacecraft around the geocentric fixed orbit go through all possible relationships equally. Since the orbital period is much less than the Earth's rotation period, the effect of the finite data length in the limit of many orbits, is given, to 1st order, by the residual assymmetry in the trace of the orbit as the Earth turns under the orbit. Since the Earth turns under the orbit once in 24 hours, the relative assymmetry in $n(\Omega)$ will be given by a maximum of (12 hrs)/(6 mo) $=3\times10^{-3}$. This number is just above the level of the order of magnitude criterion for diagonal dominance based on the assumption that all the off diagonal elements in m are equal as given in (B.18). (See Appendix B for a more detailed discussion.) We must, thus, examine this effect in more detail.

The assymmetry is a periodic step type function in ϕ with a 2π period and an amplitude 0.003. (For $\phi_a<\phi<\phi_b$, w is less by 0.003 than w for other values of ϕ). Since the ϕ dependence of $Y_{\ell m}$ is given by $e^{im\phi}$, the relative size of $|T_{\ell m\ell' m'}|$ to $|T_{\ell m\ell' m}|$ will be given by the the absolute value of (m-m')th harmonic amplitude of the fourier transform of a periodic step type function. The absolute value this harmonic is less than $0.003*2/(\pi|m-m'|)$ regardless of the width of the step (Selby, 1974). Therefore the criterion for convergence of the iterative inversion without assuming the off diagonal matrix elements are equal, (B.17) (See section B for more detail), can be written as:

$$0.5 > \mathrm{MAX}_{\ell,\ell'}\ |T_{\ell m\ell' m'}|/|T_{\ell m\ell' m}| = 0.002*2\sum_{m=1}^{\ell_m}(1/m)$$

$$=0.004\int_1^{\ell_m} dx/x \qquad (7.2)$$

$$= 0.004\ \ln(\ell_m)$$

$$0.5 > 0.02$$

where we are using the worst case conditions of $\ell,\ell' = \ell_m$ and m=0. Notice that the diagonal dominance criterion is more than met. The inclination of the orbit an angle z from a polar orbit will not change this result since we did not assume any particular $w(\theta)$ for the infinite trajectory length case to obtain the relative size of the step function in ϕ.

Off diagonal T-matrix terms in m will be produced by higher order spherical harmonic terms in the gravity potential through their effect on the trajectory estimate $\vec{r}(t)$. (In our angular integration model, this will produce ϕ dependence in $w(\vec{r}_0)$ through $\vec{r}_0(t)$'s influence on $n(\vec{r}_0)$.) Terms in the gravity field with the index $\pm m'$ will cause coupling terms in T between m and $m\pm m'$. However, all gravity potential spherical harmonic terms with $|m'|>0$ are less than 3×10^{-6} of the 1/r term (Gray, 1972) so we expect the relative size of terms off diagonal in m due to this effect to be on the order of 3×10^{-6} or less. (8.18), as mentioned above, states that the iterative inversion will converge if the relative size of the off diagonal elements is less than 0.001. Thus, this effect should not prevent the full matrix from converging iteratively.

Another effect which must be considered is roll and yaw of the satellites with frequencies equal to $nv/(2\pi)$ (n= 1,2,3,.....) producing T terms between m and $m\pm m'$. Because the orbit is polar, however, this would not produce terms coupling different m's but terms coupling different ℓ's. Also, since this effect would produce range rate data which would alias the effect of gravity terms, GSFC and APL have taken great pains to ensure that this effect will be measured and taken out of the range rate data before further analysis.

Lunar and Solar effects are also too small to effect the convergence of the iterative inversion of the T-matrix and they will usually be removed from the range rate residual by the least squares fit which determines the approximate trajectory.

8. CONCLUSIONS

The approach discussed in this paper of examining the symmetries of an operator representation of the observable proved very fruitful in simplifying the solution of the matrix equation for determining the gravity potential from low-low satellite range rate data. This still leaves the even larger problem of determining the matrix elements of the equation. This problem may also be simplified by utilizing the T-matrix in the circular orbit infinite trajectory approximation, which can be very quickly calculated (See Appendix A.), as a zeroth order approximation for the actual matrix. Further study along these lines will probably prove very promising. In addition, the circular orbit infinite trajectory approximation should prove very useful in studying the effects of various system errors and interactions on the errors in the coefficients of the spherical harmonic expansion of the gravity potential. This approach may also prove very fruitful in simplifying other problems in satellite geodecy and orbit determination.

APPENDIX A. CALCULATING THE T-MATRIX IN THE CIRCULAR ORBIT APPROXIMATION

The effect of P on $Y_{\ell m}$ can be calculated by using the following formulas (Messiah, 1966,V.1, Appendix B):

$$\partial/\partial\theta = (1/2)(e^{-i\phi}L_{+} - e^{i\phi}L_{-}) \tag{A.1}$$

where:

$$L_{\pm} = e^{\pm i\phi}(\pm\frac{\partial}{\partial\theta} + i\cot(\theta)\frac{\partial}{\partial\phi}) \tag{A.2}$$

and where:

$$L_{\pm}Y_{\ell m} = (\ell(\ell+1) - m(m\pm1))^{\frac{1}{2}} Y_{\ell,m\pm1} \tag{A.3}$$

If we now turn the full formalism of quantum mechanics, we can obtain a representation of the T-operator. In bra-ket notation (Messiah,1966), one can write the matrix elements of T as:

$$T_{\ell m\ell' m'} = \tfrac{1}{2}\sum_{\pm} \langle \ell m|P^{\dagger}w(\theta)P|\ell' m'\rangle \tag{A.4}$$

where the superscript † means the hermetian adjoint of the operator and where the $w(\theta)$ is put between $P^{\dagger}$ and P to indicate that the P operators only operate on the $Y_{\ell m}$ functions. Thus the T operator is:

$$T = \tfrac{1}{2}\sum_{\pm} (e^{\theta 6\backslash 6\pm}-1)w(\theta)(e^{\pm\partial/\partial\theta}-1) \tag{A.5}$$

where the hermetian adjoint of $\partial/\partial\theta$ is written as $\theta 6\backslash 6$ to emphasize that it operates in the backward direction.

If we expand the exponentials, collect terms of the same order in p, and perform the sum over the two directions of the orbit, we obtain:

$$T = \sum_{n=1}^{\infty}\sum_{j=1}^{2n-1} \frac{(\frac{6}{\theta 6})^{2n-j}\, p^{2n}\, w(\theta)(\frac{\partial}{\partial\theta})^{j}}{(2n-j)!\qquad j!} \tag{A.6}$$

The lowest order term in p, T_1 is given as:

$$T_1 = (\theta 6\backslash 6)p^2 w(\theta)(\partial/\partial\theta). \tag{A.7}$$

Setting $w'(r)=1$, we can write $w(\theta)$ as:

$$w(\theta) = Nrev/(\pi\sin\theta). \tag{A.8}$$

From a recursion relation derived from the fact that $Y_{1,\pm1}$ is proportional to $e^{\pm i\phi}\sin\theta$ (Mertzbacher, 1961), one can show that the "operator" $1/\sin\theta$ operating on $Y_{\ell m}$ yields:

$$Y_{\ell m}/\sin\theta = (2\ell+1)^{\frac{1}{2}} \sum_{j=o}^{j_m} \left[\frac{(2\ell-2j-1)\, F_{2j}^{\ell\mp m}}{F_{2j+2}^{\ell\pm m}}\right]^{\frac{1}{2}} e^{\pm i\phi}\, Y_{\ell 2j-1, m\mp\ell} \tag{A.9}$$

where F_m^n, the number of permutations of m object out of n, is:

$$F_m^n = n(n-1)(n-2).....(n-m+1) \tag{A.10}$$

and where:

$$\ell - 2j_m - 1 \geq |m+1| \tag{A.11}$$

Using (A.1), (A.3), (A.6), (A.9), and the orthonormality condition (6.6), a closed formula can be written for the T-matrix elements as a sum of coefficients which are calculable functions of ℓ,m,ℓ',m', and p without having to perform any numerical integrations. This could be set up in recursive form on a computer and accomplished without using a great deal of computer time.

APPENDIX B. SOLVING THE MATRIX EQUATIONS

B.1 DIRECT METHODS

Before proceeding it is useful set up some simplifying terminology. The matrix equation to be solved is given by:

$$TX = B \tag{B.1}$$

where T and B are known and X is to be solved for. T is a square matrix of size NxN, B is an NxM matrix (a column vector when M=1), and the solution X is an NxM matrix. In the case of finding the solution of the inversion of T, B is the NxN identity matrix, I, and $X=T^{-1}$. When performing certain operations on the equation in finding the solution, it is useful to introduce the concept of the augmented matrix, T^a. T^a is an Nx(N+M) matrix formed by augmenting the N columns of T with the M columns of B; that is:

$$T^a = T\ (+)\ B \tag{B.2}$$

where (+) indicates the dimensional addition of the columns of T and B together.

The various direct numerical methods used to solve matrix equations and invert matrices fall into 3 basic catagories, Triangular Gaussian elimination methods (Doolittle,Crout, etc.), Full Gaussian elimination (Gauss-Jordan), and sequential transformation methods (LU decompostion, partitioned matrices, Householder) (Riess, 1981; Gastinel, 1970; Detoma and Wardrip, 1982; Ralston and Rabinowitz, 1978). The sequential transformation methods are usually used only for special cases to take advantage of special symmetries such as large blocks of zero elements (LU and partitioning) or when only a small amount of memory is available (Householder). For the general case on large computers, usually one of the first two catagories is used.

Both of the first two catagories rely on Gaussian elimination (Riess, 1981; Gastinel, 1970). This consists of turning the off diagonal elements of a pivotal column (full), l, or a section of the pivotal column (triangular) of T into zeros by operating on T^a with:

$$T^{a(n+1)}_{ij} = T^{a(n)}_{ij} - (T^{(n)}_{il} / T^{(n)}_{lj})\, T^{a(n)}_{ll} \tag{B.3}$$

for all j not equal l in the Jordan method and for all j greater than l in the triangular method. This is performed N-1 times with l = 1 to N-1 to produce I(+)X in the Jordan method and T"(+)B' in the triangular method where T" is an upper triangular matrix. In the Jordan method the row j=l of T^a is also operated on by dividing the lth row by T_{ll}. (The complication of pivoting to minimize the error will not be discussed here (Riess, 1981; Gastinel, 1970).) In the triangular method, X is found by back-solving the modified equation as follows: Since T" is upper triangular, the lowest row of the equation is of the form $T"_{NN} X_{Nj} = B_{Nj}$, so it can be solved for X_{Nj} by dividing B_{Nj} by $T"_{NN}$. The value of X_{Nj} can now be used in the next lowest row of equation to find $X_{N-1,j}$, and this in turn can be used to find $X_{N-2,j}$, etc., until the whole equation is solved.

For M=1, and T symmetric, the number of operations to perform triangular Gaussian elimination (The triangular method takes fewer or as many operations as the Jordan method for all cases (Riess, 1981).) is approximately $(1/3)N^3$ real floating point operations (flop) (Riess, 1981; Gastinel, 1970). When M=N and T is symmetric (inversion) it takes approximately $(4/3)N^3$ flop.

Using this method to invert T, for T complex, it takes 4 times as many real operations as for T real. Thus for complex and symmetric, $(4/3)N^3$ (real) flop are required to find A and $(16/3)N^3$ (real) flop are required to invert T.

It is not enough just to show that large numbers of the matrix elements are zero or near zero; when a matrix is inverted using one of the various Guassian elimination techniques zeros and near zeros can be back-filled with non-small values very quickly during the factoring stage unless there is some symmetry to prevent this from happening (Riess, 1981; Duff, 1981). To see how fast the non-zeros turn into zeros, consider the following. Suppose we have a large NxN matrix with a relatively small number, k, of non-zero off diagonal elements in each row, with the non-zero elements occuring in a random pattern from row to row. In the factoring process of Guassian elimination each row of the matrix T other than a pivotal row, l, is transformed by the relation (B.3). If $T_{jj}^{(n)}$ were zero or near zero and $T_{jl}^{(n)}$ and $T_{lj}^{(n)}$ were non-small, one can see that $T_{jj}^{(n+1)}$ would become a non-small number. This is what is called back-filling. After operating on the matrix elements with l pivotal rows and columns, because the probability of $T_{jj}^{(n)}$ being zero is virtually 1 when there are only a small number of non-zero off diagonal elements, one can show that the average number of non-zero terms in the remaining columns grows approximately as $k2^l$ until the number of non-zero elements per row in the remaining columns becomes comparable to N. To keep this from happening, the zeros in one row must be correlated to the zeros in another row to a very high order and must remain correlated during the elimination operatations.

B.2 ITERATIVE METHODS

The two principal iterative methods are the Jacobi method and the Gauss-Seidel method (Riess, 1981; Gastinel, 1970). The Jacobi method finds the (n+1)th estimate of X from the (n)th estimate by:

$$X_{im}^{(n+1)} = \left(B_{im} - \sum_{j \neq i} T_{ij} X_j^{(n)}\right)/T_{ii} \qquad (B.4)$$

The Gauss-Seidel method uses the most current estimate for $X_{im}^{(n)}$, which for k<i is $X_{jm}^{(n+1)}$. Each iteration takes $2N^2$ flop for M=1 and $2N^3$ for inverting a matrix when T is symmetric. Thus, there is no gain in using this technique for inverting matrices, but there is a very substantial gain for M=1 as long as the solution converges in a relatively small number of steps.

B.3 THE CONVERGENCE OF ITERATIVE SOLUTIONS

If T is diagonally dominant and non-singular, the Jacobi, Gauss-Seidel, and other similar iterative methods for finding the inverse of a matrix or solving matrix equations will converge regardless of the first guess

(Riess, 1981; Gastinel, 1970). Diagonal dominance is defined by:

$$1 > \mathrm{Max}_i \sum_j{}' |T_{ij}|/|T_{ii}| \qquad (B.5)$$

where Σ' means the sum over j with j not equal to i and Max_i means the largest value for i = 1 to N. In fact if we define q as:

$$q = \mathrm{Max}_i \sum_j{}' |T_{ij}|/|T_{ii}| \qquad (B.6)$$

one can show that after n iterations:

$$||\Delta X^{(n)}||/||\Delta X^{(0)}|| \leq q^n \qquad (B.7)$$

where $||\Delta X^{(n)}||$ is the largest error in the nth estimate of the solution, X. This means that, starting with T_{ij} as a first guess for X, and given q =1/2, the matrix elements would converge to 2^{-n} times the largest element in n iterations or approximately to a precision of 2^{-n} in n iterations. If the matrices are complex, as stated above each iteration in the Jacobi or Gauss-Seidel methods requires $8N^2$ (real) flop. Thus, obtaining a result with 2^{-n}precision requires only $8N^2$xn flop. For 64 bit precision, this becomes $512N^2$ (real) flop.

Diagonal dominance is a stringent condition for large matrices. If all the of diagonal elements were the same, (B.5) would become:

$$|T_{ij}|/|T_{ii}| = q/(N-1) \qquad (B.8)$$

For N=41,253 and q =1/2, this condition is $|T_{ij}/T_{ii}| < 1.2\text{x}10\text{-}5$.

B.4 ITERATIVE METHOD FOR DETERMINING THE EXACT COEFFICIENTS.

In this section, we derive an iterative method which solves for A using X', the inverse of T', where T' is the T-matrix with all elements off diagonal in m set to zero. The method produces A to 64 bit precision in less than $1\text{x}10^{12}$ (real) flop. (See Sections B.5 and 7 for proof of convergence.) It can produce A to any desired precision with corespondingly fewer or more flop.

If we observe that:

$$T = T' + \Delta T, \qquad (B.9)$$

we can write:

$$TA = (T' + \Delta T)A = L. \qquad (B.10)$$

Multiplying both sides of (B. 9) by X', we obtain:

$$(I + X'\,\Delta T)A = X'L. \qquad (B.11)$$

This equation can now be solved by the Gauss-Seidel or Jacobi methods if the matrix elements of T off diagonal in m are small since $I+X'\Delta T$ has no matrix elements diagonal in m which are off diagonal in ℓ. (See Sections B.5 and 7 for proof of convergence.)

Calculating A from (B.11) is dominated by the number of operations in the multiplication of X' by ΔT and in the iterative proceedure. Since X' is diagonal in m, and both X'and ΔT are symmetric, it takes $8N\,\ell_m^3/3 = 5.1\times10^{11}$ (real) flop to perform the multiplication. Each iteration of the solution takes $8N^2$ (real) flop. Assuming the solution will converge 64 iterations or less (See Section B.3.), the iterative solution will take $512N^2 = 5.5\times10^{11}$ (real) flop. This means that the total number of operations to find A is 1.06×10^{12} (real) flop. This is a factor of 88 fewer flop than our original estimate based on $(4/3)41{,}253^3 = 9.4\times10^{13}$ flop.

B.5 CONVERGENCE CRITERION FOR MATRIX ELEMENTS OFF DIAGONAL IN m

Based on the iterative method of the previous section, iterative convergence criteria for the T-matrix elements off diagonal in m will be derived.

Since T has no diagonal terms in m and X' has only diagonal terms in m, we note that $I+X'\Delta T$ is equal to I for diagonal terms in m,and equal to $X'\Delta T$ for off diagonal terms in m. The criterion for convergence of the iterative solution of (B.11) is that $I+X'\Delta T$ be diagonally dominant as given by (B.5) and (B.6), which in this case, with the noted properties of $I+X'\Delta T$, become:

$$1 > q = \mathrm{Max}_{\ell m} \sum_{\ell}{}' \sum_{m}{}' \left| \sum_{\ell''} X'_{\ell m \ell'' m} \Delta T_{\ell'' m \ell' m'} \right| . \qquad \text{(B.12)}$$

Noting that:

$$||T|| = \mathrm{Max}_i \sum_j{}' |T_{ij}| \qquad \text{(B.13)}$$

is a matrix norm of T which satisfies the Cauchy-Schwarz inequality (Riess, 1982), we can write:

$$||X'\Delta T|| < ||X'||\,||\Delta T|| . \qquad \text{(B.14)}$$

Thus, from (B.12) and (B.14), we obtain:

$$q < ||X'||\,||\Delta T|| . \qquad \text{(B.15)}$$

But $||X'||$ is on the order of $1/||T'||$, so we can write the approximate relation:

$$q < \mathrm{MAX}_{m,\ell,\ell'} \sum_{\ell''}{}' \sum_{m'}{}' |T_{\ell m \ell'' m''}| \Big/ \sum_{\ell''}{}' |T_{\ell'' m \ell' m}| \qquad \text{(B.16)}$$

Assuming $|T_{\ell m \ell'' m''}|$ is on the order or bigger than $|T_{\ell'' m \ell' m}|$ (For this matrix, we expect the off diagonal elements to get smaller as m and m' differ.), we can "divide out" the sum over ℓ'' in the numerator. This yields the following approximate relation:

$$q < \mathrm{MAX}_{\ell,\ell',m} \sum_{m'}' |T_{\ell m \ell' m'}| / |T_{\ell m \ell' m}| \qquad (B.17)$$

where $\mathrm{MAX}_{\ell,\ell',m}$ means the maximum value ranging over all m, ℓ and ℓ'. (B.17), though of somewhat dubious derivation, is probably good for order of magnitude calculations.

A crude estimate for diagonal dominance can be obtained from (B.17) by setting all the off diagonal elements equal. Setting $q = 0.5$, for the worst case of ℓ and ℓ' equal to 180 and m equal to 0, we obtain:

$$|T_{\ell m \ell' m'}| / |T_{\ell m \ell' m}| < q/(2\ell_m + 1) = 0.001 \qquad (B.18)$$

where the value given is for $q = 0.5$.

B.6 PERTURBATION THEORY METHOD FOR DETERMINING THE COVARIANCE MATRIX

From (4.16), the covariance matrix can be determined if we determine T^{-1} and χ^2. To determine T^{-1} for this purpose, we don't need an exact solution, but only an approximate one good enough for error estimates. The following method will obtain an approximate solution for T^{-1} in only 5×10^{11} (real) flop.

We want the solution to:

$$TX = I \qquad (B.19)$$

where I is the identity matrix.

Suppose we have a solution:

$$T'X' = I \qquad (B.20)$$

where T is close to T'. Then by manipulating (B.19) and (B.20), we can generate:

$$X - X' = (I - X'T)T^{-1} \qquad (B.21)$$

If we use X', the separation $T = T' + \Delta T$ from Section B.4, and make the approximate substitution $T^{-1} = X'$, we obtain the following approximate formula (1st order perturbation solution):

$$T^{-1} = X' - X'\Delta T X' \qquad (B.21)$$

Given both $X'\Delta T$ and X' (from the solution to $TA = L$ in Section B.4), it takes $8N\ \ell_m^3/3$ (real) flop to produce $X'TX'$ and $4\ \ell_m^3/3$ (real) flop to perform the remaining subtraction. The actual χ^2 can be calculated from (4.17) using $\bar{y}^2$ defined by (4.18) with the integral in (4.18) changed back to the integral over the trajectory. For 3.9×10^6 data points, calculating $\bar{y}^2$ takes 8×10^5 (real) flop and calculating A^+L takes only $3N = 2.6 \times 10^5$ (real) flop. Thus, it takes approximately $8N\ \ell_m^3/3$ (real) $= 5.1 \times 10^{11}$ (real) flop to produce this estimate of the covariance.

ACKNOWLEDGEMENT

The author would like to acknowledge the help of the many persons at Goddard Space Flight Center and the Applied Physics Laboratory who cheerfully supplied a great deal of unpublished material and verbal information on GRM and the matrix inversion problem.

REFERENCES

W. Briggs, Bendix Field Engineering Corporation, Columbia, Maryland, private communication based on experience with the inversion of a 10,000x10,000 matrix, 1984.

E. Detoma and S. C. Wardrip, "Useful Statistical Techniques for Time and Frequency Data Reduction", NASA/Goddard Spaceflight Center internal report (unpublished), 1982.

I. Duff, ed., SPARSE MATRICES AND THEIR USES, Academic Press, 1981.

N. Gastinel, LINEAR NUMERICAL ANALYSIS, Academic Press, 1970.

E. Gray, ed., AMERICAN INSTITUTE OF PHYSICS HANDBOOK, 3rd ed., McGraw-Hill, 1972.

W. Heisman and H. Moritz, PHYSICAL GEODESY, Freeman and Co., 1967.

J. Jackson, CLASSICAL ELECTRODYDNAMICS, Wiley and Sons, 1962.

E. Mertzbacher, QUANTUM MECHANICS, Wiley and Sons, 1961.

A. Messiah, QUANTUM MECHANICS, Wiley and Sons, 1966.

A. Ralston and P. Rabinowitz, A FIRST COURSE IN NUMERICAL ANALYSIS, McGraw-Hill, 1978.

J. Riess, NUMERICAL ANALYSIS, Addison-Wesley, 1982.

S. Selby, ed., CRC STANDARD MATHEMATICAL TABLES, 22nd ed., CRC Press, 1974.

D. Smith, R. Langel, and T. Keating, "Geopotential Research Mission (GRM)", NASA/Goddard Space Flight Center document (no I.D. number), August, 1982.

M. Tinkham, GROUP THEORY AND QUANTUM MECHANICS, McGraw-Hill, 1964.

F. O. vonBun, D. Smith, W. Kahn, S. Bergson-Willis, T. Keating, et. al., private communications, NASA/Goddard Space Filght Center, 1980-1983.

G. Weiffenbach, V. Pisacani, et. al, private communications, Johns Hopkins University Applied Physics Laboratory, 1980-1983.

J. Wolberg, PREDICTION ANALYSIS, D. Van Nostrand, 1967.

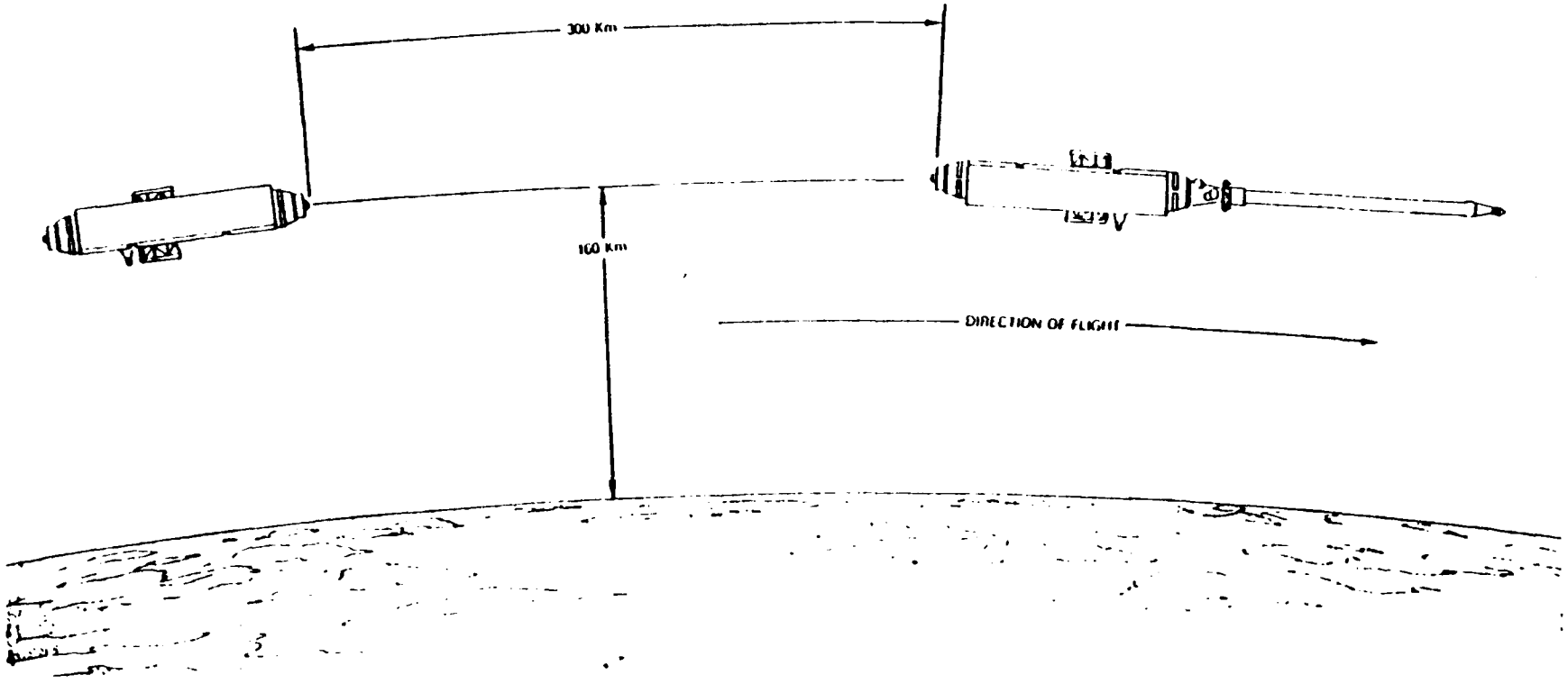

Figure 1. The GRM Satellite Configuration (Courtesy of F. O. vonBun, NASA/Goddard Space Flight Center).

DEPARTMENT OF THE AIR FORCE
AIR FORCE GEOPHYSICS LABORATORY (AFSC)
HANSCOM AIR FORCE BASE, MASSACHUSETTS 01731

REPLY TO ATTN OF LWG/Lt Warner

SUBJECT Minutes, Gravity Gradiometer Conference, 12-13 February 1985

TO Conference Attendees

1. Please find attached a copy of the meeting minutes, presentations (if individually requested), and list of conference attendees. The minutes were compiled by Dr. Chris Jekeli and me from abstracts submitted by various presenters and notes taken at the conference. In some cases our notes may have been sketchy resulting in our interpretation of questions and responses after each presentation. In all cases we attempted to report each presentation correctly and adequately.

2. I have reserved the same facilities at the USAF Academy for next year's conference to be held 11-12 February 1986. We'll start requesting papers late this summer. Registration will proceed soon after.

3. Thank you for your interest in gravity gradiometry. We look forward to your continuing support.

DONNA L. WARNER
Conference Coordinator

1 Atch: Minutes